

Surface Properties And Catalytic Activity Of Manganese Ferros spinels

*Thesis submitted to the
Cochin University of Science And Technology
in partial fulfilment of the
requirements for the degree of*

**Doctor of Philosophy
In
Chemistry**

In the Faculty of Science

By

NISHAMOL KANAT

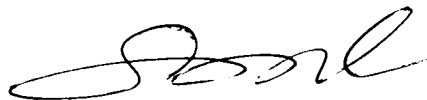
*Department of Applied Chemistry
Cochin University of Science And Technology
Kochi – 682 022*

April - 2002

CERTIFICATE

This is to certify that the thesis herewith is an authentic record of research work carried out by Ms. Nishamol Kanat under my supervision, in partial fulfilment of the requirements for the degree of Doctor of Philosophy of Cochin University of Science and Technology, and further that no part thereof has been presented before for any other degree.

Kochi- 682 022
30th April 2002



Dr. S. SUGUNAN
(Supervising teacher)
Professor in Physical Chemistry
Department of Applied Chemistry
Cochin University Science And Technology
Kochi-682 022

CONTENTS

Chapter 1	Introduction & Literature Survey	Page No
1.1	Catalysis	1
1.2	Transition metal oxides as catalysts	4
1.3	Ferrites	6
1.4	Spinels	6
1.5	Methods of preparation	6
1.6	Spinel structure	9
1.6.1	Distribution of metal ions over different sites	12
1.6.2	Factors determining the cation distribution	13
1.6.3	The surface of catalytically active spinel phase	16
1.7	Spinels as catalysts	17
1.8	Transport studies	21
1.9	Acid-base properties	23
1.9.1	Surface electron properties	24
1.9.2	Temperature programmed desorption studies	26
1.9.3	Thermogravimetry of desorption of basic molecules	29
1.9.4	Cyclohexanol decomposition	30
1.10	Reactions selected for the present study	32
1.11	Objectives of the present work	33
	References	34
Chapter 2	Experimental	
2.1	Catalyst preparation	41
2.1.1	Materials	41
2.1.2	Preparation of different compositions of manganese ferrosinels	41
2.2	Catalyst characterization	43
2.2.1	X-ray diffraction analysis	43
2.2.2	Inductively Coupled Plasma (ICP) analysis	44
2.2.3	Scanning Electron Microscope (SEM) analysis	45
2.2.4	Diffuse Reflectance Infra-Red Fourier Transform (DRIFT) Spectroscopy	46
2.2.5	Thermogravimetric (TG) analysis	47
2.2.6	Surface area determination (BET method)	47
2.2.7	Transport studies	48
2.2.8	Mössbauer Spectroscopy	50
2.2.9	Acid-base property studies	52
2.3	Catalytic activity studies	54

Chapter 3	Characterization And Surface Properties	
3.1	Physical characterization	57
3.1.1	X-ray diffraction analysis	57
3.1.2	Scanning Electron Microgram (SEM) analysis	64
3.1.3	Inductively Coupled Plasma (ICP) analysis	64
3.1.4	Diffuse Reflectance Infra-Red Fourier Transform (DRIFT) Spectra	64
3.1.5	Thermogravimetric (TG) analysis	67
3.1.6	Surface area and pore volume measurements	68
3.1.7	Transport studies	70
3.1.7.1	DC electrical conductivity measurements	70
3.1.7.2	Hall effect measurements	73
3.1.8	Mössbauer Spectra	75
3.1.9	Cation distribution	78
3.2	Surface properties-acidity/basicity	80
3.2.1	Temperature programmed desorption of ammonia (NH ₃ -TPD) method	80
3.2.2	TG desorption of pyridine/2,6-DMP	87
3.2.3	Surface electron properties	89
3.2.4	Cyclohexanol decomposition	97
	References	102
Chapter 4	Acylation And Alkylation Reactions	
4.1	Section I-Friedel-Crafts Benzoylation of Aromatic Compounds	104
4.1.1	Benzoylation of activated benzenes (toluene, xylene and anisole)	107
4.1.1.1	Benzoylation of toluene	107
4.1.1.1.1	Effect of catalyst loading	107
4.1.1.1.2	Effect of reaction temperature	109
4.1.1.1.3	Effect of duration of reaction run	110
4.1.1.1.4	Effect of toluene/BOC molar ratio	111
4.1.1.1.5	Effect of moisture	113
4.1.1.1.6	Comparison of catalyst composition	114
4.1.1.1.7	Catalyst reusability	122
4.1.1.1.8	Mechanism of benzoylation reaction	124
4.1.1.2	Benzoylation of xylenes	126
4.1.1.2.1	Benzoylation of isomeric xylenes	129
4.1.1.3	Benzoylation of anisole	130
4.1.2	Benzoylation of deactivated benzenes (benzene and halobenzenes)	133
4.1.2.1	Benzoylation of benzene	133
4.1.2.2	Benzoylation of halobenzenes	138
4.2	Section-II Aniline Alkylation	142
4.2.1	Process optimization	146

4.2.1.1	Effect of methanol to aniline molar ratio	147
4.2.1.2	Effect of reaction temperature	148
4.2.1.3	Effect of flow rate	149
4.2.2	Comparison of catalyst composition	150
4.2.3	Mechanism of aniline alkylation	161
4.3	Section III - Phenol Alkylation	163
4.3.1	Process optimization	165
4.3.1.1	Effect of methanol to phenol molar ratio	165
4.3.1.2	Effect of reaction temperature	165
4.3.1.3	Effect of flow rate	167
4.3.1.4	Effect of water in the feed	168
4.3.2	Comparison of catalyst composition	169
4.3.3	Mechanism of phenol alkylation	179
	References	182
Chapter 5	Oxidation Reactions	
5.1	Section I- Phenol Hydroxylation	188
5.1.1	Process optimization	191
5.1.1.1	Effect of catalyst loading	191
5.1.1.2	Effect of reaction temperature	192
5.1.1.3	Effect of reaction time	193
5.1.1.4	Effect of hydrogen peroxide to phenol volume ratio	194
5.1.1.5	Effect of pH of the reaction medium	195
5.1.1.6	Effect of solvent	196
5.1.2	Comparison of catalyst composition	196
5.1.3	Mechanism of phenol hydroxylation	203
5.2	Section II-Oxidative Dehydrogenation of Ethylbenzene	207
5.2.1	Process optimization	208
5.2.1.1	Effect of air flow rate	209
5.2.1.2	Effect of reaction temperature	211
5.2.1.3	Effect of flow rate	212
5.2.2	Comparison of catalyst composition	213
5.2.3	Mechanism of ODH of ethylbenzene	224
	References	228
Chapter 6	Summary And Conclusions	
6.1	Summary of the work	232
6.2	Conclusions	235
6.3	Further scope of the work	237

Introduction

1.1 Catalysis

A catalyst always helps a reaction to alter its rate. The history of catalysis began from 1796 with the studies by von Marum on the dehydrogenation of alcohol using metals. However, the term catalysis was defined by J. J. Berzelius in 1836 as a process in which a relatively small amount of a foreign material, called a catalyst, augments the rate of the reaction without being consumed in the reaction. A good catalyst must possess both high activity and long-term stability. But the most important quality is its selectivity, which reflects its ability to direct conversion of reactants in a specific way.

Modern industries are learning more and more about the applications and benefits of catalysts and the different ways to bring down the cost of production. The specificity of a catalyst enables a chemical process to proceed more efficiently with less waste. Catalytic process technologies generally involve less capital investment, lower operating costs, higher purity products and reduce environmental hazards. Hence, catalysis is of crucial importance to the chemical industry. The more well defined areas of industrial catalysis are petroleum, pharmaceutical and environmental catalysis. In the present day, catalysis research and industrial catalyst development are dependent largely upon the impulses and the needs of the market, the ecological circumstances, i.e., environmental protection, the extensive utilization of the starting materials and above all, the development of reaction specific catalysts. We must expect that in the 21st century energy production, various modes of transport, chemical and petroleum industry, metallurgy and other industries involving chemical treatment will become world wide and more safe by the use of catalytic technologies leading to the purification of exhaust gases, waste water and other harmful by-products. Various techniques and concepts of solid state are applied for synthesizing and modifying catalysts with required structure and chemical properties. Thus it goes without saying that the modern chemical industries cannot operate without proper study of catalysts and their specific action.

Traditionally, this field is divided into homogeneous and heterogeneous catalysis. By definition, a catalytic reaction in which the reactants and the catalyst are in the same phase, is homogeneous catalysis and if the reactants and the catalysts are in different phases, it is heterogeneous catalysis. Each of these catalytic processes possesses its own advantages and disadvantages. The strongest impulse for developing new, more efficient and more selective catalyst systems is related to environmental compatibility. Looking at the different industrial areas, in particular in the production of fine chemicals and in the pharmaceutical industry, a lot of by-products and wastes are produced. The so called E-factor i.e., the ratio of the amount of by-products to the amount of product is not acceptable. The reason is the use of stoichiometric amount of homogeneous Brönsted acids such as HF, H₂SO₄, H₃PO₄, HNO₃, etc. and Lewis acids such as AlCl₃, BF₃, FeCl₃, etc. By-products in the form of salts due to the neutralization of the acids are also produced. That is also true for the application of Brönsted and Lewis bases in the field of organic multi-step syntheses and in each step there is a loss of starting material. The synthesis of fine chemicals and pharmaceuticals generates large amounts of wastes, which is due in particular to the fact that most of the reactions are stoichiometric or use environmentally non-friendly homogeneous catalysts. The substitution of these polluting and corrosive homogeneous catalysts by solid catalysts, which do not possess such disadvantages, is one of the main industrial challenges. Besides the environmental improvement, heterogeneous catalysis has many technical advantages, in particular easy separation of products, easy development of continuous processes and possibility of catalyst regeneration. Due to these striking properties, the field of heterogeneous catalysis is one of the rapidly expanding areas in chemical industry.

In recent years, considerable advances have been achieved in the study of surface structure and mechanism of the catalytic reaction. A heterogeneous catalyst performs by providing an alternative reaction pathway with lower energy of activation. Heterogeneous catalysts interact with reactants and enhance the rate of chemical reactions. This interaction may be chemical and physical processes, which are fundamental to any heterogeneous catalytic system. The overall catalytic reaction rate depends on these chemical and physical processes or steps. Each of these steps contributes to a greater or lesser extent to the overall reaction rate.

The general steps involved in heterogeneous catalysis are:

- External diffusion: Transfer of the reactants from the bulk fluid phase to the fluid-solid interface and external surface of the catalyst particle.
- Internal diffusion (if particle is porous): Intraparticle transfer into the catalyst particle.
- Adsorption: Physisorption and chemisorption of reactants at the surface (sites) of the catalyst particle.
- Surface reaction: Chemical reaction of adsorbed species to produce adsorbed products; this is the intrinsic or true chemical reaction step.
- Desorption: Release of adsorbed products by the catalyst.
- Internal diffusion: Transfer of products to outer surface of the catalyst particle.
- External diffusion: Transfer of products from fluid-solid interface into the reaction stream.

From experience it is possible to narrow the range of solids that are likely to catalyze a certain type of chemical reactions. Heterogeneous catalysts can be classified according to their electrical conductivity as conductors, semiconductors and insulators. Table 1.1 shows such classification and the type of reactions for each type of catalyst.

Table 1.1 Classification of heterogeneous catalysts.

Classification	Conductor	Semiconductor	Insulator
Materials	Metals	Metal oxides and sulphides	Metal oxides
Examples	Fe, Co, Ni, Ru, Rh, Pd, Ir, Pt, Ag, Cu.	NiO, CuO, ZnO, Cr ₂ O ₃ , V ₂ O ₅ , etc., WS ₂ , MoS ₂ , etc.	Zeolites, Al ₂ O ₃ , SiO ₂ -MgO, Al ₂ O ₃ + Cl or F
Types of Reactions	Hydrogenation, Dehydrogenation, Hydrogenolysis, Oxidation, Reduction	Oxidation, Reduction, Hydrogenation, Dehydrogenation, Denitrogenation, Desulphurization, etc.	Hydration, Dehydration, Isomerization, Polymerization, Cracking, etc.

1.2 Transition metal oxides as catalysts

Transition metal oxides are technologically important materials that have found to be relevant in chemical applications. Transition metal oxides are the proficient components in catalysts employed in many reactions such as oxidation, reduction, oxidative and non-oxidative dehydrogenation, ammoxidation, metathesis and water gas shift reaction for the production of hydrogen.

Many transition metal oxides are non-stoichiometric. It is known that the interaction of the oxide with its constituents in the gas phase generates defects or coordinatively unsaturated sites. These defects or coordinatively unsaturated sites are important in surface chemistry, which are mainly responsible for the adsorptive and catalytic properties of the transition metal oxides. Due to the formation of these defects, various cations may be differently distributed between the surface and bulk of the single as well as in the multi-component transition metal systems. When the concentration of the defects at the surface of the oxide surpasses a certain critical value, ordering of defects or formation of new bi-dimensional surface phase may occur, resulting often in a dramatic enhancement of catalytic activity and selectivity [1-3]. As an example, nickel oxide mixed with SiO_2 [4], $\text{SiO}_2\text{-Al}_2\text{O}_3$ [5] and NiSO_4 [6] are highly active for the dimerization of olefins and the active site for this reaction is found to be the low valent nickel at the surface of the system.

Transition metal oxides possess acid-base properties. Titania and zirconia attracted much attention because these are good supports for metal catalysts and change to super acids on combining with small amount of sulphate. Hydrated Nb_2O_5 and Ta_2O_5 are making an impact for their application as unusual solid acids and showed excellent stability as a catalyst for esterification, hydrolysis and hydration reactions [7-11]. Oxides of Cr, Mo and W are seldom used as single oxides but are used as mixed oxides with alumina and silica for hydrogenation, dehydrogenation, skeletal isomerization of hydrocarbons, polymerization of olefins and hydrodesulphurization [12-16]. Probably due to the high oxidation activity of manganese oxides, very few studies have been reported for their acid-base properties. MnO_2 has been claimed to be efficient for the hydration of nitriles to amides, in which the acidic character of the catalyst is involved

[17, 18]. Re_2O_7 supported on alumina exhibited strong acid sites and are efficient catalysts for the metathesis of olefins [19]. Fe_2O_3 is regarded to be weakly acidic and basic and Fe_2O_3 obtained by heat-treating of FeSO_4 showed maximum acidity and catalytic activity at the calcination temperature of 700°C for several reactions [20-24]. The acidic sites in Co and Ni oxides are due to the presence of coordinatively unsaturated Co and Ni ions and are established to be active for the dimerization of olefins [4-6]. ZnO is considered as amphoteric and the acidity and basicity increase when ZnO is mixed with other oxides [25-28] and thereby the catalytic activity is enhanced.

Analysis of the voluminous patent literature concerning the selective oxidation of hydrocarbons clearly indicates that majority of the efficient catalysts for these processes are transition metal oxides. Their efficiency in oxidation reactions depends not only on their redox properties but also on their acid-base properties. Numerous works are reported to correlate the acid-base properties of mixed transition metal oxides with the catalytic activity /selectivity in selective oxidation of hydrocarbons [29, 30].

The catalytic abatement of NO_x has engrossed the interest of many laboratories world wide because of the stringent regulations for the NO_x emissions. Transition metal oxides (for example, oxides of Cu, Co, Fe, Mn, Ti, and V) show promising results when added as promoters or co-catalysts [31-34].

Transition metal oxides are efficient systems in relation to their adsorption behaviour of reaction products. Their catalytic oxidation of CO is performed by a series of reaction steps, while the adsorption of CO proceeds quickly and is limited only by the desorption of CO_2 . It has been known for a long time that copper oxides display high catalytic activity for the oxidation of CO [35-38]. A number of other transition metal oxide systems, Cu-Cr-O, Cu-Al-O, Mn-Mg-Al-O, Mn-Al-Mg-O, Mn-perovskite and Ni-Cu-Cr-O also have been identified to be active over a wide range of compositions [39].

Ternary transition metal oxides with general formula AB_2O_4 , where A and B are the metal cations, having the spinel structure show greater structural stability and catalytic activity. In the present investigation, manganese-iron based spinel oxides of chromium, cobalt, nickel, copper and zinc are chosen.

1.3 Ferrites

Mixed metal oxides with iron (III) oxides as their main component are known as ferrites. Ferrites crystallizes in three different crystal types namely, magnetoplumbite, garnet and spinel and accordingly they can be classified into three groups (Table 1.2).

Table 1.2 Crystal type of ferrites.

Type	Structure	General Formula	Example
Magnetoplumbite	Hexagonal	$A^{II}Fe_{12}O_{19}$	$BaFe_{12}O_{19}$
Garnet	Cubic	$Ln^{III}Fe_2O_4$	$Ln^{III} = Y, Sm, Eu, Gd, Tb, Dy, Ho, Er, Tm \text{ and } Lu$
Spinel	Cubic	$A^{II}Fe_2O_4$	$A^{II} = Cd, Co, Mg, Ni \text{ and } Zn$

1.4 Spinel

The simplest among the ferrites are the spinel type. Simple ferros spinels ($A^{II}Fe_2O_4$), as well as mixed ferros spinels of the general composition $A_x^{II}B_{1-x}^{III}Fe_2O_4$ are known. The interesting structural, electrical, magnetic and catalytic properties of these compounds are governed by their chemical composition. So special care must be taken in the preparation stages of these compounds to get ferros spinels with specific properties.

1.5 Methods of preparation

Ferrites can be prepared by almost all the existing techniques of solid state chemistry, leading to a wide variety of forms: thin and thick films, single crystals and polycrystalline aggregates. The ideal characteristics of ferrite powders are:

- Small particle size
- Narrow distribution in particle size
- Dispersed particles
- High purity
- Homogeneous composition

For the exact reproducibility of the ferrite particles utmost care must be taken during the preparation stages. Minor changes in the preparation method can drastically alter their properties.

The oldest method of preparation of ferrites is the *ceramic method*. The precursor compounds are usually iron oxide ($\alpha\text{-Fe}_2\text{O}_3$) and oxides or carbonates of the other cations in the desired ferrite and these are ground well by mechanical milling. But this method cannot produce fine particles and extended milling introduces significant quantities of undesired impurities and the distribution in particle size becomes extremely wide. The major drawback found for this method is the lack of homogeneity of the material prepared. Again, the high temperature (1200 K) required to complete solid state reactions leads to drastic decrease in surface area of the resulting material by sintering.

Ferrite powders with all the ideal characteristics mentioned above can be prepared by various new methods. Their common feature is that the mixing of components takes place at the atomic or molecular scale. *Co-precipitation* is a very suitable method for the creation of homogeneous catalyst components or for the moulding of precursors with a definite stoichiometry, which can easily be converted to the active catalyst [40]. This method is based on the stoichiometric mixing of aqueous solutions of chlorides, nitrates and sulphates of Fe^{3+} , and of divalent Ni, Co, Mg, Ba, Sr, etc., in the concentrations required for the ferrite composition and their simultaneous precipitation in the form of hydroxides by NaOH [41-45]. This is followed by filtration, washing and calcination of the product to form the oxide. The morphology, the texture, the structure and the size of the particles can be accurately controlled by altering the pH of the solution, temperature and nature of the reagents [46]. By this method ferrite particles with a narrow size distribution in the range 50-500 nm may be obtained, with high purity.

The *precursor method* allows the preparation of ferrites with a precise stoichiometry. It involves the synthesis of a compound (precursor) in which the reactants are present in the required stoichiometry. Upon heating in air (1200-1500 K), the precursor decomposes to yield the ferrite [47-49]. Particles with high magnetization, high purity and size in the range 20-60 nm can be obtained by this method.

Sol gel techniques are receiving much attention because they can be applied to a wide variety of materials; they offer the possibility of controlling not only the size and distribution of particles, but also their shape. A broad range of ferrites with any desired shape can be prepared by this technique [50-52]. The process involves the preparation of a sol, which is a dispersion of a solid and a dispersed phase in a liquid (dispersion medium). The sol is prepared by mixing concentrated solutions containing the cations of interest, with an organic solvent as dispersion medium. The sol is then destabilized by adding water, leading to the formation of a gel. This is transformed to the solid phase by high pressure heating whereby the liquid contained in the gel is transformed into supercritical vapours.

Spray-drying technique of preparation of ferrites involves precipitation from a concentrated solution of cations by solvent evaporation. To ensure that the particle size remains small, the concentrated solution is atomized at high pressure into fine droplets of 100-500 μm diameter; the solvent is rapidly evaporated by an upward stream of hot gas. Several alternative methods are currently under development, as an efficient way to control the texture, composition, homogeneity and structural properties of the ferrite particles [53-57].

In *freeze drying* method, the aqueous, concentrated solution is atomized into fine droplets, and are rapidly frozen by blowing into low temperature bath such as ice-acetone, or liquid nitrogen. The droplets are then dried in vacuum and the anhydrous salts are calcined to produce fine powders. Ni-Zn ferrites have been obtained from freeze-drying with high density and small and uniform grain size [58].

Combustion synthesis is a novel method for the preparation of fine particles of ferrites making use of the exothermic redox reaction between metal nitrate and tetraformal triazine or oxalic acid dihydrazine [59]. In this process stoichiometric ratio of nitrates is dissolved in the minimum amount of water in a pyrex dish; the fuel is added and is heated at 350°C in a muffle furnace. A heating rate of 75°C/min is used to obtain good combustion. This method can be used for the synthesis of Ni-Zn and Co spinels.

In addition to the above-discussed methods, some other methods like *molten salt synthesis* [60] and *shock wave synthesis* [61] are also applied in the ferrite synthesis.

1.6 Spinel structure

The spinel structure was first determined by Bragg and Nishikawa [62]. The unit cell of a spinel contains eight formula units and hence can be represented as $8[AB_2O_4]$. The 32 oxygen anions per unit cell form a face centered cubic (fcc) lattice in which two kinds of interstitial sites are present namely, (i) 64 tetrahedral sites, surrounded by 4 oxygens (A site) and (ii) 32 octahedral sites, surrounded by 6 oxygen ions (B sites). Of these, 8 tetrahedral holes ($1/8^{\text{th}}$ of the tetrahedral interstices) and 16 octahedral interstices ($1/2$ of the octahedral interstices) are occupied by metal ions. The unit cell of an ideal spinel structure is shown in Fig. 1.1. It is convenient to divide the unit cell into eight edges of length $a/2$ to show the arrangements of the A and B sites (Fig. 1.2). The space group is $Fd\bar{3}m$ (O_h^7). The oxygen atoms have four-fold coordination, formed by three B cations and A cation. The nearest neighbours of a tetrahedral site, octahedral site and oxygen anion site are shown in Fig.1.3.

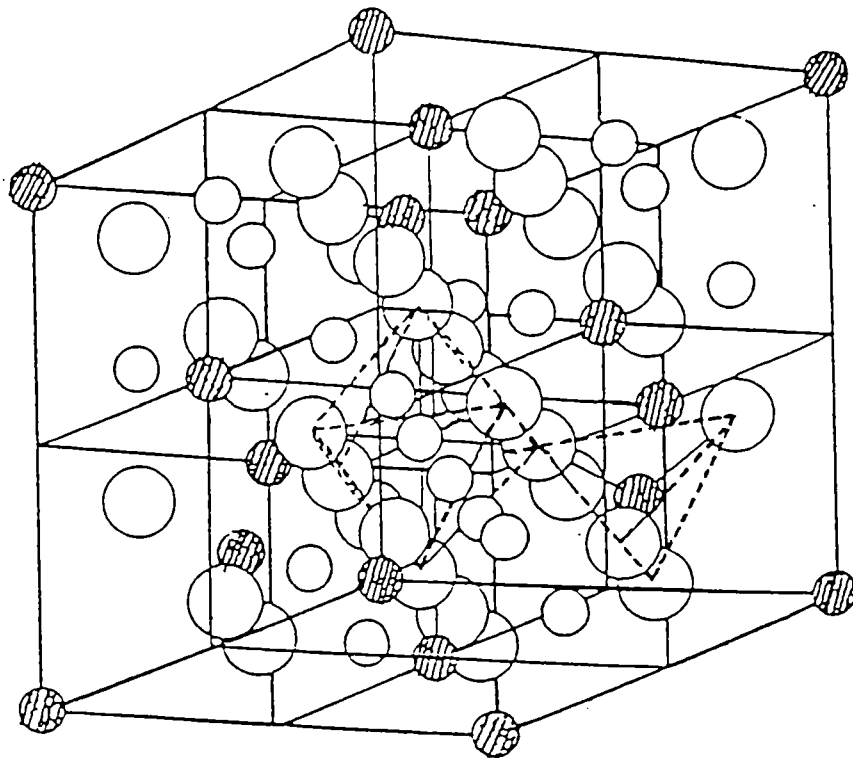


Fig. 1.1 The unit cell of an ideal spinel structure. Hatched circles indicate A cations, unhatched circles indicate B cations and large unhatched circle indicate oxygen anions.

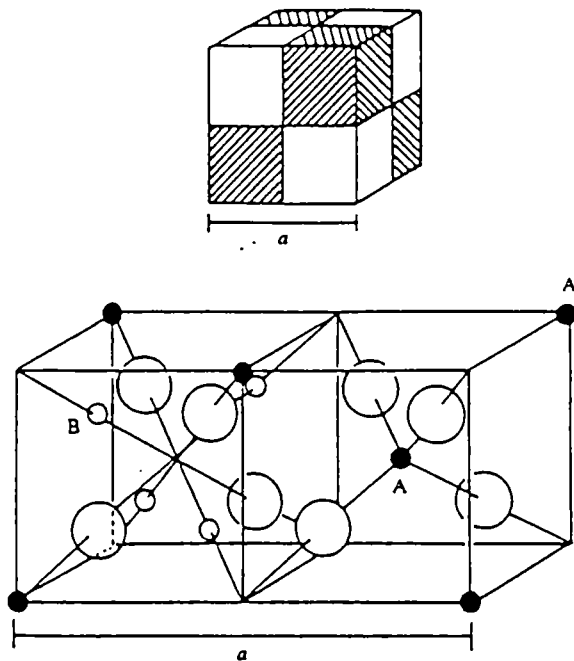


Fig. 1.2 The spinel structure. The unit cell can be divided into octants; tetrahedral cations A, octahedral cations B and oxygen atoms (large circles) are shown in two octants.

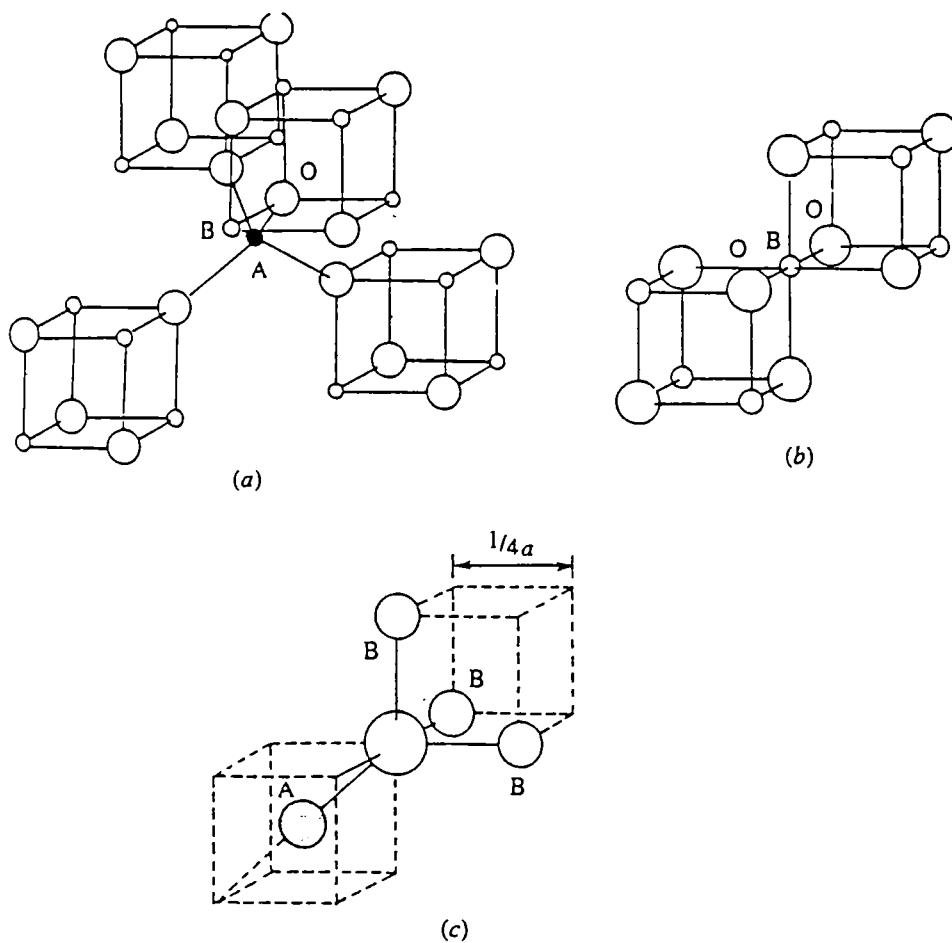


Fig. 1.3 Nearest neighbours of (a) a tetrahedral site, (b) an octahedral site and (c) oxygen anion.

The ideal situation is never realized as the oxygen anions in the spinel structures are generally not located at the exact positions of the fcc sublattice. The interstices available in an ideal close packed structure of rigid oxygen anions can incorporate only those metal ions with radius $r_{\text{tetra}} \leq 0.30 \text{ \AA}$ in tetrahedral sites and only those ions with radius, $r_{\text{octa}} \leq 0.55 \text{ \AA}$ in octahedral sites. So in order to accommodate larger cations such as Co, Cu, Mn, Mg, Ni and Zn, the lattice has to be expanded. The difference in the expansion of the octahedral and tetrahedral sites is characterized by a parameter called oxygen parameter (u). In all ideal spinels, the parameter ' u ' has a value in the neighbourhood of 0.375. But in actual spinel lattice this ideal pattern is slightly deformed, usually corresponds to $u > 0.375$. ' u ' increases because the anions in the tetrahedral sites are forced to move in the [111] direction to give space to the larger A cations, but without changing the overall $\bar{4}3m$ symmetry. Octahedra become smaller and assume $3m$ symmetry. In Table 1.3, interatomic distances are given as a function of the unit cell parameter ' a ' and the oxygen parameter ' u ' [63, 64].

Table 1. 3 Interatomic distances and site radii in spinels AB_2O_4 , as a function of unit cell edge (a) and oxygen parameter (u).

Tetra-tetra separation A-A	$a (3/4)^{1/2}$
Tetra – octa separation A-B	$a (11/8)^{1/2}$
Octa – octa separation B-B	$a (2/4)^{1/2}$
Tetra – O separation A-O	$a [3(u-0.25)]^{1/2}$
Octa – O separation B-O	$a (3u^2-2.75 u + 43/64)^{1/2} \quad a (5/8-u)$
O-O tetrahedral edge O-O	$a (2(2u-0.5))^{1/2}$
O-O shared octa edge O-O	$a [2(1-2u)]^{1/2}$
O-O unshared octa edge O-O	$a (4u^2 -3u + 11/16)^{1/2}$
Tetrahedral radius	$a [3(u-0.25)]^{1/2} - R_0$
Octahedral radius	$a (3u^2-2.75u + 43/64)^{1/2} - R_0 \quad a (5/8-u) - R_0$

u is defined with unit cell origin at an A site and R_0 is the oxide ion radius.

1.6.1 Distribution of metal ions over different sites

Normal, Inverse and Random Spinels

The interesting and useful electrical, magnetic and catalytic properties of the spinels are governed by the distribution of metal ions among the octahedral and tetrahedral sites of the spinel lattice. As mentioned earlier, the general formula of the spinel is AB_2O_4 , where A and B cations occupy the tetrahedral and octahedral sites respectively. Many different cation combinations may form a spinel structure and it is almost enough to combine any three cations with a total charge of eight to balance the charge of the anions. The following combinations

A = +2, B = +3	as in	NiFe ₂ O ₄
A = +4, B = +2	as in	Co ₂ GeO ₄
A = +1, B = +3, +4	as in	LiFeTiO ₄
A = +1, B = +3	as in	Li _{0.5} Fe _{2.5} O ₄
A = +1, B = +2, +5	as in	LiNiVO ₄

and

A = +6, B = +1	as in	Na ₂ WO ₄ , are known.
----------------	-------	--

The structure and the cation distribution of the spinels have been discussed by Verway and Heilman [65]. If A denotes a divalent cation and B, a trivalent one, the cation distribution is usually indicated as (A)[B₂]O₄, where the square brackets indicate the octahedral site occupancy and the cation in the parenthesis are located in the tetrahedral sites. This is the so called *normal* distribution, in which the tetrahedral sites are occupied only by the A- type ions and the octahedral sites by the B -type ions. The A ions of a normal spinel occupy the 8 tetrahedral sites of the Oh⁷ space group and have a point symmetry T_d. The B ions of a normal spinel occupy the 16 octahedral sites of the Oh⁷ space group and have point symmetry D_{3d}. Another extreme cation distribution is, (B)[AB]O₄, as pointed out by Barth and Posnjak [66]. In this case the B cations occupy the tetrahedral sites and all the A cations together with the other half of the B cations occupy the octahedral sites. This type of spinel configuration is called *inverse* spinels. Datta and Roy [67] and Hafner and Laves [68] have shown that there are many *intermediate* or *random* spinels which are in between the pure normal and pure inverse

arrangements. This can be represented as $(A_{(1-x)} B_x) [A_x B_{(2-x)}] O_4$, where x is the degree of inversion, with a value of zero for normal and one for the inverse distribution. This intermediate spinel structure is due to the average distribution of all the ions about all the spinel cation positions (Table 1.4).

Table 1.4 Cation distribution, lattice parameter (a) and oxygen parameter (u) for several spinels.

	Distribution	$a(\text{\AA})$	u
Normal	(Cd)[Fe ₂]	8.7050	0.3935
	(Zn)[Fe ₂]	8.5632	0.3865
Inverse	(Fe)[CoFe]	8.3500	0.3810
	(Fe)[CuFe]	8.3690	0.3800
	(Fe ³⁺)[Fe ²⁺ Fe ³⁺]	8.3940	0.3798
	(Fe)[Li _{0.5} Fe _{1.5}]	8.3300	0.3820
	(Fe)[NiFe]	8.3390	0.3823
Random	(Mg _(1-x) Fe _x)[Mg _x Fe _(2-x)]	8.3600	0.3820 ($x = 0.10$)
	(Mn _(1-x) Fe _x)[Mn _x Fe _(2-x)]	8.5110	0.3865 ($x = 0.85$)
	(Mo _(1-x) Fe _x)[Mo _x Fe _(2-x)]	8.5010	0.3751 ($x = 0.50$)

1.6.2 Factors determining the cation distribution

The physical and chemical properties of spinels depend not only on the kinds of cations in the lattice, but also their distribution over the available crystal sites. It is thus of major importance to understand the factors which influence the site occupancy.

The factors that contribute to the total lattice energy in spinels are:

- (i) elastic energy
- (ii) electrostatic (Madelung) energy
- (iii) crystal field stabilization energy
- (iv) polarization effects

The elastic energy refers to the degree of distortion of the crystal structure due to the difference in ionic radii assuming that ions adopt a spherical shape. Smaller cations, with ionic radii of 0.225-0.4 Å, should occupy tetrahedral sites, while cations of radii 0.4- 0.73 Å should enter octahedral sites. This distribution leads to a minimum in lattice strain. Since trivalent cations are usually smaller than divalent ones, a tendency towards the inverse arrangement would be expected.

The detailed Madelung energy calculations for spinels [69], show that this energy is dependent on the u parameter. For $u > 0.379$, the normal distribution is more stable, while for lower u values, the inverse arrangement possesses a higher Madelung constant. The presence of two kinds of cation on octahedral sites in inverse spinels leads to an additional contribution to the Madelung energy. The critical u value then becomes 0.381 [70]; Madelung energy is higher for the normal spinel if $u > 0.381$, and the inverse, ordered spinel is more stable for $u < 0.381$.

The application of the crystal field theory to the understanding of cation site preference was first suggested by Romeijn [71]. Dunitz and Orgel [72] and simultaneously McClare [73] have calculated the octahedral site preference energies of transition metal ions in oxides using crystal field theory (CFT) and is given in Table 1.5.

The data show that the systems with d^5 and d^{10} configurations have no crystal field stabilization energy and hence no site preference. The d^1 system has the highest octahedral site preference energy. The d^4 and d^9 ions can be further stabilized by Jahn-Teller distortion. In the regular O_h symmetry, octahedra of surrounding anions is elongated or compressed in the z direction to give D_{4h} symmetry, the doublet (e_g) and triplet (t_{2g}) levels split [74]. The splitting of the doublet is larger. In the case of elongation, the d_z^2 orbital is stabilized compared to the $d_{x^2-y^2}$ orbital. $Fe[CuFe]O_4$, $Mn[ZnMn]O_4$, $Cr[NiCr]O_4$ and $Zn[Mn_2^{3+}]O_4$ are examples of tetragonally distorted spinels.

The last factor to be discussed is polarization effects. Polarization may simply be considered as the degree of distortion of the electronic charge density around an ion. This can arise from the negligible distortion and effective removal of an electron from one ion towards its neighbour, giving rise to a purely covalent bond and a purely ionic

bond, respectively. With regard to transition metal ions in spinels, only spherically symmetric ions (d^5 and d^{10}) can show tendency for covalency. In this case, tetrahedral sites are preferred. Cations which show covalent affinity for tetrahedral environments are Fe^{3+} , Ga^{3+} , In^{3+} and, more strongly, Zn^{2+} and Cd^{2+} . Spinel with the former cations tend, therefore, to be inverse while those with the latter tend to be normal.

When the various factors are counterbalancing, there can be a completely random arrangement of metal ions among the eight tetrahedral sites and sixteen octahedral sites.

Table 1.5 Crystal field stabilisation energies for transition-metal cations on octahedral and tetrahedral spinel sites.

Number of d electrons	Theoretical cfs in terms of Dq		Cations	Estimated octahedral site preference energies, eV
	Octahedral	Tetrahedral		
1	4	6	Ti^{3+}	0.33
2	8	12	V^{3+}	0.53
3	12	8	V^{2+} Cr^{3+}	1.37 2.02
4	6	4	Mn^{3+} Cr^{2+}	1.10 0.74
5	0	0	Fe^{3+} Mn^{2+}	0 0
6	4	6	Fe^{2+} Co^{3+}	0.17 0.82
7	8	12	Co^{2+}	0.09
8	12	8	Ni^{2+}	0.99
9	6	4	Cu^{2+}	0.68
10	0	0	Zn^{2+}	0

1.6.3 The surface of catalytically active spinels

The surface structure and properties of spinels are of wide interest. The principal and interesting question to ask is, which plane, which coordination and which valency states are responsible for the catalytic activity and selectivity in spinels? There are many reports that the tetrahedral sites in spinels are not active [75-77]. The fact that the tetrahedral sites are not active could originate from stronger metal-oxygen bonds due to the lower valency and coordination number. Moreover, the tetrahedral sites are not accessible to the reactants [78]. In the literature, usually only the low-index planes are taken into consideration when discussing the surface of spinels [75, 79-81]. Following the suggestion by Knözinger and Ratnaswami [75] and using their notation one can distinguish six different low-index surface planes, which are shown in Fig. 1.4. From the figure it follows that A (111), C (110), E (100), and F (100) planes have both tetrahedral and octahedral sites on the surface, while B (111) and D (110) planes expose only octahedrally coordinated cations.

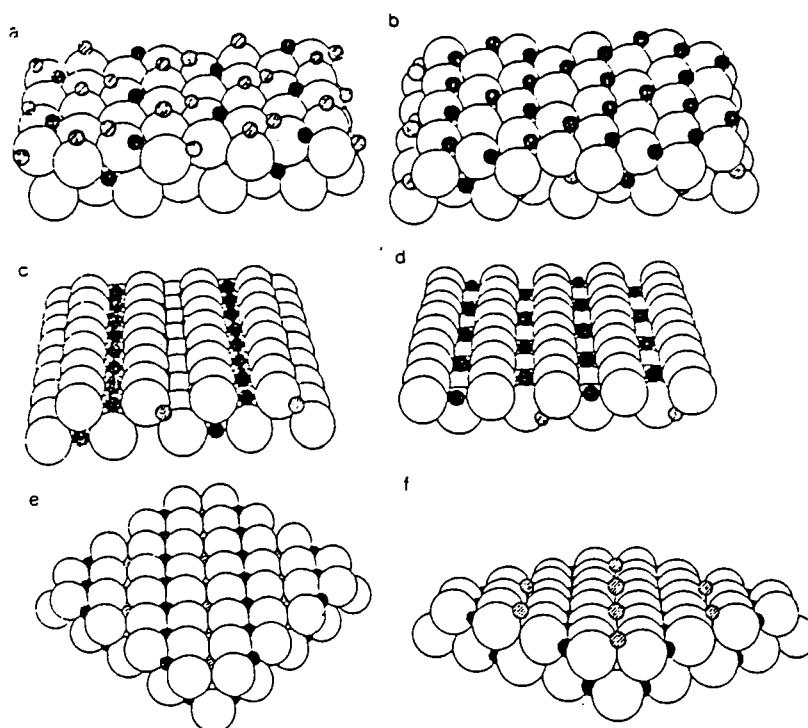


Fig. 1.4 The low-index planes of a normal spinel structure: (a) A (111), (b) B (111), (c) C (110), (d) D (110), (e) E (100), (f) F (100). The open spheres represent the oxygen anions, the solid spheres the octahedral cations and hatched spheres the tetrahedral cations.

According to Ziolkowski and Barbaux [79], from the theoretical calculations, the A (111) and D (110) planes are preferred in the surface, but these predictions do not form a final conclusion. Shelef and coworkers [80-82] made an experimental attempt to elucidate the surface structure of spinels using the low energy ion scattering (LEIS) and they support the idea that the tetrahedrally coordinated cations are not accessible for the reactant molecules.

Beaufils and Barbaux [76, 77] investigated the surface composition of normal spinel oxides by differential neutron diffraction (D.N.D) techniques and concluded that the surface of spinel consists of a mixture of (110) and (111) planes. By comparing the experimental results of D.N.D with some models involving argon-oxygen distances, they observed that these planes contain only octahedral cations and oxygen anions respectively. Jacobs *et al.* [78] confirmed this by the LEIS technique. By substitution of the Mn and Co cations in different sites in the spinel structure of Mn_3O_4 and Co_3O_4 by other cations which are not active in the selective reduction of nitrobenzene to nitrosobenzene, they studied the role of these sites in the catalytic reaction. Their results confirmed the idea that octahedral ions are exposed almost exclusively at the surface of the spinel oxide powders and only these sites participate in the reaction. The only two low-index planes of the spinel structure, which can satisfy this condition, are identified as B (111) and D (110). The absence of occupied tetrahedral sites at the surface is a more general property of spinels.

1.7 Spinel as catalysts

Ternary oxides crystallizing with spinel structure exhibit interesting catalytic properties. However, individual metal oxides lose their catalytic activity rapidly owing to ageing and coke formation on the catalyst surface. The spinel lattice imparts extra stability to the catalyst under various reaction conditions, so that these systems sustained activity for longer periods [83]. In spinel systems correlation between catalytic activities and the electric and the magnetic properties are often found; this is a direct consequence of the dependence of both properties on the nature of the ions, their charges, and their distributions among octahedral and tetrahedral sites. Jacobs *et al.* in their recent work revealed that octahedral sites are exposed almost exclusively at the surface of spinel

oxide and the catalytic activity of such systems is mainly due to the octahedral cations [78]. The tetrahedral ions are either inactive or contributing only a little to the catalytic properties [85]. The lower activity of the tetrahedral ions comes from the fact that the metal oxygen bonds will be stronger due to lower coordination number and hence such cations are less accessible to the reactants.

Among the spinel compounds, ferrites have been used as effective catalysts for a number of industrially important reactions such as oxidative dehydrogenation of hydrocarbons, hydrodesulphurization of petroleum crude, treatment of automobile exhaust gases, oxidation of CO, etc. The catalytic effectiveness of ferrites for many such reactions arises because of the ease with which iron can exchange its oxidation state between 2 and 3. Even if reduction of Fe^{3+} to Fe^{2+} occurs, spinel structure remains unaltered and upon reoxidation the original state can be regained [85].

Many single and mixed oxides have been mentioned as catalysts for the oxidative dehydrogenation (ODH) of olefins. Bajas *et al.* reported MgFe_2O_4 as an efficient catalyst for the oxidative dehydrogenation of hydrocarbons containing 4 to 6 carbon atoms [86]. Gibson and Hightower made kinetic and mechanistic studies of oxidative dehydrogenation of butene to butadiene over magnesium ferrite using deuterium and ^{14}C labelled isotopic traces [87]. Their kinetic studies showed that the reaction is zero order in oxygen and first order in olefin at low partial pressures of butene. They suggested a modified Rennard-Massoth mechanism for the reaction in which the butene adsorption site is postulated to be an anion vacancy. Zinc-chromium and magnesium-chromium ferrites with spinel structure are superior catalysts for the oxidative dehydrogenation of butene to butadiene [83, 88, 89]. The Cr^{3+} ions, incorporated into octahedral site in spinel lattice, inhibit the bulk reduction of the catalyst and increase its activity and selectivity for the reaction. Cares *et al.* reported CoFe_2O_4 , as a better catalyst over CuFe_2O_4 for the dehydrogenation reaction [90]. A probable reason for the difference in activity of two catalysts is the greater reducibility of the copper ions relative to the cobalt ions as suggested by the authors.

Methyl tertiary -butyl ether (MTBE) is an octane number enhancer as well as an emission reducing agent present in much of the unleaded gasoline today. Improvements

in the catalytic higher alcohol synthesis (production of isobutanol and methanol for downstream synthesis to MTBE) from syn gas are necessary in order for the reaction pathway to become economically viable. A commercially available Zn/Cr spinel catalyst is Engelhard Zn-0312. Epling *et al.* promoted this commercial catalyst with varying amount of potassium and cesium [91-94]. Their results indicate that a better catalyst for the production of an equimolar mixture of isobutanol and methanol can be achieved by promoting the Zn/Cr spinel by Cs rather than K and Cr, which are found to be unnecessary for higher alcohol syntheses and possibly detrimental. Further, the authors prepared a series of Zn/Cr/ Mn spinel catalysts promoted with Cs and Pd in which some of the Cr atoms have been replaced by Mn and the resulting data indicate that Mn improves the catalytic properties of Cs promoted spinels [95, 96].

Another important reaction catalyzed by oxidic spinels is selective reduction of nitrobenzene to nitrosobenzene, which is an intermediate of various organic syntheses leading to widely used antioxidants. Maltha *et al.* investigated the active sites of some manganese and cobalt spinels in the selective reduction of nitrobenzene and showed that Mn and Co ions in the octahedral positions are responsible for the catalytic activity [97]. Ziolkowski *et al.* report that spinels of nominal composition $Zn_{(1-x)}Mn_xAl_2O_4$, ($0 \leq x \leq 3$) are active, selective and are stable catalysts for the selective reduction of nitrobenzene to nitrosobenzene [98]. A series of mixed cobalt aluminium oxides with spinel structure showed high activity for this reaction and the catalytic activity is related to the concentration of cobalt ions on the catalyst surface [99]. This is in agreement with the operation of the Mars-van Krevelen mechanism.

The production of oxygen gas for many years relied on the electrolysis of water. The heterogeneous decomposition of hydrogen peroxide is a convenient alternative to the electrolysis of water for the production and storage of oxygen gas. Cobalt ferrite ($CoFe_2O_4$) catalyzes, the decomposition of hydrogen peroxide to the same extent as expensive noble metal oxides such as silver oxide, platinum and palladium black [100]. The high activity of cobalt-iron spinel oxide system towards the peroxide decomposition was explained by a redox-couple mechanism in which the presence of Co^{II} ion at the

octahedral lattice sites of the cobalt spinel oxide structure initiated a cyclic electron transfer process [100-102].

There are many studies in search of a spinel compound with optimum catalytic activity for the peroxide decomposition. Investigations on the catalytic properties of $\text{Co}_x\text{Fe}_{3-x}\text{O}_4$, $\text{Ni}_x\text{Fe}_{3-x}\text{O}_4$ and $\text{Cu}_x\text{Fe}_{3-x}\text{O}_4$ ($0 < x < 3$) in strong alkaline media have shown that the activity follows the order $\text{Co} > \text{Cu} > \text{Ni}$ [101, 103-105]. Attempts on the intrinsic catalytic power of ferros spinels with stoichiometry, $\text{M}^{\text{II}}\text{Fe}_2\text{O}_4$ ($\text{M}^{\text{II}} = \text{Mn, Co, Ni, Cu, Zn}$ and Cd) for hydrogen peroxide decomposition in neutral medium ($\text{pH} = 6.6$) have shown that ferros spinels with $\text{M}^{\text{II}} = \text{Mn}$ and Co are highly active and $\text{M}^{\text{II}} = \text{Ni, Cu, Zn}$ and Cd are moderately active [104]. Senguptha *et al.* tried the peroxide decomposition over a series of manganese ferros spinels, $\text{Mn}_x\text{Fe}_{3-x}\text{O}_4$ ($0 < x < 3$) and out of which $\text{Mn}_{2.5}\text{Fe}_{0.5}\text{O}_4$ promises to be a potential cost effective substitute for the noble metal oxides [107].

The Fischer-Tropsh synthesis for the production of hydrocarbons from syn gas has been studied over manganese ferros spinels by Maiti *et al.* and compared its activity and selectivity compared with pure iron oxides or elemental iron [108]. The mixed iron manganese catalysts with spinel phase results in stable activity. The low concentration of manganese promotes the formation of olefins, whereas high manganese catalysts promote the formation of saturated hydrocarbons. In a recent work Cabet *et al.* and Tihay *et al.* investigated the catalytic behaviour of Co-Fe oxides with spinel phase in the hydrogenation of carbon monoxide in the Fischer – Tropsh synthesis and they proved the ability of such catalysts to produce $\text{C}_2\text{-C}_4$ olefins [109, 110].

Nitrogen oxides and soot particulates emitted from diesel engine have been causing serious problems to global environment and human health. Ternary AB_2O_4 ($\text{A} = \text{Mg, Co, Cu, Ni}$ and Zn and $\text{B} = \text{Cr, Fe}$ and Mn) spinel type oxides catalyses the simultaneous removal of NO_x and diesel soot to form carbon dioxide, nitrogen and nitrous oxide and the superiority of spinels to constituent simple metal oxides and their mixture is confirmed [111]. The catalytic performance of the spinels depends significantly on the constituent metal cations and CuFe_2O_4 is the most excellent system with highest selectivity to nitrogen formation, lowest selectivity to nitrous oxide and provides intermediate ignition temperature of soot [112].

Chlorinated organic compounds are highly toxic for the environment. The catalytic hydrodechlorination of polychlorinated aromatic compounds [1,2,4-trichlorobenzene → benzene] using Ni catalysts with spinel structure is found to be a promising attempt to reduce the environmental pollution [113]. NiAl_2O_4 prepared by the low temperature method catalyze the exhaustive dehydrogenation with no loss in activity, which can occur as a result of the toxicity of the hydrogen chloride produced. Nickel spinel systems are also found to be active catalysts for ozone decomposition reaction to obtain highly reactive atomic oxygen, which is able to oxidize harmful organic compounds at room temperature [114].

1.8 Transport studies

Ferrites attracted the attention of physicists and technologists since they are magnetic semiconductors. Both semiconductors and magnetic materials exhibit interesting properties that could be used in electronic devices. Semiconductors find endless uses in electronic devices while ferrites find application as passive devices in a multitude of devices due to their high electrical resistivity, low eddy current losses and appropriate dielectric loss. They are used nowadays in industry as transformer cores, TV yokes, telephone receivers, loud speakers, permanent magnets and memory devices.

Spinel ferrites, in general are semiconductors with their conductivity values varying between 10^2 and 10^{-11} $\text{ohm}^{-1} \text{cm}^{-1}$. The conductivity is due to the presence of Fe^{2+} and M^{3+} (M = metals like Co, Ni, etc.). The presence of Fe^{2+} results in n-type and presence of M^{3+} in p-type behaviour. The conductivity arises due to the mobility of extra electron (from Fe^{2+}) or the positive hole (M^{3+}) through the crystal lattice.

The conduction mechanism in ferrites is quite different from that of semiconductors. In semiconductors the charge carriers occupy states in wide energy band. But the charge carriers in ferrites are localized at the magnetic atoms. In ferrites, the cations are surrounded by close-packed oxygen anions and the electrons associated with particular ion will largely remain isolated. Hence a localized electron model is more appropriate in the case of ferrites rather than the electron band model. Also, in ferrites the temperature dependence of mobility affects the conductivity whereas the carrier concentration is unaffected.

Many models have been suggested to account for the electrical properties in ferrites [115-121]. The factors that differentiate electrical behaviour of ferrites from that of semiconductors, led to hopping electron model [122-124]. The conductivity in these systems is found to be due to the electronic exchange between Fe^{2+} and Fe^{3+} ions, distributed on crystallographically equivalent lattice points [125]. Niko'skii [126] has shown that the hopping of electrons between Fe^{2+} and Fe^{3+} ions, arranged in non-equivalent points (ie. octahedral and tetrahedral sites) could also play a substantial role in the conduction process. The hopping probability depends upon (i) the separation between the ions involved and (ii) the activation energy. Assuming all the Fe^{2+} ions in the octahedral sites to participate in the hopping transport, the number of charge carriers (n) works out to be of the order of 10^{22} cm^{-3} . Since mobility is very low, the conductivity is low, even though n is large.

The electrical properties of the ferrites are affected by the distribution of cations in the octahedral and tetrahedral sites, preparation conditions, particle size and particle growth effects. The electrical properties of manganese ferrites have been studied by many investigators [127-132]. Among them, Lotgerring [132] has investigated the semiconducting properties of the ferrite system, $\text{Mn}_{1+x}\text{Fe}_{2-x}\text{O}_4$ and explained the observation on the basis of Verwey hopping mechanism. A systematic study of the electrical conductivity of manganese magnesium ferrites as a function of composition and temperature has been made by Venugopal *et al.* [133]. They divided the mixed ferrites under study into two groups. The mixed ferrites of group I have a slight excess of cations and show n-type conduction, whilst those of group II have a cation deficiency and show p-type conduction. The mechanism of the electrical conduction is explained in terms of the oxidation of Fe^{2+} ions by Mn^{3+} ions on octahedral sites. Perchiik *et al.* [134] suggested a hopping theory for the description of transport phenomena in the case of $\text{Mn}_{0.4}\text{Mg}_{0.6}\text{Fe}_2\text{O}_4$ in the temperature range 300 to 800 K.

Various research groups evaluated certain important parameters of a semiconductor such as the energy gap, lattice frequencies and activation energies involved in the lattice deformation and compared with those obtained in the case of cobalt and nickel ferrite systems [135-137]. Jonker studied the electrical conductivity of

a series of ferrites $\text{Co}_{1-x}\text{Fe}_{2+x}\text{O}_4$ and observed two regions of conductivity. One region is of low conductivity containing Co^{2+} and Co^{3+} ions and is of p-type semiconduction. The other region was of high conductivity containing Fe^{2+} and Fe^{3+} and it is the n-type semiconduction. The DC resistivity of a nickel ferrite with composition $\text{Ni}_{0.2}\text{Cu}_{0.8}\text{Fe}_{1.9}\text{Mn}_{0.1}\text{O}_4$ has been measured from room temperature to 300°C by Sinha *et al.* [138]. It was pointed out that large value of dc resistivity indicates low mobilities and high effective mass for the carriers.

Of late, the chemists are interested in the electrical properties of ferrites for the kinetic and mechanistic studies of various reactions. Narasimhan *et al.* studied the decomposition of isopropyl alcohol on $\text{MgAl}_{2-x}\text{Fe}_x\text{O}_4$ ($0 \leq x \leq 2$) and correlated the catalytic activity with the electrical conductivity of the systems [85]. Their results showed that there is no correlation between the dehydration activity and electrical conductivity. Thus electrical properties of the catalysts do not seem to play any role in the dehydration reaction. But the dehydrogenation activity varies linearly with activation energy for conduction. The higher the degree of n-type conductivity, the higher is the dehydrogenation activity.

Cares and Hightower supported the Rennard-Kehl mechanism of zero order oxygen dependence on oxidative dehydrogenation of butene to butadiene by the electrical conductivity measurements on cobalt ferrite [90]. Ghorpade *et al.* prepared a series of $\text{CuCr}_{2-x}\text{Fe}_2\text{O}_4$ ($0 \leq x \leq 2$) and evaluated the electrical conductivity and correlated the activation energy for conduction with the liquid-phase benzene alkylation reaction [139]. The activation energy goes on decreasing as 'x' increases from 0 to 1 and the decrease in activation energy increases the formation of diphenylmethane. The small magnitude of the activation energy or the energy gap rules out the possibility of holes taking part in the reaction.

In the present investigation manganese ferrosinels of Cr, Co, Ni, Cu and Zn are chosen. The materials are prepared by the soft-chemical route and their electrical properties such as conductivity, carrier mobility and hole effects are correlated to various reactions studied.

1.9 Acid- base properties

Surface acidity and basicity investigations have received considerable attention in recent years, since they play important role in many catalytic reactions. In the case of reactions that have been recognized to be catalyzed by acid sites on a catalyst surface, basic sites also act more or less as active sites in cooperation with acid sites. The catalyst having suitable acid-base pair sites sometimes show pronounced activity, even if the acid-base strength of a bi-functional catalyst is much more weaker than the acid or base strength of simple acid or base. For example, ZrO_2 , which is weakly acidic and basic show higher activity for C-H bond cleavage than highly acidic $SiO_2-Al_2O_3$ or highly basic MgO [140]. A systematic investigation of the activity and selectivity of a catalyst and acid-base property (strength, amount and type) enabled the development of an optimum catalyst with desired acid-base properties for a specific reaction. Development in this area has given rise to numerous methods for exploring these properties.

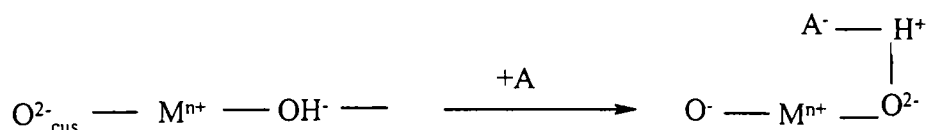
1.9.1 Surface electron donating properties

The electron donor strength of the metal oxide can be defined as the conversion power of an electron acceptor adsorbed on the surface into its anion radical [141]. The electron donor sites are associated with surface hydroxyl groups and with defect centres involving oxide ions. Study of electron donor properties of metal oxides by the adsorption of electron acceptors of various electron affinity values has been a well established technique. The first work of this type is the one reported by Flockart *et al.* [142], who investigated the electron donor properties of an alumina surface by the adsorption of tetracyanoethylene (TCNE). Similar studies on single metal oxides and binary metal oxides have also been reported by several other workers [143-148].

If a strong electron acceptor is adsorbed on the metal oxide, its anion radical is formed at strong as well as weak donor sites present on the surface. On the other hand, if a weak electron acceptor is adsorbed, the formation of anion radical is expected only at the strong donor sites. In the case of a very weak electron acceptor adsorption, its anion radical will not be formed even at the strongest donor sites. The electron donating capacity can be expressed as the limiting electron affinity value at which free radical

anion formation is not observed at the metal surface. Thus by comparing the limiting amount of the electron acceptor adsorbed on the catalyst surface and the electron affinity values of the respective electron acceptor used, it is possible to get an insight into the strength and distribution of the electron donor sites on the surface.

A detailed investigation of electron donating sites on oxide surfaces has been carried out by Cordishi *et al.* [149, 150]. They correlated electron donating sites on the surface with the Lewis basicity. The donor sites is proposed to be a coordinatively unsaturated oxygen ion, (O^{2-}_{cus}) associated with a nearby OH^- group, whose proton interacts with the radical anion formed giving stability. Thus Brønsted acidity stabilized the radical ion formed and the active site can be considered as acid-base pair as shown below.



Meguro *et al.* reported adsorption of electron acceptors on alumina and according to them surface hydroxyl groups are responsible for the electron donating properties of the oxides [148]. The ionization potential of hydroxyl group is comparatively small (about 2.6 eV in gas phase) [151], and therefore an oxidation-reduction process of the type, $OH^- + EA \rightarrow OH + EA^-$, where EA is an electron acceptor can be included.

Electron acceptors such as 7,7,8,8-tetracyanoquinodimethane (TCNQ), 2,5-dichloro-*p*-benzoquinone (DCQ), *p*-dinitrobenzene (PDNB) and *m*-dinitrobenzene with electron affinity values 2.84, 2.30, 1.77 and 1.26 eV respectively are extensively used for probing electron donor sites on the surface [141]. Esumi *et al.* carried out the adsorption of 2,3,5,6-tetrachloro-*p*-benzoquinone (chloranil) with electron affinity value 2.40 eV from acidic and basic solvents on metal oxides such as alumina and titania. They could successfully correlate the amount of chloranil adsorbed with acid-base interaction at the interface. Meguro *et al.* studied the adsorption of electron acceptors with electron affinity values from 1.26 to 2.84 eV on the surface of alumina by measuring the adsorption isotherms, esr and electronic spectra [152]. They observed that radical

concentration decreased as the electron affinities of electron acceptors decreased from 2.84 to 1.77 and thus it was noted that the radical concentration formed were directly related to the electron affinity values of the respective electron acceptor employed.

Esumi and coworkers investigated the solvent effects on the acid-base interaction of the electron acceptors (TCNQ and chloranil) with the metal oxide such as alumina and titania [153, 154]. They could see that the amount of electron acceptors adsorbed and the concentration of anion radicals formed decreased with an increase in acid-base interaction between the electron acceptor and the organic solvents used. Drago equation [155] was applied to understand the nature of interaction of different solvents with TCNQ. It was observed that acid-base enthalpy between TCNQ and the organic liquids increased in the order 1,4 dioxane > ethyl acetate > acetonitrile. So the electron acceptor adsorption is greatly depressed by the interaction between TCNQ and acetonitrile.

The effect of calcination temperature on the electron donating property of zirconia was studied by Esumi *et al.* [156]. An increase of calcination temperature reduces the amount of electron acceptor adsorbed indicating the reduction of OH⁻ on the surface. Above 900°C the amount of adsorbed species again increased due to the formation of surface oxide ions.

Sugunan *et al.* investigated the electron donor properties of rare earth oxides such as Pr₆O₁₁ [157], CeO₂ [158], Sm₂O₃ [159], La₂O₃ [160] and Nd₂O₃ [161, 162] and their mixed oxides with alumina as a function of composition and activation temperature. It was found that the number of both strong and weak donor sites was increased with increase in calcination temperature. The extent of electron transfer was characterized by magnetic measurements. During adsorption, magnetic moment decreased and reached a limiting value at the same concentration at which the limiting amount of electron acceptor was adsorbed.

1.9.2 Temperature programmed desorption studies

Temperature programmed desorption of basic molecules such as ammonia, pyridine, n-butylamine, etc. is an accepted technique extensively used to characterize the acid strength as well as acid amount on a solid catalyst surface [163-166]. When gaseous

bases are adsorbed on acid sites the one which is adsorbed on a strong acid site is more stable than the one which is adsorbed on a weak acid site and is more hard to desorb. As elevated temperatures stimulate the evacuation of the adsorbed bases from the acid sites, those at weaker sites will be evacuated preferentially. Thus, the proportion of the adsorbed base evacuated at different temperatures can give a measure of acid strength. Also, the amount of gaseous base, which a solid acid can adsorb chemically from the gaseous state can be taken as a measure of the amount of acid sites on its surface. The advantage of TPD method over the other techniques is that it allows the study of the catalyst under conditions more or less similar to that of reaction and that the acid amount for a solid at high temperatures (several hundred degree centigrade) can be determined.

The NH_3 -TPD method is widely employed to characterize the acidity of solid catalysts [167-178]. Ammonia is an excellent probe molecule for testing the acidic properties of solid catalysts, because its strong basicity and small molecular size allow the determination of acidic sites of any strength and type [167, 168]. Though ammonia-TPD method is unable to distinguish the type of acid sites (Lewis and Brønsted acidic sites) it gives the total acidity and acidity of solid catalyst at any temperature region. The NH_3 -TPD spectra are often poorly resolved and experimental artifacts such as change in the activation treatment and curve deconvolution methods can give insights on site distribution and heat of desorption. Thus, on the basis of complementary characterization results, a fairly reliable interpretation of the NH_3 -TPD pattern can be attained [178].

Generally, IR spectroscopy [173, 174], calorimetric [172] and TPD techniques are employed to achieve information on the interaction of NH_3 with solid acids. Kijenski *et al.* [179] reported that when NH_3 is chemisorbed on a surface having acidic properties, it can interact with acidic protons, electron acceptor sites and hydrogen from neutral or weakly acidic hydroxyls. The NH_3 adsorbed on a surface can be retained either by hydrogen bonding via one of its hydrogen atoms to a surface oxygen atom or oxygen of the hydroxyl group or by the transfer of protons from surface OH to ammonia [180]. These two interactions involve neighbouring anions or OH groups. The strongest interaction is the coordination to an electron deficient atom. The dissociative adsorption

in the form of surface NH_2 or NH and OH is also possible. Another mode of interaction is the complete transfer of H^+ from Bronsted sites to produce NH_4^+ .

Trombetta *et al.* made NH_3 -TPD study on mono and bi-pillared smectites [181]. The desorption of ammonia was run between 373 and 873 K to allow the total evacuation of ammonia molecules. By this technique they work out the total acidity per unit area of montmorillonite and saponite. From the relative amounts of ammonia desorbed at different temperatures (measure of the strength of the adsorbing site), they observed that pillared montmorillonite carry stronger sites than the layer surface, while the reverse is observed for the saponite. In all the samples they observed that majority of NH_3 desorbed between 473 and 573 K.

Sato *et al.* studied the TPD of ammonia adsorbed on cation-exchanged ZSM-5 [182]. The TPD spectrum of ammonia showed two distinct peaks for H-ZSM-5, indicating the existence of strong (a peak at 723 K) and weak (a peak at 463 K) acid sites. Hashimoto *et al.* describes a method which calculates the density function of activation energy for desorption of ammonia by analyzing the TPD spectrum of ammonia [183].

The heat of adsorption of a base is clearly a measure of the acid strength on a solid surface [164]. Tsutsumi *et al.* plotted differential heat of adsorption for ammonia on $\text{SiO}_2\text{-Al}_2\text{O}_3$ and SiO_2 against the surface coverage [184]. Heat of adsorption corresponding to acid strength increases with increasing alumina content in $\text{SiO}_2\text{-Al}_2\text{O}_3$.

Arena *et al.* made a characterization study of the surface acidity of solid catalysts by temperature programmed desorption of basic probe molecules such as ammonia, pyridine and benzene [178]. According to them, TPD of adsorbed ammonia is a reliable method to feature the strength but not the nature (Lewis and Brønsted) of surface acid sites in solid acid catalysts. Mathematical analysis of NH_3 -TPD spectra highlights the presence of weak, medium and strong acid sites on all the catalysts and also enables their quantitative estimation. A comparative evaluation of the TPD patterns of ammonia, pyridine and benzene sheds light on the nature (Lewis and Brønsted) of the acidic sites.

1.9.3 Thermogravimetry of desorption of basic molecules

The thermogravimetry (TG) of desorption of basic molecules is an existing method for the estimation of the acid amount together with the acid strength of a solid catalyst [164]. Pyridine has been the most widely used base for the acid characterization purposes, due its interaction with both Brönsted and Lewis acid sites [185-191]. The thermodesorption study of the pyridine adsorbed samples gives the total acid amount on the solid surface. Thus this method supports the results obtained from NH₃-TPD method.

Recently, it has been shown that sterically hindered dimethylpyridines can be used successfully to characterize acid surfaces through their chemisorption measurements [190]. The adsorption of 2,6-dimethylpyridine (2,6-DMP) is weaker than that of pyridine, even though the former is a stronger base. This indicates the presence of steric hindrance of methyl groups adjacent to nitrogen atom for the adsorption of methylpyridines [191]. The most important features of these molecules, when compared with pyridine, are their higher basicity (the pK_a is 6.7 for 2,6-DMP and 5.2 for pyridine) and their specificity for protonic centers. In the case of an acid catalyst, fluorinated γ -Al₂O₃, which contains both Brönsted and Lewis acid sites, pyridine fails in titrating the Brönsted acidity mainly due to the low surface concentration of these sites capable of interacting with pyridine. 2,6-DMP is a more convenient probe molecule for the specific determination of Brönsted acidity [192, 195].

The possibility of determination of Brönsted acidic sites in solid catalysts using 2,6-dimethylpyridine as a probe molecule is established by several authors [189-191, 193, 194]. Satsuma *et al.* examined the possibility of use of dimethylpyridines (2,6-DMP and 3,5-DMP) as probe molecules on metal oxides for the determination of the acid strengths of Brönsted and Lewis acid sites [196]. From the IR spectra of 2,6-DMP adsorbed on alumina, they showed that 2,6-DMP is held coordinatively on Lewis acid sites at lower temperature. By employing the appropriate purging temperature, 2,6-DMP is eliminated selectively from the Lewis acid sites and selective adsorption of 2,6-DMP on Brönsted acid sites is achieved. It is also demonstrated that the profiles of TPD studies of both 2,6- and 3,5-DMP ensure the measurement of the amount of Brönsted and Lewis acid sites on solid catalysts.

1.9.4 Cyclohexanol decomposition

Alcohols are amphoteric and they interact with both acidic and basic sites. The utility of alcohol decomposition as a test reaction for acid-base property studies of metal oxides is well established [27, 29, 197-202]. It was observed that metal oxides catalyze both dehydration and dehydrogenation of alcohols. Dehydration of alcohol leads to an olefin and dehydrogenation forms an aldehyde (in the case of primary alcohols) or a ketone (in the case of secondary alcohols) and hydrogen. At elevated temperatures, decomposition may involve C-C bond cleavage giving products like CO, CO₂ etc. At near ambient temperatures ether can be a major product.

According to the generally accepted concept, dehydration is an acid catalyzed reaction whereas dehydrogenation, which proceeds by a concerted mechanism, is due to the combined effect of both acidic and basic sites on the system. Thus, dehydration activity gives the direct measure of the acidity of the system, whereas the ratio of the dehydrogenation activity to the dehydration activity gives the basicity of the system [85, 203].

One of the most widely studied alcohol decomposition reaction for the acidity-basicity correlation is the cyclohexanol decomposition. The amphoteric nature of cyclohexanol permits its interaction with both acidic and basic sites. As a result of this, dehydration and dehydrogenation are catalyzed by the oxide systems forming cyclohexanol and cyclohexanone (Fig. 1.5).

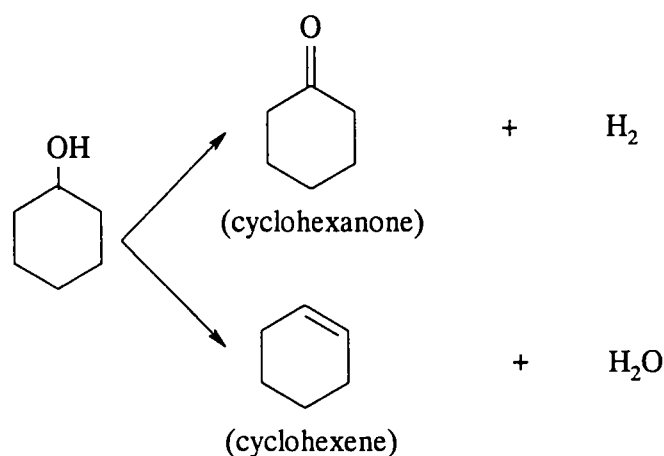


Fig. 1.5. Scheme of decomposition of cyclohexanol

Bezouhanava *et al.* have noticed cyclohexanol decomposition as an easy and reliable method to determine the functionality of metal oxide catalysts [204]. They correlated the dehydrogenation activity to the existence of basic sites originating from the lattice oxygen. Stronger acid sites are needed for dehydration of cyclohexanol compared to other secondary and tertiary alcohols like isopropyl alcohol or tertiary butyl alcohol. The test reaction of cyclohexanol decomposition was done over HZSM-5, HY, SAPO, MAPO molecular sieves and commercial chromite catalysts to characterize their acid-base properties [205].

Rachel *et al.* have studied the selectivity for dehydrogenation reaction in the decomposition of cyclohexanol as a function of copper loading assisted by the predominantly basic character of ZrO₂ in CuO/ZrO₂ catalyst [206]. The influence of copper ions in the octahedral sites of spinel catalysts on the transformation of cyclohexanol to cyclohexanone was studied by Jebarathinam *et al.* also. Their investigation indicates that Cu⁺ at the octahedral sites is more active than Cu⁰ for the dehydrogenation of cyclohexanol [207]. The same authors studied the effect of Zr²⁺ in NiFe₂O₄ matrix on the catalytic decomposition of cyclohexanol. Introduction of Zr²⁺ in NiFe₂O₄ matrix creates strong basic sites and facilitates the dehydrogenation of cyclohexanol to cyclohexanone [208].

Aramendia *et al.* observed an increase in selectivity towards cyclohexanone in the decomposition reaction of cyclohexanol by doping sodium carbonate in zinc phosphate. Addition of Na₂CO₃ during the synthetic procedure increases the surface basicity of the resultant solids and it enhances the dehydrogenation rate of cyclohexanol [209]. Catalytic decomposition of cyclohexanol over Mg_{1-x}Zn_xAl₂O₄ reported by Joshi and coworkers established the correlation among transport properties, surface acidity and catalytic behaviour [210]. Investigations on alumina by Pines *et al.* spot out to the formation of methylcyclopentene on stronger acidic sites, which is formed by the isomerization of cyclohexene [211].

1.10 Reactions selected for the present study

(a) Acylation of aromatic compounds

Benzoylation under Friedel-Crafts acylation reactions are important in organic synthesis and provide fundamental and useful method for the preparation of aromatic ketones in chemical industry, which are used in the manufacture of weed killers, dye intermediates, etc. An attempt is made to eliminate the disadvantages of homogeneous catalytic processes by replacing the hazardous homogeneous catalysts such as AlCl_3 , TiCl_4 , FeCl_3 , SnCl_4 , etc. by solid acid catalysts. A detailed description of these reactions is given in chapter 4.

(b) Alkylation of aniline and phenol

Alkylation of aniline and phenol are industrially outstanding reactions due to the numerous use of the alkylated products. Alkylation of aniline gives both C-alkylated and N-alkylated products and of these, N-alkylated ones such as N-methylaniline and N,N-dimethylaniline are more synthetically valuable. Alkylation of phenol gives a wide range of products and among them, cresols and xylenols are the most important ones. Chapter 4 deals with a detailed discussion of each type of these reactions.

(c) Phenol hydroxylation

Phenol hydroxylation is one of the industrially important reactions as the products namely catechol and hydroquinone are extensively used as photographic developers, ingredients for food and pharmaceutical applications and antioxidants. This reaction has an added importance for the reduction of phenolic pollutants in the aqueous effluents from industries such as pharmaceutical, chemical, petrochemical, etc. Chapter 5 covers a thorough discussion of this reaction

(d) Oxidative dehydrogenation of ethylbenzene

Oxidative dehydrogenation of ethylbenzene is an industrially important process for the production of styrene. In chapter 5, we discuss the correlation between acid-base properties of the catalyst and selective formation of styrene from ethylbenzene.

1.11 Objectives of the present work

Mixed metal oxides having spinel structure exhibit interesting structural, electrical, magnetic and catalytic properties. These systems have been found to possess extra stability under various reaction conditions and have sustained activity for longer periods. These spinel oxides are cheap and their preparation method is simple. These attractive features of spinel oxides prompted us to prepare manganese ferrosinels via low temperature co-precipitation method and investigate their catalytic properties for various reactions. The main objectives of the present work can be summarized as follows:

- ❖ To prepare manganese ferrosinels containing Cr, Co, Ni, Cu and Zn by low temperature co-precipitation method and characterize these by adopting various physico-chemical methods such as XRD, ICP, BET surface area, DRIFT, TGA, DC conductivity measurements and Hall effect measurements.
- ❖ To evaluate the surface basicity using electron acceptors of various electron affinity values.
- ❖ To estimate the surface acidity by the temperature programmed desorption of ammonia (NH_3 -TPD) and by the thermodesorption studies of pyridine and 2,6-dimethylpyridine adsorbed samples.
- ❖ To study the vapour-phase cyclohexanol decomposition reaction and to correlate the results with surface acid-base properties.
- ❖ To assess the catalytic activity of the samples towards the industrially important reaction, namely Friedel-Crafts benzoylation of aromatic compounds.
- ❖ To evaluate the catalytic activity of the systems for aniline and phenol alkylation using methanol as the alkylating agent.
- ❖ To study the phenol hydroxylation reaction over all the prepared systems.
- ❖ Another important objective of the present work was to evaluate the catalytic activity of the systems for the oxidative dehydrogenation of ethylbenzene and to optimize the process parameters to get the synthetically valuable styrene as the major product.

References:

- [1] G. K. Borekov; Proc. 8th Intern. Congr. Catalysis, Berlin, Verlag-Chemie-Dechema, Frankfurt, Vol.3, 1984, p.231.
- [2] J. Haber; *Materials. Sci. Forum*, 25 (1988) 17.
- [3] J. Haber; (Eds., H. F. Barry and P. C. W. Mitchel), Proc. 4th Intern. Conf. Chemistry and uses of Molebdenum, Golden, CO, , Climax Molebdenum Co., AnnArbor,1982, p.395.
- [4] K. Kimura and H. Ai; *J. Catal.*, 18 (1970) 271.
- [5] H. Uchida and H. Imai; *Bull. Chem. Soc. Jpn.*, 35 (1962) 995.
- [6] K. Maruya and A. Ozaki; *Bull. Chem. Soc. Jpn.*, 46 (1973) 351.
- [7] Z. Chen, T. Iizuka and K. Tanabe; *Chem. Lett.*, (1984) 1085.
- [8] T. Iizuka, K. Ogasawara and K. Tanabe; *Bull. Chem. Soc. Jpn.*, 56 (1983) 2927.
- [9] K. Ogasawara, T. Iizuka and K. Tanabe; *Chem. Lett.*, (1984) 645
- [10] S. Okazaki, M. Kurimata, T. Iizuka and K. Tanabe; *Bull. Chem. Soc. Jpn.*, 60 (1987) 37.
- [11] Mitusubishi Chem. Co., Japan Patent Kokai, 60-082915 (1985).
- [12] D. L. Myers and J. H. Lunsford; *J. Catal.*, 99 (1986) 140.
- [13] L. Nondek, D. Mihajlova, A. Andreev, A. Palazov, and D. Shopov; *J. Catal.*, 40 (1975) 46.
- [14] K. Yamashita, S. Naito and K. Tamura; *J. Catal.*, 94 (1985) 353.
- [15] K. Maruyama, H. Hattori and K. Tanabe; *Bull. Chem. Soc. Jpn.*, 50 (1977) 86,2181.
- [16] Y. Kamiya and E. Ogata; Proc. 5th Intern. Congr. Catal., 1972, North-Holland, 1973, p.93.
- [17] L. R. Haefele and H. J. Young; *Ind Eng. Chem., Prod. Res. Rev.*, 11 (1972) 364.
- [18] H. Miura, K. Sugiyama, S. Kawakami, T. Aoyama and T. Matsuda; *Chem. Lett.*, (1982) 183.
- [19] K. Saito, T. Yamaguchi, K. Tanabe, and M. Yagi, *Bull. Chem. Soc. Jpn.*, 52 (1979) 3192.
- [20] K. Arata, K. Sato and I. Toyoshima; *J. Catal.*, 42 (1976) 221.
- [21] K. Arata, K. Yabe and I. Toyoshima; *J. Catal.*, 44 (1976) 385.
- [22] K. Arata and I. Toyoshima; *J. Catal.*, 47 (1977) 109.
- [23] K. Arata and M. Hino; *Bull. Chem. Soc. Jpn.*, 53 (1980) 535.
- [24] K. Arata, A. Fukui and I. Toyoshima, *J. Chem. Soc., Chem. Commun.*, (1978) 121.
- [25] K. Tanabe, I. Matsuzaki, I. Ichikawa and H. Hattori; *Bull. Chem. Soc. Jpn.*, 45 (1972) 47.
- [26] T. Sumiyoshi, K. Tanabe and H. Hattori; *Bull. Jap. Petrol. Inst.*, 17 (1975) 65.
- [27] M. Ai; *J. Catal.*, 50 (1977) 291.
- [28] T. Kotanigawa, M. Yamamoto, K. Shimokawa and Y. Yoshida; *Bull. Chem. Soc. Jpn.*, 44 (1971) 1961.
- [29] M. Ai and S. Susuki; *J. Catal.*, 30 (1973) 362.

- [30] Yu. Belokopytov, K. M. Kholyavalenko and M. Ya. Rubanic; *Kin. I Kataliz.*, 14 (1973) 1280.
- [31] F. Kapteijn, L. Singoredjo, A. Andreini and J. A. Moulijn; *Appl. Catal.*, 3 (1994) 173.
- [32] T. M. Yur'eva, V. V. Popovski and G. K. Boreskov; *Kinet. Catal.*, 3 (1965) 941.
- [33] H. E. Edwards and R. M. Harison; *Environ. Sci. Technol.*, 13 (1979) 673.
- [34] T. Yamashita and A. Vannice; *J. Catal.*, 163 (1996) 158.
- [35] H. Zheng; *J. Catal.*, 119 (1990) 502.
- [36] D. A. Arendarski, Z. R. Ismagilov and G. B. Baranik; *Kinet. Catal.*, 31 (1990) 1193.
- [37] F. Boccuzzi, Achiorino, M. Gargano and N. Ravasio; *J. Catal.*, 165 (1997) 140.
- [38] J. Plewa and J. Shrzypek; *Chem. Eng. Sci.*, 44 (1989) 2817
- [39] G. Xanthopoulou and G. Vekinis; *Appl. Catal.*, 19 (1998) 37
- [40] T. Takada; Proc. 3rd Inter. Conf. on Ferrites, Japan, (Eds., H. Watanabe, S. Iida and M. Sugimoto), Center for Academic Publications, Tokyo, Japan, 1980, p. 3-8.
- [41] T. Takada and M. Kiyama; Proc. 3rd Inter. Conf. on Ferrites, Japan, (Eds., Y. Hoshino, S. Iida and M. Sugimoto), University of Tokyo Press, Tokyo), 1970. p. 69-71.
- [42] D. G. Wikham, *Inorg. Synt.*, 9 (1967) 152.
- [43] B. B. Yu and A. Goldman; Proc. 3rd Inter. Conf. on Ferrites, (Eds., H. Watanabe, S. Iida and M. Sugimoto), Center for Academic Publications, Tokyo, Japan, 1980, pp. 68-73.
- [44] X. Qian and B. J. Evans; *J. Phy.*, 52 (1981) 2523
- [45] S. K. Date, C. E. Deshpande, S. D. Kulkarni and J. J. Shrotri; Proc. 5th Inter. Conf. on Ferrites, (Eds., C. M. Srivastava and M. K. Patni), Oxford and IBH Publishing Co. PVT Ltd., Bombay, India, 1989, p. 55-60.
- [46] C. Marcilly; *Rev. Inst. Fr. Pet.*, 39 (1984) 189
- [47] D. G. Wickham, E. R. Whipple and E. G. Larson, *J. Inorg. Nucl. Chem.*, 14 (1960) 217.
- [48] T. T. Srinivasan, P. Ravindranathan, L. E. Cross, R. Roy, R. Newnham, S. G. Sankar and K. C. Pagtil; *J. Appl. Phy.*, 63, (1988) 3789.
- [49] C. J. Chen, K. Bridger, S. R. Winser and V. PaiVerneker; *J. Appl. Phy.*, 63, (1988) 3786.
- [50] I. J. McColm and N. J. Clark; "Forming, Shaping and Working of High Performance Ceramics", Blackie, Glasgow, (1988) 1.
- [51] X. Fan and E. Matijevic, *J. Am. Cer. Soc.*, 71 (1988) ,C-60.
- [52] K. G. Brooks and V. R. W. Amarakoon; *J. Am. Cer. Soc.*, 74 (1991) 851.
- [53] K. Matsumoto, K. Yamaguchi and T. Fujii; *J. Appl. Phy.*, 69 (1991) 5912.
- [54] W. A. Kaczmarek, B. W. Ninham and A. Calka; *J. Appl. Phy.*, 70, (1991) 5909.
- [55] H. K. Xu, C. M. Sorenson, K. J. Klabunde and G. C. Hadjipanayis; *J. Mat. Res.*, 7 (1992) 712.
- [56] G. C. Jain, B. K. Das and R. Avtar; *Ind. J. Pur. Appl. Phy.*, 14, (1976) 796.
- [57] M. J. Ruthner; *J. de Phy.*, 38 (1977) 311.
- [58] F. J. Schnettler and D. W. Johnson; Proc. Inter. Conf. on Ferrites, (Eds., Y. Hoshino, S. Iida

- and M. Sugimoto), University of Tokyo Press, Tokyo, Japan, 1970, p. 121-124.
- [59] K. Suresh, N. R. S Kumar and K. C. Patil; *Adv. Mater.*, 3 (1991) 148.
- [60] R. H. Arendt; *J. Solid State Chem.*, 8 (1973) 339
- [61] E. L. Venturini, B. Morosin, and R. A. Graham, *J. Appl. Phys.*, 57 (1985) 3814.
- [62] W. H. Bragg; *Philosophical Magazine*, 30 (1915) 305.
- [63] R. J. Hill, J. R. Craig and G. V. Gibbs; *Phys. Chem. Miner.*, 4 (1979) 317.
- [64] H. Jagodzinski; "Crystallographic Aspects of Non-stoichiometry of Spinels", (Eds., A. Rabenau), North-Holland, Amsterdam, p.131.
- [65] E. J. W. Verwey and E. L. Heilmann; *J. Chem. Phys.*, 15 (1947) 174.
- [66] T. F. W. Barth and E. Posnjak; *Z. Krist.*, 84 (1952) 325.
- [67] R. K. Datta and K. Roy, *Nature*, 191 (1961) 169.
- [68] S. Hafner and F. Laves; *Z. Krist.*, 115 (1961) 321
- [69] E. J. W. Verwey, F. de Boer and J. H. van Santen, *J. Chem. Phys.*, 16, (1948) 1091
- [70] F. de Boer, J.H van Santen and E. J. W. Verwey; *J. Chem. Phys.*, 18, (1950) 1032.
- [71] F. C. Romeijn; *Phil. Res. Rep.*, 8 (1953) 304.
- [72] J. D. Dunitz and L. E. Orgel; *Phys. Chem. Solids*, 3 (1957) 318.
- [73] D. S. McClare; *Phys. Chem. Solids*, 3 (1957) 311.
- [74] G. Blasse; *Philips. Res. Repts. Supplement*, 3 (1964) 40.
- [75] H. Knözinger and P. Ratnasami; *Catal. Rev.-Sci.Eng.*, 17 (1979) 31.
- [76] J. P. Beaufils and Y. Barboux; *J. Chem. Phys.*, 78 (1981) 347.
- [77] J. P. Beaufils and Y. Barboux; *J. Appl. Crystallogr.*, 15 (1982) 301.
- [78] J. P. Jacobs, A. Maltha, J. G. H Reintjes, J. Drimal, V. Ponc and H. H. Brongersma, *J. Catal.*, 147 (1994) 294.
- [79] J. Ziolkowski and Y. Barboux; *J. Mol. Catal.*, 67 (1991) 199.
- [80] B. C. Lippens and J. J. Steggerda; (Eds., B.G Linsen), "Physical and Chemical Aspects of Adsorbents and Catalysts", Academic Press, New York, 1970, p.171.
- [81] H. C. Yao and M. Shelef; *J. Phys. Chem.*, 78 (1974) 2490.
- [82] M. Shelef, M. A. Z. Wheeler and H. C. Yao; *Surf. Sci.*, 47 (1975) 697.
- [83] R. J. Rennard and W. L. Kehl; *J. Catal.*, 21 (1971) 282.
- [84] J. Zilowski and Y. Barbaun; *J. Mol. Catal.*, 67 (1991) 199.
- [85] C. S. Narasimhan and C. S. Swami, *Appl. Catal.*, 2 (1982) 315.
- [86] L. Bajas, J. L. Croce and M. Gabliks; U.S Patent, 3 284 536, 1966.
- [87] M. A. Gibson and J. W. Hightower; *J. Catal.*, 41 (1976) 420.
- [88] W. L. Kehl and R. J. Rennard; U.S Patent, 3 450 788, 1969.
- [89] W. L. Kehl and R. J. Rennard, U.S Patent, 3 450 787, 1969.
- [90] W. R. Cares and J. W. High Tower, *J. Catal.*, 23 (1971) 193.

- [91] W. S. Epling, G. B. Hoflund, W. M. Hart and D. M. Minhan; *J. Catal.*, 169 (1997) 438.
- [92] W. S. Epling, G. B. Hoflund, W. M. Hart and D. M. Minhan; *J. Catal.*, 172 (1997) 13.
- [93] W. S. Epling, G. B. Hoflund and D. M. Minhan; *J. Catal.*, 175 (1998) 175.
- [94] D. M. Minhan, W. S. Epling and G. B. Hoflund; *J. Catal.*, 179 (1998) 241.
- [95] W. S. Epling, G. B. Hoflund and D. M. Minhan; *Appl. Catal.*, 183 (1999) 335.
- [96] G. B. Hoflund, W. S. Epling and D. M. Minhan; *Catal. Today*, 52 (1999) 99.
- [97] A. Maltha, K. F. Kist, B. Brunet, J. Ziolkowski, H. Onishi, Y. Iwasara and V. Ponec; *J. Catal.*, 149 (1994) 356.
- [98] J. Ziolkowski, A. M. Maltha, H. Kist, E. J. Grootendorst, H. J. M. de Groot and V. Ponec; *J. Catal.*, 160 (1996) 148.
- [99] S. Meijers, T. P. Pruys van der Hoeven, V. Ponec, J. P. Jacobs and H. H. Brongersma; *J. Catal.*, 161 (1996) 459
- [100] H. M. Cota, J. Katan, M. Chin and F. J. Schoenveis, *Nature*, London, 203 (1964) 1281.
- [101] J. R. Goldstein and A. C. C. Tseung; *J. Mater. Sci.*, 7 (1972) 1383.
- [102] G. Blasse; *Philips. Res. Rep.*, 18 (1963) 383.
- [103] S. V. S Prasad and S. Rao; Proc. of the National Symposium on Advances in Catalysis- Science and Technology, Baroda, India, January 1985 edited by T.S.R Prasad Rao (Wiley Eastern Limited, New Delhi, 1985) 1985, pp. 241-248.
- [104] A. I. Onuchukwu; *J. Chem. Soc. Faraday Trans. I*, 80 (1984) 1447.
- [105] A. I. Onuchukwu and A. B. Zuru; *Mater. Chem. Phys.*, 15 (1986) 131.
- [106] P. Lahiri and S. K. Senguptha; *Can. J. Chem.*, 69 (1991) 33.
- [107] S. K. Senguptha and P. Lahiri; *Ind. J. Tech.*, 30 (1992) 172.
- [108] G. C. Maiti, R. Malessa, U. Lochner, H. Papp and M. Barends; *J. Catal.*, 16 (1985) 215.
- [109] C. Cabot, A. C. Roger, A. Kienmann, S. Lakamp and G. Pourroy; *J. Catal.*, 173 (1998) 64.
- [110] F. Tihay, G. Pourroy, M. R. Plouet, A. C. Roger and A. Kienmann; *Appl. Catal.*, 206 (2001) 29
- [111] W. F. Shangquan, Y. Teraoka and Kagawa; *Appl. Catal.*, 8 (1996) 217.
- [112] W. F. Shangquan, Y. Teraoka and Kagawa; *Appl. Catal.*, 16 (1998) 149.
- [113] Y. Cesteros, P. Salagre, F. Medina and J. E. Sueiras; *Appl. Catal.*, 25 (2000) 213.
- [114] D. Mehandjiev, A. Naydenov and G. Iwanov; *Appl. Catal.*, 206 (2001) 13.
- [115] G. H. Jonker; *J. Phy. Chem. Solids*, 9 (1959) 165.
- [116] R. R. Dogoadge, A. A. Cherenko and C. Yu; *Sov. Phys. Solid State*, 3 (1961) 2698.
- [117] R. R. Heiks; *Phys. Rev.*, 99 (1955) 1232.
- [118] N. Rezlescu, D. Condurache, P. Petrariu and E. Luca; *J. Amer. Ceram. Soc.*, 57 (1974) 40.
- [119] W. Haubenreisser; *Phys. Stat. Solid.*, 21 (1961) 390S.
- [120] B. Lorentz and D. Ihle; *Phys. Stat. Solid.*, 63 (1974) 599.
- [121] B. Lorentz and D. Ihle; *Phys. Stat. Solid.*, 69 (1975) 451.

- [122] E. J. W. Verwey and J. H. de Boer; *Rec. Trav. Chim. Phys. Bas.*, 55 (1936) 531.
- [123] A. A. Samokhvalov and A. G. Rustamov; *Sov. Phys. Solid State*, 6 (1964) 749.
- [124] A. A. Samokhvalov and A. G. Rustamov; *Sov. Phys. Roy. Soc.*, 49 (1937) 59.
- [126] A. P. Niko'skii; *Sov. Phys. Solid State*, 8 (1960) 960.
- [127] K. H. Rao, S. B. Raju, K. Aggarwal and R. G. Mendiratta; *J. Appl. Phys.*, 52(3) (1981) 1376.
- [128] K. P. Belov, E. P. Srina and O. A. Malikov; *Sov. Phys. Solid State*, 4 (1963) 2072.
- [129] K. P. Belov, A. A. Popova and E. V. Talalaeva; *Sov. Phys. Crystallography*, 3 (1960) 738.
- [130] M. Rosenberg, P. Nicolau and I. Bunget; *Phys. Stat. Sol.*, 4 (1964) K121.
- [131] M. Rosenberg, P. Nicolau and I. Bunget; *Phys. Stat. Sol.*, 4 (1964) K125.
- [132] F. K. Lotgerring; *J. Phys. Chem. Solids*, 25 (1964) 95.
- [133] P. Venugopal Reddy, T. Sheshagiri Rao and S.M.D Rao; *J. Less. Com. Met.*, 79 (1981).
- [134] F. B. Perchik, Yu. K. Shalabutov and P. A. Markovia; *Sov. Phys. Solid State*, 19 (1977) 517.
- [135] G. H. Jonker; *J. Phys. Chem. Solids*, 9 (1959) 165.
- [136] P. V. Reddy and T. S. Rao, *Phy. Stat. Sol.(a)*, 77 (1983) K63.
- [137] D. Elwell, B. A. Griffiths and R. Parker; *Brit. J. Appl. Phys.*, 17 (1966) 587.
- [138] J. K. Sinha and Pran Kishan; *Ind. J. Pure and Appl. Phys.*, 2 (1964) 200.
- [139] S. P. Ghorpade, V. S. Darshane and S. G. Dixit; *Appl. Catal.*, 166 (1998) 135.
- [140] T. Yamaguchi, Y. Nakano and K. Tanabe; *Chem. Lett.*, 1976, 677.
- [141] K. Esumi and K. Meguro; *J. Colloid and Interface Sci.*, 66(1) (1978) 192.
- [142] B. D. Flockart, I. R. Leith and R. C. Pink; *Trans. Faraday Soc.*, 65 (1969) 54.
- [143] K. Esumi and K. Meguro; *Bull. Chem. Soc. Jpn.*, 55 (1982) 1647.
- [144] R. S. Davidson and R. M. Slater; *J. C. S Faraday I*, 72 (1976) 2426.
- [145] M. Che, C. Naccache and B. Imlik; *J. Catal.*, 24 (1972) 328.
- [146] H. Hosaka, T. Fujiwara and K. Meguro; *Bull. Chem. Soc. Jpn.*, 44 (1971) 2616.
- [147] K. Esumi, H. Shimada and K. Meguro; *Bull. Chem. Soc. Jpn.*, 50 (1977) 2795.
- [148] B. D. Folkhart, Kong Yong Liew and R. C. Pink; *J. Catal.*, 32 (1974) 20.
- [149] D. Cordischi, V. Indovina and A. Cimino; *J. C. S. Faraday I*, 70 (1974) 2189.
- [150] D. Cordischi, V. Indovina and A. Cimino, *J. C. S. Faraday Trans.*, 72 (10) (1976) 2341.
- [151] J. B. Perri; *J. Phys. Chem.*, 69 (1965).
- [152] K. Meguro and K. Esumi; *J. Colloid and Interface Sci.*, 59(1) (1977) 93.
- [153] K. Esumi, K. Miyata and K. Meguro, *Chem. Soc. Jpn.*, 58 (1985) 3524.
- [154] K. Esumi, K. Miyata, F. Waki and K. Meguro, *Bull. Chem. Soc. Jpn.*, 59 (1986) 3363.
- [155] R. S. Drago, L. B. Parr and C. S. Chambelain; *J. Am. Chem. Soc.*, 99 (1977) 3203.
- [156] K. Esumi and K. Meguro; *Bull. Chem. Soc. Jpn.*, 55 (1982) 315.
- [157] S. Sugunan, G. D. Devika Rani and P. A. Unnikrishnan; *J. Mater. Sci. Technol.*, 10(1994) 425.

- [158] S. Sugunan and J. M. Jalaja; *Collect. Czech. Chem. Commun.*, 59 (1994) 2605
- [159] S. Sugunan and J. J. Malayan; *J. Adhesion Sci. Technol.*, 9 (1) (1995) 73.
- [160] S. Sugunan and K. B. Sherly; *Ind. J. Chem.*, 32(A) (1993) 689.
- [161] S. Sugunan and G. D. Devika Rani; *Ind. J. Chem.*, 32 (A) (1993) 993.
- [162] S. Sugunan and G. D. Devika Rani; *J. Mater. Sci.*, 29 (1993) 4811.
- [163] R. J. Cvetanovic and Y. Amenomiya; *Adv. Catal*, 17 (1967) 103.
- [164] K. Tanabe; "Solid Acids and Bases-Their Catalytic Properties", Kodansha, Tokyo, Academic Press, New York, 1970.
- [165] K. Tanabe, M. Misono, Y. Ono and H. Hattori; "Solid Acids and Bases", Kodansha-Elsevier, Tokyo, 1989
- [166] A. Corma; *Chem. Rev.*, 95 (1995) 559.
- [167] W. E. Farneth and R. J. Gorte; *Chem. Rev.*, 95 (1995) 615.
- [168] H. G. Karge and V. Dondur; *J. Phys. Chem.*, 94 (1990) 765.
- [169] H. G. Karge, V. Dondur and J. Weitkamp; *J. Phys. Chem.*, 95 (1991) 283.
- [170] M. C. Abella, A. P. Velasco, M. F. Goniez and J. B. Riyarola; *Langmuir*, 13 (1997) 2596.
- [171] H. Matsushashi, H. Motoj and K. Arata, *Catal. Lett.*, 26 (1994) 325.
- [172] S. B. Sharma, B. I. Meyers, D. T. Chem and J. A. Dunesic; *Appl. Catal.*, 102 (1993) 253.
- [173] N. Y. Topsoc, K. Pederson and E. G. Derouane; *J. Catal.*, 70 (1981) 41.
- [174] C. V. Hidalgo, H. Itoh, T. Hattori, M. Niwa and Y. Hurakami; *J. Catal.*, 85 (1984) 362.
- [175] W. Reschetilowski, and K. P. Wendlandt; *J. Chem. Soc. Faraday Trans. I*, 85 (1989) 2941.
- [176] G. I. Kapustin, T. R. Brueva, A. L. Klyachko and B. Wichterlova; *Appl. Catal.*, 42 (1988) 239.
- [177] K. Chao, B. -H Chiou, C. -C. Cho and S. -Y Jeng; *Zeolites*, 4 (1984) 2.
- [178] F. Arena, R. Dario and A. Parmaliana; *Appl. Catal.*, 170 (1998) 127.
- [179] J. Kijenski and A. Baiker; *Catal. Today*, 5 (1989) 1.
- [180] A. Auroux and A. Antonella; *J. Phys. Chem.*, 94 (1990) 6371.
- [181] M. Trombetta, G. Busca, M. Lenarda, L. Storaro, R. Ganzerla, L. Piovesan, A. J. Lopez, M. Alcantara-Rodriguez and E. Rodriguez-Castellon; *Appl. Catal.*, 193 (2000) 55.
- [182] H. Sato, N. Ishii, K. Hirose and S. Nakamura, Proc. 7th Intern. Zeolite Conf., (Eds., Y. Murakami *et al.*) Kodansha, Tokyo and Elsevier, Amsterdam, 1986, p.755.
- [183] K. Hashimoto, T. Masuda and T. Mori; Proc. 7th Intern. Zeolite Conf., (Eds., Y. Murakami *et al.*) Kodansha, Tokyo and Elsevier, Amsterdam, 1986, p.503.
- [184] K. Tsutsumi, S. Haigiwara and H. Takahashi, *Bull. Chem. Soc. Jpn.*, 48 (1975) 3576.
- [185] J. B. Peri and R. B. Hamman; *J. Phys. Chem.*, 64 (1960) 1526.
- [186] E. P. Parry; *J. Catal.*, 2 (1963) 371.
- [187] M. R. Basila and T. R. Kantner; *J. Phys. Chem.*, 71 (1967) 467.
- [188] T. R. Huges and H. M. White; *J. Phys. Chem.*, 71 (1967) 2193.

- [189] J. Dewing, G. T. Monks and B. Youll; *J. Catal.*, 44 (1976) 226.
- [190] H. A. Benesi; *J. Catal.*, 28 (1973) 176.
- [191] H. Knözinger; *Adv. Catal. Relat. Subj.*, 25 (1976) 184.
- [192] P. A. Jacobs and C. F. Heylen; *J. Catal.*, 34 (1974) 2.
- [193] E. R. A. Matulewicz, F. P. J. M. Kerkhof, J. A. Moulijn and H. J. Reitsma; *J. Colloid Interface Chem.*, 77 (1980) 110.
- [194] A. Corma, C. Rodellas and V. Formes; *J. Catal.*, 88 (1984) 374.
- [195] H. Miyata and J. B. Moffat; *J. Catal.*, 62 (1980) 357.
- [196] S. Sato, M. Tokumitsu, T. Sodesawa and F. Nozaki; *Bull. Chem. Soc. Jpn.*, 64 (1991) 1005.
- [197] A. Satsuma, Y. Kamiya, Y. Westi and T. Hattori; *Appl. Catal.*, 194-195 (2000) 253.
- [198] M. Ai; *Bull. Chem. Soc. Jpn.*, 50 (1977) 2597.
- [199] M. A. Aramendia, V. Borau, I. M. Garcia, C. Jimenez, A. Marinas, J. M. Marinas, A. Porras and F. J. Urbano; *Appl. Catal.*, 184 (1999) 115.
- [200] H. Vinek, H. Noller, M. Ebel and K. Schwarz; *J. Chem. Soc. Faraday Trans. I*, 73 (1977) 734.
- [201] A. Auroux and A. Gervasini; *J. Catal.*, 131 (1991) 190.
- [202] G. R. Dube and V. S. Darshane; *J. Mol. Catal.*, 79 (1993) 285.
- [203] M. P. Rosynek, R. J. Koprowski and G. N. Dellisante; *J. Catal.*, 122 (1990) 80.
- [204] C. Bezouhanava and M. A. Al-Zihari, *Catal. Lett.*, 11 (1991) 245.
- [205] K. V. V. S. B. S. R Murthy, B. Srinivas, S. J. Kulkarni, M. Subrahmanyam and P. Kanta Rao; "Catalysis : Modern Trends", (Eds., N. M. Gupta and D. K. Chakrabarty) 1995, Narosa publishing House, New Delhi, India.
- [206] A. Rachel, V. Durgakumari and P. Kanta Rao, "Catalysis : Modern Trends" (Eds., N. M. Gupta and D.K Chakrabarty) 1995, Narosa publishing House, New Delhi, India
- [207] N. J. Jebarathinam and V. Krishnaswamy; "Catalysis : Modern Trends", (Eds., N. M. Gupta and D. K. Chakrabarty) 1995, Narosa publishing House, New Delhi, India.
- [208] N. J. Jebarathinam and V. Krishnaswamy; "Catalysis: Present and Future", (Eds., P. Kantha Rao and B. S. Benwal), Publication and Information Directorate, New Delhi, p. 288.
- [209] M. A. Aramendia, V. Borau, C. Jimenez, J. M. Marinas and F. J. Romero, *J. Catal.*, 151 (1995) 44.
- [210] M. V. Joshi, S. G. Oak and V. S. Darshane; "Catalysis : Modern Trends" (Eds., N. M. Gupta and D. K. Chakrabarty) 1995, Narosa publishing House, New Delhi, India
- [211] H. Pines and C. N. Pillai; *J. Am. Chem. Soc.*, 82 (1960) 2401.

Experimental

This chapter gives a detailed description of the catalyst preparation and pretreatment conditions, materials used, the techniques used to characterize the catalyst, the experimental set up and measures used for the catalytic activity study.

2.1 Catalyst preparation

The catalytic activity strongly depends on the methods of preparation and pretreatment conditions apart from the reaction parameters. Small variations in the preparation conditions radically alter the performance of the catalyst. So intense care must be taken during the selection of materials and preparation of the systems.

2.1.1 Materials

Analar grade $\text{Mn}(\text{NO}_3)_2 \cdot 4\text{H}_2\text{O}$, $\text{Fe}(\text{NO}_3)_3 \cdot 9\text{H}_2\text{O}$, $\text{Cr}(\text{NO}_3)_3 \cdot 9\text{H}_2\text{O}$, $\text{Co}(\text{NO}_3)_2 \cdot 6\text{H}_2\text{O}$, $\text{Ni}(\text{NO}_3)_2 \cdot 6\text{H}_2\text{O}$, $\text{Cu}(\text{NO}_3)_2 \cdot 3\text{H}_2\text{O}$, $\text{Zn}(\text{NO}_3)_2 \cdot 6\text{H}_2\text{O}$ and NaOH from Merck were used as such without further purification.

2.1.2 Preparation of different compositions of manganese ferros spinels

Five series of manganese ferros spinels of formula, $\text{Mn}_{(1-x)}\text{B}_x\text{Fe}_2\text{O}_4$ (B is a metal cation like Cr, Co, Ni, Cu or Zn, and $x = 0, 0.2, 0.4, 0.6, 0.8$ and 1.0) were prepared for the present work. Their compositions and labelling are summarized in the following table (Table 2.1.1).

For the synthesis of all compositions of manganese ferros spinels low temperature co-precipitation method reported by Date *et al.* [1] was adopted. The co-precipitation method is preferred over the usual ceramic method as the ferrites prepared by former route provide chemically homogeneous and fine particles. And between the two usual co-precipitation routes, viz. oxalate and hydroxide the latter is preferred for achieving higher surface areas. The present study, accordingly employed hydroxide route co-precipitation method for the synthesis of the systems. Metals were precipitated as their hydroxides from their nitrate solutions using sodium hydroxide as the precipitant alkali.

Table 2.1.1 Catalyst compositions and labelling of different series of manganese ferrosinels.

x	Catalyst composition	Catalyst labelling
Cr_xMn_(1-x)Fe₂O₄ - series		
0.0	MnFe ₂ O ₄	MF
0.2	Cr _{0.2} Mn _{0.8} Fe ₂ O ₄	MCrF-0.2
0.4	Cr _{0.4} Mn _{0.6} Fe ₂ O ₄	MCrF-0.4
0.6	Cr _{0.6} Mn _{0.4} Fe ₂ O ₄	MCrF-0.6
0.8	Cr _{0.8} Mn _{0.2} Fe ₂ O ₄	MCrF-0.8
1.0	CrFe ₂ O ₄	CrF
Co_xMn_(1-x)Fe₂O₄ - series		
0.0	MnFe ₂ O ₄	MF
0.2	Co _{0.2} Mn _{0.8} Fe ₂ O ₄	MCoF-0.2
0.4	Co _{0.4} Mn _{0.6} Fe ₂ O ₄	MCoF-0.4
0.6	Co _{0.6} Mn _{0.4} Fe ₂ O ₄	MCoF-0.6
0.8	Co _{0.8} Mn _{0.2} Fe ₂ O ₄	MCoF-0.8
1.0	CoFe ₂ O ₄	CoF
Ni_xMn_(1-x)Fe₂O₄ - series		
0.0	MnFe ₂ O ₄	MF
0.2	Ni _{0.2} Mn _{0.8} Fe ₂ O ₄	MNiF-0.2
0.4	Ni _{0.4} Mn _{0.6} Fe ₂ O ₄	MNiF-0.4
0.6	Ni _{0.6} Mn _{0.4} Fe ₂ O ₄	MNiF-0.6
0.8	Ni _{0.8} Mn _{0.2} Fe ₂ O ₄	MNiF-0.8
1.0	NiFe ₂ O ₄	NiF
Cu_xMn_(1-x)Fe₂O₄ - series		
0.0	MnFe ₂ O ₄	MF
0.2	Cu _{0.2} Mn _{0.8} Fe ₂ O ₄	MCuF-0.2
0.4	Cu _{0.4} Mn _{0.6} Fe ₂ O ₄	MCuF-0.4
0.6	Cu _{0.6} Mn _{0.4} Fe ₂ O ₄	MCuF-0.6
0.8	Cu _{0.8} Mn _{0.2} Fe ₂ O ₄	MCuF-0.8
1.0	CuFe ₂ O ₄	CuF
Zn_xMn_(1-x)Fe₂O₄ - series		
0.0	MnFe ₂ O ₄	MF
0.2	Zn _{0.2} Mn _{0.8} Fe ₂ O ₄	MZnF-0.2
0.4	Zn _{0.4} Mn _{0.6} Fe ₂ O ₄	MZnF-0.4
0.6	Zn _{0.6} Mn _{0.4} Fe ₂ O ₄	MZnF-0.6
0.8	Zn _{0.8} Mn _{0.2} Fe ₂ O ₄	MZnF-0.8
1.0	ZnFe ₂ O ₄	ZnF

Solutions of the metal nitrates in the required stoichiometric ratios were prepared and mixed and rapidly added to the 5.3 M NaOH solution with vigorous stirring. Due to the exothermic nature of the precipitation reaction, the temperature of the slurry rose to 45°C. The pH of the final slurry was carefully adjusted between 10 and 11. The precipitate was kept overnight for ageing and then washed several times with double distilled water until free from nitrate ions and alkali. It was filtered, dried in an air oven at 80°C for 36 h and were calcined at 500°C for 5 h to achieve complete spinel phase formation. The dried materials were powdered and sieved below 75 µm mesh.

2.2 Catalyst characterization

All the prepared catalysts were characterized by different physico-chemical techniques viz. XRD, inductively coupled plasma (ICP) analysis, scanning electron microscopy (SEM), surface area measurements (BET), thermogravimetric analysis (TGA), DRIFT spectroscopy, Mössbauer spectroscopy and acidity-basicity measurements by various methods like electron acceptor adsorption studies, temperature programmed desorption of ammonia and thermogravimetric analysis using pyridine/dimethylpyridine as probe molecules. A brief discussion of the various methods adopted is presented below.

2.2.1 X-Ray Diffraction analysis

XRD is one of the widely used and versatile techniques for the qualitative and quantitative analysis of the solid phases [2]. The purity of the substance, transition to different phases, allotropic transformation, lattice constants and presence of foreign atoms in the crystal lattice can also be recognized by this technique. The XRD method involves the interaction between the monochromatic X-rays (like Cu K_α or Mo K_α) with family of planes (identified by a system of Miller Indices, hkl) in the polycrystalline material. A fixed wavelength is chosen for the incident radiation and the Bragg's peaks are identified as a function of scattering angle 2θ. The interplanar distances (d spacing) are calculated from the Bragg's equation,

$$n\lambda = 2d \sin\theta,$$

where λ is the X-ray wave length and n is an integer called order of reflection.

The mean crystallite size of a material can also be determined from the broadening of an X-ray diffraction peak, which is inversely proportional to crystallite size and this can be achieved by following the Scherrer method using the formula,

$$t = 0.9 \lambda / \beta \cos \theta$$

which is derived from Bragg's equation. 't' is the thickness of the crystal and β = FWHM (half the width of the peak with maximum intensity).

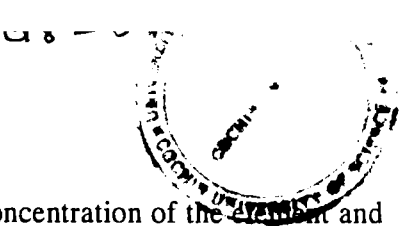
The XRD patterns of the catalyst samples were taken using Rigaku D-Max C X-ray diffractometer. A stationary Ni filtered Cu K_{α} radiation ($\lambda = 1.5404 \text{ \AA}$) and a movable detector, which measures the intensity of diffracted radiation as a function of 2θ are the main parts of the instrument.

2.2.2 Inductively coupled plasma (ICP) analysis

Inductively Coupled Plasma (ICP) is an analytical technique used for the determination of the elemental composition of the samples. The primary goal of ICP is to get elements to emit specific light of characteristic wavelength, which can then be measured. The technology for the ICP method was first employed in the early 1960's with the intention of improving upon crystal growing techniques.

ICP hardware [3] is designed to generate plasma, which is a gas in which atoms are present in an ionized state. The basic set up of an ICP consists of sample introduction system (nebulizer), ICP torch, radio frequency generator, transfer optics, spectrometer and computer interface. Argon is commonly used as both the intermediate gas and inner or carrier gas.

An ICP requires that the elements, which are to be analyzed, be in aqueous solution. The nebulizer transforms the aqueous solution into an aerosol. The light emitted by the atoms of an element in the ICP must be converted to an electrical signal that can be measured quantitatively. This is accomplished by resolving the light into its component radiation (nearly always by means of a diffraction grating) and then measuring the light intensity with a photomultiplier tube at the specific wavelength for each element line. The light emitted by the atoms or ions in the ICP is converted to electrical signals by the photomultiplier in the spectrometer. The intensity of the electron



signal is compared with measured intensities of known concentration of the element and the concentration is computed. Each element will have many specific wavelengths in the spectrum, which could be used for analysis.

Advantages of using an ICP include its ability to identify and quantify all elements with the exception of argon since many wavelengths of varied sensitivity are available for determination of any element. ICP is suitable for all concentrations from ultratrace levels to major components. Detection limits are generally low for most elements with a typical range of 1-100 g/L. Probably the prevalent advantage of employing an ICP when performing quantitative analysis is the fact that multi-elemental analysis can be accomplished, and quite rapidly. A complete multielement analysis can be undertaken in a period as short as 30 seconds, consuming only 0.5 mL of sample solution.

The ICP analysis of the samples was done using ARL 3410 ICP atomic emission spectrometer.

2.2.3 Scanning electron microscope (SEM) analysis

Scanning electron microscopy (SEM) is based on the strong interaction of electrons with matter and appreciable scattering by quite small atomic clusters. Electrons can be conveniently deflected and focused by electric or magnetic fields so that magnified real-space images can be formed in addition to simple diffraction patterns. This property of electron beam is used in SEM analysis. In SEM, the electron optics act before the specimen is reached to convert the beam into a fine probe, which can be as small as 100 Å in diameter at the specimen surface [4]. The technique is of high interest in catalysis because of its high spatial resolution. However, a serious drawback is that the results need not be really representative of the whole sample. This can be overcome by making many analyses at different locations of the sample particles and for many catalyst particles.

SEM analysis of the samples was done using Stereoscan 440: Cambridge, U.K scanning electron microscope.

2.2.4 Diffuse Reflectance Infrared Fourier Transform (DRIFT) spectroscopy

Infrared spectroscopy (IR) is widely used in the field of characterization of heterogeneous catalysts. Identification of the structural features of the catalyst itself, adsorbed and dispersed species and their structure, metal-metal interaction, reaction intermediates on the catalyst surface etc. are some of the important informations obtained from infrared spectral studies. The introduction of Diffuse Reflectance Infrared Fourier Transform (DRIFT) spectroscopy [5, 6] has improved the application of infrared spectroscopy by giving valuable informations which are inherent in a mid-IR (4000 – 200 cm^{-1}) spectrum. The diffuse reflectance spectrum of a dilute sample of 'infinite depth' (i.e., up to 3mm) is usually calculated with reference to the diffuse reflectance of the pure diluents to yield the reflectance, $R_{i\bar{\lambda}}$. $R_{i\bar{\lambda}}$ is related to the concentration of the sample, c , by the Kubelka-Munk (K-M) equation [7]:

$$f(R_{i\bar{\lambda}}) = (1-R_{i\bar{\lambda}})^2/2R_{i\bar{\lambda}} = 2.303ac/s$$

where 'a' is the absorptivity and 's' is the scattering coefficient. The scattering coefficient depends on both particle size and degree of sample packing; thus the K-M function can be used for accurate quantitative analysis, provided the particle size and packing method are strictly controlled. For good diffuse reflectors plots of the K-M function, $f(R_{i\bar{\lambda}})$, are analogous to absorbance plots for transmission spectra. Care must be taken in applying the K-M equation when $R_{i\bar{\lambda}}$ is much less than about 30% since deviations from linearity can occur when the sample concentration is high. Diluting ensures deeper penetration of the incident beam, thus increasing the contribution to the spectrum of the transmission and internal reflection component.

The technique of diffuse reflection spectroscopy has been used successfully in many fields as an adjunct to better-known spectroscopic methods, and is often useful where traditional techniques fail. In spinel ferrites the metal cations are distributed in two different environments and the spinel phase formation can be well assigned by the appearance of two IR bands [8, 9]. Usually these two IR bands are hidden in ordinary FTIR spectroscopy. The infrared spectra of the prepared samples were recorded by a DR-IR (Shimadzu) in the range 400-1400 cm^{-1} .

2.2.5 Thermogravimetric (TG) analysis

Thermogravimetric analysis is used in catalyst characterization procedure as an important tool to provide valuable information regarding drying ranges, hydration, decomposition temperature, stability limits, etc. In thermogravimetry, the weight of a sample is recorded over a period of time while its temperature is being raised linearly. A thermogram is obtained by plotting weight of the sample (on ordinate) against temperature (on abscissa). The horizontal regions of the thermogram indicated the stability of the sample, while weight loss is indicated by the curved portions. DTG is the first derivative plot of the TG curve from which a better understanding of the weight loss can be obtained from the dip in the curve.

The thermogravimetric analysis of the ferrite samples was carried out using Shimadzu TGA-50. The heating rate was 20°C / minute in nitrogen atmosphere.

2.2.6 Surface area determination (BET method)

The Brunauer, Emmett and Teller (BET) method [10] has been adopted as a standard procedure for surface area determination. By the introduction of a number of simplifying assumptions, the BET theory extends Langmuir model to multilayer adsorption. In the BET theory, it is assumed that the solid surface possesses uniform, localized sites and the adsorption at one site does not affect adsorption at neighbouring sites. It is further assumed that the adsorption is multilayer and the heat of adsorption of the second and the subsequent layers are identical and is equal to the liquefaction of the adsorbate. The BET equation can be represented as,

$$\frac{p}{v(p_0 - p)} = \frac{1}{C v_m} + \frac{(C - 1)p}{C v_m p_0}$$

Here, C = a constant for a given system at a given temperature and related to the heat of adsorption, v = volume adsorbed at equilibrium pressure p, v_m = volume of the adsorbate necessary to form a monolayer on the surface and p₀ = saturated vapour pressure of the adsorbate.

The BET equation demands a linear relation between $p/[v(p_0 - p)]$ and p/p_0 , where slope = $(C-1)/Cv_m$ and y intercept = $1/Cv_m$. From the slope and y-intercept, v_m can

be calculated. The specific surface area of the sample is then calculated using the relation,

$$\text{Surface area (m}^2 \text{ g}^{-1}\text{)} = \frac{V_m N_0 a_m}{22414 \times \text{weight of the catalyst}}$$

where a_m = average area occupied by the nitrogen molecule (1.62 \AA^2) and N_0 = Avagadro number.

Micrometrics Gemini analyzer was used to determine the surface area with nitrogen as adsorbate. Previously activated samples were degassed at 200°C under nitrogen flow for 2 h and then brought to 77 K using liquid nitrogen.

2.2.7. Transport studies

Ferrites are semiconductors and exhibit interesting electrical properties. The electrical properties of the ferrites vary drastically with the minute changes in the composition. Recently, it has been found that the electrical properties of the ferrites are involved in determining the catalytic properties [11]. DC conductivity measurements and Hall effect measurements were done to investigate the transport properties of different series of manganese ferrites.

(a) Activation energy determination (DC conductivity measurements)

The temperature dependence of the DC conductivities allowed the determination of the activation energy (energy gap between the valence and conduction band). At temperatures above room temperatures charge carriers are additionally transferred by thermal excitation from the valence band to the conduction band. The temperature dependence in this case is essentially described by an exponential function:

$$\sigma_{dc} = \sigma_0 \exp(-E_a/\kappa T)$$

where E_a = energy gap or activation energy, κ = Boltzmann's constant, T = absolute temperature.

The logarithm of this equation is, $\ln \sigma_{dc} = \ln \sigma_0 - (E_a/\kappa T)$. This equation is of the form, $y = mx + C$. A plot of $\ln \sigma_{dc}$ (as ordinate) at different temperatures against $1/T$ (as abscissa) gives a straight line with $\ln \sigma_0$ as y-intercept (C) and $(-E_a/\kappa)$ as slope (m).

The DC conductivity measurements were done using two-probe method. The pellets were prepared from the sample (2 g) by applying a pressure of 7 tones; the thickness of the pellets was varied between 0.80 and 0.90 cm. The pellet was placed in a conductivity cell in which the temperature can be varied from room temperature to 120°C by a digital temperature controller and this was measured by a Fe-K thermocouple kept on the sample. A bias voltage of 20 V was applied and the current flowing across the sample was measured by a Keithley Picoammeter/ voltage source (Model 487). All the measurements were carried out under dynamic vacuum. The acquisition and analysis of the data were completely automated by employing the LabVIEW software.

(b) Hall effect measurements

The history of the Hall effect begins in 1879 when Edwin H. Hall discovered that a small transverse voltage appeared across a current-carrying thin metal strip in an applied magnetic field. The importance of the Hall effect is underscored by the need to determine accurately carrier density, electrical resistivity, and the mobility of carriers in semiconductors. The Hall effect provides a relatively simple method for doing this. Because of its simplicity, low cost, and fast turnaround time, it is an indispensable characterization technique for semiconductors.

The basic physical principle underlying the Hall effect is the Lorentz force. When an electron moves along a direction perpendicular to an applied magnetic field, it experiences a force acting normal to both directions and moves in response to this force and the force effected by the internal electric field. For an n-type semiconductor the carriers are predominately electrons. Assume that a constant current 'I' flows along the x-axis from left to right in the presence of a z-directed magnetic field. Electrons subject to the Lorentz force initially drift away from the current line toward the negative y-axis, resulting in an excess surface electrical charge on the side of the sample. This charge results in the Hall voltage, a potential drop across the two sides of the sample (the force on holes is toward the same side because of their opposite velocity and positive charge). This transverse voltage is the Hall voltage V_H and its magnitude is equal to IB/qnd , where, 'I' is the current, 'B' is the magnetic field, 'd' is the sample thickness, and 'q'

(1.602×10^{-19} C) is the elementary charge. If n_s is the charge carrier density, one then obtains the equation,

$$n_s = IB/q |V_H|$$

Thus, by measuring the Hall voltage V_H and from the known values of I , B , and q , one can determine the density of charge carriers (n_s) in semiconductors. The Hall voltage is negative for n-type semiconductors and positive for p-type semiconductors. The resistance R_s of the semiconductor can be conveniently determined by use of the van der Pauw resistivity measurement technique (four probe method). Since sample resistance involves both charge carrier density and mobility, one can determine the Hall mobility from the equation,

$$\mu = |V_H|/R_s I B = 1/(qn_s R_s).$$

The Hall effect measurements of the manganese ferrosipinel systems were done with MMR (H-50) instrument.

2.2.8 Mössbauer spectroscopy

Mössbauer spectroscopy is a versatile technique to yield better understanding of the oxidation state, phase transitions, magnetic properties and electronic environment of the mössbauer active elements in the catalysts and of the particle size of the samples. Mössbauer spectroscopy is based on Mossbauer effect, which is the recoil-free emission of γ -radiation from a solid radioactive material [12]. This radiation can be absorbed by stationary atoms, and is best observed in isotopes, which have long-lived low-lying excited nuclear energy states (^{57}Fe is the best example of this).

A transmission Mössbauer spectrometer is very simple, and typically consists of a γ -ray source, the absorber (sample) and a detector. The γ -ray source is excited ^{57}Fe nuclei, produced by the decay of ^{57}Co isotope. Approximately 90% of the ^{57}Fe nuclear excited state decays through the intermediate level to produce 14.4 K eV gamma radiation. These gamma photons can then be absorbed by ^{57}Fe in a sample. The source is moved relative to the absorber, shifting the energy spectrum due to the Doppler effect. The spectrum is plotted as percent transmission versus source velocity (energy).

The interpretation of the Mössbauer spectrum is mainly done through the analysis of Mössbauer parameters such as isomer shift (δ), center shift (CS), quadrupole splitting (ΔE_Q), hyperfine magnetic field (H) and line width (I). All these parameters are expressed in velocity units, mm/s except for hyperfine magnetic field, which is expressed in Tesla.

The isomer shift (δ), is the energy difference between source and absorber nuclei resulting from the effects including differences in valence state, spin state and coordination of the absorber atoms [13]. Experimentally one observes a single line shifted from a reference zero point by an isomer shift plus the second order Doppler shift (SOD), a small thermal shift due to atomic vibrations. The contribution from SOD is similar in most standard materials, so for the purpose of comparison the isomer shift is always taken to be equal to the center shift.

The quadrupole splitting (ΔE_Q), is the splitting of the energy levels caused by the interaction between the nuclear quadrupolar moment and an electric field gradient (EFG) at the nucleus. It depends on the valence and spin state of the absorber atoms as well as the coordination and degree of distortion of the crystallographic site. Experimentally one observes a doublet with components of equal intensity and line width in the ideal random absorber case. The quadrupole splitting is given by the energy separation between the components.

The interaction of the nuclear dipole moment of the nucleus and a hyperfine magnetic field causes a splitting of the nuclear energy levels, resulting in six peaks for ^{57}Fe spectra in the simplest case. For an ideal random absorber with no quadrupole interaction the line width of the peaks are equal with intensity ratio, 3:2:1:1:2:3. The separation of peaks 1 and 6 is proportional to the magnitude of the hyperfine magnetic field.

The line width is expressed in full width at half maximum of the peak height (FWHM). The peaks are broadened beyond the natural line width by effects due to equipment (vibrational, thermal and electronic problems), the source (self-absorption resulting from decay) and the sample (thickness broadening, next nearest neighbour effects and dynamic processes such as relaxation).

The room temperature Mössbauer spectra of the ferrites were obtained using a constant acceleration Mössbauer spectrometer.

2.2.9 Acid-base property studies

Acid base properties of the solid catalysts play decisive role in determining the catalytic activity and selectivity. Four independent methods are adopted for the thorough understanding of acid-base properties of manganese ferros spinels such as temperature programmed desorption of ammonia, thermodesorption studies of pyridine/2,6-dimethylpyridine adsorbed samples, electron donating property studies and decomposition of cyclohexanol.

(a) Temperature programmed desorption (TPD) of ammonia

The NH₃-TPD method is widely employed in characterizing the acidity of solid catalysts. This is an easy method used to find out the total acidity as well as acid strength distribution.

The pellets were prepared from the sample (about 0.75 g) using a pelletiser and activated at 500°C for 2 h. The accurately weighed pellets were placed in a home built stainless steel reactor of internal diameter 1 cm and length 15 cm kept in a cylindrical furnace. The temperature of the reactor is maintained using a temperature controller and the temperature was measured by an Al-Cr thermocouple kept inside the furnace. The sample was degassed at 300°C using a flow of nitrogen for half an hour. It was then allowed to cool to room temperature and a definite amount of ammonia is injected into the reactor and allowed to adsorb uniformly over the catalyst surface. The physisorbed ammonia was flushed out using a flow of nitrogen gas. Under a controlled temperature programme, the amount of chemisorbed ammonia leached out for each 100°C in the temperature range 100°- 600°C was trapped into H₂SO₄ solution (0.025 N) and ammonia desorbed was determined by back titration with NaOH solution (0.025 N).

$$\text{Amount of ammonia desorbed} = \frac{\Delta V \times N_{\text{NaOH}} \times 5 \times 17}{\text{Weight of the sample}}$$

where ΔV is the difference titre values of NaOH between blank H_2SO_4 and the ammonia trapped H_2SO_4 at each temperature. The acid strength distribution was obtained from a plot of the amount of ammonia desorbed against temperature.

(b) TGA of pyridine/2,6-dimethylpyridine adsorbed samples

The thermodesorption studies of pyridine and 2,6-dimethylpyridine (2-DMP) adsorbed samples were implemented to investigate the relative amount of total acidity and Brønsted acidic sites in manganese ferros spinels.

The catalyst samples activated at $500^\circ C$ for 2 h were kept in two different desiccators saturated with pyridine and 2, 6-dimethylpyridine vapours, respectively. For the effective and uniform adsorption the samples were kept inside the desiccator for 48 h. After this, the weight loss of the adsorbed samples was measured by thermogravimetric analysis operating between 40 to $600^\circ C$ at a rate of $20^\circ C / \text{minute}$. For the pyridine adsorbed samples, the weight loss between $100^\circ-200^\circ C$, $201^\circ-400^\circ C$ and $401^\circ-600^\circ C$ are considered to be measures of weak, medium and strong acid sites, respectively. Since the 2,6-DMP weakly bound to Lewis acid sites get desorbed below $300^\circ C$ [14], the weight loss between $301^\circ-400^\circ C$, $401^\circ-500^\circ C$ and $501^\circ-601^\circ C$ are considered to be measures of weak, medium and strong acid sites, respectively.

(c) Electron donating property study

Adsorption of electron acceptors has been investigated to study and characterize the electron donating property of the system. The following electron acceptors were used.

7,7,8,8-tetracyanoquinodimethane (TCNQ) [Merck- Schuchardt] was purified by repeated crystallization from acetonitrile [15], 2,3,5,6-tetra-chloro-4-benzoquinone (chloranil) [Sisco Research Laboratories PVT. Ltd.] was crystallized from benzene before use [16]. Chloroform was used as the solvent for the crystallization of *p*-dinitrobenzene (PDNB) [17]. SQ grade acetonitrile [Qualigens Fine Chemicals] was purified by passing through silica gel for drying followed by distillation with P_2O_5 and the fraction between $79-82^\circ C$ was collected.

The following procedure was adopted for adsorption studies. The catalyst samples were activated at 500°C for 2 h prior to each experiment. The adsorption study was carried out over 0.5 g catalyst placed in a 25 mL cylindrical glass tube fitted with a mercury sealed stirrer. 10 mL of solution of an electron acceptor in acetonitrile was then admitted to the catalyst. Stirring was continued for 4 h in a mechanically driven stirrer at room temperature and atmospheric pressure in a thermostated bath, and centrifuging the solution collected the oxide. The amount of electron acceptor adsorbed was determined from the difference in concentration of the electron acceptor in solution before and after adsorption, which was measured by means of a Shimadzu UV-VIS spectrophotometer. The λ_{max} of electron acceptors in acetonitrile is 393.5 nm for TCNQ, 288 nm for chloranil and 262 nm for PDNB.

The Langmuir type adsorption isotherms were obtained by plotting equilibrium concentration of electron acceptors against amount of electron acceptors adsorbed. From the Langmuir adsorption isotherms, limiting amount of electron acceptor adsorbed was calculated.

2.2.10 Catalytic activity studies

The reactions studied for the present work can be put under two categories as liquid-phase reactions and vapour-phase reactions. Under the liquid phase reactions, benzylation of aromatics and phenol hydroxylation and under vapour phase reaction, aniline alkylation, phenol methylation and oxidative dehydrogenation of ethylbenzene were carried out.

(a) Liquid-phase reactions

For the liquid-phase reactions, the reagents in the required molar ratio was taken in a 50 mL double necked round bottom flask fitted with water condenser and guard tube. The reaction was carried out in an oil bath and the temperature of the reaction was controlled using a dimmerstat. Using a magnetic stirrer attained the uniform stirring of the reaction mixture. The product formed was analyzed by gas chromatography (Chemito GC 8610, flame ionization detector, appropriate columns) and the products were identified by GC-MS.

(b) Vapour-phase reactions

The vapour-phase experiments were performed at atmospheric pressure in a fixed bed, vertical, down-flow, quartz reactor of 2 cm I.D and 30 cm length placed inside a double-zone furnace. 0.5 g of the catalyst activated at 500°C for 2 h is positioned in the centre of the reactor in such a way that the catalyst is sandwiched between the layers of inert silica beads. The upper portion of the reactor served as a vaporizer cum pre-heater. The temperature measurements were done using a temperature controller and a Cr-Al thermocouple was placed at the centre of the catalyst bed. A home built syringe pump fed the liquid reactant mixture. The products of the reaction were collected downstream from the reactor in a receiver connected through a cold water-circulating condenser. The products were collected at various time intervals and analyzed by GC (Chemito GC 8610, flame ionization detector, appropriate columns) and the products were identified by GC-MS.

References:

- [1] P. S. Anilkumar, J. J. Shrotri, S. D. Kulkarni, C. E. Deshpande and S. K. Date; *Matt. Lett.*, 27 (1996) 293.
- [2] C. Whiston; "X-ray Methods", (Eds., F. E. Prichard), ACOL, Thames Polytech., London, 1991.
- [3] D. A. Skoog; "Principles of Instrumental analysis", 3rd Edn., Saunders College Publishing, 1985, p.294.
- [4] A. Howie; "Characterisation of Catalysts", (Eds. J. M. Thomas and R. M. Lambert), John Wiley, New York, 1980, p.114.
- [5] M. P. Fuller and P. R. Griffiths; *Anal. Chem.*, 58 (1978) 1906.
- [6] J. P. Blitz; "Modern Techniques in Applied Molecular Spectroscopy", (Eds., F. M. Mirabella), John Wiley, New York, 1998, p.213.
- [7] P. Kubelka and F. Munk; *Z. Tech. Phys.*, 12 (1931) 593.
- [8] R. D. Waldron; *Phy. Rev.*, 99 (1955) 1727.
- [9] W. B. White and B. A. DeAngelis; *Spectrochimica Acta*, 23A (1967) 985.
- [10] S. Brunauer, P. h Emmett and E. Teller; *J. Am. Chem. Soc.*, 60 (1938) 309.
- [11] S. P. Deshpande, V. S. Darshane and S. G. Dixit; *Appl. Catal.*, 166 (1998) 135.
- [12] C. N. Banwell and E. M. McCash; "Fundamentals of Molecular Spectroscopy", 4th Edn., Tata McGraw-Hill Publishing Company Ltd., New Delhi, 1995.
- [13] R. C. Burns and T. C. Solberg; "Spectroscopic characterization of Minerals and their Surfaces", (Eds., L. M. Coyne, S.W.S. McKeever and D.F. Blake), ACS symposium series, American Chemical Society, Washington DC, 1990, p. 262-283.
- [14] A. Satsuma, Y. Kamiya, Y. Westi and T. Hattori, *Appl. Catal.*, 194-195 (2000) 253.
- [15] D. S. Acker and W.R. Hertler; *J. Am.Chem. Soc.*, 84 (1962) 3370.
- [16] L. F. Fiesser and M. Fiesser; "Reagents for Organic Synthesis", John Wiley, New York, 1967, p.125.
- [17] B. S. Furness, A. J. Hannaford, V. Roger, P. W. G. Smith and A. R. Tatchel; "Vogel's Text Book of Practical Organic Chemistry", 4th Edn., ELBS, London, 1978, p.708.
- [18] A. I. Vogel; "A Text Book of Practical Organic Chemistry", 3th Edn., ELBS, London, 1973, p.407.

Characterization And Surface properties

3.1 Physical characterization

The manganese ferrites prepared by co-precipitation technique were characterized by adopting various physical methods such as XRD analysis, SEM analysis, inductively coupled plasma analysis, diffuse reflectance infrared studies, surface area measurements, thermal analysis, transport studies and Mössbauer spectra.

3.1.1 X-ray diffraction analysis

Every crystalline substance has a unique X-ray powder pattern because the line position depends on unit cell size, and line intensity depends on the type of atoms present and on their arrangement in the crystal [1]. The X-ray diffractograms of the powdered samples were recorded using Rigaku (model D/MAX-VC) instrument with Cu K α radiation and are presented in Fig.3.1.1 - 3.1.6. Fig.3.1.1 shows the influence of calcination temperature on the XRD pattern of MnFe $_2$ O $_4$. It can be seen that the intensity of the peaks turns out to be sharper with increase in calcination temperature and this suggests the growth of particle size and increase of crystallinity at higher calcination temperatures. At 80°C the XRD pattern is broader, indicative of the gradual but incomplete formation of spinel phase [2]. It was observed that only at a calcination temperature of 500°C, the spinel phase was formed and hence it was taken as the optimum calcination temperature for the prepared ferrites. The theoretical (from JCPDS Card Data) and experimental d_{hkl} values for simple ferrosinels such as MnFe $_2$ O $_4$, CrFe $_2$ O $_4$, CoFe $_2$ O $_4$, NiFe $_2$ O $_4$, CuFe $_2$ O $_4$ and ZnFe $_2$ O $_4$ are presented in Table 3.1.1. It can be seen that the experimental data are well coordinated with the theoretical data. Interestingly, it was also observed that the mixed ferrites of the Cr-Mn, Co-Mn, Ni-Mn, Cu-Mn and Zn-Mn series gave much identical XRD patterns with those of the corresponding simple ferrosinels. In the systems studied, the compositional differences are due to different proportion of the atoms Cr, Co, Ni, Cu and Zn in pure MnFe $_2$ O $_4$. These atoms have close atomic numbers and so, much alike XRD patterns.

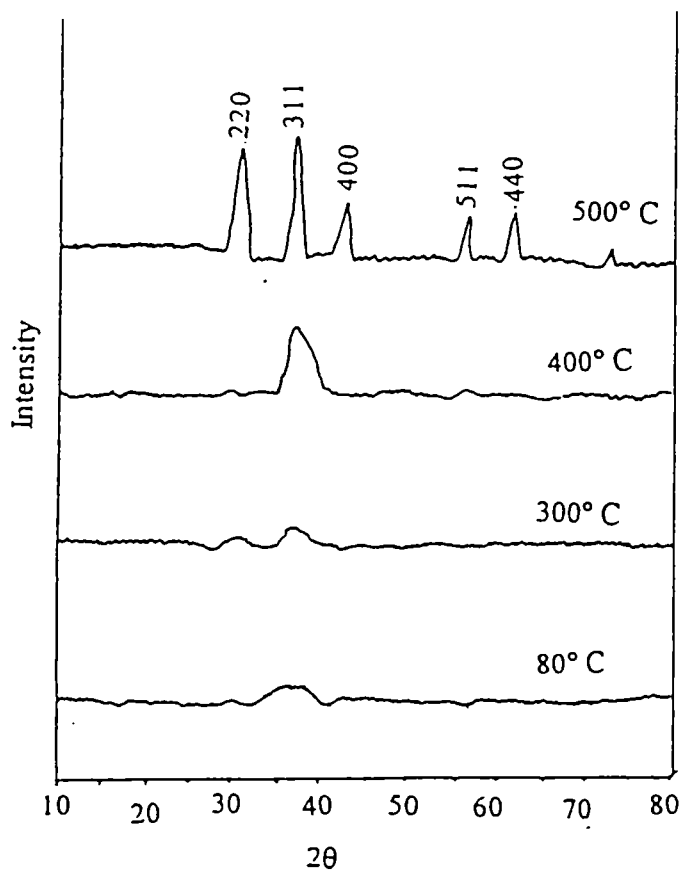


Fig. 3.1.1 XRD patterns of MnFe₂O₄ calcined at different temperatures.

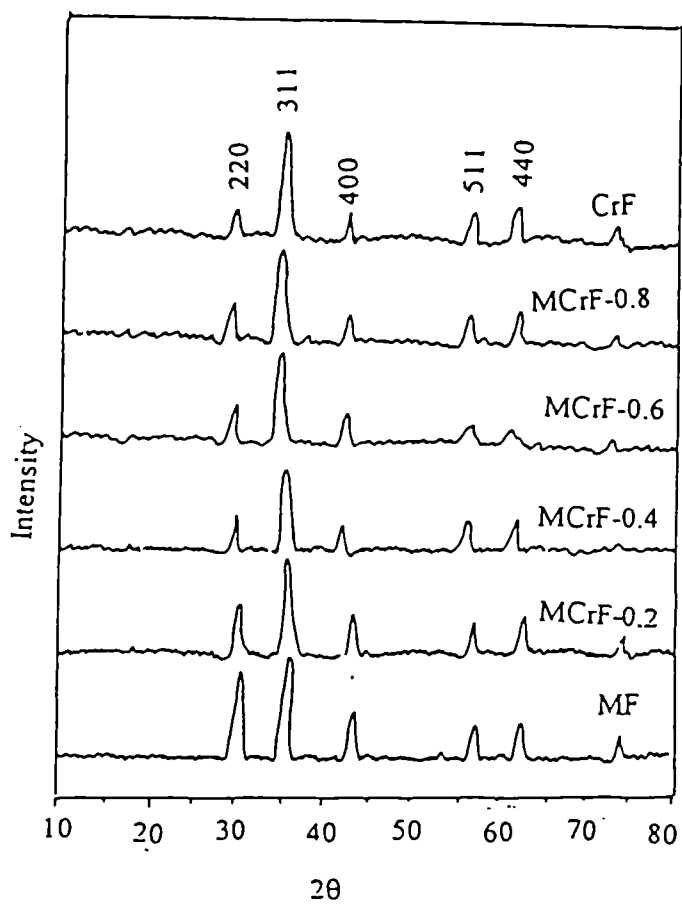


Fig. 3.1.2 XRD patterns of Cr_xMn_(1-x)Fe₂O₄ (x = 0, 0.2, 0.4, 0.6, 0.8 and 1)- systems.

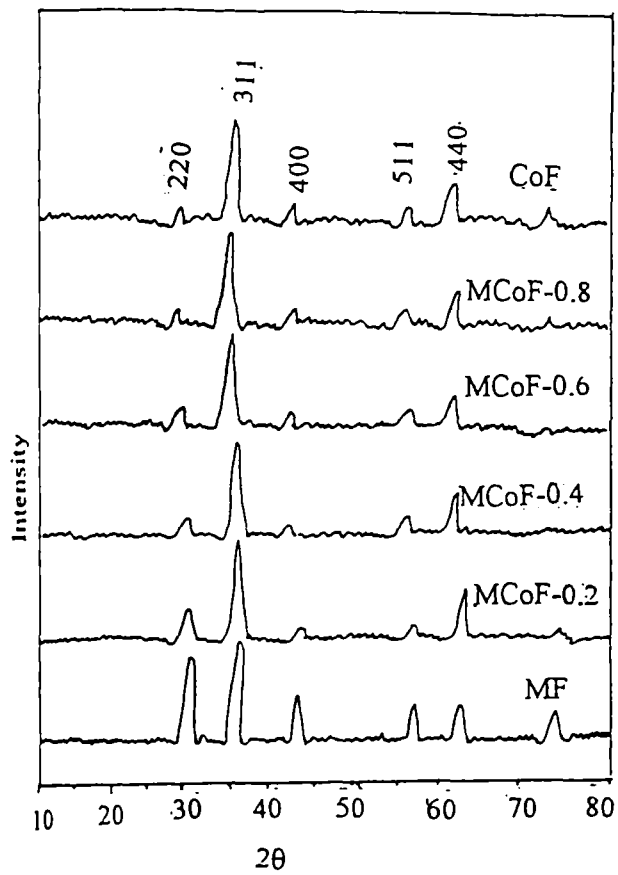


Fig 3.1.3 XRD patterns of $\text{Co}_x\text{Mn}_{(1-x)}\text{Fe}_2\text{O}_4$ ($x = 0, 0.2, 0.4, 0.6, 0.8$ and 1)- systems.

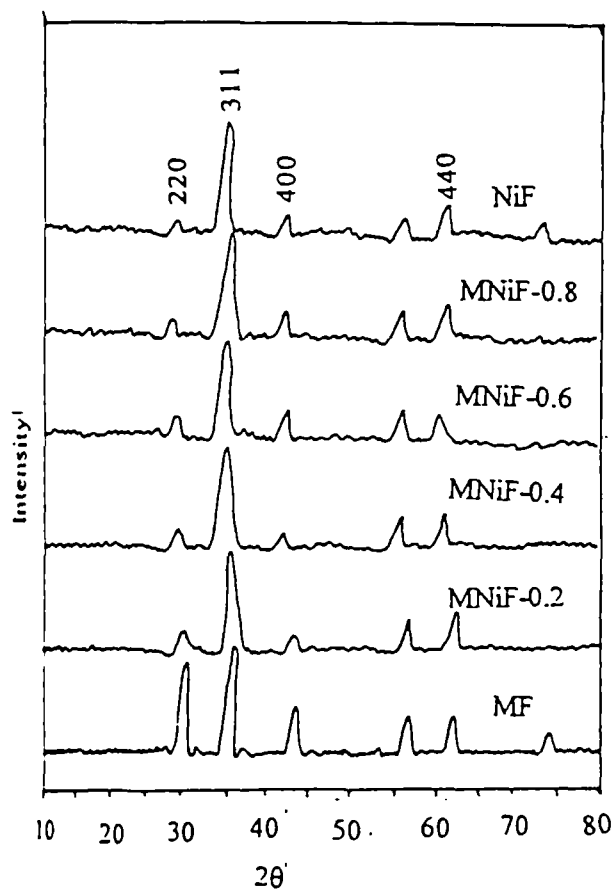


Fig 3.1.4 XRD patterns of $\text{Ni}_x\text{Mn}_{(1-x)}\text{Fe}_2\text{O}_4$ ($x = 0, 0.2, 0.4, 0.6, 0.8$ and 1)- systems.

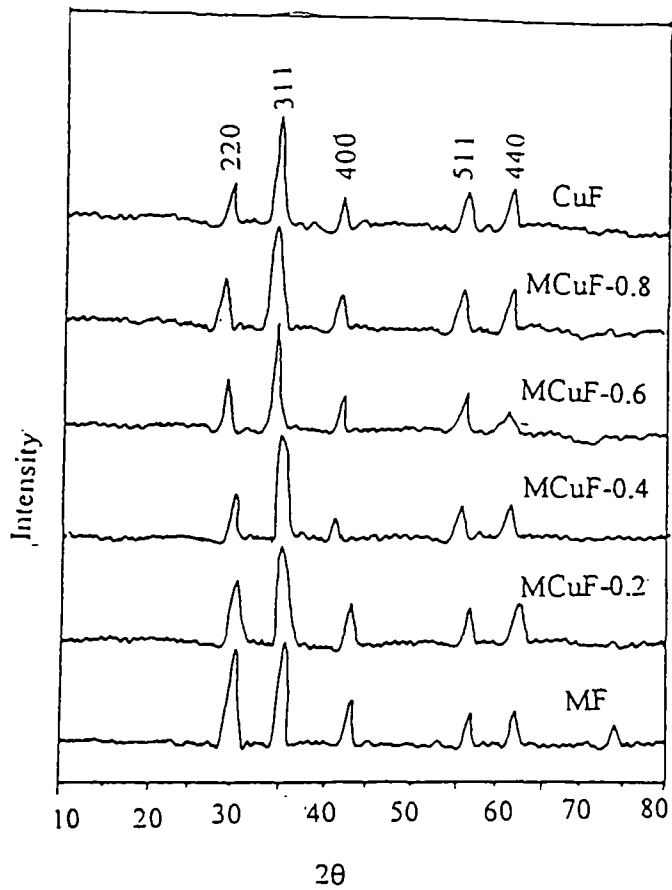


Fig. 3.1.5 XRD patterns of $\text{Cu}_x\text{Mn}_{1-x}\text{Fe}_2\text{O}_4$ ($x = 0, 0.2, 0.4, 0.6, 0.8$ and 1)- systems.

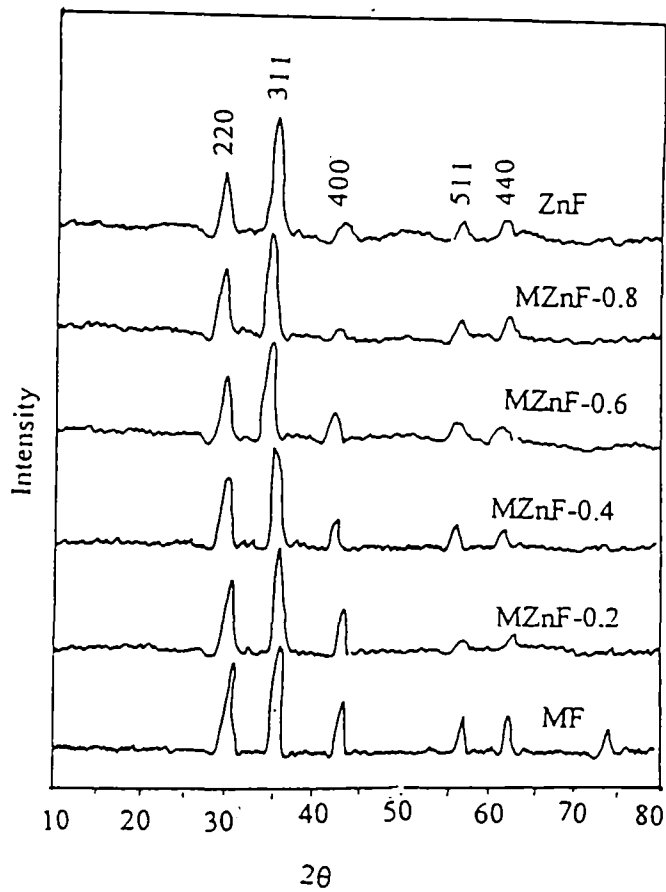


Fig. 3.1.6 XRD patterns of $\text{Zn}_x\text{Mn}_{1-x}\text{Fe}_2\text{O}_4$ ($x = 0, 0.2, 0.4, 0.6, 0.8$ and 1)- systems.

Table 3.1.1. Experimental and theoretical XRD data for simple ferros spinels.

Sample	System	JCPDS data		Experimental data		hkl
		I/I ₀	d _{hkl}	I/I ₀	d _{hkl}	
MnFe ₂ O ₄	Cubic	35	3.005	35	3.004	220
		100	2.553	100	2.551	311
		40	1.503	39	1.501	440
CrFe ₂ O ₄	Cubic	35	1.635	35	1.632	511
		30	2.902	30	2.901	220
		100	2.554	100	2.553	311
CoFe ₂ O ₄	Cubic	30	1.421	30	1.420	440
		35	1.618	35	1.615	511
		30	2.972	30	2.970	220
NiFe ₂ O ₄	Cubic	100	2.557	100	2.556	311
		35	1.483	35	1.485	440
		35	1.617	35	1.616	511
CuFe ₂ O ₄	Cubic	25	2.965	25	2.963	220
		100	2.559	100	2.558	311
		35	1.487	35	1.486	440
ZnFe ₂ O ₄	Cubic	30	1.612	30	1.610	511
		30	2.962	30	2.961	220
		100	2.560	100	2.559	311
ZnFe ₂ O ₄	Cubic	30	1.503	30	1.501	440
		25	1.613	25	1.611	511
		35	2.984	34	2.982	220
ZnFe ₂ O ₄	Cubic	100	2.563	100	2.563	311
		35	1.491	35	1.490	440
		30	1.624	30	1.623	511

The average crystallite size of the samples can be determined from the Scherrer equation:

$$t = 0.9 \lambda / \beta \cos \theta$$

where t = average particle size, λ = wavelength of the x-ray used, θ = glancing angle and β = FWHM (half the width of the peak with maximum intensity). The crystallite size of MnFe_2O_4 at different heat treatments is presented in Table 3.1.2. It can be seen that the crystallite size of the sample is increased with increase in calcination temperature. The crystallite size of different series of manganese ferrosinels is presented in Table 3.1.3. No significant observations can be attained from the crystallite size with reference to the various metal cation incorporation into the manganese ferrosinels.

Table 3.1.2. Heat treatment schedules and crystallite size Values of MnFe_2O_4 .

Heat treatment schedule	Crystallite size (nm)
Dried at 80°C/ 36 h	12
Calcined at 300°C/ 5 h	15
Calcined at 400°C/ 5 h	17
Calcined at 500°C/ 5 h	21

The qualitative phase analysis is based on the positions and intensities of the XRD peaks. It is observed that the different series of manganese ferrosinels under investigation are cubic. It is possible to derive mathematical relationship between unit cell parameter or lattice constant (a), interplanar spacing (d) and Miller Indices (hkl) and the relationship for the cubic system can be represented as:

$$d = a / (h^2 + l^2 + k^2)^{1/2}$$

Using this relationship, the lattice constants for various manganese ferrosinels are found out and are presented in Table 3.1.3. It was observed that the unit cell parameter vary with the ionic radii and the site occupancy of the incorporated metal cations. Thus the progressive incorporation of Cr^{3+} , Co^{2+} , Ni^{2+} and Cu^{2+} ions into the octahedral sites and Zn^{2+} ions into the tetrahedral sites of the manganese ferrite increased the lattice constant.

Table 3.1.3. Crystallite size and lattice constants of different series of manganese ferros spinels

Catalyst	Crystallite size (nm)	Lattice constant (Å)
MnFe ₂ O ₄	21.00	8.461
Cr _{0.2} Mn _{0.8} Fe ₂ O ₄	39.41	8.462
Cr _{0.4} Mn _{0.6} Fe ₂ O ₄	47.52	8.464
Cr _{0.6} Mn _{0.4} Fe ₂ O ₄	52.37	8.465
Cr _{0.8} Mn _{0.2} Fe ₂ O ₄	56.38	8.467
CrFe ₂ O ₄	58.11	8.468
Co _{0.2} Mn _{0.8} Fe ₂ O ₄	25.17	8.463
Co _{0.4} Mn _{0.6} Fe ₂ O ₄	30.01	8.467
Co _{0.6} Mn _{0.4} Fe ₂ O ₄	34.62	8.471
Co _{0.8} Mn _{0.2} Fe ₂ O ₄	36.55	8.475
CoFe ₂ O ₄	37.83	8.478
Ni _{0.2} Mn _{0.8} Fe ₂ O ₄	28.51	8.472
Ni _{0.4} Mn _{0.6} Fe ₂ O ₄	32.67	8.475
Ni _{0.6} Mn _{0.4} Fe ₂ O ₄	37.37	8.477
Ni _{0.8} Mn _{0.2} Fe ₂ O ₄	42.77	8.480
NiFe ₂ O ₄	45.30	8.484
Cu _{0.2} Mn _{0.8} Fe ₂ O ₄	23.59	8.472
Cu _{0.4} Mn _{0.6} Fe ₂ O ₄	27.19	8.478
Cu _{0.6} Mn _{0.4} Fe ₂ O ₄	30.23	8.482
Cu _{0.8} Mn _{0.2} Fe ₂ O ₄	33.58	8.485
CuFe ₂ O ₄	35.65	8.488
Zn _{0.2} Mn _{0.8} Fe ₂ O ₄	30.12	8.481
Zn _{0.4} Mn _{0.6} Fe ₂ O ₄	33.57	8.484
Zn _{0.6} Mn _{0.4} Fe ₂ O ₄	38.72	8.488
Zn _{0.8} Mn _{0.2} Fe ₂ O ₄	43.22	8.493
ZnFe ₂ O ₄	49.10	8.501

3.1.2 Scanning Electron Microgram (SEM) analysis

The scanning electron microgram of MnFe_2O_4 at three different calcination temperatures were taken and are presented in Fig. 3.1.7. The XRD data are supported by the observations from scanning electron micrographs. Fig. 3.1.7.(a) shows fine grains of uniform size of $\approx 5 \text{ \AA}$, Fig. 3.1.7.(b) presents larger grains of $\approx 50 \text{ \AA}$ and still larger and perfect grains of $\approx 500 \text{ \AA}$ are seen in Fig. 3.1.7.(c). The progressively increased grain growth or particle size is due to the higher calcination temperatures.

3.1.3 Inductively Coupled Plasma (ICP) analysis

The stoichiometry of the compositions of the prepared ferrite samples was checked by ICP analysis and the results obtained are given in Table 3.1.4. It has been found that there is a good agreement between the experimentally obtained weight percentage of the elements and the theoretically calculated weight percentage.

3.1.4. Diffuse Reflectance Infrared Fourier Transform (DRIFT) spectra

The DRIFT spectra of all samples calcined at 500°C were taken in the $400\text{-}1400 \text{ cm}^{-1}$ wave number region. The spectra typically show two strong infrared bands ν_1 and ν_2 around 700 cm^{-1} and 500 cm^{-1} respectively. The DRIFT spectra of representative manganese ferrites are shown in Fig. 3.1.8. According to Waldron *et al.* [3] and White *et al.* [4], the high frequency band at 700 cm^{-1} is due to the stretching vibration of the tetrahedral M-O bond and the low frequency band at 500 cm^{-1} is due to the vibration of the octahedral M-O bond. The basis for their conclusion is as follows:

In spinel lattice, every oxygen anion is bonded to three octahedral and one tetrahedral cation as shown in Fig. 3.1.8 (i). The three octahedral bonds are perpendicular to each other and provide an isotropic force field in the three directions if the tetrahedral bond was absent. The tetrahedral cation M_T introduces a supplementary force in a preferential direction along $M_T\text{-O}$ bond. This is responsible for the ν_1 mode in which the oxygen is forced to oscillate

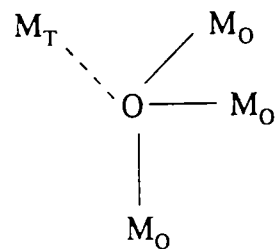
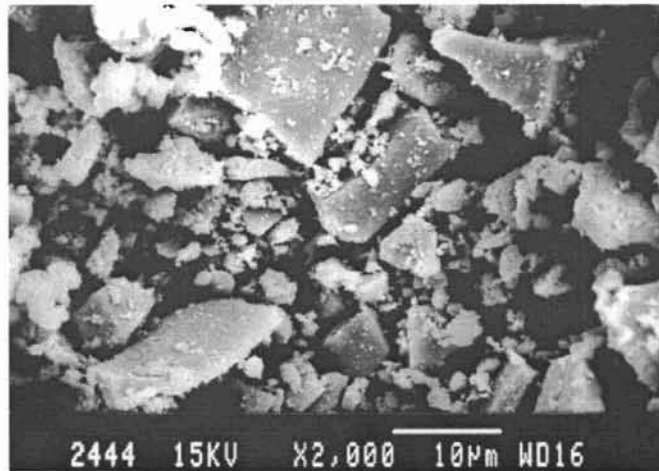
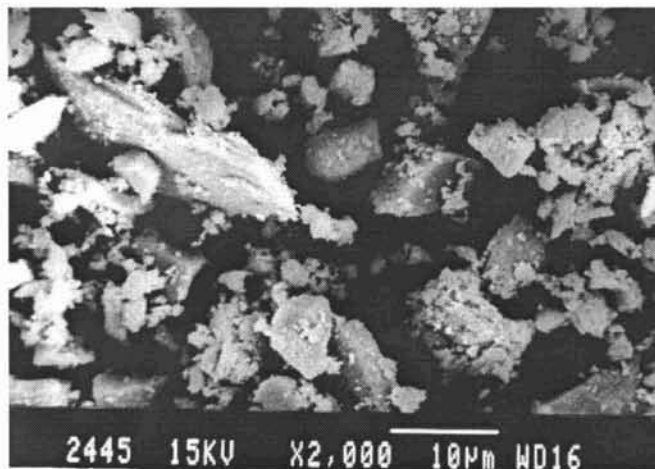


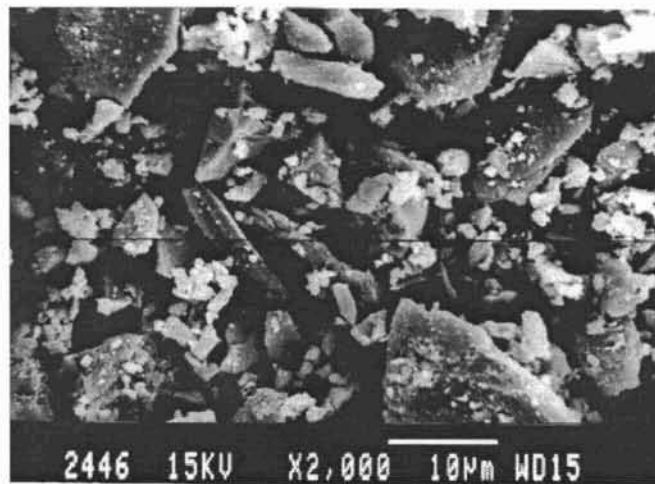
Fig.3.1.8 (i). The nearest neighbours of oxygen anion in the spinel lattice. M_T : tetrahedral cation and M_O : octahedral cation.



(a) 80°C



(b) 300°C



(c) 500°C

Fig. 3.1.7 Scanning electron micrographs (SEM) of MnFe_2O_4 calcined at different temperatures.

Table 3.1.4. ICP analysis data for different series of manganese ferrites

Catalyst composition	Metal ion concentration (wt %)	
$\text{Cr}_x\text{Mn}_{(1-x)}\text{Fe}_2\text{O}_4$ - series	Cr^{3+}	Mn^{2+} & Mn^{3+}
MnFe_2O_4	--	23.82 (23.82)
$\text{Cr}_{0.2}\text{Mn}_{0.8}\text{Fe}_2\text{O}_4$	4.50 (4.52)	19.09 (19.10)
$\text{Cr}_{0.4}\text{Mn}_{0.6}\text{Fe}_2\text{O}_4$	9.05 (9.06)	14.35 (14.36)
$\text{Cr}_{0.6}\text{Mn}_{0.4}\text{Fe}_2\text{O}_4$	13.63 (13.63)	9.59 (9.60)
$\text{Cr}_{0.8}\text{Mn}_{0.2}\text{Fe}_2\text{O}_4$	18.22 (18.22)	4.80 (4.81)
CrFe_2O_4	22.83 (22.83)	--
$\text{Co}_x\text{Mn}_{(1-x)}\text{Fe}_2\text{O}_4$ - series	Co^{2+}	Mn^{2+} & Mn^{3+}
MnFe_2O_4	--	23.82 (23.82)
$\text{Co}_{0.2}\text{Mn}_{0.8}\text{Fe}_2\text{O}_4$	5.08 (5.09)	18.99 (19.00)
$\text{Co}_{0.4}\text{Mn}_{0.6}\text{Fe}_2\text{O}_4$	10.14 (10.15)	14.19 (14.19)
$\text{Co}_{0.6}\text{Mn}_{0.4}\text{Fe}_2\text{O}_4$	15.16 (15.17)	9.43 (9.43)
$\text{Co}_{0.8}\text{Mn}_{0.2}\text{Fe}_2\text{O}_4$	20.15 (20.16)	4.68 (4.69)
CoFe_2O_4	25.12 (25.12)	--
$\text{Ni}_x\text{Mn}_{(1-x)}\text{Fe}_2\text{O}_4$ - series	Ni^{2+}	Mn^{2+} & Mn^{3+}
MnFe_2O_4	--	23.82 (23.82)
$\text{Ni}_{0.2}\text{Mn}_{0.8}\text{Fe}_2\text{O}_4$	5.05 (5.07)	18.98 (18.99)
$\text{Ni}_{0.4}\text{Mn}_{0.6}\text{Fe}_2\text{O}_4$	10.09 (10.11)	14.18 (14.19)
$\text{Ni}_{0.6}\text{Mn}_{0.4}\text{Fe}_2\text{O}_4$	15.12 (15.10)	9.43 (9.43)
$\text{Ni}_{0.8}\text{Mn}_{0.2}\text{Fe}_2\text{O}_4$	20.07 (20.09)	4.68 (4.70)
NiFe_2O_4	25.03 (25.04)	--
$\text{Cu}_x\text{Mn}_{(1-x)}\text{Fe}_2\text{O}_4$ - series	Cu^{2+}	Mn^{2+} & Mn^{3+}
MnFe_2O_4	--	23.82 (23.82)
$\text{Cu}_{0.2}\text{Mn}_{0.8}\text{Fe}_2\text{O}_4$	5.47 (5.47)	18.90 (18.91)
$\text{Cu}_{0.4}\text{Mn}_{0.6}\text{Fe}_2\text{O}_4$	9.92 (9.92)	14.06 (14.08)
$\text{Cu}_{0.6}\text{Mn}_{0.4}\text{Fe}_2\text{O}_4$	16.17 (16.17)	9.29 (9.31)
$\text{Cu}_{0.8}\text{Mn}_{0.2}\text{Fe}_2\text{O}_4$	21.40 (21.38)	4.60 (4.62)
CuFe_2O_4	26.55 (26.56)	--
$\text{Zn}_x\text{Mn}_{(1-x)}\text{Fe}_2\text{O}_4$ - series	Zn^{2+}	Mn^{2+} & Mn^{3+}
MnFe_2O_4	--	23.82 (23.82)
$\text{Zn}_{0.2}\text{Mn}_{0.8}\text{Fe}_2\text{O}_4$	5.62 (5.62)	18.86 (18.88)
$\text{Zn}_{0.4}\text{Mn}_{0.6}\text{Fe}_2\text{O}_4$	11.14 (11.14)	14.03 (14.04)
$\text{Zn}_{0.6}\text{Mn}_{0.4}\text{Fe}_2\text{O}_4$	16.56 (16.57)	10.76 (10.78)
$\text{Zn}_{0.8}\text{Mn}_{0.2}\text{Fe}_2\text{O}_4$	21.74 (21.75)	4.58 (4.59)
ZnFe_2O_4	27.12 (27.12)	--

* The quantities in the parentheses indicate theoretical values.

along the M_T-O bond, and thus appears as a stretching vibration of the tetrahedral group. Vibration of this group corresponds to the highest restoring force and thus assigned to the high-frequency absorption band. If we consider an oxygen vibration at right angles with the preceding one, the restoring force due to the tetrahedral cation M_T will be negligible. This leads to ν_2 modes, which may be considered as a stretching vibration of the octahedral bond. Thus, the appearance of two strong IR bands at around 700 cm^{-1} and 500 cm^{-1} confirmed the formation of spinel phase.

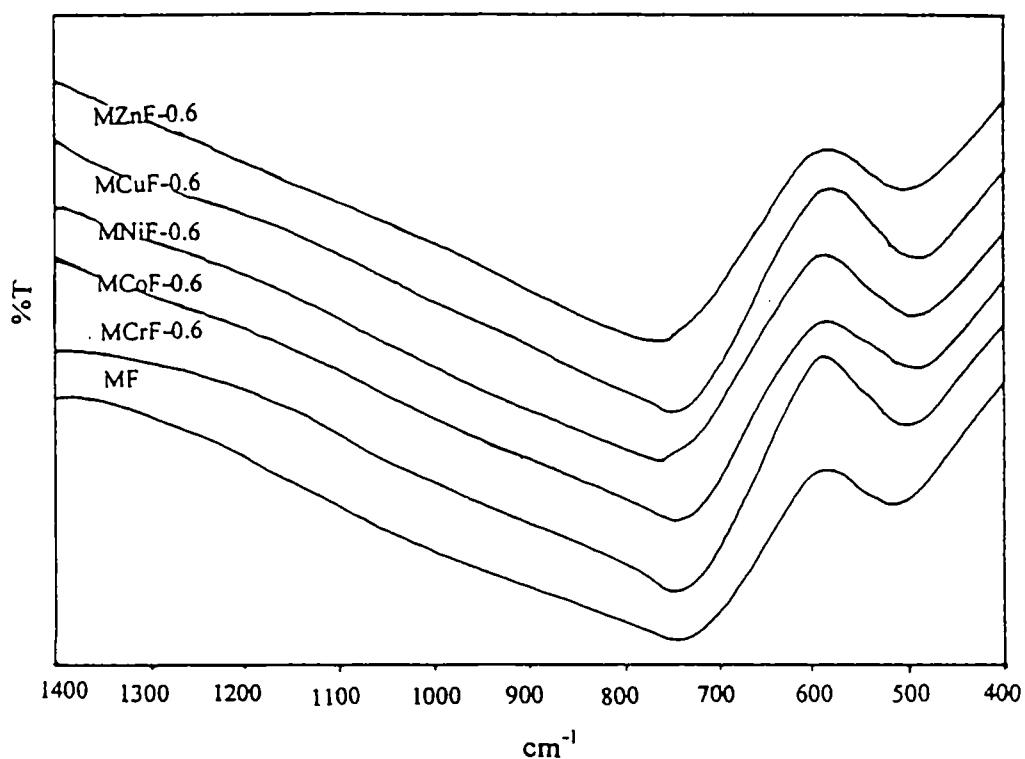


Fig. 3.1.8. DRIFT spectra of representative manganese ferros spinels

3.1.5 Thermogravimetric (TG) Analysis

The TGA curve for $MnFe_2O_4$ is plotted with percentage weight loss as a function of temperature (Fig. 3.1.9). The Fig. 3.1.9 is also fitted with the resultant derivative curve (DTG), which is plotted with the corresponding derivative of the percentage weight loss against the temperature. A sharp dip observed near 100°C is due to the desorption of the physisorbed water. The fairly horizontal behaviour of both the TG and DTG curves indicated the thermal stability of the sample. A small dip can be

observed in the 350 – 400°C temperature region. Since the sample is precipitated from the respective nitrate solutions, some amount of the nitrate may present in adsorbed form and the decomposition of nitrate at 350°C is responsible for the small dip in the TGA-DTG plot.

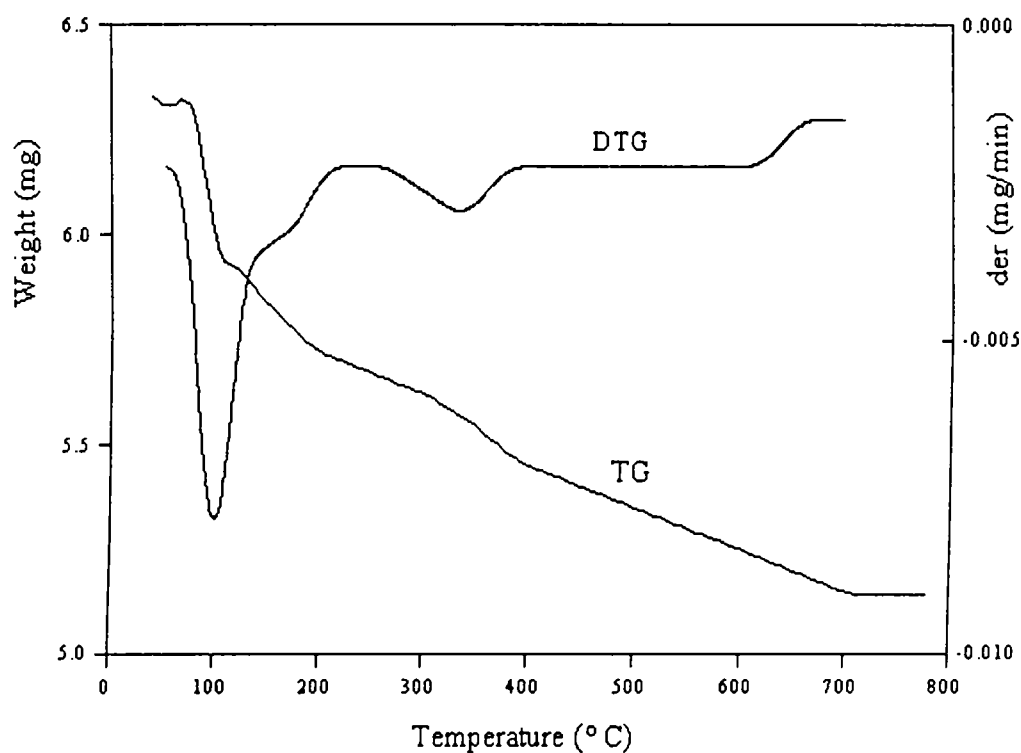


Fig. 3.1.9 TG-DTG curves of MnFe_2O_4

3.1.6 Surface area and pore volume measurements

The BET and Langmuir surface areas and total pore volume of the different compositions of the ferrite samples calcined at 500°C were measured by nitrogen adsorption at liquid nitrogen temperature (Micrometrics Gemini Analyzer). The data are shown in Table 3.1.5. The different series of ferrites prepared by the controlled low temperature co-precipitation technique possess high surface areas. It was observed that MnFe_2O_4 having the highest surface area among the manganese ferros spinels under investigation, possesses lowest average crystallite size calculated from the XRD line broadening (Table 3.1.3). The incorporation of metal cations such as Cr^{3+} , Co^{2+} , Ni^{2+} , Cu^{2+} and Zn^{2+} decreased the surface area to some extent.

Table 3.1.5. Surface areas and total pore volume of different series of manganese ferrospinels.

Catalyst	Surface Area (m ² /g)		Pore volume (cm ³ /g)
	BET	Langmuir	
MnFe ₂ O ₄	153.3	221.2	0.5023
Cr _{0.2} Mn _{0.8} Fe ₂ O ₄	65.32	100.96	0.1774
Cr _{0.4} Mn _{0.6} Fe ₂ O ₄	54.31	84.52	0.1730
Cr _{0.6} Mn _{0.4} Fe ₂ O ₄	47.58	77.31	0.1678
Cr _{0.8} Mn _{0.2} Fe ₂ O ₄	41.06	69.14	0.1514
CrFe ₂ O ₄	35.76	54.62	0.1430
Co _{0.2} Mn _{0.8} Fe ₂ O ₄	112.95	175.25	0.3875
Co _{0.4} Mn _{0.6} Fe ₂ O ₄	105.28	202.72	0.3836
Co _{0.6} Mn _{0.4} Fe ₂ O ₄	97.23	170.15	0.3789
Co _{0.8} Mn _{0.2} Fe ₂ O ₄	85.78	158.36	0.3719
CoFe ₂ O ₄	75.63	149.03	0.3614
Ni _{0.2} Mn _{0.8} Fe ₂ O ₄	103.3	202.2	0.3899
Ni _{0.4} Mn _{0.6} Fe ₂ O ₄	97.4	173.3	0.3830
Ni _{0.6} Mn _{0.4} Fe ₂ O ₄	86.8	166.2	0.3730
Ni _{0.8} Mn _{0.2} Fe ₂ O ₄	74.5	155.8	0.3690
NiFe ₂ O ₄	63.2	149.1	0.3386
Cu _{0.2} Mn _{0.8} Fe ₂ O ₄	137.56	218.59	0.4018
Cu _{0.4} Mn _{0.6} Fe ₂ O ₄	125.95	194.31	0.3967
Cu _{0.6} Mn _{0.4} Fe ₂ O ₄	118.65	184.23	0.3932
Cu _{0.8} Mn _{0.2} Fe ₂ O ₄	112.60	176.52	0.3897
CuFe ₂ O ₄	93.84	168.75	0.3792
Zn _{0.2} Mn _{0.8} Fe ₂ O ₄	95.68	162.91	0.2712
Zn _{0.4} Mn _{0.6} Fe ₂ O ₄	82.36	150.25	0.2701
Zn _{0.6} Mn _{0.4} Fe ₂ O ₄	74.23	141.26	0.2632
Zn _{0.8} Mn _{0.2} Fe ₂ O ₄	65.28	129.36	0.2491
ZnFe ₂ O ₄	56.31	106.75	0.2253

3.1.7 Transport studies

Recently the electrical properties of the ferrites attracted the attention of chemists as these characteristics have been found to play an important role in determining the catalytic activities and selectivities in reactions [5-7]. These properties vary drastically with the small changes in the composition of ferrite systems. The conductivity in ferrites arises due to the mobility of an extra electron (from Fe^{2+}) or positive hole (M^{3+}) through the crystal lattice [8]. The movement is ascribed by a hopping mechanism in which the charge carriers jump from one ionic site to the next.

DC electrical conductivity measurements (two-probe method) were made to determine the energy gap between the valence and conduction band (activation energy). To determine the type of charge carriers (electrons or holes) and their mobility in the system, Hall effect measurements were adopted.

3.1.7.1 DC electrical conductivity measurements

The determination of activation energy of solids by DC conductivity measurements has been well established [9-11]. Here, two-probe method was used for the conductivity study. The pelletized sample was kept in the conductivity cell and the corresponding current across the sample was determined. The resistance (R) can be calculated from the value of voltage and current using ohms law ($R = V/I$). Once R is known, resistivity (ρ) of the sample can be calculated by the formula, $\rho = RA/I$, where A is the area of the sample and I is the thickness of the sample. DC conductivity measurements of all the samples were measured from room temperature to 120°C. A voltage of 20 V was applied across the pellet. The room temperature conductivity values of all the samples varied between 10^{-6} and $10^{-3} \Omega^{-1} \text{cm}^{-1}$. The electrical conductivity-temperature behaviour was found to obey Wilson's law, $\sigma_{dc} = \sigma_0 \exp(E_a/\kappa T)$. Here σ_{dc} is the conductivity in $\Omega^{-1} \text{cm}^{-1}$, T is the absolute temperature, κ is the Boltzmann constant, E_a is the activation energy and σ_0 is the y intercept obtained by plotting $\ln \sigma_{dc}$ at different temperatures against $10^3/\kappa T$. This indicated the semiconducting behaviour of all the compounds under investigation. The activation energy calculated for different series of manganese ferros spinels is shown in Table 3.1.6.

Table 3.1.6. Activation energy for different series of manganese ferrosinels

Catalyst	Activation Energy (eV)
MnFe ₂ O ₄	0.400
Cr _{0.2} Mn _{0.8} Fe ₂ O ₄	0.560
Cr _{0.4} Mn _{0.6} Fe ₂ O ₄	0.608
Cr _{0.6} Mn _{0.4} Fe ₂ O ₄	0.667
Cr _{0.8} Mn _{0.2} Fe ₂ O ₄	0.701
CrFe ₂ O ₄	0.748
Co _{0.2} Mn _{0.8} Fe ₂ O ₄	0.247
Co _{0.4} Mn _{0.6} Fe ₂ O ₄	0.201
Co _{0.6} Mn _{0.4} Fe ₂ O ₄	0.182
Co _{0.8} Mn _{0.2} Fe ₂ O ₄	0.166
CoFe ₂ O ₄	0.140
Ni _{0.2} Mn _{0.8} Fe ₂ O ₄	0.411
Ni _{0.4} Mn _{0.6} Fe ₂ O ₄	0.450
Ni _{0.6} Mn _{0.4} Fe ₂ O ₄	0.482
Ni _{0.8} Mn _{0.2} Fe ₂ O ₄	0.513
NiFe ₂ O ₄	0.557
Cu _{0.2} Mn _{0.8} Fe ₂ O ₄	0.301
Cu _{0.4} Mn _{0.6} Fe ₂ O ₄	0.265
Cu _{0.6} Mn _{0.4} Fe ₂ O ₄	0.225
Cu _{0.8} Mn _{0.2} Fe ₂ O ₄	0.272
CuFe ₂ O ₄	0.295
Zn _{0.2} Mn _{0.8} Fe ₂ O ₄	0.571
Zn _{0.4} Mn _{0.6} Fe ₂ O ₄	0.689
Zn _{0.6} Mn _{0.4} Fe ₂ O ₄	0.741
Zn _{0.8} Mn _{0.2} Fe ₂ O ₄	0.829
ZnFe ₂ O ₄	0.917

(a) $\text{Cr}_x\text{Mn}_{(1-x)}\text{Fe}_2\text{O}_4$ - type systems ($x = 0, 0.2, 0.4, 0.6, 0.8$ and 1.0)

It can be seen from Table 3.1.6 that the progressive substitution of Mn by Cr proportionately increases the activation energy in this series of ferrites. Increase of Cr^{3+} ion concentration in the octahedral sites of manganese ferrites increases the activation energy for electrical conduction from 0.400 to 0.888 eV. Cr^{3+} being a d^3 ($t_{2g}^3 e_g^0$ – half-filled t_{2g} state) system is very stable and its orbitals have much lower energy than Mn^{3+} ($d^4 - t_{2g}^3 e_g^1$). Replacement of smaller Mn^{3+} by larger Cr^{3+} ions in the octahedral sites increases the lattice constant. These factors are accounted for the increased activation energy.

(b) $\text{Co}_x\text{Mn}_{(1-x)}\text{Fe}_2\text{O}_4$ - type systems ($x = 0, 0.2, 0.4, 0.6, 0.8$ and 1.0)

It is evident from Table 3.1.6 that the successive substitution of Mn by Co decreases the activation energy. The addition of Co^{2+} ions in the octahedral sites of pure manganese ferrite decreases the energy gap from 0.400 to 0.140 eV. Co^{2+} , a d^7 ($t_{2g}^6 e_g^1$) system, possesses high energy and its orbitals are unstable. This factor is mainly responsible for the low activation energy of this series of ferrites.

(c) $\text{Ni}_x\text{Mn}_{(1-x)}\text{Fe}_2\text{O}_4$ - type systems ($x = 0, 0.2, 0.4, 0.6, 0.8$ and 1.0)

The progressive replacement of Mn by Ni in the pure manganese ferrite increases the activation energy of the series. The added Ni^{2+} ions those entered into the octahedral sites increase the activation energy from 0.400 to 0.557 eV. In this case, Ni^{2+} is a d^8 ($t_{2g}^6 e_g^2$ – half filled e_g state) system, which is stable and its orbitals possess lower energy than the Mn^{3+} ion which has d^4 ($t_{2g}^3 e_g^1$) configuration. Also the ionic radius of Ni^{2+} is larger than the ionic radius of Mn^{3+} . This increases the lattice constant of the series. These two factors synergistically increase the activation energy of this series.

(d) $\text{Cu}_x\text{Mn}_{(1-x)}\text{Fe}_2\text{O}_4$ - type systems ($x = 0, 0.2, 0.4, 0.6, 0.8$ and 1.0)

The successive Cu doping into the octahedral sites of the manganese ferrite first decreases the activation energy up to $x = 0.6$ (from 0.400 to 0.225 eV) and increased gradually with increase in 'x' value. Cu^{2+} is a d^9 ($t_{2g}^6 e_g^3$) system. So, it is highly unstable and has much higher energy than Mn^{3+} ions. But the ionic radius of Cu^{2+} is higher than the ionic radius of Mn^{3+} and this increases the lattice constant of the series.

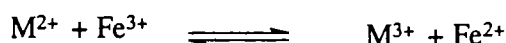
The increase in ionic radius is the predominating factor, which accounts for the high activation energy at larger 'x' values.

(e) $Zn_xMn_{(1-x)}Fe_2O_4$ - type systems (x = 0, 0.2, 0.4, 0.6, 0.8 and 1.0)

Since Zn^{2+} ions prefer tetrahedral sites rather than octahedral sites, the added Zn ions make their accumulation in the tetrahedral sites. The activation energy of the series increases appreciably from 0.400 eV to 0.917 eV with increase in 'x' values. The Zn^{2+} ion, a d^{10} ($t_{2g}^6 e_g^{10}$ – completely filled t_{2g} and e_g states) system is highly stable and its orbitals possess much lower energy than the Mn^{3+} ions. Moreover, the ionic radius of Zn^{2+} is much higher than Mn^{3+} , which increased the lattice parameter. These factors together account the high activation energy of this series.

3.1.7.2 Hall effect measurements

Hall effect is widely used in the interpretation of conduction mechanism in ferrites [12-16]. The interpretation of Hall effect is straightforward and gives precise results. Hall effect measurements were used to determine the concentration, mobility and nature of current carriers in manganese ferros spinels. Here we used a four-probe method. The sign of the thermo emf gives vital information about the type of conduction in semiconductors: whether it is p-type or n-type. If the sign of the thermo emf is positive, the conduction is p-type and if it is negative, the conduction is n-type. The conduction mechanism in manganese ferros spinels can be represented as:

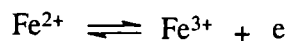


where M = Mn or the incorporated metal. Thus the conduction mechanism in n-type ferrites is predominantly due to the hopping of electrons from Fe^{2+} to Fe^{3+} ions. On the other hand, the conduction mechanism in p-type ferrites can be ascribed to the jumping of holes between M^{3+} and M^{2+} ions. The mechanism of the electrical conduction in manganese ferros spinels can be explained in terms of the oxidation of Fe^{2+} ions by M^{3+} ions on octahedral sites. The type of charge carriers, amount of carriers and the mobility of the carriers of different series of manganese ferrites are shown in Table 3.1.7.

Table 3.1.7. Data for different series of manganese ferros spinels obtained from Hall effect measurements

Catalyst	Type of charge carriers	Amount of charge carriers (cm ⁻³)	Mobility (cm ² /V s)
MnFe ₂ O ₄	electrons	2.60 x 10 ¹³	- 84.20
Cr _{0.2} Mn _{0.8} Fe ₂ O ₄	holes	2.07 x 10 ⁹	+ 0.58
Cr _{0.4} Mn _{0.6} Fe ₂ O ₄	holes	2.79 x 10 ⁹	+ 0.67
Cr _{0.6} Mn _{0.4} Fe ₂ O ₄	holes	3.76 x 10 ⁹	+ 0.76
Cr _{0.8} Mn _{0.2} Fe ₂ O ₄	holes	4.37 x 10 ⁹	+ 0.84
CrFe ₂ O ₄	holes	4.52 x 10 ⁹	+ 0.93
Co _{0.2} Mn _{0.8} Fe ₂ O ₄	holes	1.03 x 10 ¹²	+ 2.58
Co _{0.4} Mn _{0.6} Fe ₂ O ₄	holes	6.83 x 10 ¹²	+ 3.07
Co _{0.6} Mn _{0.4} Fe ₂ O ₄	holes	12.37 x 10 ¹²	+ 3.36
Co _{0.8} Mn _{0.2} Fe ₂ O ₄	holes	18.32 x 10 ¹²	+ 3.64
CoFe ₂ O ₄	holes	28.57 x 10 ¹²	+ 3.97
Ni _{0.2} Mn _{0.8} Fe ₂ O ₄	holes	0.03 x 10 ¹⁰	+ 1.85
Ni _{0.4} Mn _{0.6} Fe ₂ O ₄	holes	4.23 x 10 ¹⁰	+ 2.31
Ni _{0.6} Mn _{0.4} Fe ₂ O ₄	holes	8.37 x 10 ¹⁰	+ 2.66
Ni _{0.8} Mn _{0.2} Fe ₂ O ₄	holes	11.63 x 10 ¹⁰	+ 2.81
NiFe ₂ O ₄	holes	14.07 x 10 ¹⁰	+ 3.12
Cu _{0.2} Mn _{0.8} Fe ₂ O ₄	holes	0.07 x 10 ¹³	+ 1.38
Cu _{0.4} Mn _{0.6} Fe ₂ O ₄	holes	1.18 x 10 ¹³	+ 1.79
Cu _{0.6} Mn _{0.4} Fe ₂ O ₄	holes	3.78 x 10 ¹³	+ 1.86
Cu _{0.8} Mn _{0.2} Fe ₂ O ₄	holes	9.72 x 10 ¹³	+ 1.94
CuFe ₂ O ₄	holes	13.76 x 10 ¹³	+ 2.12
Zn _{0.2} Mn _{0.8} Fe ₂ O ₄	holes	0.12 x 10 ¹¹	+ 2.18
Zn _{0.4} Mn _{0.6} Fe ₂ O ₄	holes	1.01 x 10 ¹¹	+ 2.99
Zn _{0.6} Mn _{0.4} Fe ₂ O ₄	holes	4.66 x 10 ¹¹	+ 3.16
Zn _{0.8} Mn _{0.2} Fe ₂ O ₄	holes	10.52 x 10 ¹¹	+ 3.34
ZnFe ₂ O ₄	holes	15.18 x 10 ¹¹	+ 3.62

It can be seen from Table 3.1.7 that except for MnFe_2O_4 , in all the other systems holes are the majority charge carriers. In MnFe_2O_4 , electrons are the charge carriers and n-type conduction is operating. Therefore for this n-type ferrite, the most probable mechanism is electron hopping between Fe^{2+} and Fe^{3+} ions as:



This process is expected to take place between two adjacent octahedral sites in a spinel lattice. Also it is observed that the concentration and mobility of these charge carriers (electrons) in the system are highly appreciable. On incorporating metal cations into MnFe_2O_4 the charge carriers are shifted from electrons to holes. Though the concentration of holes are comparable with the concentration of electrons, their mobility is much less than that of electrons present in MnFe_2O_4 .

3.1.8. Mössbauer Spectra

In catalysis, Mössbauer spectroscopy is primarily employed for the characterization of catalysts. This technique gives a better understanding of the oxidation state [17-19], phase transitions [20], magnetic properties [21] and electronic environment of the Mössbauer active elements in the catalysts and of the particle size of the samples. The room temperature Mössbauer spectrum of MnFe_2O_4 calcined at 500°C is given in Fig. 3.1.10. The Mössbauer spectrum is fitted with two partially superimposed sextets and one doublet. The Mössbauer parameters for the spectrum are given in Table 3.1.8.

The Mössbauer spectrum of MnFe_2O_4 is composed of two sextets with hyperfine fields 51.26 and 48.43 T, corresponding to octahedral and tetrahedral sites, respectively [22-24].

The isomer shift (δ) values were found out with respect to the metallic iron (^{57}Fe). The spectrum of ferric iron is shifted in a positive direction relative to the metallic iron because of the decrease in electronic charge density at its nucleus following the loss of the 4s electrons. The spectrum of the ferrous iron is shifted to even larger positive velocities because of the screening effect of the additional 3d electrons on the 3s electrons which increases the radial distribution of 3s electrons and further decreases

Table 3.1.8 Mössbauer parameters of MnFe_2O_4 .

Type of splitting	Isomer shift (δ) (± 0.02 mm/s)	Quadrupole splitting (Δ) (± 0.04 mm/s)	Line width (± 0.04 mm/s)	Intensity (%)
Sextets				
Hyperfine field (51.26 T)	0.50	-0.11	0.70	40.80
Hyperfine field (48.43 T)	0.40	-0.21	0.48	52.78
Doublet	0.24 ± 0.02	0.81	0.97	59.20

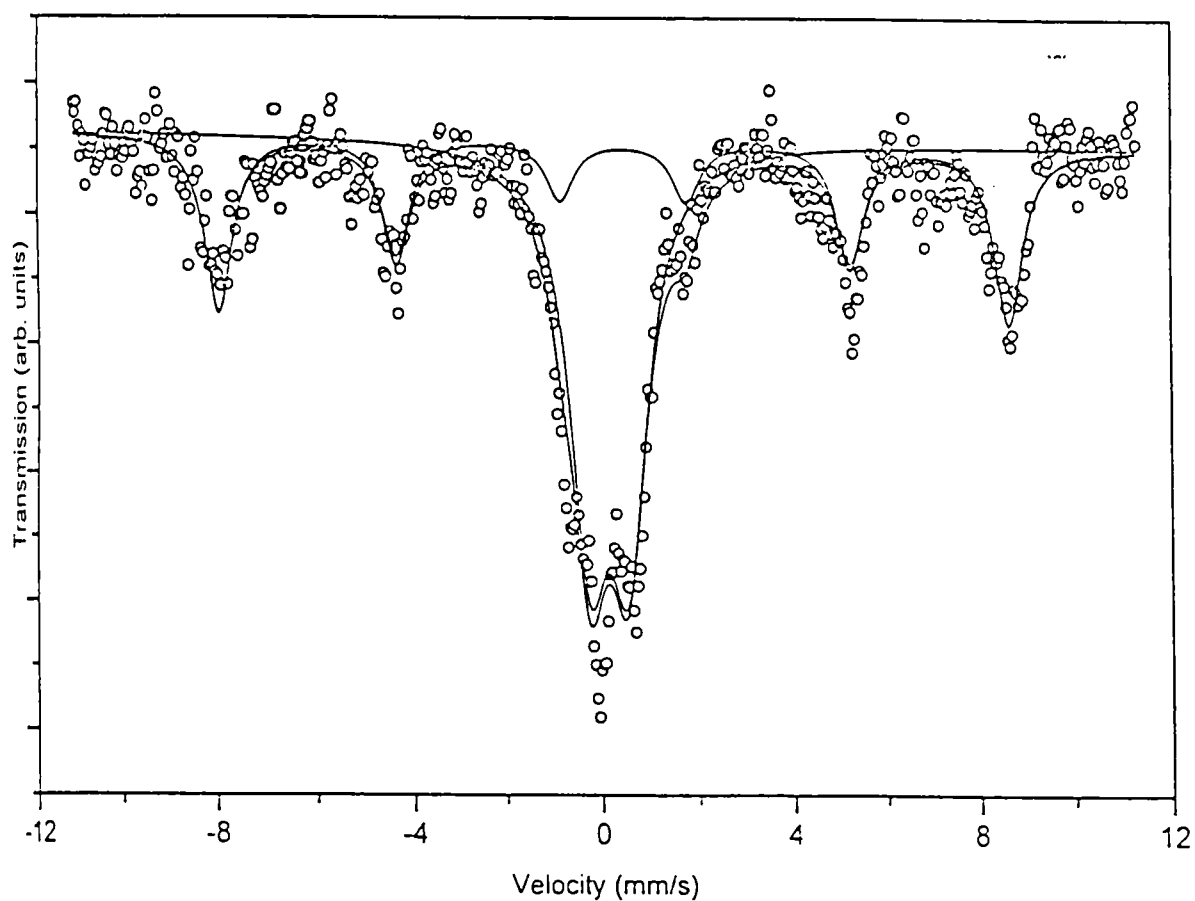


Fig. 3.1.10. The room temperature Mössbauer spectrum of MnFe_2O_4 calcined at 500°C

their electron charge density at the nucleus. The magnitude of the effects may vary over wide ranges depending on covalency effects and spin states. In ferrites, Fe^{2+} ions are d^6 ($t_{2g}^4 e_g^2$) systems with $0.4 \Delta_o$ crystal field stabilization energy and Fe^{3+} ions are d^5 ($t_{2g}^3 e_g^2$) systems with zero crystal field stabilization energy due to oxygen anions. The characteristic Mössbauer isomer shift range for Fe^{2+} is within 1.10 to 1.30 mm/s [25] and for Fe^{3+} , it is within 0.2 to 0.5 mm/s [26] with respect to the metallic iron. The isomer shift values (δ) from both the doublet and sextets correspond to Fe^{3+} ions, both in the tetrahedral and octahedral sites. Since MnFe_2O_4 is a partially inverse spinel, we expect Fe^{2+} ions in the octahedral sites. But, isomer shift values corresponding to Fe^{2+} ions are not observed. It is because the concentration of Fe^{2+} ions in the system is much lower when compared to the concentration of Fe^{3+} ions. Also, due to the presence of Fe^{2+} and Fe^{3+} ions in the octahedral sites, the difference in the two valence states is averaged out by rapid electron exchange at room temperature. It is evident from Table 3.1.8 that δ values of Fe^{3+} ions in the octahedral site (hyperfine field- 51.26 T) is 0.10 mm/s more positive than the Fe^{3+} ions in the tetrahedral site (hyperfine field- 48.43 T).

The quadrupolar splitting (Δ) exhibited by ^{57}Fe reflected the asymmetry of the electric field gradient (EFG) experienced by Fe^{3+} and Fe^{2+} ions in the system. In the case of Fe^{2+} ion, the EFG at ^{57}Fe nucleus may be due to the non-spherical distribution of 3d electrons ($t_{2g}^4 e_g^2$). However, Fe^{3+} ion possesses half filled 3d configuration ($t_{2g}^3 e_g^2$), the EFG arises from the neighbouring ions. Since MnFe_2O_4 is 50% inverted [27], the tetrahedral site contains Mn^{2+} and Fe^{3+} ions. Both these ions are d^5 systems. The Fe^{3+} ion experiences no chemical disorder and hence the tetrahedral sites have no EFG. The cubic symmetry of the tetrahedral site is thus maintained. But the octahedral Fe^{3+} ions experience EFG due to the surrounded metal ions of large size and asymmetric distribution of electrons and also due to the surrounded oxygen anions. Thus, the crystallographic site of Fe^{3+} ions in the octahedral site does not have a cubic symmetry, but a trigonal symmetry.

The Mössbauer line widths are a measure of the chemical disorder around the Mössbauer nuclei. So, it is clear from the Table 3.1.8 that the chemical disorder around the Mössbauer nuclei in octahedral site is more than that in the tetrahedral site.

For materials exhibiting magnetic ordering the degeneracy of the nuclear spin state is lifted and the Mössbauer spectrum will be characterized by a hyperfine pattern. The Mössbauer spectrum of MnFe_2O_4 is composed of two partially superimposed six-line spectra (sextet). Hence MnFe_2O_4 possesses magnetic behaviour. Gager and Hobson [28] observed two superimposed hyperfine pattern for magnetite. According to them these are due to the hyperfine splitting of Fe^{3+} ion in the tetrahedral site and hyperfine splitting of Fe^{2+} and Fe^{3+} ions in the octahedral site. It can be observed from Fig.3.1.10 that at the lower velocity region of the spectrum, the superimposed hyperfine lines corresponding to the transitions associated with the tetrahedral and octahedral sites are somewhat resolved. The line width of the transitions associated with the tetrahedral sites are temperature independent while that of transitions related with octahedral sites increases with decrease in temperature. The decrease in temperature slows down the electron exchange between the Fe^{2+} and Fe^{3+} ions and thus both the Fe centre can be distinguished in the spectrum.

3.1.9. Cation distribution

The cation distribution of the different series of manganese ferros spinels can be found out from the X-ray intensity calculations [29], Mössbauer spectral analysis data [30-32] and theoretical calculations. Table 3.1.9 gives the cation valency distribution of five series of manganese ferros spinels. It can be seen that the partially inverse MnFe_2O_4 , is turned to fully inverse CrFe_2O_4 by the step-wise increment of Cr ions into the octahedral sites of the former. The same trend is observed for the other systems like $\text{Co}_x\text{Mn}_{(1-x)}\text{Fe}_2\text{O}_4$, $\text{Ni}_x\text{Mn}_{(1-x)}\text{Fe}_2\text{O}_4$ and $\text{Cu}_x\text{Mn}_{(1-x)}\text{Fe}_2\text{O}_4$. But in the case of $\text{Zn}_x\text{Mn}_{(1-x)}\text{Fe}_2\text{O}_4$ system, the successive incorporation of zinc ions changed the partially inverse manganese ferros spinel to the normal spinel, ZnFe_2O_4 . We have observed that the type and concentration of metal ions in the tetrahedral and octahedral sites of different series of manganese ferros spinels play a crucial role in their surface properties and catalytic activities.

Table 3.1.9 Cation distribution of different manganese ferros spinels.

Catalyst	Cation valency distribution
MnFe ₂ O ₄	(Mn _{0.5} ²⁺ Fe _{0.5} ³⁺) _{tet} [Fe _{0.5} ²⁺ Fe ³⁺ Mn _{0.5} ³⁺] _{oct} O ₄ ²⁻
Cr _{0.2} Mn _{0.8} Fe ₂ O ₄	(Mn _{0.4} ²⁺ Fe _{0.6} ³⁺) _{tet} [Fe _{0.6} ²⁺ Fe _{0.8} ³⁺ Mn _{0.4} ³⁺ Cr _{0.2} ³⁺] _{oct} O ₄ ²⁻
Cr _{0.4} Mn _{0.6} Fe ₂ O ₄	(Mn _{0.3} ²⁺ Fe _{0.7} ³⁺) _{tet} [Fe _{0.7} ²⁺ Fe _{0.6} ³⁺ Mn _{0.3} ³⁺ Cr _{0.4} ³⁺] _{oct} O ₄ ²⁻
Cr _{0.6} Mn _{0.4} Fe ₂ O ₄	(Mn _{0.2} ²⁺ Fe _{0.8} ³⁺) _{tet} [Fe _{0.8} ²⁺ Fe _{0.4} ³⁺ Mn _{0.2} ³⁺ Cr _{0.6} ³⁺] _{oct} O ₄ ²⁻
Cr _{0.8} Mn _{0.2} Fe ₂ O ₄	(Mn _{0.1} ²⁺ Fe _{0.9} ³⁺) _{tet} [Fe _{0.9} ²⁺ Fe _{0.2} ³⁺ Mn _{0.1} ³⁺ Cr _{0.8} ³⁺] _{oct} O ₄ ²⁻
CrFe ₂ O ₄	(Fe ³⁺) _{tet} [Fe ²⁺ Cr ³⁺] _{oct} O ₄ ²⁻
Co _{0.2} Mn _{0.8} Fe ₂ O ₄	(Mn _{0.4} ²⁺ Fe _{0.6} ³⁺) _{tet} [Fe _{0.4} ²⁺ Fe ₁ ³⁺ Mn _{0.4} ³⁺ Co _{0.2} ²⁺] _{oct} O ₄ ²⁻
Co _{0.4} Mn _{0.6} Fe ₂ O ₄	(Mn _{0.3} ²⁺ Fe _{0.7} ³⁺) _{tet} [Fe _{0.3} ²⁺ Fe ₁ ³⁺ Mn _{0.3} ³⁺ Co _{0.4} ²⁺] _{oct} O ₄ ²⁻
Co _{0.6} Mn _{0.4} Fe ₂ O ₄	(Mn _{0.2} ²⁺ Fe _{0.8} ³⁺) _{tet} [Fe _{0.2} ²⁺ Fe ₁ ³⁺ Mn _{0.2} ³⁺ Co _{0.6} ²⁺] _{oct} O ₄ ²⁻
Co _{0.8} Mn _{0.2} Fe ₂ O ₄	(Mn _{0.1} ²⁺ Fe _{0.9} ³⁺) _{tet} [Fe _{0.1} ²⁺ Fe ₁ ³⁺ Mn _{0.1} ³⁺ Co _{0.8} ²⁺] _{oct} O ₄ ²⁻
CoFe ₂ O ₄	(Fe ³⁺) _{tet} [Fe ³⁺ Co ³⁺] _{oct} O ₄ ²⁻
Ni _{0.2} Mn _{0.8} Fe ₂ O ₄	(Mn _{0.4} ²⁺ Fe _{0.6} ³⁺) _{tet} [Fe _{0.4} ²⁺ Fe ₁ ³⁺ Mn _{0.4} ³⁺ Ni _{0.2} ²⁺] _{oct} O ₄ ²⁻
Ni _{0.4} Mn _{0.6} Fe ₂ O ₄	(Mn _{0.3} ²⁺ Fe _{0.7} ³⁺) _{tet} [Fe _{0.3} ²⁺ Fe ₁ ³⁺ Mn _{0.3} ³⁺ Ni _{0.4} ²⁺] _{oct} O ₄ ²⁻
Ni _{0.6} Mn _{0.4} Fe ₂ O ₄	(Mn _{0.2} ²⁺ Fe _{0.8} ³⁺) _{tet} [Fe _{0.2} ²⁺ Fe ₁ ³⁺ Mn _{0.2} ³⁺ Ni _{0.6} ²⁺] _{oct} O ₄ ²⁻
Ni _{0.8} Mn _{0.2} Fe ₂ O ₄	(Mn _{0.1} ²⁺ Fe _{0.9} ³⁺) _{tet} [Fe _{0.1} ²⁺ Fe ₁ ³⁺ Mn _{0.1} ³⁺ Ni _{0.8} ²⁺] _{oct} O ₄ ²⁻
NiFe ₂ O ₄	(Fe ³⁺) _{tet} [Fe ³⁺ Ni ²⁺] _{oct} O ₄ ²⁻
Cu _{0.2} Mn _{0.8} Fe ₂ O ₄	(Mn _{0.4} ²⁺ Fe _{0.6} ³⁺) _{tet} [Fe _{0.4} ²⁺ Fe ₁ ³⁺ Mn _{0.4} ³⁺ Cu _{0.2} ²⁺] _{oct} O ₄ ²⁻
Cu _{0.4} Mn _{0.6} Fe ₂ O ₄	(Mn _{0.3} ²⁺ Fe _{0.7} ³⁺) _{tet} [Fe _{0.3} ²⁺ Fe ₁ ³⁺ Mn _{0.3} ³⁺ Cu _{0.4} ²⁺] _{oct} O ₄ ²⁻
Cu _{0.6} Mn _{0.4} Fe ₂ O ₄	(Mn _{0.2} ²⁺ Fe _{0.8} ³⁺) _{tet} [Fe _{0.2} ²⁺ Fe ₁ ³⁺ Mn _{0.2} ³⁺ Cu _{0.6} ²⁺] _{oct} O ₄ ²⁻
Cu _{0.8} Mn _{0.2} Fe ₂ O ₄	(Mn _{0.1} ²⁺ Fe _{0.9} ³⁺) _{tet} [Fe _{0.1} ²⁺ Fe ₁ ³⁺ Mn _{0.1} ³⁺ Cu _{0.8} ²⁺] _{oct} O ₄ ²⁻
CuFe ₂ O ₄	(Fe ³⁺) _{tet} [Fe ³⁺ Cu ²⁺] _{oct} O ₄ ²⁻
Zn _{0.2} Mn _{0.8} Fe ₂ O ₄	(Zn _{0.2} ²⁺ Mn _{0.4} ²⁺ Fe _{0.4} ³⁺) _{tet} [Fe _{0.4} ²⁺ Fe _{1.2} ³⁺ Mn _{0.4} ³⁺] _{oct} O ₄ ²⁻
Zn _{0.4} Mn _{0.6} Fe ₂ O ₄	(Zn _{0.4} ²⁺ Mn _{0.3} ²⁺ Fe _{0.3} ³⁺) _{tet} [Fe _{0.3} ²⁺ Fe _{1.4} ³⁺ Mn _{0.3} ³⁺] _{oct} O ₄ ²⁻
Zn _{0.6} Mn _{0.4} Fe ₂ O ₄	(Zn _{0.6} ²⁺ Mn _{0.2} ²⁺ Fe _{0.2} ³⁺) _{tet} [Fe _{0.2} ²⁺ Fe _{1.6} ³⁺ Mn _{0.2} ³⁺] _{oct} O ₄ ²⁻
Zn _{0.8} Mn _{0.2} Fe ₂ O ₄	(Zn _{0.8} ²⁺ Mn _{0.1} ²⁺ Fe _{0.1} ³⁺) _{tet} [Fe _{0.1} ²⁺ Fe _{1.8} ³⁺ Mn _{0.1} ³⁺] _{oct} O ₄ ²⁻
ZnFe ₂ O ₄	(Zn ²⁺) _{tet} [Fe ₂ ³⁺] _{oct} O ₄ ²⁻

3.2 Surface properties- acidity/basicity

The study of surface acidity and basicity of solids are important as these properties have decisive roles in determining the catalytic activities and selectivities in reactions. The strength of the sites exposed on the surface and their distribution depends greatly upon the catalytic composition. The present system of ferrites studied contains normal spinels, inverse spinels and mixed spinels. According to many authors [33-40], whatever be the type of spinel, the octahedral sites are exposed almost exclusively at the catalyst surface of the spinel oxides and so the catalytic performance is greatly dependent on the composition of the octahedral sites. Hence, the relative acid-base properties of the cations present in the octahedral sites are relevant in determining the acidity and basicity of the systems.

To determine the surface acidity, three independent methods were implemented – (1) temperature programmed desorption of ammonia, (2) thermodesorption studies of pyridine and 2,6-dimethylpyridine adsorbed samples and (3) vapour-phase decomposition of cyclohexanol. For evaluating the basicity of the systems, adsorption studies of electron acceptors of different electron affinity values were carried out.

3.2.1 Temperature programmed desorption of ammonia (NH₃-TPD) method

Temperature Programmed Desorption (TPD) analysis permits to identify the strength, the number and the type of active sites that are available on the catalyst surface. The NH₃-TPD method is an easy, rapid and quantitative method, widely employed in characterizing the acidity of solid catalysts. The technique consists in desorbing, by a linear temperature rate, a reactive gas such as ammonia previously chemisorbed on the surface. This method permits the determination of both protonic and cationic acidities.

Owing to the smaller size and strong basicity, ammonia can get adsorbed on acidic sites of any strength and type. The surface OH groups (Brønsted type) and exposed cations (Lewis type) are responsible for the acidity generation in a solid catalyst surface. Different modes of adsorption of ammonia on the catalyst surface are shown in Fig.3.2.1. These modes comprise adsorption at Brønsted and Lewis acidic sites. The first two modes of adsorptions, 'a' and 'b' in Fig. 3.2.1 are weak and the strongest interaction occurs when ammonia is coordinatively bonded on Lewis site.

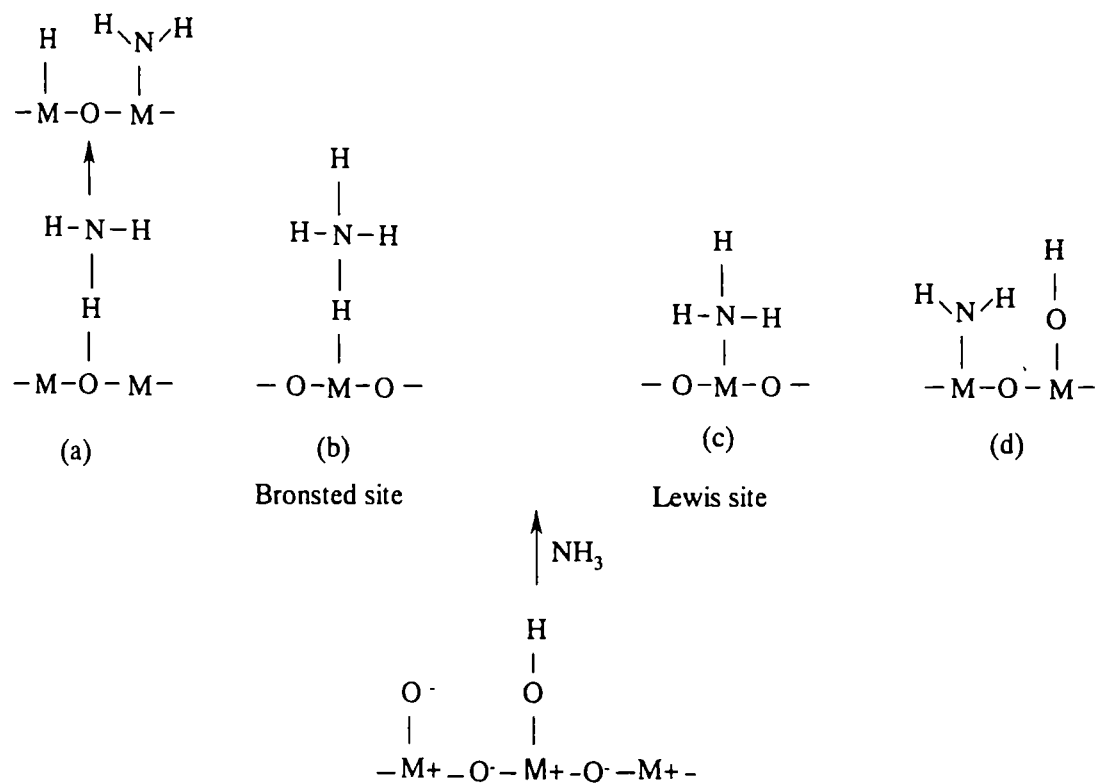


Fig. 3.2.1. Different modes of adsorption of ammonia on oxide surface

The NH_3 -TPD studies of different series of manganese ferros spinels were done in the temperature range $100 - 600^\circ\text{C}$. A definite amount of ammonia is injected into the sample in the reactor and allowed to adsorb over the catalyst surface in a uniform manner. This is followed by evacuation for 20 minutes to remove the weakly adsorbed ammonia. The measurements were taken from 100°C to avoid the physisorbed ammonia. It was observed that below 100°C , a bulk amount of ammonia was desorbed indicating the capacity of the sample to physisorb a large quantity of ammonia. The ammonia desorbed in the temperature range of $100 - 600^\circ\text{C}$ is divided into three different temperature regions ($^\circ\text{C}$) such as $100-200$, $201-400$ and $401-600$ and assigned as weak, medium and strong acid sites respectively. The NH_3 -TPD profiles for the catalysts were also drawn with amount of ammonia desorbed as a function of temperature. The area of the peaks corresponds to the amount of acid sites in that temperature region. Two major shoulders or peaks were observed for many of the systems, while only one hump was seen for a few systems. Various conclusions derived for different series of manganese ferros spinels are presented in the following sections.

(a) $\text{Cr}_x\text{Mn}_{(1-x)}\text{Fe}_2\text{O}_4$ - type systems ($x = 0, 0.2, 0.4, 0.6, 0.8$ and 1.0)

The acidity of this series of systems in the weak, medium and strong regions are presented in Table 3.2.1. The NH_3 -TPD profiles obtained for this series are shown in Fig.3.2.2.

Table 3.2.1. The acid site distribution for $\text{Cr}_x\text{Mn}_{(1-x)}\text{Fe}_2\text{O}_4$ system

x	NH_3 Desorbed (10^{-3}mmolm^{-2})			
	weak	medium	strong	Total
0.0	3.85	4.27	8.38	16.5
0.2	3.88	4.31	2.37	10.6
0.4	3.97	4.39	2.12	10.5
0.6	4.02	4.41	1.95	10.4
0.8	4.08	4.45	1.80	10.3
1.0	4.15	4.50	1.61	10.2

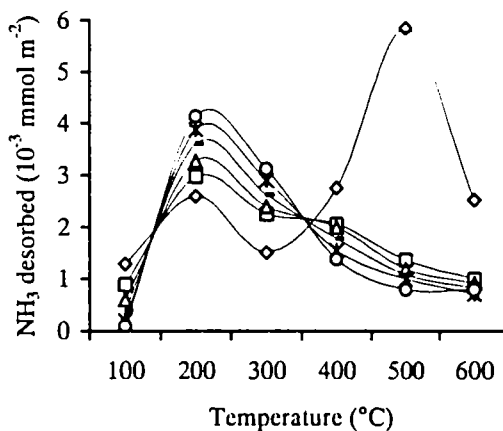


Fig. 3.2.2. Ammonia-TPD profiles for $\text{Cr}_x\text{Mn}_{(1-x)}\text{Fe}_2\text{O}_4$ system

It can be seen from Table 3.2.1 that the progressive addition of chromium ions into the pure manganese ferrosphel decreases the total acidity as well as acidity in the strong region whereas the weak and the medium acidic sites were somewhat pronounced. NH_3 -TPD method lacks in discriminating the type of acid sites (Brönsted and Lewis). However, it is generally accepted that evacuation of ammonia adsorbed surface at 400°C removes most of the Brönsted acid sites [41]. Again, it is implied that the coordinatively bound ammonia on the strong Lewis acid site can be desorbed only at higher temperatures and the acidity in the strong region can be due to the strong Lewis acid sites. The acidity in the weak plus medium region is due to the Brönsted and weak Lewis acid sites. From Fig. 3.2.1, it can be seen that except for MnFe_2O_4 , all the other systems in this series possess only one peak around 200°C due to the lack of strong Lewis sites. Also, from the cation distribution (Table 3.1.9) it can be seen that this series of ferrites contain Mn^{3+} , Fe^{3+} , Fe^{2+} and Cr^{3+} ions in the octahedral site and relative

concentration of these ions are mainly responsible for the acidity of the individual systems. The successive substitution of Mn by Cr decreased the amount of Fe³⁺ ions in the octahedral sites and this is the reason for the decrease in the strong acidity values and subsequent increase in the weak plus medium acidity.

(b) Co_xMn_(1-x)Fe₂O₄ - type systems (x = 0, 0.2, 0.4, 0.6, 0.8 and 1.0)

Table 3.2.2 presents the acidity values of Co-Mn series in the weak, medium and strong regions and the NH₃-TPD profiles for this series are depicted in Fig. 3.2.3.

Table 3.2.2. The acid site distribution for Co_xMn_(1-x)Fe₂O₄ system

x	NH ₃ Desorbed (10 ⁻³ mmolm ⁻²)			
	weak	medium	strong	Total
0.0	3.85	4.27	8.38	16.50
0.2	3.86	4.70	7.80	16.36
0.4	3.88	4.86	7.53	16.27
0.6	3.90	4.90	7.33	16.13
0.8	3.93	5.00	7.14	16.07
1.0	3.95	5.04	7.04	16.03

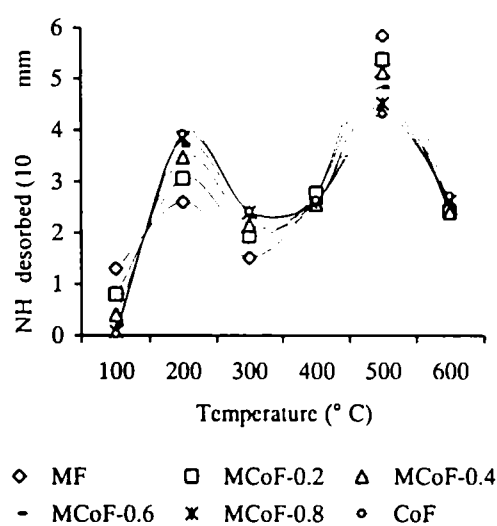


Fig. 3.2.3. Ammonia-TPD profiles for Co_xMn_(1-x)Fe₂O₄ system

It is evident from Table 3.2.2 that the successive incorporation of Co²⁺ ions into the octahedral sites of the manganese ferrosphel increases both the weak and medium acidity. But, the total acidity as well as the acidity in the strong acid region was abridged slightly. Thus, the cobalt incorporation increased either the Brönsted or weak Lewis acid sites or both and decreased the strong Lewis acid sites. The ammonia-TPD profiles (Fig. 3.2.3) for this series showed two peaks or shoulders for all the compositions. The peak maximum for the first region appeared at around 200°C and the second peak maximum was at around 500°C. The shifting of peak maximum towards the right indicates the presence of stronger acid sites. Thus, all the compositions of this series contain

comparable amounts of Brönsted and Lewis acid sites. Moreover, this series of ferrites contain Mn^{3+} , Fe^{3+} , Fe^{2+} and Co^{2+} ions in the octahedral site (Table 3.1.9). The successive substitution of Mn by Co did not change the concentration of Fe^{3+} ions in the octahedral site and hence the variation of acidity is due to the relative concentration of Mn^{3+} and Co^{2+} ions.

(c) $Ni_xMn_{(1-x)}Fe_2O_4$ - type systems ($x = 0, 0.2, 0.4, 0.6, 0.8$ and 1.0)

The acidity distribution on weak, medium and strong regions of Ni-Mn series of ferrites is presented in Table 3.2.3 and Fig. 3.2.4.

Table 3.2.3. The acid site distribution for $Ni_xMn_{(1-x)}Fe_2O_4$ system

x	NH_3 Desorbed ($10^{-3} mmol m^{-2}$)			
	weak	medium	strong	Total
0.0	3.85	4.27	8.38	16.50
0.2	3.82	4.32	7.00	15.14
0.4	3.83	4.35	6.88	15.06
0.6	3.86	4.36	6.78	15.00
0.8	3.88	4.38	6.70	14.96
1.0	3.91	4.41	6.58	14.90

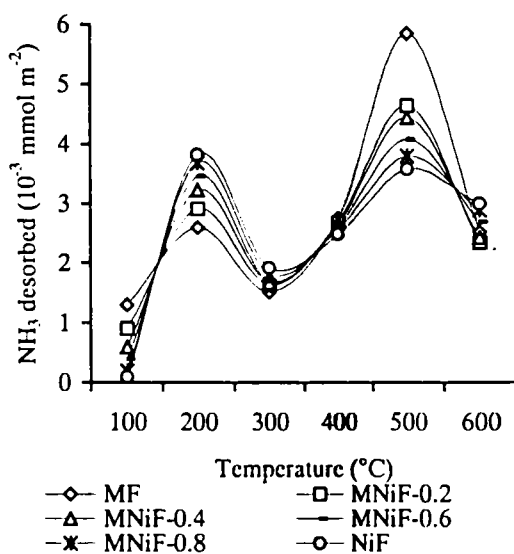


Fig. 3.2.4. Ammonia-TPD profiles for $Ni_xMn_{(1-x)}Fe_2O_4$ system

It is clear from Table 3.2.3 that weak plus medium acidity of the series is enhanced to certain extent by the incorporation of nickel into the octahedral sites of the pure manganese ferrosphenel. But acidity at the stronger region due to the Lewis acid sites is reduced. All the compositions of this series exhibited two peak maxima at around 200°C and 500°C showing that the systems in this series contain appreciable amount of Brönsted and Lewis acid sites. The octahedral sites of this series of ferrites contain Mn^{3+} , Fe^{3+} , Fe^{2+} and Ni^{2+} ions (Table 3.1.9). Like the Co-Mn series, here also, the concentration of Fe^{3+} in the octahedral site is not changed by the successive

incorporation of Ni^{2+} . Hence, the variation in acidity is mainly due to the relative concentration of Mn^{3+} and Ni^{2+} ions in the octahedral sites.

(d) $\text{Cu}_x\text{Mn}_{(1-x)}\text{Fe}_2\text{O}_4$ - type systems ($x = 0, 0.2, 0.4, 0.6, 0.8$ and 1.0)

Table 3.2.4 presents the acidity values in the weak, medium and strong regions of Cu-Mn series. The ammonia-TPD curves for this series of ferrites showing the acidity distribution in all the temperature regions is presented in Fig. 3.2.5.

Table 3.2.4. The acid site distribution for $\text{Cu}_x\text{Mn}_{(1-x)}\text{Fe}_2\text{O}_4$ system

x	NH_3 Desorbed (10^{-3}mmolm^{-2})			
	weak	medium	strong	Total
0.0	3.85	4.27	8.38	16.50
0.2	3.84	4.31	5.84	13.99
0.4	3.86	4.33	5.94	14.13
0.6	3.88	4.36	6.47	14.71
0.8	3.90	4.38	7.33	15.61
1.0	3.91	4.41	8.10	16.42

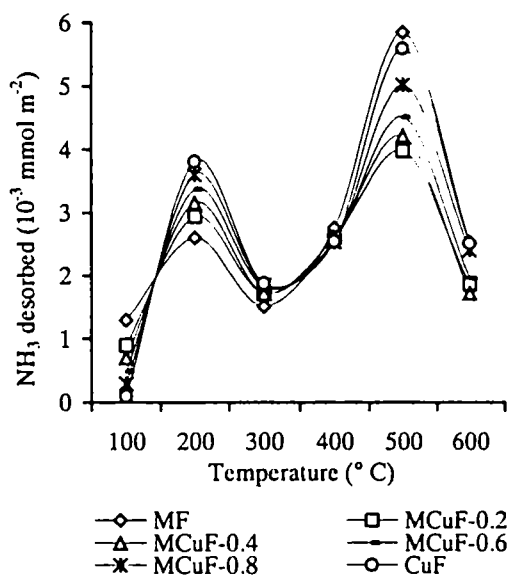


Fig. 3.2.5. Ammonia-TPD profiles for $\text{Cu}_x\text{Mn}_{(1-x)}\text{Fe}_2\text{O}_4$ system

The copper doping in pure manganese ferros spinel increased the weak plus medium acidity as can be seen from Table 3.2.4. The strong acidity first showed a reduction and then an enhancement with further addition of copper. The Cu^{2+} ions in the octahedral sites create surface defects and thereby enhancing the strong Lewis acidity and this is more pronounced in CuFe_2O_4 . All the compositions of the series hold two peak maxima at around 200°C and 500°C . The higher peak at 500°C indicates the presence of large amount of Lewis acid sites. Again, it is evident from the cation distribution that the octahedral sites of this series contain Mn^{3+} , Fe^{3+} , Fe^{2+} and Cu^{2+} ions and the successive increase in copper content did not alter the concentration of Fe^{3+} ions.

Therefore, the difference in the relative concentration of Cu^{2+} ions and Mn^{3+} ions in the octahedral sites are accountable for the variation in acidity of the systems.

(e) $\text{Zn}_x\text{Mn}_{(1-x)}\text{Fe}_2\text{O}_4$ - type systems ($x = 0, 0.2, 0.4, 0.6, 0.8$ and 1.0)

The total acidity and acidity values in the weak, medium and strong regions of the Zn-Mn series of ferrites are presented in Table. 3.2.5. The ammonia-TPD curves for the series are shown in Fig. 3.2.6.

Table 3.2.5. The acid site distribution for $\text{Zn}_x\text{Mn}_{(1-x)}\text{Fe}_2\text{O}_4$ system

x	NH_3 Desorbed (10^{-3}mmolm^{-2})			
	weak	medium	strong	Total
0.0	3.85	4.27	8.38	16.50
0.2	1.63	1.85	8.57	12.05
0.4	1.42	1.67	8.71	11.80
0.6	1.30	1.45	8.92	11.67
0.8	1.15	1.19	9.13	11.47
1.0	1.02	1.05	9.25	11.32

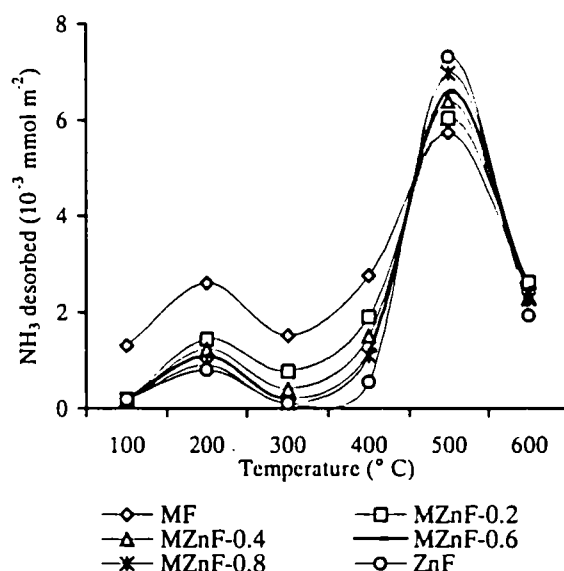


Fig. 3.2.6. Ammonia-TPD profiles for $\text{Zn}_x\text{Mn}_{(1-x)}\text{Fe}_2\text{O}_4$ system

The addition of zinc ions into the pure manganese ferrosipinel decreased the weak and medium acidity to a great extent. But the strong acidity is enhanced by an appreciable amount (Table 3.2.5). Though the ammonia-TPD curves (Fig.3.2.6) for this series possess two peak maxima, the one around 500°C is highly prominent than the one around 200°C indicating the enhancement in the strong Lewis acidity. The octahedral sites of this series of ferrites contain Mn^{3+} , Fe^{2+} and Fe^{3+} ions (Table 3.1.9). The addition of zinc into the pure manganese ferrosipinel causes its accumulation in the tetrahedral sites and pushes isomorphically Fe^{3+} ions into the octahedral site. This increases the concentration of Fe^{3+} ions in the octahedral sites and enhances the strong acidity.

3.2.2 TG desorption of pyridine/2,6-dimethylpyridine

The potential of use of pyridine and 2,6-dimethylpyridine as probe molecules for the determination of acid strength of solid acids has recently attained increased applications. Since pyridine gets adsorbed on both Brönsted and Lewis acid sites, thermodesorption study of pyridine adsorbed samples gives the total acid amount of the solid surface. Thus, this method can be used as a support for the results obtained from NH₃-TPD method. But 2,6-dimethylpyridine (2,6-DMP) adsorbs strongly on Brönsted acid sites and forms weak bonds with Lewis acid sites [42]. According to Satsuma *et al.* [43] the 2,6-DMP weakly bound to Lewis acid sites, get desorbed below 300°C. Hence thermodesorption study of 2,6-dimethylpyridine adsorbed samples beyond 300°C can give the measure of Brönsted acid sites. The detection of Brönsted acid sites by 2,6-DMP may be due to its stronger basicity (higher pK_a value) than that of pyridine [43].

These methods of determining the total acidity and Brönsted acidity have been done for different series of manganese ferros spinels. The samples were activated at 500°C for 2 h and kept in two different desiccators saturated with pyridine and 2,6-dimethylpyridine vapours at room temperature for 48 h. These samples were then subjected to thermogravimetric analysis and the percentage of weight loss per unit surface area was determined. The heating rate was 20°C/minute in nitrogen atmosphere. In the case of pyridine adsorbed samples, the percentage of weight loss per unit surface area in the temperature region 100-600°C is divided into weak (100-200°C), medium (201-400°C) and strong (401-600°C) acid sites (Table 3.2.6). For 2,6-dimethylpyridine adsorbed samples the percentage of weight loss per unit surface area in the temperature region 301-600°C is divided into weak (301-400°C), medium (401-500°C) and strong (501-600°C) acid sites (Table 3.2.7). The conclusions made for different series of manganese ferros spinels are discussed in the following sections.

It is confirmed that the results obtained from the thermodesorption studies of pyridine adsorbed samples can be used as a support for the NH₃-TPD studies. The total acidity values and the acidity in the weak, medium and strong regions for different series of manganese ferros spinels obtained from TGA of pyridine adsorbed samples are in good agreement with the data for acidity from NH₃-TPD studies.

Table 3.2.6 Acidity measurement by TG analysis of pyridine adsorbed samples.

Catalyst	Pyridine Desorbed (%wt loss) $10^2 \text{ m}^{-2} \text{ g}$			
	Weak	Medium	Strong	Total
MnFe ₂ O ₄	0.868	1.117	1.496	3.481
Cr _{0.2} Mn _{0.8} Fe ₂ O ₄	0.881	1.131	0.421	2.433
Cr _{0.4} Mn _{0.6} Fe ₂ O ₄	0.882	1.135	0.405	2.422
Cr _{0.6} Mn _{0.4} Fe ₂ O ₄	0.884	1.139	0.391	2.414
Cr _{0.8} Mn _{0.2} Fe ₂ O ₄	0.886	1.141	0.373	2.400
CrFe ₂ O ₄	0.888	1.143	0.355	2.386
Co _{0.2} Mn _{0.8} Fe ₂ O ₄	0.877	1.129	1.181	3.187
Co _{0.4} Mn _{0.6} Fe ₂ O ₄	0.880	1.133	1.170	3.183
Co _{0.6} Mn _{0.4} Fe ₂ O ₄	0.882	1.135	1.152	3.169
Co _{0.8} Mn _{0.2} Fe ₂ O ₄	0.885	1.137	1.143	3.165
CoFe ₂ O ₄	0.888	1.139	1.130	3.157
Ni _{0.2} Mn _{0.8} Fe ₂ O ₄	0.869	1.119	1.122	3.110
Ni _{0.4} Mn _{0.6} Fe ₂ O ₄	0.870	1.121	1.116	3.107
Ni _{0.6} Mn _{0.4} Fe ₂ O ₄	0.871	1.123	1.108	3.102
Ni _{0.8} Mn _{0.2} Fe ₂ O ₄	0.872	1.125	1.093	3.090
NiFe ₂ O ₄	0.874	1.128	1.076	3.078
Cu _{0.2} Mn _{0.8} Fe ₂ O ₄	0.870	1.121	0.927	2.918
Cu _{0.4} Mn _{0.6} Fe ₂ O ₄	0.872	1.124	0.987	2.938
Cu _{0.6} Mn _{0.4} Fe ₂ O ₄	0.873	1.127	1.125	3.125
Cu _{0.8} Mn _{0.2} Fe ₂ O ₄	0.875	1.129	1.149	3.153
CuFe ₂ O ₄	0.877	1.131	1.171	3.179
Zn _{0.2} Mn _{0.8} Fe ₂ O ₄	0.301	0.545	1.515	2.361
Zn _{0.4} Mn _{0.6} Fe ₂ O ₄	0.257	0.521	1.562	2.340
Zn _{0.6} Mn _{0.4} Fe ₂ O ₄	0.231	0.504	1.597	2.332
Zn _{0.8} Mn _{0.2} Fe ₂ O ₄	0.213	0.478	1.621	2.312
ZnFe ₂ O ₄	0.198	0.437	1.668	2.303

Table 3.2.7. Acidity measurement by TGA of 2,6-dimethylpyridine adsorbed samples.

Catalyst	2,6-dimethylpyridine desorbed (%wt loss)			
	Weak	Medium	Strong	Total
MnFe ₂ O ₄	0.320	0.276	0.229	0.825
Cr _{0.2} Mn _{0.8} Fe ₂ O ₄	0.162	0.097	0.041	0.300
Cr _{0.4} Mn _{0.6} Fe ₂ O ₄	0.137	0.091	0.033	0.261
Cr _{0.6} Mn _{0.4} Fe ₂ O ₄	0.124	0.083	0.0226	0.233
Cr _{0.8} Mn _{0.2} Fe ₂ O ₄	0.113	0.072	0.023	0.208
CrFe ₂ O ₄	0.108	0.061	0.018	0.187
Co _{0.2} Mn _{0.8} Fe ₂ O ₄	0.291	0.201	0.191	0.683
Co _{0.4} Mn _{0.6} Fe ₂ O ₄	0.282	0.197	0.172	0.651
Cr _{0.6} Mn _{0.4} Fe ₂ O ₄	0.263	0.191	0.160	0.614
Cr _{0.8} Mn _{0.2} Fe ₂ O ₄	0.257	0.180	0.151	0.588
CoFe ₂ O ₄	0.251	0.173	0.142	0.566
Ni _{0.2} Mn _{0.8} Fe ₂ O ₄	0.321	0.274	0.229	0.824
Ni _{0.4} Mn _{0.6} Fe ₂ O ₄	0.321	0.274	0.228	0.823
Ni _{0.6} Mn _{0.4} Fe ₂ O ₄	0.320	0.273	0.227	0.820
Ni _{0.8} Mn _{0.2} Fe ₂ O ₄	0.319	0.271	0.227	0.817
NiFe ₂ O ₄	0.319	0.270	0.224	0.814
Cu _{0.2} Mn _{0.8} Fe ₂ O ₄	0.318	0.256	0.201	0.775
Cu _{0.4} Mn _{0.6} Fe ₂ O ₄	0.311	0.242	0.197	0.775
Cu _{0.6} Mn _{0.4} Fe ₂ O ₄	0.307	0.237	0.191	0.735
Cu _{0.8} Mn _{0.2} Fe ₂ O ₄	0.304	0.221	0.182	0.707
CuFe ₂ O ₄	0.298	0.218	0.173	0.689
Zn _{0.2} Mn _{0.8} Fe ₂ O ₄	0.326	0.297	0.161	0.784
Zn _{0.4} Mn _{0.6} Fe ₂ O ₄	0.317	0.280	0.153	0.750
Zn _{0.6} Mn _{0.4} Fe ₂ O ₄	0.313	0.273	0.142	0.728
Zn _{0.8} Mn _{0.2} Fe ₂ O ₄	0.301	0.253	0.137	0.691
ZnFe ₂ O ₄	0.293	0.232	0.131	0.606

It is assumed that the weak plus medium acidity obtained from NH₃-TPD studies and TGA of pyridine adsorbed samples are mainly due to Brönsted as well as weak Lewis acid sites. From Table 3.2.7, it is clear that the relative amount of Brönsted acidity is reduced by the successive incorporation of chromium ions into the manganese ferros spinels in mixed Cr-Mn series. Thus the enhancement in the weak Lewis acidity is responsible for the improved weak plus medium acidity as evident from the NH₃-TPD studies and TGA of pyridine adsorbed samples. Similar observations are seen in the cases of mixed Co-Mn series, Ni-Mn series and Cu-Mn series. But, in the case of mixed Zn-Mn series both the Brönsted acidity as well as the weak Lewis acidity is reduced by the successive incorporation of zinc ions into the manganese ferros spinel.

3.2.3. Surface electron donating properties

The utility of electron acceptor adsorption for the study of the electron donor property of the catalyst surface has been well established. Electron donor strength of a surface is defined as the conversion power of an adsorbed electron acceptor into its anion radical. It can be expressed as the limiting electron affinity value at which free radical anion formation is not observed. The limiting amount of the electron acceptors adsorbed on the catalysts surface depends on nature of the donor sites and also on the electron affinity of the electron acceptors used. Thus, by a comparison between the limiting concentration of electron acceptors adsorbed and the electron affinity values of the respective electron acceptors, information regarding the strength and distribution of the electron donor sites can be obtained.

The electron acceptors selected for the study were tetracyanoquinodimethane (TCNQ), 2,3,5,6-tetra-chloro-4-benzoquinone (chloranil) and *p*-dinitrobenzene (PDNB) with electron affinity values 2.84, 2.40 and 1.77 eV respectively. The adsorption experiments were done for different series of manganese ferros spinels activated at 500°C for 2 h. Acetonitrile is used as the solvent for the adsorption studies. The limiting amount was estimated from the Langmuir plot where the amount of the electron acceptor adsorbed (mmol m⁻²) was plotted as a function of equilibrium concentration (mmol dm⁻³) of the electron acceptor in solution. The limiting amount of TCNQ gives a measure of total amount of basic sites whereas limiting amount of chloranil signifies the measure of

moderate and strong basic sites. The difference between the limiting amounts of TCNQ and chloranil represents a measure of weaker basic sites. The results obtained for different series of manganese ferros spinels are discussed in the following sections. Negligible adsorption of PDNB in all systems indicated the absence of very strong basic sites.

(a) $\text{Cr}_x\text{Mn}_{(1-x)}\text{Fe}_2\text{O}_4$ - type systems ($x = 0, 0.2, 0.4, 0.6, 0.8$ and 1.0)

Table 3.2.8 represents the limiting amounts of electron acceptors for Cr-Mn series of ferrites. The total basicity of this series, as evident from the limiting amount of TCNQ adsorbed follows the order: $\text{MnFe}_2\text{O}_4 \lll \text{Cr}_{0.2}\text{Mn}_{0.8}\text{Fe}_2\text{O}_4 < \text{Cr}_{0.4}\text{Mn}_{0.6}\text{Fe}_2\text{O}_4 < \text{Cr}_{0.6}\text{Mn}_{0.4}\text{Fe}_2\text{O}_4 < \text{Cr}_{0.8}\text{Mn}_{0.2}\text{Fe}_2\text{O}_4 \approx \text{CrFe}_2\text{O}_4$.

It can be seen that the incorporation of Cr^{3+} ions into the octahedral sites of the pure manganese ferros spinel enhanced the moderate to strong basic sites very significantly as evident from the steady increase in the limiting amount of the chloranil adsorbed. The weak basic sites represented by the difference in the limiting amounts of TCNQ and chloranil did not follow any trend during the successive substitution of Mn by Cr. From the cation distribution (Table 3.1.9) it can be seen that MnFe_2O_4 is a partially inverse spinel and the inverse nature increases with progressive incorporation of chromium ions into the octahedral sites. This isomorphically replaces the more acidic

Table. 3.2.8 Limiting amounts of TCNQ, Chloranil and (TCNQ-Chloranil) for Cr-Mn series of ferrites

Catalyst	Limiting amount ($10^{-4} \text{ mmolm}^{-2}$)		
	TCNQ	Chloranil	TCNQ-Chloranil
MnFe_2O_4	10.71	2.60	8.11
$\text{Cr}_{0.2}\text{Mn}_{0.8}\text{Fe}_2\text{O}_4$	55.52	22.79	32.73
$\text{Cr}_{0.4}\text{Mn}_{0.6}\text{Fe}_2\text{O}_4$	56.28	25.19	31.09
$\text{Cr}_{0.6}\text{Mn}_{0.4}\text{Fe}_2\text{O}_4$	57.58	30.67	26.91
$\text{Cr}_{0.8}\text{Mn}_{0.2}\text{Fe}_2\text{O}_4$	59.01	35.29	23.72
CrFe_2O_4	60.61	38.58	22.03

Fe^{3+} from the more active octahedral sites to the hindered tetrahedral sites and increased the amount of less acidic Cr^{3+} ions in the octahedral sites. All these factors are responsible for the increased basicity of this series. The adsorption isotherms of TCNQ and chloranil in acetonitrile over different compositions of mixed Cr-Mn series of ferrites are presented in Fig. 3.2.7 and in Fig. 3.2.8.

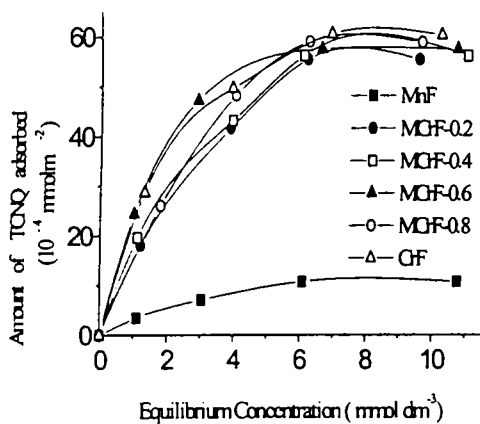


Fig. 3.2.7 Adsorption isotherms of TCNQ in acetonitrile over mixed Cr-Mn series of ferrites.

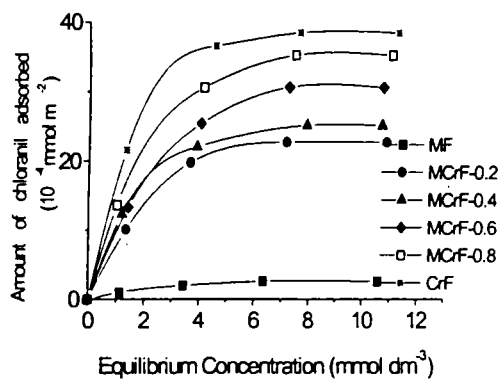


Fig. 3.2.8 Adsorption isotherms of chloranil in acetonitrile over mixed Cr-Mn series of ferrites.

(b) $\text{Co}_x\text{Mn}_{(1-x)}\text{Fe}_2\text{O}_4$ - type systems ($x = 0, 0.2, 0.4, 0.6, 0.8$ and 1.0)

The limiting amounts of TCNQ and chloranil adsorbed for different compositions of Co-Mn series of ferrites are shown in Table 3.2.9. The addition of cobalt ions into the octahedral sites of manganese ferrosipinel increased all the regions of basicity slightly. It is understood from the cation distribution (Table 3.1.9) that the progressive incorporation of cobalt ions converted the partially inverse MnFe_2O_4 into an inverse spinel. But this shifting of spinel type did not alter the concentration of Fe^{3+} ions in the octahedral sites. Therefore, the ratio of $\text{Co}^{2+}/\text{Mn}^{3+}$ is mainly responsible for the slightly improved basicity of this series of ferrites.

Table. 3.2.9 Limiting amounts of TCNQ, Chloranil and (TCNQ-Chloranil) adsorbed for Co-Mn series of ferrites.

Catalyst	Limiting amount (10^{-4} mmol m^{-2})		
	TCNQ	Chloranil	TCNQ-Chloranil
MnFe ₂ O ₄	10.71	2.60	8.11
Co _{0.2} Mn _{0.8} Fe ₂ O ₄	15.68	7.39	8.29
Co _{0.4} Mn _{0.6} Fe ₂ O ₄	16.38	8.08	8.30
Co _{0.6} Mn _{0.4} Fe ₂ O ₄	17.19	8.87	8.32
Co _{0.8} Mn _{0.2} Fe ₂ O ₄	17.88	9.52	8.36
CoFe ₂ O ₄	18.58	9.93	8.65

The adsorption isotherms of TCNQ and chloranil in acetonitrile over mixed Co-Mn series of ferrites are presented in Fig. 3.2.9 and Fig. 3.2.10.

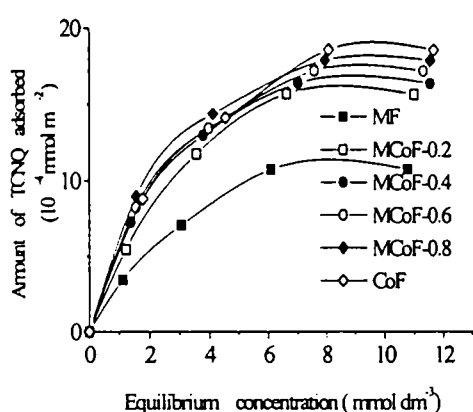


Fig. 3.2.9. Adsorption isotherms of TCNQ in acetonitrile over mixed Co-Mn series of ferrites.

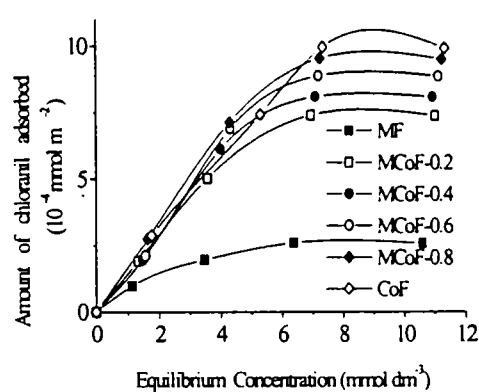


Fig. 3.2.10. Adsorption isotherms of chloranil in acetonitrile over mixed Co-Mn series of ferrites.

(c) Ni_xMn_(1-x)Fe₂O₄ - type systems (x = 0, 0.2, 0.4, 0.6, 0.8 and 1.0)

Table 3.2.10 represents the limiting amounts of electron acceptors (TCNQ and chloranil) adsorbed for different compositions of Ni-Mn series of ferrites. The adsorption isotherms of TCNQ and chloranil in acetonitrile over mixed Ni-Mn series of ferrites are presented in Fig. 3.2.11 and in Fig. 3.2.12.

Table. 3.2.10 Limiting amounts of TCNQ, Chloranil and (TCNQ-Chloranil) adsorbed for Ni-Mn series of ferrites.

Catalyst	Limiting amount (10^{-4} mmol m^{-2})		
	TCNQ	Chloranil	TCNQ-Chloranil
$MnFe_2O_4$	10.71	2.6	8.11
$Ni_{0.2}Mn_{0.8}Fe_2O_4$	20.81	6.41	14.39
$Ni_{0.4}Mn_{0.6}Fe_2O_4$	22.47	7.00	15.47
$Ni_{0.6}Mn_{0.4}Fe_2O_4$	23.13	7.58	15.52
$Ni_{0.8}Mn_{0.2}Fe_2O_4$	24.97	7.92	16.05
$NiFe_2O_4$	25.52	8.91	16.61

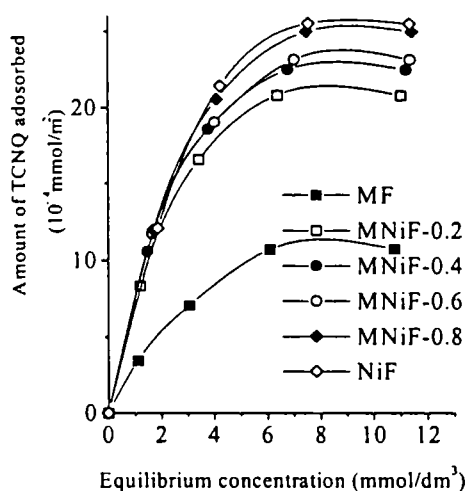


Fig. 3.2.11 . Adsorption isotherms of TCNQ in acetonitrile over mixed Ni-Mn series of ferrites.

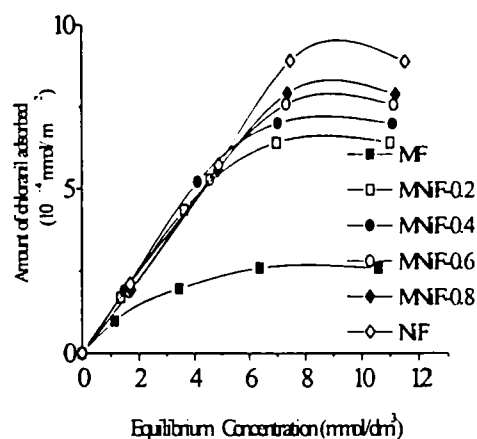


Fig. 3.2.12 . Adsorption isotherms of chloranil in acetonitrile over mixed Ni-Mn series of ferrites.

It can be seen from Table 3.2.10 that the basicity of this series follows the order: $MnFe_2O_4 \gg Ni_{0.2}Mn_{0.8}Fe_2O_4 > Ni_{0.4}Mn_{0.6}Fe_2O_4 > Ni_{0.6}Mn_{0.4}Fe_2O_4 > Ni_{0.8}Mn_{0.2}Fe_2O_4 > NiFe_2O_4$. Thus the increment in nickel content in the octahedral

positions of pure manganese ferros spinels enhanced the basicity in the various types of basic sites as evident from the limiting amounts of TCNQ and chloranil adsorbed. Like the Co-Mn series, here also the increment in nickel content in the octahedral sites did not alter the concentration of more acidic Fe^{3+} in the octahedral site. The variation of basicity in different compositions of Ni-Mn series depend strongly on the $\text{Ni}^{2+}/\text{Mn}^{3+}$ ratio in the octahedral sites.

(d) $\text{Cu}_x\text{Mn}_{(1-x)}\text{Fe}_2\text{O}_4$ - type systems ($x = 0, 0.2, 0.4, 0.6, 0.8$ and 1.0)

The limiting amount of the electron acceptors adsorbed over different compositions of Cu-Mn series of ferrites are presented in Table 3.2.11.

Table 3.2.11 Limiting amounts of TCNQ, Chloranil and (TCNQ-Chloranil) adsorbed for Cu-Mn series of ferrites.

Catalyst	Limiting amount (10^{-4} mmol m^{-2})		
	TCNQ	Chloranil	TCNQ-Chloranil
MnFe_2O_4	10.71	2.6	8.11
$\text{Cu}_{0.2}\text{Mn}_{0.8}\text{Fe}_2\text{O}_4$	22.91	2.52	20.39
$\text{Cu}_{0.4}\text{Mn}_{0.6}\text{Fe}_2\text{O}_4$	24.65	2.48	22.17
$\text{Cu}_{0.6}\text{Mn}_{0.4}\text{Fe}_2\text{O}_4$	26.95	2.44	24.51
$\text{Cu}_{0.8}\text{Mn}_{0.2}\text{Fe}_2\text{O}_4$	28.32	2.31	26.01
CuFe_2O_4	30.01	2.27	27.74

The copper doping into the octahedral sites of manganese ferros spinel increased the limiting amounts of TCNQ adsorbed appreciably, but slightly decreased that of chloranil. The difference between the limiting amounts of TCNQ and chloranil, which represents the weaker basic sites is enhanced with increased copper doping. In this series of ferrites the concentration of Fe^{3+} ions for the different compositions are the same and the variation in donor properties of the series hence depend on the $\text{Cu}^{2+}/\text{Mn}^{3+}$ ratio. The adsorption isotherms of TCNQ and chloranil in acetonitrile over mixed Co-Mn series of ferrites are presented in Fig. 3.2.13. and Fig. 3.2.14.

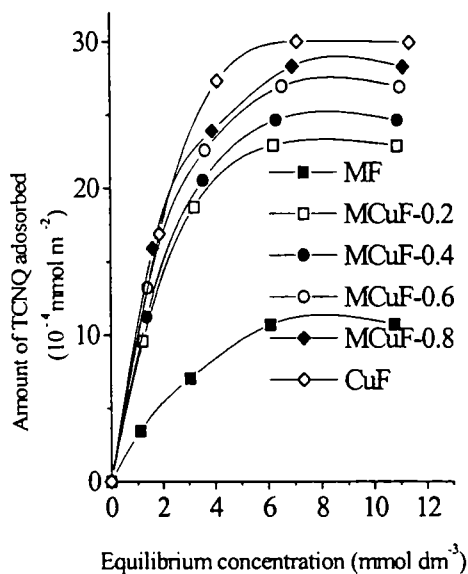


Fig. 3.2.13. Adsorption isotherms of TCNQ in acetonitrile over mixed Cu-Mn series of ferrites.

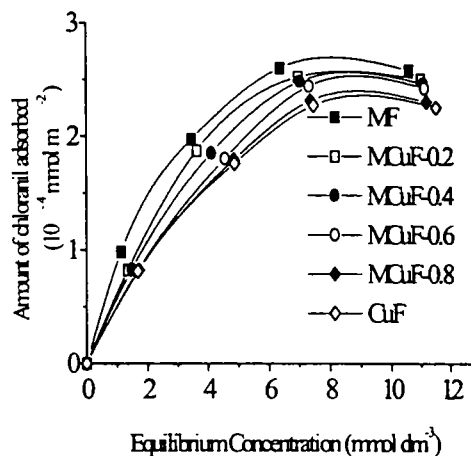


Fig. 3.2.14. Adsorption isotherms of chloranil in acetonitrile over mixed Cu-Mn series of ferrites.

(e) $Zn_xMn_{(1-x)}Fe_2O_4$ - type systems ($x = 0, 0.2, 0.4, 0.6, 0.8$ and 1.0)

The limiting amounts of TCNQ, chloranil and TCNQ-Chloranil adsorbed over different compositions of Zn-Mn series of ferrites are presented in Table 3.2.12. The data clearly reveal that the progressive substitution of Mn by Zn reduces the weak, medium as well as strong basic sites of the series. Unlike the other systems, the substitution of zinc ions into the pure manganese ferrosphenel goes to the tetrahedral sites rather than to the octahedral sites. This increases the concentration of more acidic Fe^{3+} ions in the exposed octahedral sites and are responsible for the reduced basicity of this series. The Langmuir adsorption isotherms of TCNQ and chloranil in acetonitrile over mixed Zn-Mn series of ferrites are shown in Fig. 3.2.15 and Fig. 3.2.16.

Table 3.2.12. Limiting amounts of TCNQ, Chloranil and (TCNQ-Chloranil) adsorbed for Zn-Mn series of ferrites.

Catalyst	Limiting amount (10^{-4} mmol m^{-2})		
	TCNQ	Chloranil	TCNQ-Chloranil
$MnFe_2O_4$	10.71	2.6	8.11
$Zn_{0.2}Mn_{0.8}Fe_2O_4$	10.21	2.58	7.63
$Zn_{0.4}Mn_{0.6}Fe_2O_4$	10.02	2.51	7.51
$Zn_{0.6}Mn_{0.4}Fe_2O_4$	9.91	2.49	7.42
$Zn_{0.8}Mn_{0.2}Fe_2O_4$	9.62	2.46	7.16
$ZnFe_2O_4$	9.37	2.43	6.94

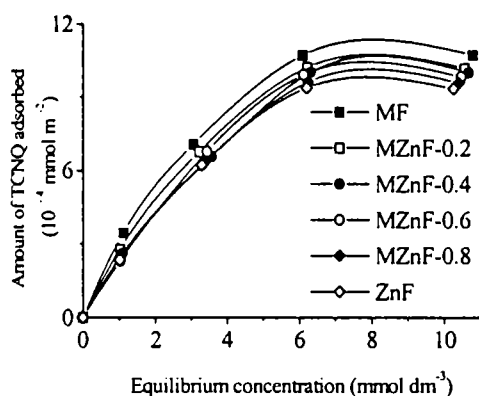


Fig.3.2.15 Adsorption isotherms of TCNQ in acetonitrile over mixed Zn-Mn series of ferrites.

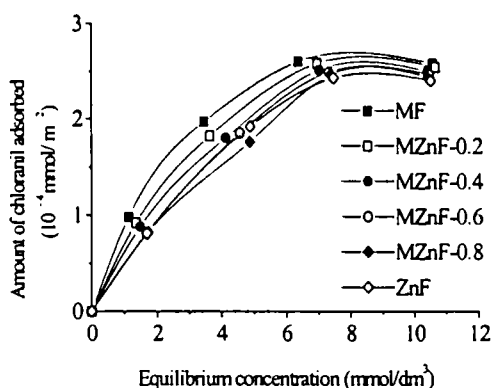


Fig.3.2.16. Adsorption isotherms of chloranil in acetonitrile over mixed Zn-Mn series of ferrites.

3.2.4. Cyclohexanol decomposition

Cyclohexanol decomposition reaction is widely studied to determine the functionality of an oxide catalyst [5, 6, 44-47]. The selectivity of the products exhibited by a catalyst is related to its surface acid-base and redox properties [48-52]. Spinel oxides contain both acidic and basic sites and the amphoteric nature of the cyclohexanol permits their interaction with acidic and basic sites. The dehydration activity resulting in the formation of cyclohexene is linked to the acidic property and the dehydrogenation

activity leading to the formation of cyclohexanone is linked to the combined effects of both acidic and basic properties [53]. A proposed mechanism [46] for the decomposition of cyclohexanol is depicted in Fig. 3.2.17.

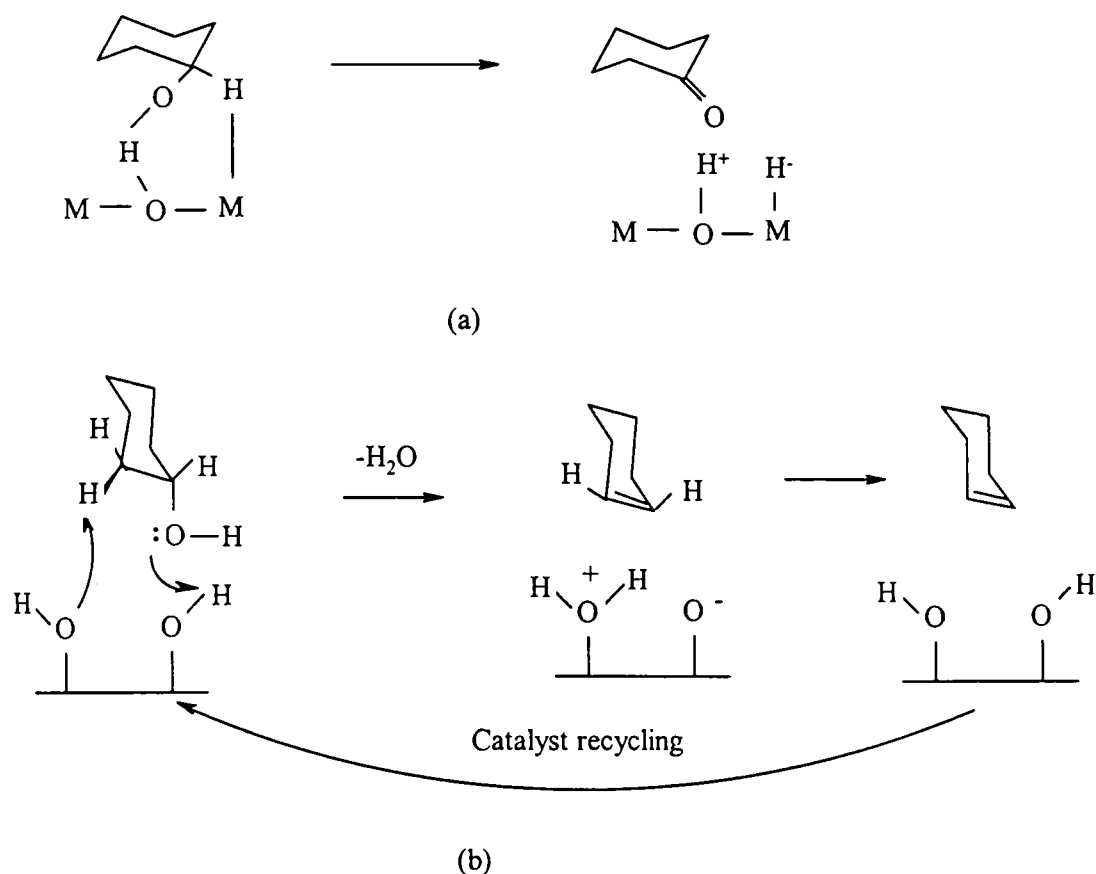


Fig. 3.2.17 Mechanism of (a) dehydrogenation and (b) dehydration of cyclohexanol on oxide surface.

Besides cyclohexene and cyclohexanone, phenol, benzene, cyclohexane and methylcyclopentene are also reported to form during this reaction [5]. The decomposition of cyclohexanol was performed over different compositions of manganese ferrites in vapour-phase at 250°C for 2 h and the products were analyzed by GC fitted with FID using carbowax column. Cyclohexene and cyclohexanone were the observed reaction products and formation of methylcyclopentene indicative of strong acidic sites [54] was not observed for any of the systems. The percentage conversion of

cyclohexanol was found to show a proportionate increase with decrease in activation energy of the catalyst. It was also observed that the Brönsted acid sites are mainly responsible for the dehydration activity of the various manganese ferrites. The data for cyclohexanol decomposition is shown in Table 3.2.13.

(a) $\text{Cr}_x\text{Mn}_{(1-x)}\text{Fe}_2\text{O}_4$ - type systems ($x = 0, 0.2, 0.4, 0.6, 0.8$ and 1.0)

The percentage conversion of cyclohexanol was decreased with increase in the chromium amount in the octahedral site of the manganese ferrites. This series of catalysts were observed as weakly acidic from the NH_3 -TPD results and is established from the highly reduced dehydration activity. Thus substitution by Cr^{3+} ions removes the acidic sites initially present in Mn-ferrite. The inverse nature of MnFe_2O_4 increased gradually with the progressive substitution of Cr^{3+} ions in the octahedral sites due to the replacement of Fe^{3+} ions to the hindered tetrahedral sites. So it is considered that Cr^{3+} ions in the octahedral site act as possible active sites for the enhanced dehydrogenation.

(b) $\text{Co}_x\text{Mn}_{(1-x)}\text{Fe}_2\text{O}_4$ - type systems ($x = 0, 0.2, 0.4, 0.6, 0.8$ and 1.0)

The progressive substitution of Mn by Co in MnFe_2O_4 enhanced the percentage conversion of cyclohexanol. The dehydration activity, which is a measure of the acidic strength, is slightly lowered with successive incorporation of Co^{2+} ions in the octahedral sub lattice. This result is in well agreement with the NH_3 -TPD studies (Table 3.2.2). The substitution of Co^{2+} ions increased the inverse nature of manganese ferrite, but did not alter the concentration of Fe^{3+} ions in the octahedral sites. Thus, the reduced dehydration activity and improved dehydrogenation activity of this series of ferrites with progressive cobalt ion substitution are due to the increased ratio of $\text{Co}^{2+}/\text{Mn}^{3+}$ in the exposed octahedral sites.

(c) $\text{Ni}_x\text{Mn}_{(1-x)}\text{Fe}_2\text{O}_4$ - type systems ($x = 0, 0.2, 0.4, 0.6, 0.8$ and 1.0)

The progressive replacement of Mn by Ni in the octahedral sub lattice of manganese ferrite reduced the percentage conversion of cyclohexanol. The dehydration activity signifying the acidic strength of the catalysts is rather decreased with nickel doping. The same trend was observed for this series from NH_3 -TPD results (Table 3.2.3). The partially inversed manganese ferrite is converted gradually to the fully

Table. 3.2.13 Reaction data for cyclohexanol decomposition over manganese ferrites.

Catalyst	Conversion (%)	Selectivity (%)		Activation Energy (eV)
		Cyclohexene	Cyclohexanone	
MnFe ₂ O ₄	57.59	91.28	8.72	0.400
Cr _{0.2} Mn _{0.8} Fe ₂ O ₄	32.18	38.52	61.48	0.560
Cr _{0.4} Mn _{0.6} Fe ₂ O ₄	29.73	37.01	62.99	0.668
Cr _{0.6} Mn _{0.4} Fe ₂ O ₄	26.43	36.25	63.75	0.760
Cr _{0.8} Mn _{0.2} Fe ₂ O ₄	24.98	35.89	64.11	0.881
CrFe ₂ O ₄	22.14	34.82	65.18	0.888
Co _{0.2} Mn _{0.8} Fe ₂ O ₄	73.72	90.80	9.20	0.247
Co _{0.4} Mn _{0.6} Fe ₂ O ₄	75.27	88.00	12.00	0.201
Cr _{0.6} Mn _{0.4} Fe ₂ O ₄	76.29	87.50	12.50	0.182
Cr _{0.8} Mn _{0.2} Fe ₂ O ₄	77.86	87.10	12.90	0.166
CoFe ₂ O ₄	78.52	86.00	14.00	0.140
Ni _{0.2} Mn _{0.8} Fe ₂ O ₄	52.57	90.76	9.24	0.411
Ni _{0.4} Mn _{0.6} Fe ₂ O ₄	49.78	89.25	10.75	0.450
Ni _{0.6} Mn _{0.4} Fe ₂ O ₄	46.29	88.98	11.02	0.482
Ni _{0.8} Mn _{0.2} Fe ₂ O ₄	44.52	85.29	14.71	0.513
NiFe ₂ O ₄	41.13	82.10	17.90	0.557
Cu _{0.2} Mn _{0.8} Fe ₂ O ₄	64.31	47.23	52.77	0.301
Cu _{0.4} Mn _{0.6} Fe ₂ O ₄	65.54	46.36	53.64	0.265
Cu _{0.6} Mn _{0.4} Fe ₂ O ₄	66.37	42.18	57.82	0.225
Cu _{0.8} Mn _{0.2} Fe ₂ O ₄	67.33	38.98	61.02	0.272
CuFe ₂ O ₄	69.03	34.91	65.09	0.295
Zn _{0.2} Mn _{0.8} Fe ₂ O ₄	45.10	80.23	19.77	0.571
Zn _{0.4} Mn _{0.6} Fe ₂ O ₄	41.28	77.36	22.64	0.689
Zn _{0.6} Mn _{0.4} Fe ₂ O ₄	34.11	74.18	25.82	0.741
Zn _{0.8} Mn _{0.2} Fe ₂ O ₄	25.79	71.98	28.02	0.829
ZnFe ₂ O ₄	18.97	69.91	30.09	0.917

Reaction temperature – 250°C, amount of catalyst – 0.5g, TOS - 2 h., flow rate – 6 mL h⁻¹.

inverse spinels by the successive incorporation of Ni^{2+} ions in the octahedral sub lattice. The variation of concentration of nickel content did not change the concentration of Fe^{3+} ions in the octahedral sub lattice. Therefore the variation in dehydration activity and the improved dehydrogenation is due to the change in concentration of Ni^{2+} ions in the octahedral sites.

(d) $\text{Cu}_x\text{Mn}_{(1-x)}\text{Fe}_2\text{O}_4$ - type systems ($x = 0, 0.2, 0.4, 0.6, 0.8$ and 1.0)

It is evident from Table 3.2.13 that copper doping in manganese ferrosipinel improved the percentage conversion of cyclohexanol. The dehydration activity is reduced radically with increase in copper content in the octahedral sites. It is interesting to note that the dehydrogenation activity of the copper substituted manganese ferrites exhibited an appreciable enhancement. Like the Co-Mn systems and Ni-Mn systems, though the partially inverse MnFe_2O_4 is changed to an inverse spinel by the progressive incorporation of copper ions, the concentration of Fe^{3+} ions in the octahedral sub lattice remained unaltered with increase in copper content. The highly enhanced dehydrogenation activity can be looked upon as the combined effect of high Lewis acidity and high oxidizing ability supplied by the Cu^{2+} ions in the octahedral sub lattice.

(e) $\text{Zn}_x\text{Mn}_{(1-x)}\text{Fe}_2\text{O}_4$ - type systems ($x = 0, 0.2, 0.4, 0.6, 0.8$ and 1.0)

The incorporation of Zn into the manganese ferrites radically reduced the cyclohexanol conversion. The acidic strength determined from the dehydration activity is reduced with zinc content. These results are in agreement with the results obtained from the NH_3 -TPD studies (Table 3.2.5). The added zinc ions enter into the tetrahedral sites of the manganese ferrite rather than the octahedral sites and increase the concentration of the Fe^{3+} ions in the octahedral sites. Thus, the partially inverse manganese ferrite is converted to the normal spinel. Thus Fe^{3+} ions in the octahedral sites are playing the main role in determining the enhanced dehydrogenation activity.

References:

- [1] C. Whiston; "X-ray Methods", (Eds., F. E. Prichard), ACOL, Thames Polytech., London, 1991.
- [2] P. S. Anilkumar, J. J. Shetri, S. D. Kulkarni, C. E. Deshpande and S. K. Date; *Mater. Lett.*, 27 (1996) 293.
- [3] R. D. Waldron; *Phy. Rev.*, 99 (1955) 1727.
- [4] W. B. White and B. A. DeAngelis; *Spectrochimica Acta*, 23A (1967) 985.
- [5] N. J. Jebrathinam and V. Krishnaswami; "Catalysis: Present and Future" (Eds., P. Kanta Rao and R. S. Beniwal), Wiley Eastern Ltd., New Delhi, 1995, p.354.
- [6] M. V. Joshi, S. G. Oak and V. S. Darshane; "Catalysis: Modern Trends"; (Eds., N. M. Gupta and D. K. Chakrabarthy), Narosha Publishing House, New Delhi, 1995, 275.
- [7] S. P. Ghorpade, V. S. Darshane and S. G. Dixit; *Appl. Catal.*, 166 (1998) 135.
- [8] B. Viswanathan and V. R. K. Murthy; " Ferrite Materials Science and Technology", Springer-Verlag and Narosha Publishing House, 1990, p. 15.
- [9] S. C. Byeon, K. S. Hong, J. G. Park and W. N. Kang; *J. Appl. Phys.*, 81(15) (1997) 7835.
- [10] D. Ravinder and K. Latha; *J. Appl. Phys.*, 75(10) (1994) 6118.
- [11] K. H. Rao, S. B. Raju, K. Agarwal and R. G. Mendiratta; *J. Appl. Phys.*, 52 (3) (1981) 1376.
- [12] K. P. Belov, E. P. Srma and O. A. Malikou; *Sov. Phys. Solid State*, 4 (1963) 2072.
- [13] K. P. Belov, A. A. Popova and E. V. Talalaeva; *Sov. Phys. Crystallography*, 3 (1960) 738.
- [14] M. Rosenberg, P. Nicolau and I. Bunget; *Phys. Stat. Sol.*, 4 (1964) K121.
- [15] M. Rosenberg, P. Nicolau and I. Bunget; *Phys. Stat. Sol.*, 4 (1964) K125.
- [16] Z. Simsa and J. Simosova; *Czech. J. Phys.*, B24 (1974) 439.
- [17] G. Amthaner and G. R. Rossman; *Phys. Chem. Minerals*, 11 (1984) 37.
- [18] G. M. Bancroft and R. G. Burns; *Geochim. Cosmochim. Acta.*, 31 (1967) 2219.
- [19] R. G. Burns; *Ann. Rev. Earth Planet. Sci.*, 9 (1981) 345.
- [20] S. J. Campell; *Astr. J. Phys.*, 37 (1984) 429.
- [21] J. M. D. Coey; "Chemical Applications of Mössbauer Spectroscopy", (Eds., G. L. Long), Plenum Press, New York, 1 (1984) 443.
- [22] B. J. Evans and S. Hafner; *J. Phys. Chem. Solids*, 29 (1968) 1573.
- [23] N. N. Greenwood and T. C. Gibb; "Mössbauer Spectroscopy", (Eds., Chapman and Hall), London, 1971, p. 258.
- [24] G. F. Goya, H. R. Rechenberg and J. Z. Jiang; *J. Appl. Phys.*, 84 (1998) 1101.
- [25] J. Jacob and H. Hobert; Proceedings of the Conference on Mössbauer Spectroscopy, Dresden, Physikalische Gesellschaft der DDR, Berlin, 1971, p. 523.
- [26] E. V. A. Ebsworth, D. W. H. Rankin and S. Cradock; "Structural Methods in Inorganic Chemistry", ELBS/Blackwell Scientific Publications, Great Britain, 1987, p. 287.

- [27] S. K. Senguptha and P. Lahiri; *Ind. J. Tech.*, 30 (1992) 172.
- [28] H. M. Gager and M. C. Hobson; *Eng.*, 11 (1) (1975) 117.
- [29] Dallal, M. N. Khan and A. Amed; *J. Mater. Sci.*, 25 (1990) 407.
- [30] M. R. De Gurie, R. C. O'Handley and G. Kalonji; *J. Appl. Phys.*, 65 (1989) 3167.
- [31] A. Watanabe, H. Yamamura, Y. Moriyoshi and S. Shirasaki; Proc. 3rd Int. Conf., (Eds., H. Watanabe, S. Idiaand M. Sugimoto), Centre for Academic Publications. Tokyo, p. 170.
- [32] C. Quintanar, V. Fuentes, M. Jimenez, S. Aburto and R. Valenzuela; *J. Magnetism and Magnetic Materials*, 54 (1986) 1339.
- [33] H. Knözinger and P. Ratnaswami; *Catal. Rev.-Sci.Eng.*, 17 (1979) 31.
- [34] J. P. Beaufils and Y. Barbaux, *J. Chem. Phys.*, 78 (1981) 347.
- [35] J. P. Beaufils and Y. Barbaux, *J. Appl. Crystallogr.*, 15 (1982) 301.
- [36] J. P. Jacobs, A. Maltha, J. G. H. Reintjes, J. Drimal, V. Ponec and H. H. Brongersma; *J. Catal.*, 147 (1994) 294.
- [37] J. Ziolkowski and Y. Barbaux, *J. Mol. Catal.*, 67(1991)199.
- [38] B. C. Lippens and J. J. Steggerda; "Physical and Chemical Aspects of Adsorbents and Catalysts", (Eds., B.G Linsen), Academic Press, New York, 1970, p.171.
- [39] H. C. Yao and M. Shelef; *J. Phys. Chem.*, 78 (1974) 2490
- [40] M. Shelef, M. A. Z Wheeler and H. C. Yao; *Surf. Sci.*, 47 (1975) 697.
- [41] A. Aurox and A. Gervasini; *J. Phys. Chem.*; 94 (1990) 6371.
- [42] P. A. Jacobs and C. F. Heylen, *J. Catal.*, 34 (1974) 2.
- [43] A. Satsuma, Y. Kamiya, Y. Westi and T. Hattori; *Appl. Catal.*, 194-195 (2000) 253.
- [44] D. Martin and Duprez; *J. Mol. Catal.*; 118 (1997) 113.
- [45] M. C. C. Costa, L.F. Hodson, R. A. W. Johnstone and D. Whitaker; *J. Mol. Catal.*, 142 (1999) 349.
- [46] C. P. Bezouhanova and M. A. Al-Zihari; *Catal. Lett.*, 11 (1991) 245.
- [47] M. Debrovolszky, P. Tetenyi and Z. Paal; *J. Catal.*, 74 (1982) 31.
- [48] K. Tanabe, M. Misono, I. Ono and N. Hattori; *Stud. Surf. Sci. Catal.*, 51 (1989).
- [49] J. M. Winterbottom; "Catalysis", Royal Soc. Chem., 4 (1981) 141.
- [50] M. Ai; *J. Catal.*, 49 (1977) 305.
- [51] A. Ouqour, G. Coudurier and J. C. Vedrine; *J. Chem. Soc. Faraday Trans.*, 89 (1993) 3151.
- [52] F. Figueras-Rocca, L. Mourgues and Y. Trambouze; *J. Catal.*, 14 (1969) 107.
- [53] M. Ai; *Bull. Chem. Soc. Jpn.*, 50 (10) (1997) 2579.
- [54] A. Bielansky and J. Haber; *Catal. Rev.*, 19 (1979) 1.

Acylation And Alkylation Reactions

This chapter presents Friedel-Crafts liquid-phase benzylation of aromatic compounds and vapour-phase alkylation of aniline and phenol. The Friedel-Crafts reaction is of wide scope, principally for introducing carbon substituents into an aromatic ring [1]. *Friedel-Crafts acylation* acylates the ring, generally using acyl halides, acids, or anhydrides and *Friedel-Crafts alkylation* attaches an alkyl group, using an alkyl halide, alcohol or olefin. The choice of the reagent and the catalyst is normally dictated by the reactivity of the aromatic substrate. Electron-rich rings (thiophene or benzene substituted by electron-donor groups) need milder electrophiles to bring about reaction, while inactivated rings (benzene or halobenzenes) need more vigorous reagent/catalyst combinations. The reaction is an aromatic electrophilic substitution, the attacking electrophile being generated by the interaction of the reagent with the acid catalyst. Of these two types of Friedel-Crafts reactions, acylations are more selective and versatile because they do not give multiple acylation products nor products with rearranged acyl groups as alkylations are prone to do.

The chapter is divided into three sections. The first section gives a detailed discussion of the liquid-phase benzylation of the aromatic compounds (benzene, activated benzenes and deactivated benzenes) using benzoyl chloride as the benzylation reagent over the five series of manganese ferrite catalysts. In addition, the effect of various reaction parameters on product distribution of toluene benzylation is studied. Catalytic activity is correlated with the acid-base properties and activation energy determined from DC conductivity measurements. The second section deals with the thorough investigation of alkylation of aniline using methanol over the prepared systems. The detailed discussion regarding the influence of factors such as reaction temperature, molar ratio, time-on-stream and contact time are also presented. The alkylation of phenol using methanol over all the present systems and the effects of various reaction parameters are depicted in the third section.

4.1 Section I - Friedel-Crafts Benzoylation of Aromatic Compounds

Friedel-Crafts acylation reactions are fundamental and important processes in organic synthesis as well as in industrial chemistry [2, 3]. Conventionally, the Friedel-Crafts acylation of aromatic hydrocarbons is carried out in a homogeneous phase by using Lewis acids such as AlCl_3 , BF_3 , ZnCl_2 , TiCl_4 , FeCl_3 , or Brønsted acids such as polyphosphoric and HF as catalysts [4-6]. However, these processes have the inconvenience of using stoichiometric or even excess amount of the catalysts for the reaction to proceed [7]. In addition, rather reaction conditions, disposal of the spent catalyst, high toxicity, tedious work-up procedures, which may induce environmental pollution, especially in industrially scale processes. While ranging in effectiveness, life time and the increasing demand for cleaner processes prompted by stringent environmental laws, solid acids may be preferred to their counterparts as they offer a number of advantages including high activity and selectivity, easy recovery, regeneration and reuse of the catalyst.

Towards this purpose, different solid acids have been tested as catalysts for the acylation of aromatic compounds. Materials such as pillared clays and rare earth exchanged pillared clays [8], Nafion-H and Nafion/silica composites [9-11], sulphated zirconia [8, 12], graphite [13] and zeolites [14-23] have been proven to catalyse this reaction.

It is reported that in spite of their high acidity HZSM-5, HY and H-beta zeolites show very low activity even for activated benzenes [24, 25]. However, there are recent reports to show the high activity of zeolites undergoing acylation reactions of activated arenes. Botella *et al.* [26] tried the acylation of toluene with acetic anhydride over beta zeolites. They found beta zeolite as a good catalyst to perform acylation of toluene with acetic anhydride at 150°C. An arene/anhydride molar ratio in between 10 and 20 is beneficial for the reasonable conversions with high selectivities to methylacetophenone (MAP). It was found that the catalytic activity is influenced by the Brønsted acidity of the zeolite and therefore low frame work Si/Al ratios lead to better yields of MAP.

Singh *et al.* observed the benzoylation of xylenes using benzoyl chloride as the benzoylating agent [27] over various zeolites. Their results reveal that *o*-xylene can be

benzoylated selectively to 3,4-dimethylbenzophenone and zeolite H-beta exhibits higher activity and selectivity than that of the other zeolite catalysts. With benzotrichloride or benzoyl chloride as the acylating agent and HZSM-5 as the catalyst, activated arenes underwent benzoylation efficiently and the reaction is found essentially regiospecific [28]. Here, the authors presumed that the Lewis acid sites (Al^{3+}) in HZSM-5 can activate benzotrichloride or benzoyl chloride by way of coordination, resulting in phenyldichlorocarbenium ion and phenylacylium ion respectively, which in turn react with the aromatic nucleus to produce benzophenones.

Hino and Arata report that solid super acids, sulphated zirconia and alumina showed activities for the benzoylation of toluene with benzoyl chloride and benzoic anhydride at temperatures below the reflux temperature of the mixture [25, 29]. The authors account another super acid system, tungsten oxide supported on zirconia, which was found to be active for the acylation reaction [30]. Further, Arata *et al.* examined the benzoylation of toluene with benzoic anhydride over metal promoted sulphated zirconia, the enhancement in the activity by the addition of Pt and Ru was observed exceedingly effective and the isomer distribution of methylbenzophenone was similar to that with the usual homogeneous reaction [31].

In an effort to promote rare earth salts as catalysts for Friedel-Crafts electrophilic substitutions, Baundry *et al.* reported the results of alkylation [32, 33] and acylation [34] reactions of activated benzene rings using reusable supported lanthanide salts as heterogeneous catalysts. The benzoylation of anisole gave high yields of products while benzene failed to react. The rate of the reaction was found to increase with substrates with electron donating groups, which stabilizes the benzoyl cation intermediate. The phosphotungstic acid supported on silica as well as its cesium salts were found active for the acylation of activated benzenes with crotonic acids as the acylating agent [35].

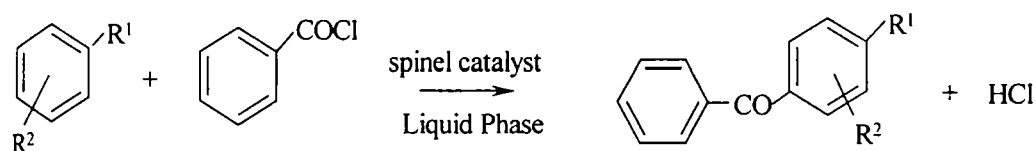
Zinc chloride impregnated on an industrial montmorillonite clay, K10, nicknamed as 'clayzic' is efficient for the acylation of anisole [36]; Cornelis *et al.* [37, 38] made the comparative analysis of the kinetic behaviours of anisole in benzoylation and acylation over this catalyst and proved that the chemisorption of anisole is not the

rate determining step. Ferrospinel of nickel, cobalt and copper and their sulphated analogues have been reported to be active for the benzoylation of toluene [39].

Though some catalysts that complete the acylation by catalytic use have been reported [40-52], substrates were limited to activated benzenes or aryl derivatives. There are only a few reports regarding the acylation of deactivated benzenes and development of more efficient and powerful catalysts is strongly demanded.

Kobayashi *et al.* report catalytic Friedel-Crafts acylation of benzene and deactivated benzenes such as chlorobenzene and fluorebenzene using $\text{Hf}(\text{OTf})_4$ and TfOH [53]. They observed both aromatic and aliphatic acid chlorides as the acylating agents reacted smoothly under the conditions to afford the corresponding aromatic ketones in good yields. Later, bismuth(III) trifluorometane, which was found as a good option for the acylation of deactivated benzenes was reported by Repichet *et al.* [54]. According to their observation, benzoyl chloride is the better acylating agent than benzoic anhydride for the acylation of deactivated benzenes.

The study of benzoylation of aromatic compounds using benzoyl chloride as the benzoylating agent and the prepared ferrite systems as catalysts is conveniently described under two headings as (i) benzoylation of activated benzenes (toluene, xylenes and anisole) and (ii) benzoylation of deactivated benzenes (benzene, fluorobenzene, chlorobenzene and bromobenzene). A schematic representation of the benzoylation of aromatic compounds using benzoyl chloride can be presented as below (Fig. 4.1.1):



where,

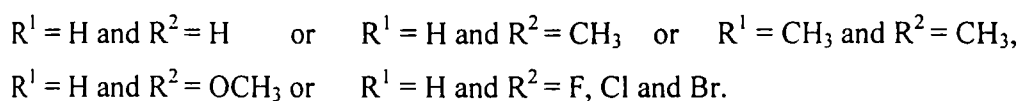


Fig 4.1.1. Schematic representation of benzoylation of aromatic compounds using benzoyl chloride.

4.1.1 Benzoylation of activated benzenes (toluene, xylenes and anisole)

The presence of an activating group in the aromatic ring makes acylation of activated benzenes more easy. In order to get the desired selective product, the use of suitable catalysts and optimization of the reaction conditions are necessary. As a representative reaction, benzoylation of toluene using benzoyl chloride (BOC) as the benzoylating agent is done for the process optimization and comparison of the activity of the prepared systems.

4.1.1.1 Benzoylation of toluene

The liquid-phase benzoylation of toluene was done by taking a mixture of toluene, benzoyl chloride and minute amount of the prepared systems as catalysts in a 50 mL double necked round bottom flask equipped with a reflux condenser in an oil bath. The reaction yielded mainly two products, which were estimated by GC and identified by GC-MS as 2-methylbenzophenone (2-MBP) and 4-methylbenzophenone (4-MBP). A small amount of a third product identified as 3- methylbenzophenone (3-MBP) is also detected. The reaction is represented schematically by the following figure (Fig. 4.1.2).

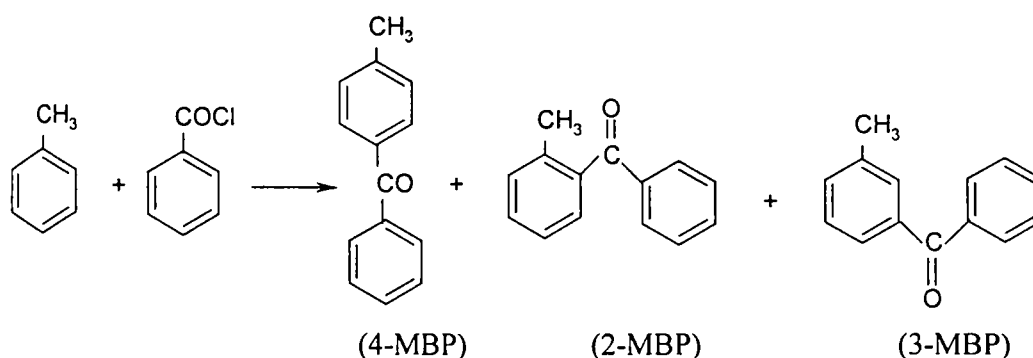


Fig.4.1.2. Scheme for the benzoylation of toluene.

The catalytic activity and product distribution greatly depend on the composition of the catalyst and also on the reaction conditions. The process optimization was carried out by varying the reaction parameters such as amount of catalyst, reaction temperature, catalyst composition, presence of moisture in the reaction mixture as well as in the catalyst and toluene/BOC molar ratio. The details of each are given in the forthcoming sections.

4.1.1.1.1 Effect of catalyst loading

In heterogeneous catalysis the amount of catalyst plays a crucial role in determining the rate of the reaction. The amount of catalyst required for the reaction was optimized by taking MnFe_2O_4 as catalyst. Prior to each experiment the catalyst was activated at 500°C for 2 h. The toluene/BOC molar ratio was taken as 10 and the reaction temperature was set at 80°C . The reaction was allowed to run for 20 minutes in an oil bath with magnetic stirring using different amount of catalysts. The effect of amount of catalyst on the percentage conversion of BOC is presented in the figure shown below (Fig.4.1.3).

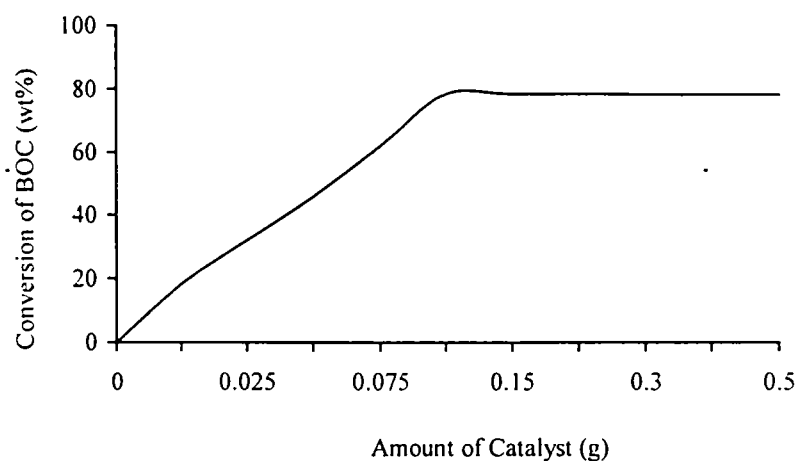


Fig 4.1.3. Effect of catalyst loading. Catalyst- MnFe_2O_4 , Reaction temperature- 80°C , Toluene/BOC molar ratio-10, Reaction time- 20 minutes.

It can be seen from the above figure that the amount of catalyst has an imperative function in the benzoylation reaction. The reaction is not occurring without the presence of a catalyst. As the amount of catalyst increased from zero grams to 0.1 g, the percentage conversion of BOC increased from 0 % up to 78.42 %. Thus the product yield was found to be proportional to the amount of the catalyst taken up to 0.1g, establishing the heterogeneity of the method. After this, the conversion of BOC to the reaction products is found to be remaining more or less constant. This trend can be explained in terms of the fact that the further increase in the catalyst amount restricts desorption of the acylated product from the catalyst surface. Thus, it is understood that

there is an optimum amount of catalyst for the effective performance and in this case, it is 0.1 g. Therefore, 0.1 g of the catalyst was used in the subsequent experiments.

4.1.1.1.2 Effect of reaction temperature

Figure 4.1.4 shows the variation of the conversion of BOC and the product distribution with reaction temperature at a time of 20 minutes. The catalyst chosen was MnFe_2O_4 and the toluene/BOC molar ratio was selected to be 10.

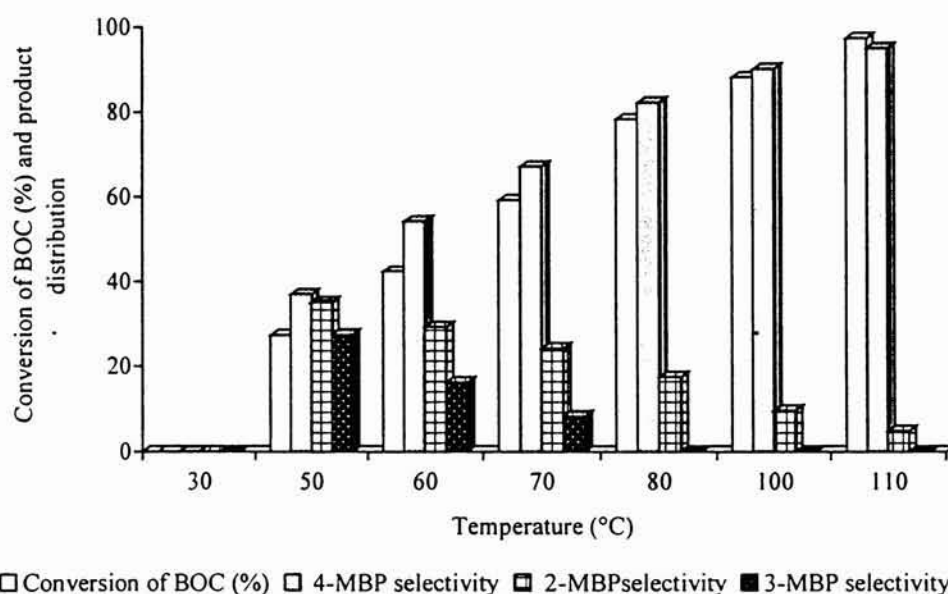


Fig. 4.1.4. Effect of reaction temperature. Catalyst- MnFe_2O_4 , Toluene/BOC molar ratio-10, Reaction time- 20 minutes.

At room temperature, conversion of benzoyl chloride is not taking place. The reaction needs diminutive temperature to activate the reactant molecules. From Fig. 4.1.4, it is clear that the conversion of BOC and selectivity to the para product, 4-MBP are increasing with the rise of temperature. This is probably due to the speedy desorption of the acylated product from the catalyst surface with increase in temperature. This facilitates the further adsorption of reactant molecules, which resulted in the increased conversion of BOC. Also, there can be the chance of formation of the bulkier products when the reaction temperature is raised, since the higher reaction temperature favours the consecutive acylation, disproportionation, alkylation and decarboxylation [26]. But no such by-products were observed even at 110°C. Though the maximum conversion of

BOC (%) and high selectivity for 4-MBP was obtained at the reaction temperature of 110°C (refluxing temperature of the reaction mixture), a reaction temperature of 80°C was selected for further studies to get the better comparative results.

4.1.1.3 Duration of reaction run

For studying the effect of reaction time on benzylation of toluene, the reaction was carried out with a toluene/BOC molar ratio of 10, at a reaction temperature of 80°C for half an hour. The filtrate was collected from the reaction mixture at a regular interval of 5 minutes for the GC analysis. The correlation between conversion of BOC, product distribution and reaction time for the benzylation of toluene over the catalyst, MnFe_2O_4 is illustrated in figure 4.1.5.

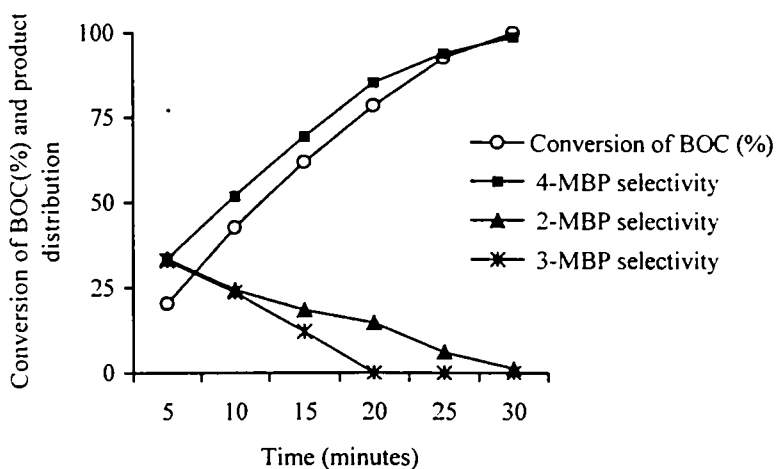


Fig.4.1.5. Effect of reaction time. Catalyst- MnFe_2O_4 , Toluene/BOC molar ratio-10, Reaction temperature- 80°C.

The conversion of BOC and selectivity for 4-MBP over MnFe_2O_4 is found to increase with increase in reaction time and reached the maximum in 30 minutes of reaction run. The increase in conversion of BOC with time, confirming the heterogeneity of the catalytic reaction. Again, the products formed during the initial run of the reaction is suspected to convert to thermodynamically more stable para product with increase in reaction time.

4.1.4 Effect of toluene/BOC molar ratio

A series of experiments were done at 80°C with different molar ratios of toluene/BOC over MnFe₂O₄. Fig. 4.1.6 shows the effect of toluene /BOC molar ratio in the reaction mixture on the activity of MnFe₂O₄ and product distribution at a fixed toluene concentration. In all the cases, 4-MBP and 2-MBP were the main reaction products identified. However, at lower toluene/BOC molar ratios (t/ b = 2.5, 5 and 7.5) a significant amount of 3-MBP was also formed in the reaction mixture. Dibenzoylated products were not observed even at lower toluene/BOC molar ratios in any of the systems.

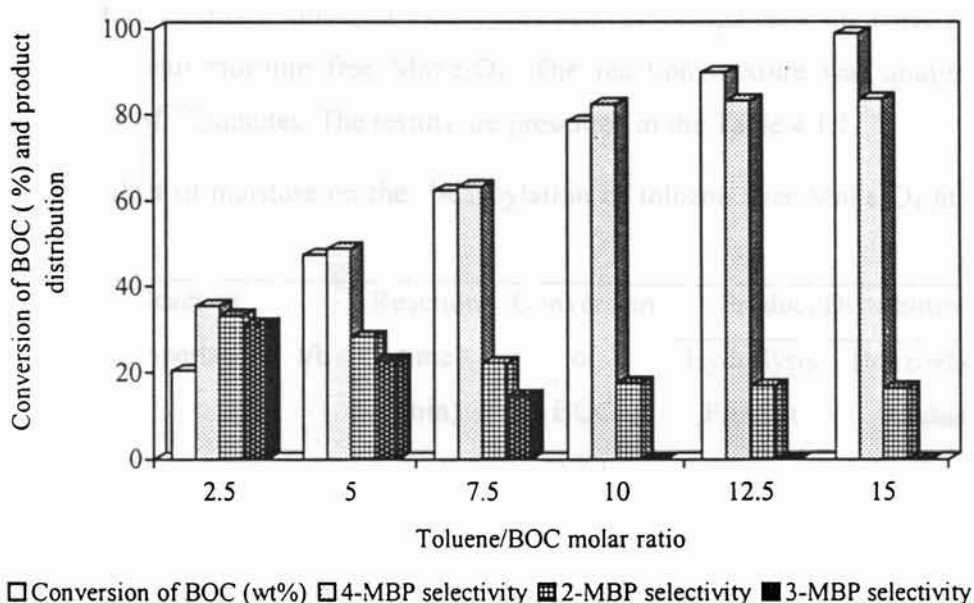


Figure 4.1.6. Effect of toluene/BOC molar ratio. Catalyst-MnFe₂O₄, Reaction temperature- 80°C, Reaction time-20 minutes.

Since toluene is taken in excess, the reaction is supposed to proceed via a pseudo unimolecular mechanism. The rate of the reaction, therefore, should vary with the concentration of the benzoyl chloride taken. From Fig. 4.1.6, it can be seen that the conversion of BOC is increased with the increase in the toluene/ BOC molar ratio. i.e., rise in concentration of BOC in the reaction mixture reduces the product yield. This contradictory observation may be due to the inhibiting effect caused by the acylated products, which can be strongly adsorbed on the catalyst surface [55]. This restricts further adsorption of the reactant molecules and thus reduces the conversion of BOC.

The inhibition would be less significant for reaction mixtures richer in toluene, which helps to desorb the ketones formed. It is seen that the selectivity for the formation of 4-MBP remains constant beyond the toluene/BOC molar ratio of 10 .

4.1.1.5 Effect of moisture

In order to study the effect of moisture in the catalyst and in the reaction mixture, the catalyst and toluene were kept in a desiccator saturated with water vapours at room temperature for 48 h. The reactions were carried out at 60°C for 1 h. by taking toluene/BOC molar ratio of 10 in a 50 mL double necked round bottom flask using about 0.1 g of moisture adsorbed MnFe₂O₄ as the catalyst. For comparison, the reaction was also performed with moisture free MnFe₂O₄. The reaction mixture was analyzed at regular intervals of 10 minutes. The results are presented in the Table 4.1.1.

Table 4.1.1. Effect of moisture on the benzoylation of toluene over MnFe₂O₄ at 60°C and t/b =10.

Catalyst	Reaction temperature	t/b	Reaction time (min)	Conversion of BOC (%)	Product Distribution	
					Hydrolysis Product	Benzoylated Product
MnFe ₂ O ₄ (adsorbed with moisture)	60°C	10	10	25.23	100	--
			20	42.12	100	--
			30	53.51	100	--
			40	61.62	100	--
			50	70.61	90	10
			60	91.48	88.53	11.47
MnFe ₂ O ₄	60°C	10	10	48.72	--	100
			20	53.48	--	100
			30	62.97	--	100
			40	71.67	--	100
			50	77.48	--	100
			60	80.96	--	100

In the presence of moisture, hydrolysis of benzoyl chloride was observed as the major reaction, leading to benzoic acid as the product in the initial stages of the reaction. After some time, the benzoylation reaction started to come about leading to the formation of 4-MBP. From data in Table 4.1.1, it can be seen that there exists an induction period for the benzoylation reaction due to the presence of adsorbed moisture on the catalyst. Induction period is the time required for replacing the adsorbed moisture by the reactants to start the catalytic reaction. With the fresh catalyst, only the benzoylation reactions were observed. From these observations it can be inferred that the Lewis acid sites are catalyzing the reaction and are initially blocked by the adsorbed moisture enhancing the hydrolysis of the benzoylating agent. Thus for benzoylation reactions with BOC as the benzoylating agent, moisture free catalysts and reactants are recommended, otherwise redundant products may come up.

4.1.1.1.6 Comparison of catalyst composition

We have prepared five series of manganese ferrosinels and for the comparison of catalyst composition, the results and discussions are conveniently made under five groups: (a) Cr-Mn series (b) Co-Mn series (c) Ni-Mn series (d) Cu-Mn series and (v) Zn-Mn series. The commercially available individual metal oxides and the conventional homogeneous catalyst AlCl_3 , were also looked for the catalytic reaction. From the product yield and considering the reaction as a pseudo unimolecular, the intrinsic rate constants in the units of $(\text{min}^{-1} \text{m}^{-2})$ was determined for each catalyst sample using the formula,

$$k (\text{min}^{-1} \text{m}^{-2}) = \frac{2.303}{t w A} \log \frac{100}{(100 - \% \text{ yield})}$$

where,

t = time of the reaction (minutes), w = weight of the catalyst (g) and A = BET surface area of the catalyst ($\text{m}^2 \text{g}^{-1}$).

(a) $\text{Cr}_x\text{Mn}_{(1-x)}\text{Fe}_2\text{O}_4$ (x = 0, 0.2, 0.4, 0.6, 0.8 and 1.0) - type systems

The percentage yield of the product, rate constant and the product distribution for different composition of the Cr- Mn series are presented in Table 4.1.2.

Table 4.1.2. Benzoylation of toluene with BOC over $\text{Cr}_x\text{Mn}_{(1-x)}\text{Fe}_2\text{O}_4$ ($x = 0, 0.2, 0.4, 0.6, 0.8$ and 1.0)- type systems.

Catalyst	Product yield (%)	Rate Constant ($10^{-3}\text{min}^{-1}\text{m}^{-2}$)	Selectivity (%)		
			4-MBP	2-MBP	3-MBP
MnFe_2O_4	78.42	4.99	82.38	17.62	---
$\text{Cr}_{0.2}\text{Mn}_{0.8}\text{Fe}_2\text{O}_4$	42.79	4.27	80.79	16.37	2.84
$\text{Cr}_{0.4}\text{Mn}_{0.6}\text{Fe}_2\text{O}_4$	33.18	3.71	76.32	22.61	1.07
$\text{Cr}_{0.6}\text{Mn}_{0.4}\text{Fe}_2\text{O}_4$	26.90	3.29	67.32	32.06	0.62
$\text{Cr}_{0.8}\text{Mn}_{0.2}\text{Fe}_2\text{O}_4$	18.34	2.40	66.37	33.63	---
CrFe_2O_4	11.57	1.71	62.73	37.27	---

Reaction Temperature- 80°C , Reaction time- 20 minutes, $t/b = 10$

The data clearly reveal that the successive incorporation of chromium ions into the pure manganese ferrosinell. MnFe_2O_4 , reduce the catalytic activity towards benzoylation reaction and also the selective formation of 4-MBP. It is evident from the NH_3 -TPD profiles of these spinels (Table 3.2.1) and from the thermodesorption studies of pyridine (Table 3.2.6) that the total acidity and also strong acidity decreased noticeably, whereas the limiting concentrations of electron acceptors were increased (Table 3.2.8). In other words, replacement of Mn by Cr decreased the acidity of the series and is confirmed from the their dehydration activity in cyclohexanol decomposition reaction (Table 3.2.13).

MnFe_2O_4 is a random spinel or partially inverse spinel and substitution of Mn by Cr replaces Fe^{3+} from the octahedral sites to hindered tetrahedral sites (Table 3.1.9). In the substituted ferrosinels, the high strength Lewis acids are provided by the octahedral Fe^{3+} ions which are more exposed on the catalyst surface. The shifting of Fe^{3+} from the octahedral sites to hindered tetrahedral sites reduces the catalytic activity of Cr-Mn series. And as far as chromium ions are concerned they do not seem to generate strong enough catalytic activity in spinels to catalyse Friedel-Crafts reactions [56].

The foremost factor seemed to be the activation energy of the catalyst, which is the energy gap between valence band and conduction band. The activation energy of the series goes on increasing with successive substitution of Mn by Cr. Figure 4.1.7 depicts the variation of rate constant and activation energy with different compositions of Cr-Mn series. The figure clearly shows the decrease in rate constant with increase in activation energy of the catalysts.

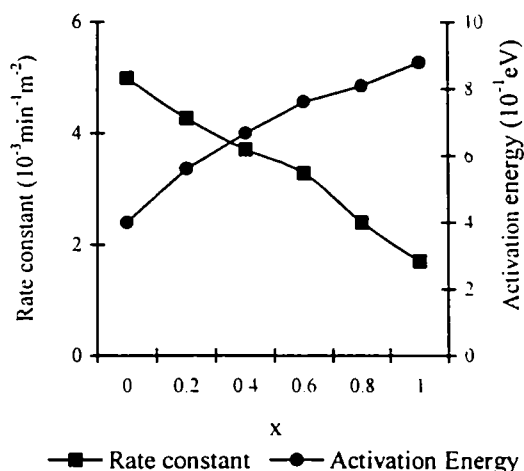


Fig.4.1.7 Variation of rate constant and activation energy with composition of $\text{Cr}_x\text{Mn}_{(1-x)}\text{Fe}_2\text{O}_4$ ($x = 0, 0.2, 0.4, 0.6, 0.8$ and 1) type catalysts

All these aforementioned factors synergistically decrease the catalytic activity of chromium substituted manganese ferrospinels.

(b) $\text{Co}_x\text{Mn}_{(1-x)}\text{Fe}_2\text{O}_4$ ($x = 0, 0.2, 0.4, 0.6, 0.8$ and 1.0) - type systems

Table 4.1.3 presents the product yield (%), rate constant and product distribution of toluene benzoylation performed over different Co-Mn systems.

Table 4.1.3. Benzoylation of toluene with BOC over $\text{Co}_x\text{Mn}_{(1-x)}\text{Fe}_2\text{O}_4$ ($x = 0, 0.2, 0.4, 0.6, 0.8$ and 1.0)- type systems

Catalyst	Product yield (%)	Rate Constant ($10^{-3} \text{ min}^{-1} \text{ m}^{-2}$)	Selectivity (%)		
			4-MBP	2-MBP	3-MBP
MnFe_2O_4	78.42	4.99	82.38	17.62	---
$\text{Co}_{0.2}\text{Mn}_{0.8}\text{Fe}_2\text{O}_4$	96.52	14.91	73.37	20.54	6.09
$\text{Co}_{0.4}\text{Mn}_{0.6}\text{Fe}_2\text{O}_4$	97.71	17.94	70.08	23.74	5.18
$\text{Co}_{0.6}\text{Mn}_{0.4}\text{Fe}_2\text{O}_4$	97.98	19.91	69.03	26.65	4.32
$\text{Co}_{0.8}\text{Mn}_{0.2}\text{Fe}_2\text{O}_4$	98.67	25.22	68.13	27.71	4.16
CoFe_2O_4	98.93	30.00	67.19	28.84	3.97

Reaction Temperature- 80°C , Reaction time- 20 minutes, t/b – 10

The acidity measurements reveal that the incorporation of Co^{2+} in manganese ferrosipinel decreases its total acidity, especially acidity in the strong region slightly (Table 3.2.2). Interestingly, we observed a greater enhancement in catalytic activity by the incorporation of Co^{2+} , though the selectivity for 4-MBP was considerably abridged. Along with 2-MBP, systems afforded 3-MBP in a significant yield.

The greater catalytic activity of the Co-Mn series can be due to the following reasons. The acylated products formed get adsorbed on the acid sites of the catalyst surface owing to its polarity, restrict further adsorption of the reactant molecules and reduce the reaction rate. Thus, catalysts having lesser amount of acidic sites promote the desorption of the acylated products and thereby increasing the catalytic activity. But when the competitive adsorption of toluene, benzoyl chloride and the benzoylated product is considered, the preponderance adsorption of the benzoylated product is less significant and this possibility is ruled out.

However, when the band gap or the activation energy of the catalysts is taken into account, substitution of Mn by Co in the pure manganese ferrosipinel lowered the activation energy of manganese ferrosipinel considerably. Figure 4.1.8 shows the variation of rate constant and activation energy with composition of Co-Mn series of ferrites. The enhancement in catalytic activity showed a proportionate increase with decrease in activation energy. Thus it can be inferred that the lowering of activation energy by the incorporation of Co^{2+} ions in the octahedral position playing the foremost role in the enhancement of benzoylation of toluene.

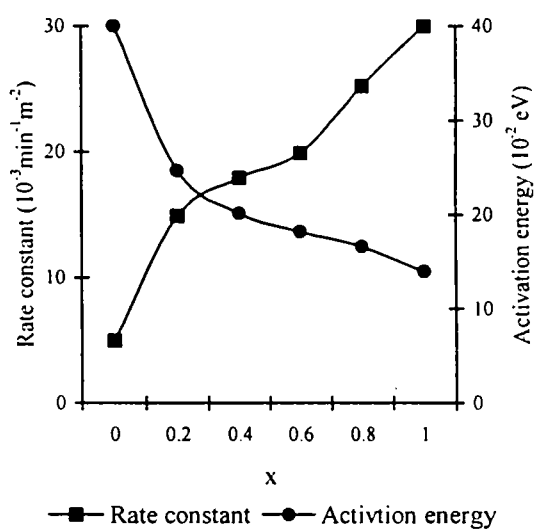


Fig.4.1.8 Variation of rate constant and Activation energy with composition of $\text{Co}_x\text{Mn}_{(1-x)}\text{Fe}_2\text{O}_4$ ($x = 0, 0.2, 0.4, 0.6, 0.8$ and 1) type catalysts.

(c) $\text{Ni}_x\text{Mn}_{(1-x)}\text{Fe}_2\text{O}_4$ ($x = 0, 0.2, 0.4, 0.6, 0.8$ and 1.0) - type systems

The catalytic activity studies in this series for the benzoylation of toluene are given in Table 4.1.4.

Table 4.1.4. Benzoylation of toluene with BOC over $\text{Ni}_x\text{Mn}_{(1-x)}\text{Fe}_2\text{O}_4$ ($x = 0, 0.2, 0.4, 0.6, 0.8$ and 1.0)- type systems

Catalyst	Product yield (%)	Rate Constant ($10^{-3}\text{min}^{-1}\text{m}^{-2}$)	Selectivity (%)		
			4-MBP	2-MBP	3-MBP
MnFe_2O_4	78.42	4.99	82.38	17.62	---
$\text{Ni}_{0.2}\text{Mn}_{0.8}\text{Fe}_2\text{O}_4$	64.23	4.91	87.23	11.24	1.53
$\text{Ni}_{0.4}\text{Mn}_{0.6}\text{Fe}_2\text{O}_4$	60.57	4.85	88.12	10.42	1.42
$\text{Ni}_{0.6}\text{Mn}_{0.4}\text{Fe}_2\text{O}_4$	57.31	4.80	89.75	9.52	0.73
$\text{Ni}_{0.8}\text{Mn}_{0.2}\text{Fe}_2\text{O}_4$	51.80	4.75	93.39	7.49	---
NiFe_2O_4	45.20	4.70	92.93	6.91	---

Reaction Temperature- 80°C , Reaction time- 20 minutes, $t/b = 10$

Though the progressive nickel addition decreased the rate constant, it enhanced the para selectivity appreciably. In these systems, we observed a decrease in total acidity and strong acid sites by the progressive nickel doping into the pure manganese ferrosphenel as evident from the NH_3 -TPD studies (Table 3.2.3) and thermodesorption studies of pyridine adsorbed samples (Table 3.2.6). The dehydration activity in cyclohexanol decomposition signifying the acidic strength of the catalysts is rather decreased (Table 3.2.13) with nickel doping whereas the limiting concentrations of electron acceptors increased (Table 3.2.10).

It is evident from the cation distribution (Table 3.1.9) that the progressive substitution of Mn^{3+} ions by Ni^{2+} ions increased the inverse nature of MnFe_2O_4 , but did not alter the concentration of Fe^{3+} ions in the octahedral sites. Hence the concentration of Ni^{2+} ions in the octahedral sites is seemed to be responsible for the catalytic activity of this series.

From the DC conductivity measurements data (Table 3.1.5) we observe an enhancement in activation energy by the successive replacement of Mn by Ni, and NiFe₂O₄ have the highest value for activation energy in this series. The reduction in catalytic activity of these systems follows the same order with increase in activation energy. Fig. 4.1.9 shows the variation of rate constant and activation energy with composition. The synergistic effect of enhancement in activation energy and reduced acidity in the Ni-Mn series decreased their catalytic activity.

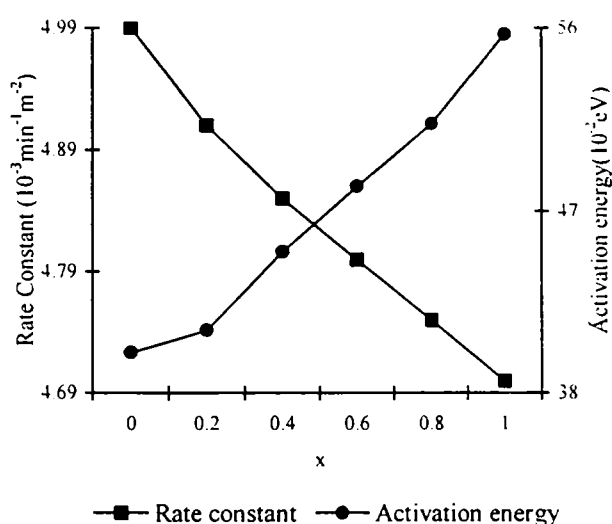


Fig.4.1.9. Variation of rate constant and activation energy with composition of Ni_xMn_(1-x)Fe₂O₄ (x = 0, 0.2, 0.4, 0.6, 0.8 and 1)- type catalysts.

(d) Cu_xMn_(1-x)Fe₂O₄ (x = 0, 0.2, 0.4, 0.6, 0.8 and 1.0) - type systems

A series of experiments were performed to evaluate the catalytic activities of different Cu-Mn ferrites. The results obtained are summarized in Table 4.1.5.

Table 4.1.5. Benzoylation of toluene with BOC over Cu_xMn_(1-x)Fe₂O₄ (x = 0, 0.2, 0.4, 0.6, 0.8 and 1.0)- type systems.

Catalyst	Product yield (%)	Rate Constant (10 ⁻³ min ⁻¹ m ⁻²)	Selectivity (%)		
			4-MBP	2-MBP	3-MBP
MnFe ₂ O ₄	78.42	4.99	82.38	17.62	---
Cu _{0.2} Mn _{0.8} Fe ₂ O ₄	89.72	8.27	74.28	18.33	7.39
Cu _{0.4} Mn _{0.6} Fe ₂ O ₄	93.79	11.03	71.18	20.85	7.97
Cu _{0.6} Mn _{0.4} Fe ₂ O ₄	95.76	13.31	69.32	22.36	8.32
Cu _{0.8} Mn _{0.2} Fe ₂ O ₄	89.68	10.11	68.37	22.40	9.23
CuFe ₂ O ₄	80.51	8.66	67.98	22.75	9.27

Reaction Temperature- 80°C, Reaction time- 20 minutes, t/b – 10

In these systems, we couldn't observe a correlation between the amount of acidic sites and the catalytic activity for toluene benzylation whereas a good correlation between the activation energy and catalytic activity was found. The analysis of the data in Table 4.1.5 shows that the catalytic activity of the manganese ferros spinel increases by the successive copper doping up to $x = 0.6$ and afterwards showed a decline in the activity. However, for the values of x above 0.6, the values of activation energy increase,

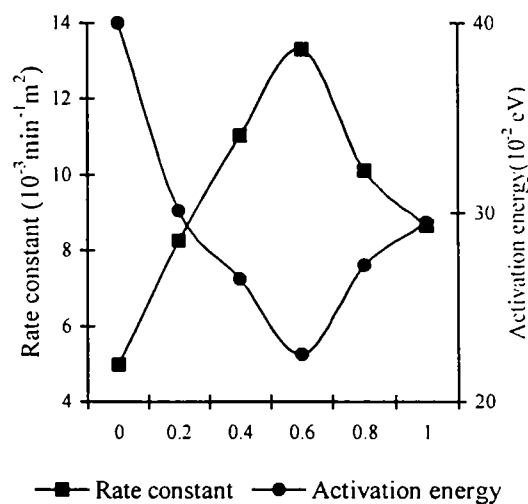


Fig.4.1.10. Variation of rate constant and activation energy with composition of $\text{Cu}_x\text{Mn}_{(1-x)}\text{Fe}_2\text{O}_4$ ($x = 0, 0.2, 0.4, 0.6, 0.8$ and 1) type catalysts.

which resulted in a decrease in the rate of the reaction. Fig. 4.1.10 clearly depicts the variation of rate constant and activation energy with composition. The selectivity for 4-MBP is considerably reduced on incorporating copper ions. Along with 2-MBP, a significant amount of 3-MBP was also formed. Though the catalytic activity of manganese ferros spinel was increased from 2 to 2.5 fold by the incorporation of copper, the systems were seemed to be poorer choice in the selective formation of 4-MBP.

(e) $\text{Zn}_x\text{Mn}_{(1-x)}\text{Fe}_2\text{O}_4$ ($x = 0, 0.2, 0.4, 0.6, 0.8$ and 1.0) - type systems

The results obtained for the benzylation of toluene over different Zn-Mn ferros spinels are summarized in Table 4.1.6.

An examination of the data in Table 4.1.6 reveals that the zinc-manganese combination somewhat decreased the rate of the reaction and the product selectivity declined drastically. The incorporation of Zn ions into the manganese ferros spinel increased the amount of strong acidic sites as evident from the NH_3 -TPD measurements (Table 3.2.5) and thermodesorption studies of the pyridine adsorbed samples (Table 3.2.6). Hence a correlation between acidity and activity could not be achieved

Table 4.1.6. Benzoylation of toluene with BOC over $Zn_xMn_{(1-x)}Fe_2O_4$ ($x = 0, 0.2, 0.4, 0.6, 0.8$ and 1.0)- type systems

Catalyst	Product yield (%)	Rate Constant ($10^{-3} \text{min}^{-1} \text{m}^{-2}$)	Selectivity (%)		
			4-MBP	2-MBP	3-MBP
$MnFe_2O_4$	78.42	4.99	82.38	17.62	---
$Zn_{0.2}Mn_{0.8}Fe_2O_4$	60.42	4.83	57.59	21.68	20.73
$Zn_{0.4}Mn_{0.6}Fe_2O_4$	52.98	4.58	58.72	21.62	19.66
$Zn_{0.6}Mn_{0.4}Fe_2O_4$	45.07	4.03	63.79	18.71	17.50
$Zn_{0.8}Mn_{0.2}Fe_2O_4$	39.78	3.88	66.07	17.61	16.32
$ZnFe_2O_4$	34.01	3.68	68.36	16.32	15.32

Reaction Temperature- 80°C , Reaction time- 20 minutes, t/b – 10

Figure 4.1.11 shows the variation of rate constant and activation energy with composition of Zn-Mn ferrite series. The substitution of Mn by Zn increased the activation energy of the systems radically. The rise in activation energy of these systems follow the order: $ZnFe_2O_4 > Zn_{0.8}Mn_{0.2}Fe_2O_4 > Zn_{0.6}Mn_{0.4}Fe_2O_4 > Zn_{0.4}Mn_{0.6}Fe_2O_4 > Zn_{0.2}Mn_{0.8}Fe_2O_4 > MnFe_2O_4$. The rate of the reaction follows the reverse order and hence, the reduction in activity can be explained by considering the factors like enhancement in activation energy with Zn^{2+} substitution.

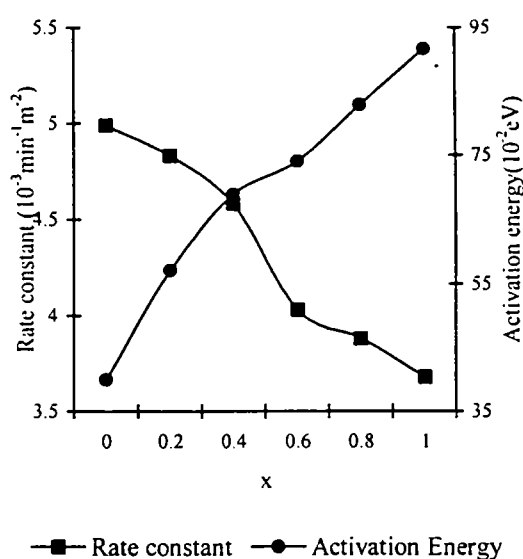


Fig.4.1.11. Variation of rate constant and activation energy with composition of $Zn_xMn_{(1-x)}Fe_2O_4$ ($x = 0, 0.2, 0.4, 0.6, 0.8$ and 1)-type catalysts.

The commercially available individual metal oxides and the conventional homogeneous catalyst $AlCl_3$, were also tested for the catalytic activity. The results are shown in the following table (Table 4.1.11).

Table 4.1.7. Benzoylation of toluene with BOC over individual metal oxides and AlCl₃.

Catalyst	Conversion of BOC (%)	Selectivity (%)		
		4-MBP	2-MBP	3-MBP
AlCl ₃	78.02	34.89	33.06	32.05
MnO ₂	1.24	100	--	--
Fe ₂ O ₃	72.87	33.64	33.76	32.6
Cr ₂ O ₃	--	--	--	--
CoO	0.78	100	--	--
NiO	0.20	100	--	--
CuO	0.25	100	--	--
ZnO	0.36	100	--	--

Reaction Temperature- 80°C, Reaction time- 20 minutes, t/b – 10

The homogenous catalyst AlCl₃ gave 78 % conversion which required more than the stoichiometric amount of the catalyst and furthermore, the product selectivity was very low. Fe₂O₃ gave reasonable percentage of conversion of BOC with low selectivity. No benzoylation reaction was observed over Cr₂O₃. Other metal oxides such as MnO₂, CoO, NiO, CuO and ZnO gave lower reactivity. The activation energy of the individual metal oxides varies in the range 2-5 eV whereas the activation energy of the different manganese ferrites varies in between 0.4 and 0.95 eV. The high activation energy of the metal oxides may be the cause for their poor activity.

4.1.1.1.7 Catalyst reusability

For checking the reusability, the catalyst was removed from the reaction mixture by filtration. It was washed thoroughly with acetone until free of reaction mixture, dried in an air oven for over night and activated at 500°C for 5 h. The same catalyst was again used for carrying out another reaction under the similar reaction conditions. As well, the catalyst was tested three times for the benzoylation of toluene. Though negligible, a decrease in conversion of BOC was observed, but the selectivity towards the formation of 4-MBP remained constant in recycling the catalyst (Table 4.1.8).

Table 4.1.8. Catalyst reusability

Number of times	Conversion of BOC (%)	Selectivity (%)		
		4-MBP	2-MBP	3-MBP
0	78.42	82.38	17.62	—
1	75.31	82.29	17.71	---
2	73.05	82.17	17.83	---
3	70.65	81.97	18.03	---

Catalyst-MnFe₂O₄, Amount of the catalyst –0.1 g, Reaction temperature- 80°C, Reaction time- 20 minutes, t/b – 10.

The small decrease in the conversion of BOC might be due to the iron leaching during the reaction. After the completion of the reaction and subsequent to the removal of the catalyst the filtrate was tested for iron with ammonium thiocyanate solution. A blood red colouration indicating the iron leaching during the reaction period was observed. Over again, the XRD of the reused catalyst after the third recycling was taken. Interestingly, we observed that the spinel phase remained intact even after the reaction. The XRD pattern of the reused catalyst retained all the distinctiveness of the fresh catalyst except for a small decrease in the intensity of the peaks (Figure 4.1.12). The lowering of intensity of XRD peaks may be due the leaching out of iron during the reaction.

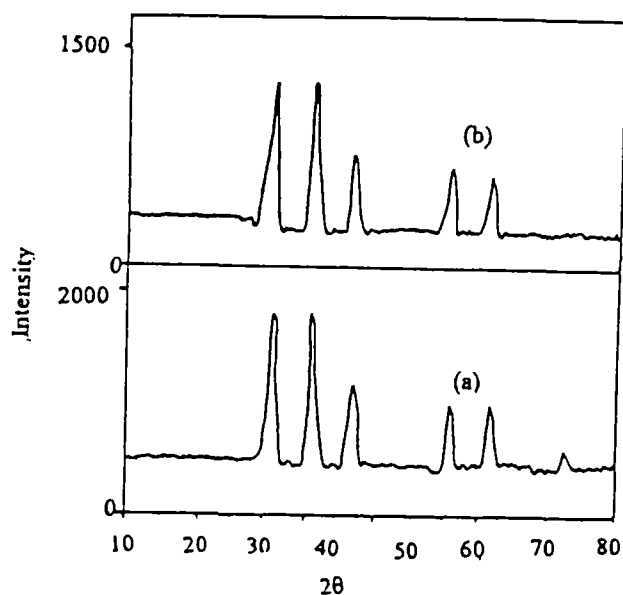


Fig. 4.1.12. XRD patterns of (a) fresh catalyst and (b) used catalyst.

Accordingly, all the spinel ferrites were found to be reusable to a large extent. The individual metal oxides and the conventional homogeneous catalyst, AlCl_3 were not found to be reusable to any possibility.

4.1.1.1.8 Mechanism of benzoylation reaction

The Friedel-Crafts acylation is an electrophilic substitution reaction.. The homogeneous Friedel-Crafts acylation requires a little more than the stoichiometric amount of the Lewis acid catalyst. Mainly two mechanisms are found to operate depending on the reaction conditions. In most cases, the active electrophile is believed to be an acylium ion, RCO^+ . In the other mechanism, the attacking species is a complex formed between the Lewis acid and the carbonyl group of the acyl halide. The acylium ion has been detected by IR spectroscopy in polar solvents such as nitrobenzene; but in non-polar solvents such as chloroform, only the complex and not the free ion is present. Regardless of which is the active electrophile, they are not as potent as those involved in other types of electrophilic substitutions.

Earlier studies on the heterogeneous Friedel-Crafts acylation of aromatic compounds reveal that both Brönsted and Lewis type of acid sites catalyse the reaction [25, 28, 31 and 38]. Arata *et al.* concluded from their reaction results on benzoylation of toluene using sulphate-supported alumina that the benzoyl cation (PhCO^+) from benzoyl chloride molecule is generated by a Brönsted site on the catalyst to form the acylated aromatics [25]. Paul *et al.*, by the mechanistic studies of benzoylation of aromatic compounds, presumed that the Lewis acid sites (Al^{3+}) in HZSM-5 catalysts promote the formation of phenylacylium ion, which in turn react with the aromatic nucleus to produce benzophenones [28].

Spinel ferrites possess both Brönsted and Lewis acid sites. It is considered that Brönsted acid sites are created by the adsorption of water on the Lewis acid sites [25] and Saur *et al.* from their studies on sulphated alumina and titania found the Brönsted acidity to be increased in the presence of moisture [57]. The study of effect of moisture on the catalyst for benzoylation of toluene showed that the rate of the reaction decreases due to moisture adsorption over the catalyst. This suggests that reaction involves the interaction of Lewis acid sites of the catalysts with benzoyl chloride. The interaction of

the Lewis acid site with BOC resulted in the formation of an electrophile ($C_6H_5CO^+$) which then attacks the toluene molecule to form methylbenzophenones. Again, from the catalyst comparison studies, it is revealed that more than the amount of acidic sites present in the system activation energy of the catalyst playing the foremost role in deciding the rate of the reaction. An easy adsorption of the aromatic substrate on the catalyst surface is hence proposed. Based on these facts, a plausible mechanism can be represented by the following figure (Fig. 4.1.13).

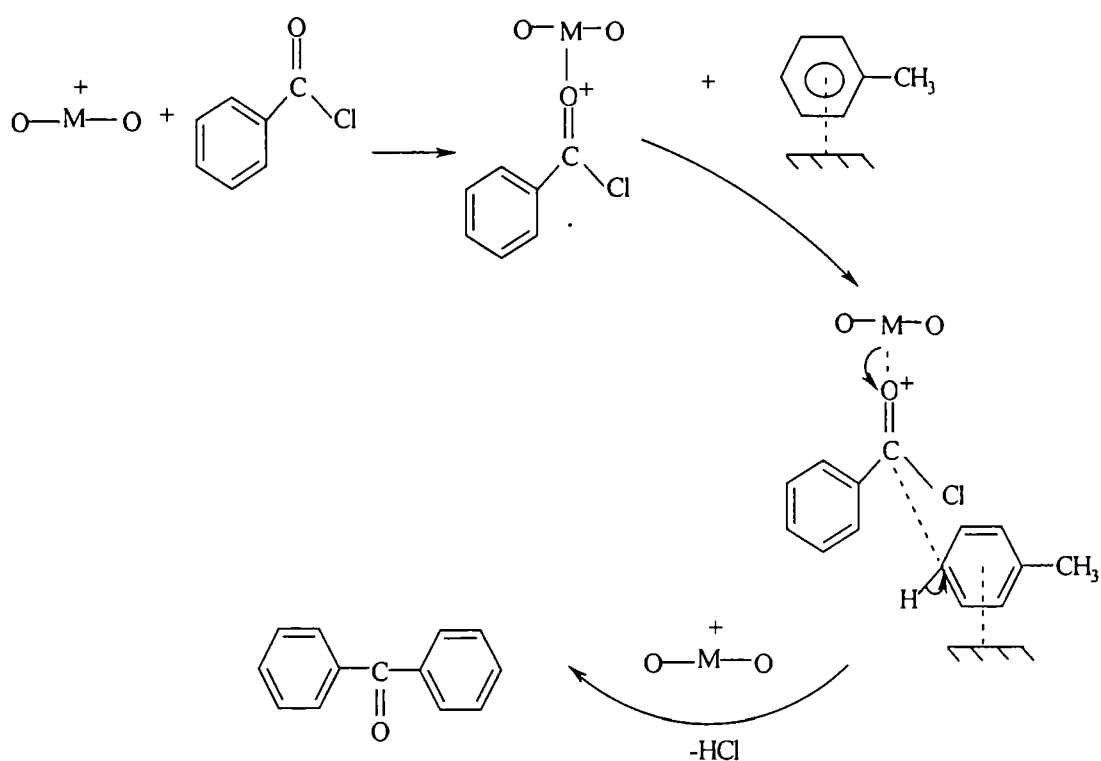


Fig. 4.1.13. Plausible mechanism of benzoylation of toluene using benzoyl chloride.

4.1.1.2 Benzoylation of xylenes

The presence of two activating methyl groups in the aromatic ring makes the acylation of xylenes more easier than toluene. Generally, zeolites are explored for the acylation of activated aromatic compounds to get the shape selective products [20, 21, 24, 58-64]. The benzoylation of *o*-xylene with benzoyl chloride was done over all the prepared ferrite systems to facilitate their activities and to compare the correlations given in the benzoylation of toluene. The major reaction product 3,4-dimethylbenzophenone is industrially important and is used for the manufacture of dyes and several organic intermediates for the production of fine chemicals.

The reaction procedure was the same as in the case of toluene benzoylation. Since xylene is an activated benzene, the reaction was very speedy with ferrite catalysts at the refluxing temperature and also several reaction products aroused. Accordingly, to get the comparable results, the reaction temperature was optimised at 50°C. The xylene/BOC molar ratio was 10 and the reaction run was carried out for 20 minutes. The reaction products were analyzed by GC and identified by GC-MS as 3,4-dimethylbenzophenone (3,4-DMBP) and 2,3-dimethylbenzophenone (2,3-DMBP). A reaction scheme can be drawn for the benzoylation of *o*-xylene with benzoyl chloride as the benzoylating agent is shown below (Figure. 4.1.14).

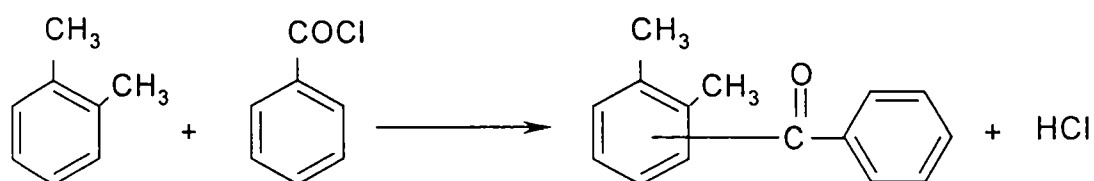


Fig. 4.1.14. Reaction scheme for benzoylation of *o*-xylene with benzoyl chloride over manganese ferros spinels.

The product yields, the rate constants and the product distribution for the benzoylation of *o*-xylene are presented in the following table (Table 4.1.9).

Table 4.1.9 Benzoylation of *o*-xylene with benzoyl chloride over manganese ferros spinels

Catalyst	Product Yield (%)	Rate Constant ($10^{-3} \text{ min}^{-1} \text{ m}^{-2}$)	Product Distribution (%)	
			3,4-DMBP	2,3-DMBP
MnFe ₂ O ₄	83.78	5.91	93.3	6.7
Cr _{0.2} Mn _{0.8} Fe ₂ O ₄	49.28	5.15	100	---
Cr _{0.4} Mn _{0.6} Fe ₂ O ₄	42.35	4.83	100	---
Cr _{0.6} Mn _{0.4} Fe ₂ O ₄	32.71	3.59	100	---
Cr _{0.8} Mn _{0.2} Fe ₂ O ₄	21.81	3.00	100	---
CrFe ₂ O ₄	18.66	2.88	100	---
Co _{0.2} Mn _{0.8} Fe ₂ O ₄	89.78	9.90	90.05	9.95
Co _{0.4} Mn _{0.6} Fe ₂ O ₄	92.52	12.31	91.22	8.78
Co _{0.6} Mn _{0.4} Fe ₂ O ₄	95.73	16.21	93.10	6.90
Co _{0.8} Mn _{0.2} Fe ₂ O ₄	98.71	25.31	95.54	4.46
CoFe ₂ O ₄	99.56	35.86	96.37	3.63
Ni _{0.2} Mn _{0.8} Fe ₂ O ₄	70.84	5.88	97.51	2.49
Ni _{0.4} Mn _{0.6} Fe ₂ O ₄	67.22	5.81	98.88	1.12
Ni _{0.6} Mn _{0.4} Fe ₂ O ₄	63.13	5.63	100	---
Ni _{0.8} Mn _{0.2} Fe ₂ O ₄	57.26	5.53	100	---
NiFe ₂ O ₄	50.19	5.44	100	---
Cu _{0.2} Mn _{0.8} Fe ₂ O ₄	85.49	7.01	91.35	8.65
Cu _{0.4} Mn _{0.6} Fe ₂ O ₄	86.52	7.96	93.46	6.54
Cu _{0.6} Mn _{0.4} Fe ₂ O ₄	87.91	8.90	96.66	3.34
Cu _{0.8} Mn _{0.2} Fe ₂ O ₄	85.62	8.59	98.59	1.41
CuFe ₂ O ₄	82.36	7.05	100	---
Zn _{0.2} Mn _{0.8} Fe ₂ O ₄	65.42	5.53	87.87	12.13
Zn _{0.4} Mn _{0.6} Fe ₂ O ₄	58.74	5.38	89.32	10.68
Zn _{0.6} Mn _{0.4} Fe ₂ O ₄	53.25	5.18	92.31	7.69
Zn _{0.8} Mn _{0.2} Fe ₂ O ₄	47.68	4.95	95.73	4.27
ZnFe ₂ O ₄	42.15	4.84	98.33	1.67

Reaction temperature- 50°C, Reaction time- 20 minutes, Amount of the catalyst-0.1 g, *o*-xylene/BOC molar ratio -10

The analysis of the data in Table 4.1.9 leads us to the following interpretations.

(a) $\text{Cr}_x\text{Mn}_{(1-x)}\text{Fe}_2\text{O}_4$ ($x = 0, 0.2, 0.4, 0.6, 0.8$ and 1.0) - type systems

The product yields and rate constants for manganese ferrospinels brought down by a long way by the progressive substitution of chromium. But in this case, the selectivity for 3,4-dimethylbenzophenone was highly appreciable. The reduction in the product yield can be due to the combined effect of increased activation energy (Table 3.1.6) and lowering of acidity (Table 3.2.1) due to chromium doping.

(b) $\text{Co}_x\text{Mn}_{(1-x)}\text{Fe}_2\text{O}_4$ ($x = 0, 0.2, 0.4, 0.6, 0.8$ and 1.0) - type systems

Though the introduction of cobalt in manganese ferrospinel enhanced the product yield dramatically, the selectivity for the 3,4-DMBP was somewhat diminished. It can be seen from the acidity measurements that the cobalt substitution in manganese ferrospinel decreased the total acidity as well as the acidity due to a strong sites to a small extent (Table 3.2.2). But a proportionate decrease in catalytic activity is not observed and so it is concluded that in this case acidity is not the core factor determining the activity. The lowering of activation energy with cobalt substitution (Table 3.1.6) supported the enhanced activity.

(c) $\text{Ni}_x\text{Mn}_{(1-x)}\text{Fe}_2\text{O}_4$ ($x = 0, 0.2, 0.4, 0.6, 0.8$ and 1.0) - type systems

Though the successive nickel doping in Ni-Mn ferrite series show reduced reaction rates, the selectivity for 3,4-DMBP increases appreciably with the nickel content. It is evident from the acidity measurements that nickel substitution decreases the acidity (Table 3.2.3). Also, the activation energy of this series is enhanced with nickel doping (Table 3.1.6). Both these factors together influence a reduction of product yield.

(d) $\text{Cu}_x\text{Mn}_{(1-x)}\text{Fe}_2\text{O}_4$ ($x = 0, 0.2, 0.4, 0.6, 0.8$ and 1.0) - type systems

The effect of copper doping in manganese ferrite is to an increase in the rate of the reaction initially, but then the rate declines with further introduction of copper content. It can be seen from the DC conductivity measurements that the lowering of activation energy with copper substitution showed an increase in the value beyond $x = 0.6$ (Table 3.1.6). So it is clear that activation energy of the catalyst is the foremost factor deciding the activity.

(e) $Zn_xMn_{(1-x)}Fe_2O_4$ ($x = 0, 0.2, 0.4, 0.6, 0.8$ and 1.0) - type systems

The zinc substitution decreased the rate of the reaction and also the selectivity for 3,4-DMBP. The enhanced acidity in the strong region with successive incorporation of zinc as evident from the NH_3 -TPD studies (Table 3.2.5) and thermodesorption studies of pyridine adsorbed samples (Table 3.2.6), found no correlation with the catalytic activity. But the DC conductivity measurements revealed that the replacement of Mn by Zn increased the activation energy (Table 3.1.6), which is the prime cause for their poor catalytic activity.

4.1.1.2.1 Benzoylation of isomeric xylenes

The position of the methyl groups on the benzene ring plays an important role in defining the type of products in xylenes. *Ortho*-, *para*- and *meta*-xylenes were separately acylated by benzoyl chloride over $MnFe_2O_4$ at $50^\circ C$ under identical reaction conditions. Different xylenes gave different product distribution and the results are shown in the following table (Table 4.1.10).

Table 4.1.10. Benzoylation of isomeric xylenes

Type of xylene	Product Yield (%)	Product distribution (%)				
		2,3-DMBP	3,4-DMBP	2,6-DMBP	2,4-DMBP	2,5-DMBP
ortho	83.78	6.71	93.29	---	---	---
para	78.57	---	---	---	---	100
meta	74.61	---	---	14.35	85.65	---

Catalyst- $MnFe_2O_4$, Reaction temperature- $50^\circ C$, xylene/BOC molar ratio-10, Reaction time-20 minutes.

The data in Table 4.1.10 reveal that the chemical reactivity of the xylenes follow the order, *o*-xylene > *p*-xylene > *m*-xylene. The benzoylation of *o*-xylene leads to the formation of 3,4-dimethylbenzophenone (3,4-DMBP) and 2,3-dimethylbenzophenone (2,3-DMBP) with high selectivity for 3,4-DMBP (93.29%). With *p*-xylene, the reaction gave cent percent 2,5-dimethylbenzophenone (2,5-DMBP). Under similar reaction conditions, *m*-xylene gave two monoacylated products, 2,6-dimethylbenzophenone (2,6-DMBP) and 2,4-dimethylbenzophenone (2,4-DMBP).

4.1.1.3 Benzoylation of anisole

Anisole functions as an excellent substrate for Friedel-Crafts acylation. Mild reaction conditions are sufficed because the alkoxy group is highly activating functional group. The benzoylation of anisole with benzoyl chloride was carried out over all the manganese ferrite samples to endorse the conclusions made under other activated benzenes discussed earlier. The experimental procedures and the reaction conditions were almost the same as in the case of previously presented aromatics. A small change in the optimization conditions required, the reaction temperature is set at 40°C. The reaction can be represented by the following scheme (Figure. 4.1.15).

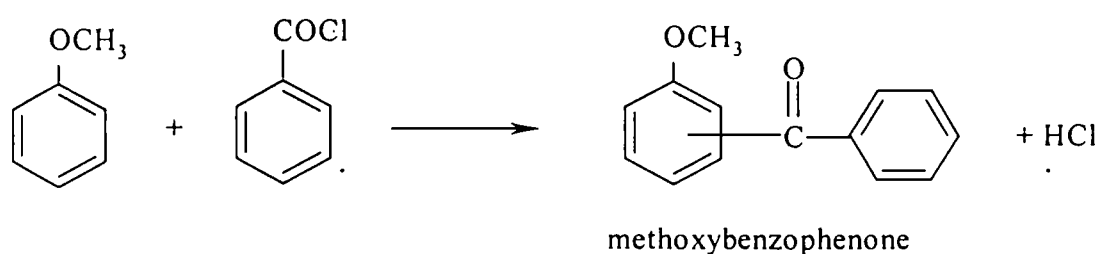
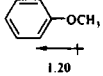


Fig. 4.1.15. Reaction scheme for benzoylation of anisole using benzoyl chloride.

The methoxy substituent in anisole increases the rate of electrophilic substitution about ten thousand fold than benzene. This activation of the benzene ring towards the electrophilic substitution may be correlated with the electron donating influence of the

substituents, as measured by molecular dipole moments (). As the methoxy group is ortho-para directing we foresee mainly two reaction products. The GC analysis data claimed the same as 4-methoxybenzophenone (4-MYBP) and 2-methoxybenzophenone (2-MYBP) as the main reaction products. A small amount of 3-methoxybenzophenone (3-MYBP) was also observed in some cases.

The product yields, the rate constants and the product distribution for the benzoylation of anisole with benzoyl chloride as the benzoylating agent are presented in the following table (Table 4.1.11).

Table 4.1.11. Benzoylation of anisole with benzoyl chloride over manganese ferros spinels

Catalyst	Product Yield (%)	Rate Constant ($10^{-3}\text{min}^{-1}\text{m}^{-2}$)	Product distribution (%)		
			4-MYBP	2-MYBP	3-MYBP
MnFe ₂ O ₄	87.58	6.79	85.74	10.72	3.52
Cr _{0.2} Mn _{0.8} Fe ₂ O ₄	57.25	6.49	80.21	15.22	4.57
Cr _{0.4} Mn _{0.6} Fe ₂ O ₄	49.98	6.30	80.78	13.98	5.24
Cr _{0.6} Mn _{0.4} Fe ₂ O ₄	42.37	5.79	81.30	12.83	5.87
Cr _{0.8} Mn _{0.2} Fe ₂ O ₄	33.25	4.90	81.87	12.11	6.02
CrFe ₂ O ₄	26.42	4.28	80.52	13.63	5.85
Co _{0.2} Mn _{0.8} Fe ₂ O ₄	91.58	10.96	67.95	21.48	10.57
Co _{0.4} Mn _{0.6} Fe ₂ O ₄	93.58	12.99	62.54	24.19	13.27
Co _{0.6} Mn _{0.4} Fe ₂ O ₄	94.51	14.87	61.91	27.81	10.28
Co _{0.8} Mn _{0.2} Fe ₂ O ₄	96.09	18.86	58.70	28.42	12.88
CoFe ₂ O ₄	96.95	22.96	52.36	29.22	18.42
Ni _{0.2} Mn _{0.8} Fe ₂ O ₄	73.52	6.34	89.73	8.46	1.81
Ni _{0.4} Mn _{0.6} Fe ₂ O ₄	69.79	6.29	91.59	8.41	---
Ni _{0.6} Mn _{0.4} Fe ₂ O ₄	66.57	6.17	93.64	6.36	---
Ni _{0.8} Mn _{0.2} Fe ₂ O ₄	60.62	6.07	95.24	4.76	---
NiFe ₂ O ₄	50.14	5.76	96.33	3.67	---
Cu _{0.2} Mn _{0.8} Fe ₂ O ₄	91.81	9.02	81.78	12.38	5.84
Cu _{0.4} Mn _{0.6} Fe ₂ O ₄	93.62	10.92	78.31	13.44	8.25
Cu _{0.6} Mn _{0.4} Fe ₂ O ₄	95.31	12.88	77.14	13.85	9.01
Cu _{0.8} Mn _{0.2} Fe ₂ O ₄	90.21	10.29	76.72	14.52	8.76
CuFe ₂ O ₄	88.43	10.28	76.34	14.88	8.78
Zn _{0.2} Mn _{0.8} Fe ₂ O ₄	70.78	6.41	70.76	27.53	1.71
Zn _{0.4} Mn _{0.6} Fe ₂ O ₄	63.88	6.19	69.14	30.08	0.78
Zn _{0.6} Mn _{0.4} Fe ₂ O ₄	57.19	5.71	68.57	31.43	---
Zn _{0.8} Mn _{0.2} Fe ₂ O ₄	51.57	5.54	67.89	32.11	---
ZnFe ₂ O ₄	45.27	5.34	67.57	32.43	---

Reaction conditions: Reaction temperature- 40°C, Reaction time- 20 minutes, Amount of catalyst-0.1 g, anisole/BOC molar ratio -10

The benzylation of anisole with benzoyl chloride under the mild reaction conditions over the manganese ferros spinels executed well. Most of the catalyst series gave more than 90% product yield. The details of the performance of each catalyst series in the benzylation of anisole are given in the following sections.

(a) $\text{Cr}_x\text{Mn}_{(1-x)}\text{Fe}_2\text{O}_4$ ($x = 0, 0.2, 0.4, 0.6, 0.8$ and 1.0) - type systems

Similar to the case of other activated benzenes such as toluene and xylenes the product yield and rate constants of benoylation of anisole over the Cr-Mn series decreased on the successive incorporation of chromium. In this case, the selectivity for the 4-methoxybenzophenone is not appreciable compared to the pure manganese ferros spinel. The increase in activation energy by the incorporation of chromium ions (Table 3.1.6) and decrease in strong acidity (Table 3.2.1) are the probable reason for their poor catalytic activity.

(b) $\text{Co}_x\text{Mn}_{(1-x)}\text{Fe}_2\text{O}_4$ ($x = 0, 0.2, 0.4, 0.6, 0.8$ and 1.0) - type systems

The successive incorporation of the cobalt into the pure manganese ferros spinel increase the rate of the reaction tremendously. But, in this case the selectivity for 4-methylbenzophenone is poor compared to the pure manganese ferros spinel. The increase in the rate of the reaction with the successive incorporation of cobalt into the manganese ferros spinel is due to the lowering of activation energy in this series.

(c) $\text{Ni}_x\text{Mn}_{(1-x)}\text{Fe}_2\text{O}_4$ ($x = 0, 0.2, 0.4, 0.6, 0.8$ and 1.0) - type systems

The progressive nickel-doping in manganese ferros spinel decreased the rate of the reaction, but increased the selectivity for the 4-methylbenzophenone. NiFe_2O_4 gave 96.3% selectivity for 4-MYBP. The nickel doping in manganese ferros spinel decreased the acidity and increased the activation energy of the series. These two factors synergistically reduced the catalytic activity.

(d) $\text{Cu}_x\text{Mn}_{(1-x)}\text{Fe}_2\text{O}_4$ ($x = 0, 0.2, 0.4, 0.6, 0.8$ and 1.0) - type systems

The copper doping increased the rate of the reaction moderately. But, this series failed in achieving high selectivity for 4-MYBP. The decrease in rate of the reaction beyond $x = 0.6$ is commensurated to the lifting up of activation energy beyond the same value of 'x'. Thus, it can be inferred that activation energy is playing the foremost role in the catalytic activity of ferros spinels in the benzylation of activated benzenes.

(e) $Zn_xMn_{(1-x)}Fe_2O_4$ ($x = 0, 0.2, 0.4, 0.6, 0.8$ and 1.0) - type systems

Though the Zn-Mn series possess enhanced acidity, it failed in progressing the rate of the reaction and also, in the selective formation of 4-MYBP. Though the formation of 3-MYBP is negligible, a significant amount of 2-MYBP is formed during the reaction. The Zn substitution increased the activation energy or the band gap of the pure $MnFe_2O_4$ and accordingly reduced the reaction rate.

4.1.2 Benzoylation of deactivated benzenes (benzene and halobenzenes)

This section presents the benzoylation of benzene and halobenzenes such as fluorene, chlorobenzene and bromobenzene. The deactivated rings need more vigorous reagent/catalyst combinations and tough reaction conditions. The aromatic substrates, which are less, activated than halobenzenes not undergo Friedel-Crafts acylation reactions.

4.1.2.1 Benzoylation of benzene

There are only a few reports regarding the benzoylation of benzene using heterogeneous catalysts [62, 65-67]. The lack of any activating group in the ring makes the acylation of benzene more difficult. The benzoylation of benzene using benzoyl chloride as the benzoylating agent was carried out over different series of manganese ferrite samples. The experimental procedures, reaction conditions and calculation methods were similar to those we have done for the benzoylation of activated benzenes, except the reaction temperature was set at $80^\circ C$ and the reaction to be run for 30 minutes. As we expected, the GC analysis data gave a single product, benzophenone. The results obtained are shown in the Table 4.1.12.

The interpretations we have made out in the case of activated benzenes are seemed to be different in the case of benzene. The series of catalysts, which showed higher activity for the benzoylation of activated benzenes, gave only moderate activity in the case of benzene benzoylation. Here, an attempt is made to correlate the acidic properties of the catalysts with the activity. The details of the catalytic performance of each series of ferrite catalysts are given in the coming sections.

Table 4.1.12. Benzoylation of benzene with benzoyl chloride over manganese ferros spinels

Catalyst	Product Yield (%)	Rate Constant ($10^{-3} \text{min}^{-1} \text{m}^{-2}$)
MnFe ₂ O ₄	66.57	2.30
Cr _{0.2} Mn _{0.8} Fe ₂ O ₄	16.22	0.90
Cr _{0.4} Mn _{0.6} Fe ₂ O ₄	13.21	0.86
Cr _{0.6} Mn _{0.4} Fe ₂ O ₄	10.51	0.77
Cr _{0.8} Mn _{0.2} Fe ₂ O ₄	8.14	0.68
CrFe ₂ O ₄	5.73	0.54
Co _{0.2} Mn _{0.8} Fe ₂ O ₄	54.01	2.26
Co _{0.4} Mn _{0.6} Fe ₂ O ₄	50.57	2.23
Co _{0.6} Mn _{0.4} Fe ₂ O ₄	47.76	2.22
Co _{0.8} Mn _{0.2} Fe ₂ O ₄	43.23	2.19
CoFe ₂ O ₄	38.71	2.15
Ni _{0.2} Mn _{0.8} Fe ₂ O ₄	49.86	2.23
Ni _{0.4} Mn _{0.6} Fe ₂ O ₄	47.18	2.20
Ni _{0.6} Mn _{0.4} Fe ₂ O ₄	42.93	2.14
Ni _{0.8} Mn _{0.2} Fe ₂ O ₄	38.06	2.10
NiFe ₂ O ₄	32.02	2.04
Cu _{0.2} Mn _{0.8} Fe ₂ O ₄	50.28	1.66
Cu _{0.4} Mn _{0.6} Fe ₂ O ₄	46.57	1.70
Cu _{0.6} Mn _{0.4} Fe ₂ O ₄	47.52	1.81
Cu _{0.8} Mn _{0.2} Fe ₂ O ₄	48.79	1.97
CuFe ₂ O ₄	47.12	2.24
Zn _{0.2} Mn _{0.8} Fe ₂ O ₄	50.88	2.47
Zn _{0.4} Mn _{0.6} Fe ₂ O ₄	47.98	2.64
Zn _{0.6} Mn _{0.4} Fe ₂ O ₄	46.13	2.77
Zn _{0.8} Mn _{0.2} Fe ₂ O ₄	42.95	2.88
ZnFe ₂ O ₄	39.57	2.97

Reaction temperature- 80°C, Reaction time- 30 minutes, Amount of catalyst-0.1 g, benzene/BOC molar ratio -10

(a) $\text{Cr}_x\text{Mn}_{(1-x)}\text{Fe}_2\text{O}_4$ ($x = 0, 0.2, 0.4, 0.6, 0.8$ and 1.0) - type systems

The catalytic activity of chromium substituted manganese ferrospinels was not appreciable for the benzoylation of benzene. The electron donating property studies revealed the increase in basicity by the chromium substitution (Table 3.2.8). The NH_3 -TPD measurements (Table 3.2.1) showed that the weak acidic sites were improved by the incorporation of chromium, whereas

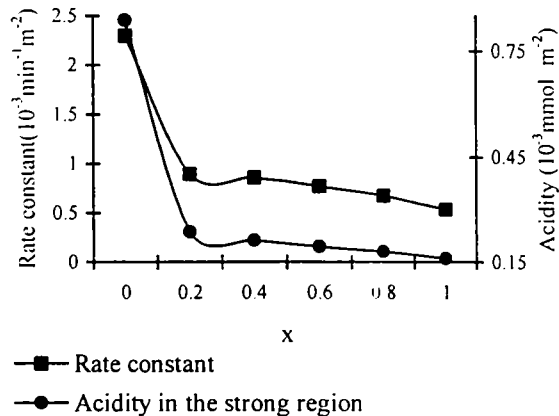


Fig.4.1.16. Variation of rate constant and acidity with composition of $\text{Cr}_x\text{Mn}_{(1-x)}\text{Fe}_2\text{O}_4$ type catalysts.

the medium and strong acidic sites got diminished. These results have been supported by the thermodesorption studies of the pyridine adsorbed chromium ferrite samples (Table 3.2.6). Figure 4.1.16 depicts the variation of rate constant and acidity in the strong region with composition of Cr-Mn series. Moreover, the activation energy or the band gap of the chromium ferrite samples bumped up on progressive chromium substitution (Table 3.1.6). All these factors together have an effect on the dullness of these series of samples towards the benzene benzoylation.

(b) $\text{Co}_x\text{Mn}_{(1-x)}\text{Fe}_2\text{O}_4$ ($x = 0, 0.2, 0.4, 0.6, 0.8$ and 1.0) - type systems

The effect of cobalt substitution in manganese ferrite is to sustain the rates of the reaction more or less unaffected. The acidity measurements by the NH_3 -TPD studies (Table 3.2.2) showed that replacement of Mn by Co in manganese ferrospinel increases both the weak and medium acidic sites, but the amount of strong acidic sites abridged slightly. The thermodesorption studies of the pyridine adsorbed samples

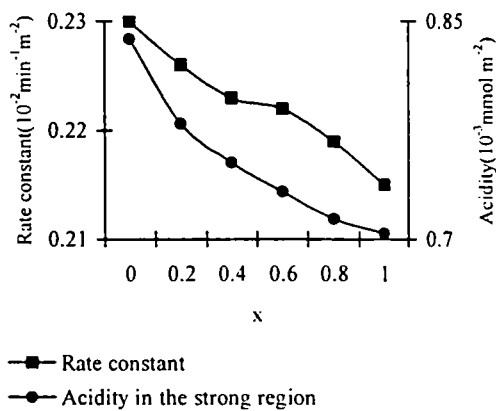


Fig.4.1.17. Variation of rate constant and Acidity with composition of $\text{Co}_x\text{Mn}_{(1-x)}\text{Fe}_2\text{O}_4$ type catalysts.

(Table 3.2.6) fairly supported this observation. The variation in rate constant and acidity in the strong region can be clearly seen in the figure 4.1.17. The strong acidic sites can be either Lewis or Brönsted sites nearer to the Lewis acid sites. We have ruled out the possibility of participation of Brönsted sites in benzoylation reactions by the moisture adsorption studies. However, the activation energy or band gap of the samples which seem to be the important factor in determining the rates of the reaction in activated benzenes, showed no correlation with the rate of benzene benzoylation. Thus, we can conclude that the acidity in the strong regions or Lewis acidic sites take the active role in the rate of benzene benzoylation.

(c) $\text{Ni}_x\text{Mn}_{(1-x)}\text{Fe}_2\text{O}_4$ ($x = 0, 0.2, 0.4, 0.6, 0.8$ and 1.0) - type systems

The rate of the reaction is seemed to be diminished on nickel incorporation into the manganese ferrosphenel. The order of catalytic activity follow the order as $\text{MnFe}_2\text{O}_4 > \text{Ni}_{0.2}\text{Mn}_{0.8}\text{Fe}_2\text{O}_4 > \text{Ni}_{0.4}\text{Mn}_{0.6}\text{Fe}_2\text{O}_4 > \text{Ni}_{0.6}\text{Mn}_{0.4}\text{Fe}_2\text{O}_4 > \text{Ni}_{0.8}\text{Mn}_{0.2}\text{Fe}_2\text{O}_4 > \text{NiFe}_2\text{O}_4$. The NH_3 -TPD profiles (Fig.3.2.4) showed the decrease in the amount of acidic sites by the incorporation of nickel in the strong acidic sites,

which are propped up by the results of thermodesorption studies of pyridine, adsorbed samples (Table 3.2.6). Fig. 4.1.18 illustrates the variation of rate constant and acidity with composition. Since the order of the rate of the reaction well commensurate with the acidity values, the gradation in catalytic activity can be explained in terms of acidity values especially in the strong acid regions. Also, the activation energy of this series is increased with nickel doping provides some involvement to the reduced catalytic activity towards benzene benzoylation.

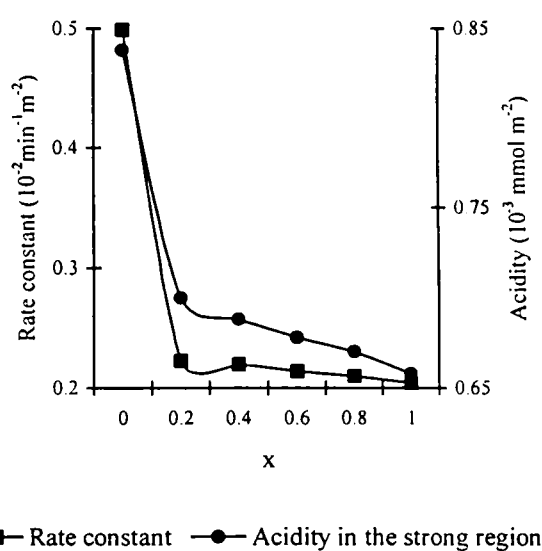


Fig.4.1.18. Variation of rate constant and Acidity with composition of $\text{Ni}_x\text{Mn}_{(1-x)}\text{Fe}_2\text{O}_4$ type catalysts.

(d) $\text{Cu}_x\text{Mn}_{(1-x)}\text{Fe}_2\text{O}_4$ ($x = 0, 0.2, 0.4, 0.6, 0.8$ and 1.0) - type systems

The replacement of Mn by Cu first decreased the rate constant and then showed an increase as Mn is being substituted with Cu. The NH_3 -TPD studies (Table 3.2.4) revealed that the copper doping decreased the amount of acidic sites in both the weak and medium regions drastically whereas, the strong acidic regions first showed a decrease and then an increase with the successive copper doping. The thermodesorption studies of the pyridine-adsorbed samples (Table 3.2.6) uphold these results. But the thermodesorption studies of the 2,6-dimethylpyridine adsorbed samples (Table 3.2.7) revealed that the incorporation of copper drastically decreased the Brönsted acidic sites. So, the relatively high catalytic activity of copper substituted systems is due to the generation of Lewis acid sites at the higher copper loadings Fig. (4.1.19).

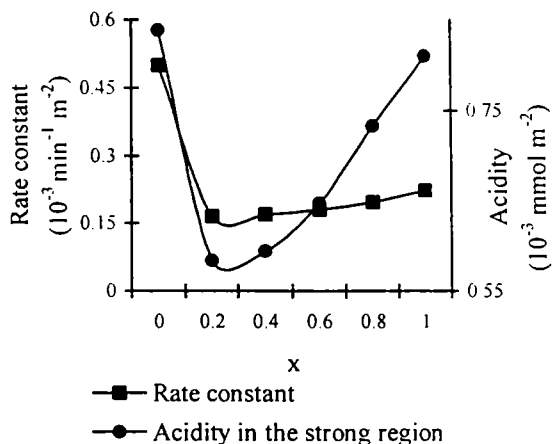


Fig.4.1.19 Variation of rate constant and acidity with composition of $\text{Cu}_x\text{Mn}_{(1-x)}\text{Fe}_2\text{O}_4$ type catalysts.

(e) $\text{Zn}_x\text{Mn}_{(1-x)}\text{Fe}_2\text{O}_4$ ($x = 0, 0.2, 0.4, 0.6, 0.8$ and 1.0) - type systems

The substitution of zinc into the manganese ferrite increased the amount of acidic sites in strong regions as evident from the NH_3 -TPD profiles (Fig. 3.2.6) and thermodesorption studies of pyridine adsorbed samples (Table 3.2.6). The same trend in activity for the benzoylation can be revealed from Table 4.1.12. The improvement in catalytic activity by the incorporation

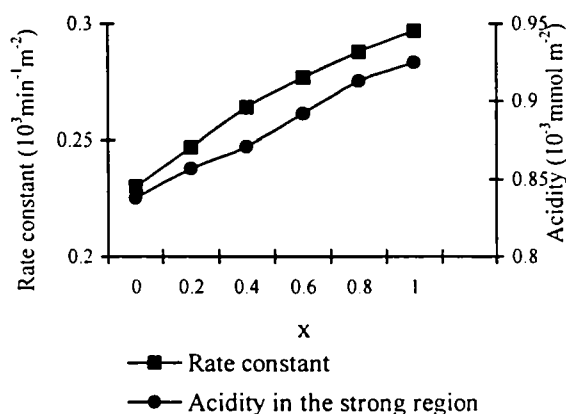
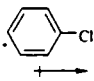


Fig.4.1.20 Variation of rate constant and acidity with composition of $\text{Zn}_x\text{Mn}_{(1-x)}\text{Fe}_2\text{O}_4$ type catalysts.

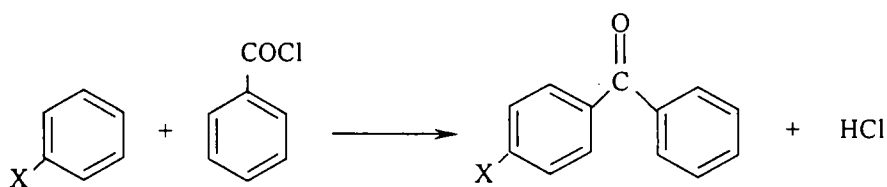
of zinc can be well explained with the enhanced strong acidity. The increase of activation energy by the successive zinc substitution in manganese ferrosphenel for the benzoylation of activated benzenes found no role in the benzene benzoylation.

4.1.2.2 Benzoylation of halobenzenes

The benzoylation of halobenzenes are more difficult than benzene. Our literature survey reveals that benzoylation of halobenzenes over heterogeneous catalysts have not been reported so far, whereas over the homogeneous catalysts a few reports have been found [53, 54]. If the atom bonded to the ring has one or more non-bonding valence shell electron pairs, as do halogens, electrons may flow into the aromatic ring by p-pi conjugation (resonance) and the charge distribution in the ring is greatest at sites ortho and para to the substituent. Although halogen atoms have non-bonding valence electron pairs that participate in p-pi conjugation, their strong inductive effect predominates, and

hence compounds such as chlorobenzene are less reactive than benzene ( ; dipole moment – 1.56 D).

The benzoylation of halobenzenes such as fluorobenzene, chlorobenzene and bromobenzene was done using benzoyl chloride as the benzoylating agent over the ferrite samples. For each aromatic substrate, the reaction temperature was set at the refluxing temperature of the reaction mixture and the reaction was carried out for 45 minutes to get the comparable yields. Though the benzoylation of halobenzenes give ortho and para product, our catalysts lead to only the para product with satisfactory percentage of product yield. The rate constants and product yield for the benzoylation of halobenzene are shown in Table 4.1.13



Where, X = F, Cl and Br

Figure.4.1.21. Scheme for benzoylation of halobenzenes using benzoyl chloride over ferrite catalysts.

Table 4.1.13 Benzoylation of halobenzenes with benzoyl chloride over manganese ferrosinels

Catalyst	fluorobenzene (Reaction temperature - 80°C)		chlorobenzene (Reaction temperature-132°C)		bromobenzene (Reaction temperature-140°C)	
	Product yield (%)	Rate constant ($10^{-3}\text{min}^{-1}\text{m}^{-2}$)	Product yield (%)	Rate constant ($10^{-3}\text{min}^{-1}\text{m}^{-2}$)	Product yield (%)	Rate constant ($10^{-3}\text{min}^{-1}\text{m}^{-2}$)
MnFe ₂ O ₄	58.25	1.25	63.64	1.46	70.18	1.73
Cr _{0.2} Mn _{0.8} Fe ₂ O ₄	9.27	0.33	14.14	0.52	19.22	0.72
Cr _{0.4} Mn _{0.6} Fe ₂ O ₄	7.37	0.31	11.52	0.50	15.89	0.70
Cr _{0.6} Mn _{0.4} Fe ₂ O ₄	6.12	0.29	9.73	0.48	12.98	0.65
Cr _{0.8} Mn _{0.2} Fe ₂ O ₄	4.66	0.26	8.01	0.45	10.63	0.61
CrFe ₂ O ₄	3.85	0.24	6.43	0.41	8.42	0.55
Co _{0.2} Mn _{0.8} Fe ₂ O ₄	45.91	1.20	51.54	1.41	58.26	1.70
Co _{0.4} Mn _{0.6} Fe ₂ O ₄	43.21	1.18	48.37	1.37	55.38	1.68
Co _{0.6} Mn _{0.4} Fe ₂ O ₄	40.23	1.16	45.14	1.35	52.44	1.67
Co _{0.8} Mn _{0.2} Fe ₂ O ₄	35.32	1.13	39.81	1.32	46.36	1.62
CoFe ₂ O ₄	30.45	1.08	34.56	1.27	40.61	1.56
Ni _{0.2} Mn _{0.8} Fe ₂ O ₄	42.88	1.19	47.73	1.38	54.14	1.66
Ni _{0.4} Mn _{0.6} Fe ₂ O ₄	39.54	1.13	44.14	1.31	50.76	1.60
Ni _{0.6} Mn _{0.4} Fe ₂ O ₄	35.27	1.09	40.19	1.29	45.87	1.55
Ni _{0.8} Mn _{0.2} Fe ₂ O ₄	30.28	1.06	35.14	1.27	39.84	1.50
NiFe ₂ O ₄	24.48	0.98	29.09	1.21	34.51	1.48
Cu _{0.2} Mn _{0.8} Fe ₂ O ₄	51.61	1.16	57.85	1.39	64.12	1.64
Cu _{0.4} Mn _{0.6} Fe ₂ O ₄	48.53	1.15	54.39	1.36	60.88	1.63
Cu _{0.6} Mn _{0.4} Fe ₂ O ₄	47.12	1.19	52.53	1.39	58.56	1.64
Cu _{0.8} Mn _{0.2} Fe ₂ O ₄	46.55	1.22	51.24	1.40	57.16	1.66
CuFe ₂ O ₄	41.94	1.25	46.42	1.46	51.41	1.69
Zn _{0.2} Mn _{0.8} Fe ₂ O ₄	42.92	1.30	48.13	1.52	52.87	1.79
Zn _{0.4} Mn _{0.6} Fe ₂ O ₄	40.42	1.39	45.11	1.61	50.13	1.87
Zn _{0.6} Mn _{0.4} Fe ₂ O ₄	38.93	1.46	44.18	1.72	48.57	1.96
Zn _{0.8} Mn _{0.2} Fe ₂ O ₄	37.43	1.58	42.72	1.88	45.92	2.08
ZnFe ₂ O ₄	35.96	1.74	39.78	1.98	42.52	2.16

Reaction conditions: Reaction time- 45 minutes, Amount of catalyst-0.1 g, halobenzene/BOC molar ratio -10.

The trends in catalytic activity of the ferrite series for the benzoylation of halobenzene well resemble with the results obtained for benzene benzoylation. The reactivity of halobenzenes for the benzoylation reaction over the ferrite catalysts follows the order, fluorobenzene < chlorobenzene < bromobenzene. Thus, the inductive effect of the halogens seemed to be the decisive factor in determining the reactivity of the halobenzenes.

(a) $\text{Cr}_x\text{Mn}_{(1-x)}\text{Fe}_2\text{O}_4$ ($x = 0, 0.2, 0.4, 0.6, 0.8$ and 1.0) - type systems

The Cr-Mn series showed poor activity for the benzoylation of halobenzene. The acidity measurements by the NH_3 -TPD method (Table 3.2.1) and the thermodesorption studies of the pyridine adsorbed samples (Table 3.2.6) show that except for the enhancement in acidity values in the weak regions, chromium addition decreases the acidic sites in all the other regions especially in the strong regions. So, the radical decrease in catalytic activity can be correlated to the reduction in acidic sites by the incorporation of chromium ions.

(b) $\text{Co}_x\text{Mn}_{(1-x)}\text{Fe}_2\text{O}_4$ ($x = 0, 0.2, 0.4, 0.6, 0.8$ and 1.0) - type systems

The rate of the reaction slightly reduced by successive incorporation of Co into the manganese ferros spinel. The incorporation of cobalt improved the acidity values of manganese ferrite in the weak and medium regions, but strong acidic values diminished gradually (Table 3.2.2). Thus, the gradual diminution in catalytic activity is associated with the trivial decrease in acidic values in the strong regions.

(c) $\text{Ni}_x\text{Mn}_{(1-x)}\text{Fe}_2\text{O}_4$ ($x = 0, 0.2, 0.4, 0.6, 0.8$ and 1.0) - type systems

The progressive nickel doping in manganese ferros spinel seemed to decrease the rate of the reaction. The nickel doping decreased the acidity values of manganese ferros spinel especially in the strong region (Table 3.2.3), which is found to be the prime cause for their decreased reaction rate.

(d) $\text{Cu}_x\text{Mn}_{(1-x)}\text{Fe}_2\text{O}_4$ ($x = 0, 0.2, 0.4, 0.6, 0.8$ and 1.0) - type systems

Initially, the copper doping decreased the reaction rate, and showed an increase in the rate with further incorporation of copper. The trend in activation energy with copper doping found no correlation with reaction rate for the benzoylation of

halobenzene. The incorporation of copper into the manganese ferros spinel, decreased the acidity values in the weak and medium acidic regions (Table 3.2.4). The acidic sites in the strong region first declined with copper substitution, and then increased with additional amount of copper. Thus, the gradation in their rate constants for the benzylation of halobenzene can be correlated to the acidity in the strong regions.

(e) $Zn_xMn_{(1-x)}Fe_2O_4$ ($x = 0, 0.2, 0.4, 0.6, 0.8$ and 1.0) - type systems

To a greater extent the substitution of Mn by Zn increased the rate of the reaction. This can be well correlated with the enhancement in the acidity in the strong region as evident from the NH_3 -TPD measurements (Fig. 3.2.5). The rise in activation energy with Zn substitution (Table 3.1.6) showed no effect in the benzylation of deactivated benzenes.

Comparison of activated and deactivated benzenes

It can be seen from the aforementioned sections that different compositions of manganese ferros spinels effectively catalysed the benzylation of activated as well as deactivated benzenes. We have observed that the decisive properties of the catalyst in deciding the catalytic activity for activated and deactivated benzenes are different. The acylation of benzenes and more particularly that of deactivated halobenzenes is a much difficult reaction than the acylation of the activated benzenes. It is evident that in the case of activated benzenes like toluene, xylenes and anisole, the aromatic ring is highly activated and therefore less acidity of the samples is sufficient to bring about such reactions [68]. Thus, the adsorption of the activated aromatic substrate over the catalyst become easier and the following surface reactions seemed to determine the rate of the reaction. For this, activation energy of the catalysts is more involved than the acidity. Since, in the case of benzene and halobenzenes, the aromatic ring is not activated or deactivated, the adsorption of the aromatic substrate over the catalyst is difficult. Here, the adsorption of the aromatic substrate over the catalyst has more involvement in determining the rate of the reaction and hence the acidity of the catalysts plays the decisive role.

4.2 Section II – Aniline Alkylation

This section presents the vapour-phase alkylation of aniline using methanol as the alkylating agent over the ferrite samples. The effect of various reaction parameters such as methanol to aniline molar ratio, time-on-stream, catalyst composition, reaction temperature and flow rate on product distribution are discussed in this section. The reaction products of the alkylation of aniline with methanol are N-, N,N'-, N,C-, C- and C,C'- (at high temperatures only) derivatives. The C-alkylated products are formed through the intramolecular transformations of the N-alkylated products. Methylation of aniline is industrially important owing to the wide uses of various substituted anilines like N-methylaniline (NMA), N,N-dimethylaniline (NNDMA), toluidines and xyloidines [1-3]. It is possible to selectively synthesize N-alkylated products, which are industrially more important by controlling the reaction parameters and acidity of the catalysts. The industrial applications of the various alkyl anilines are presented in the following table (Table 4.2.1).

Table 4.2.1 Industrial applications of various alkyl anilines.

Alkylanilines	Applications
N-methylaniline	Intermediate for paper and textile dyes, drugs, perfumes and explosives. Polymerization initiator for unsaturated polyester, resins and plastics and rubber accelerators. NMA is widely used as acid acceptor for semi-synthetic antibiotics.
N,N-dimethylaniline	Intermediate for the manufacture of vanillin, Michler's ketone, methyl violet and dyes. It can be also used as a solvent, an alkylating agent and a stabilizer. NNDMA can be used in photochemical dechlorination at room temperatures.
Toluidines	Intermediate for agricultural chemicals, dye stuffs, pharmaceuticals and colour photographic developers.
Xyloidines	Intermediate for drugs.

In recent years, chemists have turned their attention to the use of environmentally friendly catalysts instead of mineral acids. Bhattacharya and Nandi [4] have reported the liquid-phase dialkylation of aniline using mineral acids. Prolonging the residence period beyond 2 h not only decreased the conversion of aniline but also resulted in the increased formation of undesirable tarry products. The use of aluminium alkoxides and halides as catalysts has also been reported [5-7]. Another common method of alkylation uses dimethyl sulphate or alkyl halide, which are toxic and corrosive, as alkylating agents [8]. In order to avoid these problems alkylation reactions can be performed under vapour-phase conditions using solid acids as catalysts and non-toxic alkylating agents such as methanol.

With the increasing awareness of environmental issues, studies on solid acids are being pursued intensively due to their ecofriendly nature and the potential to replace the conventional Friedel-Crafts type systems. Towards this purpose, different solid catalysts such as oxides [9-15], multimetallic catalysts [16], Raney-Nickel [17], zeolites [18-26], AEL type molecular sieves [27, 28] and clays [29-34] have been tried for the alkylation of aniline.

The vapour-phase methylation of aniline by methanol has been extensively studied [5, 7, 35-40]. Low temperature normally favours N-alkylation and high temperature favours ring alkylation by Hoffmann-Martius rearrangement [7] or dehydration of methanol to alkenes or dimethyl ether, which can then methylate the ring [41]. There are enough evidences in the literature to show the formation of N- and C-methylanilines [37, 42, 43]. Trotta *et al.* [38] and Fu and Ono [39] reported the selective N-methylation of aniline with dimethyl carbonate. At high temperatures N,N-dimethylaniline undergoes isomerisation to give N-methyltoluidines.

An-Nan Ko *et al.* [9] investigated the aniline methylation over γ -alumina, which produced successively NMA and NNDMA. They assumed the reaction to be pseudo unimolecular. The second methylation leading to NNDMA exhibited higher rate constant and lower activation energy. It is also observed that the selectivity of NNDMA increased with increasing reaction temperature and methanol/aniline molar ratio.

With the intention of investigating the influence of acidity of catalyst for aniline alkylation, Narayanan *et al.* [32] selected three transition metal oxides with different acid strengths viz., Cr_2O_3 , ZrO_2 and V_2O_5 and impregnated on K10 montmorillonite and silica. Chromia is a strong Lewis acid, zirconia is amphoteric and vanadia is weakly acidic. The authors observed that a 10 wt% vanadia loaded SiO_2 and K10 promoted aniline alkylation more efficiently than the respective chromia or zirconia impregnated catalysts. Though aniline conversion depends on acidity, the authors did not find any linear or quantitative relationship between the two. Again, they [30] characterized the acidic sites in vanadia impregnated on to K10 and silica and came to the conclusion that the presence of a combination of Brønsted and Lewis acidic sites on the catalyst surface favours the aniline alkylation reaction.

Aluminophosphate-based molecular sieves are found to be good options for aniline alkylation reaction with high selectivity to N-alkylated products. Prasad and Rao [44] studied the alkylation of aniline by methanol over $\text{AlPO}_4\text{-5}$ catalyst with the aid of a parallel study on the reaction of NNDMA to speculate on the possible mechanism. They observed the formation of NMA at lower temperature, which is subsequently converted to NNDMA, which itself isomerises to N-methyltoluidine (NMT) as the temperature is increased. Isomerization occurs largely by the carbocation mechanism, as demonstrated by studying the reaction of NNDMA.

According to Elangaovan *et al.* [28], weak and moderate acid sites are sufficient for N-alkylation, whereas strong acid sites are mandatory for C-alkylation. The cobalt and zinc incorporated aluminophosphates designated as CoAPO-5 and ZAPO-5 gave a considerable amount of N-methyltoluidine (NMT) apart from NMA and NNDMA owing to their strong acidic sites. Though CoAPO-11 and ZAPO-11 possess strong acidic sites, NMT is not produced which is attributed to their smaller pore size. The authors proposed that the smaller pores might not be sufficient for the formation of NMT. Singh *et al.* [27] correlated the acidity-basicity function of ALPO-11, SAPO-11, MAPSO-11 and ZSM-5 with the activity of the catalysts and product pattern of the methylation of aniline. The selectivity of NNDMA is more in the reaction catalyzed by SAPO-11, compared to ALPO-11. This can be accounted from the relatively stronger acid sites present in

SAPO-11 which might be necessary for the consecutive methylation of aniline for NNDMA formation.

A wide variety of metal orthophosphates have also been employed as catalysts for aniline alkylation. Aramendia *et al.* [45] tested various magnesium orthophosphates with different structures and acid-base properties as catalysts for aniline methylation. They observed that the catalysts were selectively active for the N-alkylation of aniline with methanol as they yield no C-alkylated product. Also, the magnesium pyrophosphates were found to be more active than the magnesium orthophosphates. Further, the authors [46] used Na₂CO₃-impregnated magnesium orthophosphate for the alkylation of aniline with methanol. The progressive carbonate loading in the catalysts neutralized the acidic sites in magnesium orthophosphates by the basicity of Na₂CO₃. The overall conversion decreased with increase in Na₂CO₃ content, but the selectivity towards NMA increased.

Woo *et al.* [47, 48] investigated the selective alkylation of aniline with methanol over several metallosilicates. They suggested that strong acid sites are active sites that yield C-alkylated products and coke, medium acid sites yield NNDMA and NMT and weak acid sites give NMA.

Chen *et al.* [43] found HZSM-5 zeolite modified by alkali metal species to boost the selectivity towards NNDMA. The ion-exchanged KHZSM-5 exhibited high conversion and selectivity for NNDMA. Although, Cs⁺ ion provided the highest basicity, it resulted in the lowest NNDMA yield over CsZSM-5. Su *et al.* [26] studied aniline alkylation over different zeolites. The zeolites X and Y exchanged with K, Rb or Cs are more basic and favour the production of N-alkylates. The zeolites with more acidic cations such as Li and Na lead to C-alkylation.

Ivanova *et al.* [49] performed ¹³C NMR to investigate the mechanism of aniline alkylation with methanol on HY zeolite [49]. The results point to the existence of two types of strongly adsorbed methanol species, one with solid-like characteristics and another with liquid-like characteristics corresponding to more mobile 'intra-crystalline' methanol. The strongly adsorbed species are attributed to the adsorption complexes of methanol with aniline and surface methoxy species, respectively. Among all the species

observed, only methoxy species are shown to be responsible for aniline alkylation, which take place in the temperature range of 373 to 523 K.

A schematic representation of various reaction pathways of aniline alkylation using methanol as the alkylating agent is shown in Fig. 4.2.1.

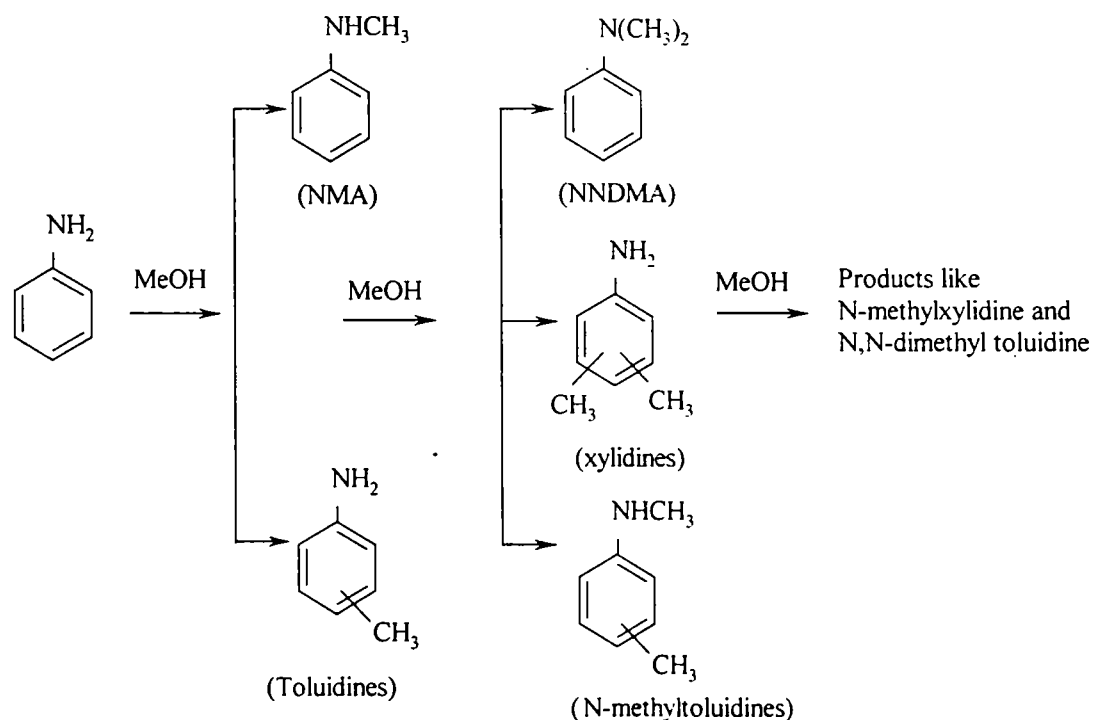


Fig. 4.2.1 Reaction scheme of aniline alkylation using methanol as the alkylating agent.

The vapour-phase aniline alkylation using methanol as the alkylating agent was done over the five series of manganese ferrosinels. We observed that the ferrite systems could produce mainly N-alkylated products with very high selectivity towards NMA. Unlike the other conventional systems the activities of our spinel systems remained for longer durations.

4.2.1 Process optimization

The alkylation reactions were carried out in a fixed-bed down –flow silica reactor of 1 cm ID and 30 cm length in the temperature range 250-550°C under atmospheric pressure. 0.5 g of the catalyst activated at 500°C for 2h was taken for each run and was placed at the center of the reactor. The temperature was controlled by a Cr-Al

thermocouple placed inside the reactor. The feed mixture (aniline and methanol) was admitted to the reactor by means of a syringe pump. Evolved gases from the reactor were passed through a condenser and on to a collector that allowed liquids to be withdrawn at required time intervals. Volume hourly space velocity (VHSV) was varied from 3 mL h⁻¹ to 9 mL h⁻¹. The products were analysed by gas chromatography (Chemito GC 8610, flame ionization detector, SE 30 column, 2 m length). A blank run with no catalyst was carried out at 350°C in the reactor indicated negligible thermal reaction.

4.2.1.1. Effect of methanol to aniline molar ratio

The change in conversion and product distribution for aniline alkylation at different molar ratios of MeOH to aniline at 350°C and volume space velocity of 5 mL h⁻¹ is shown in Fig.4.2.2.

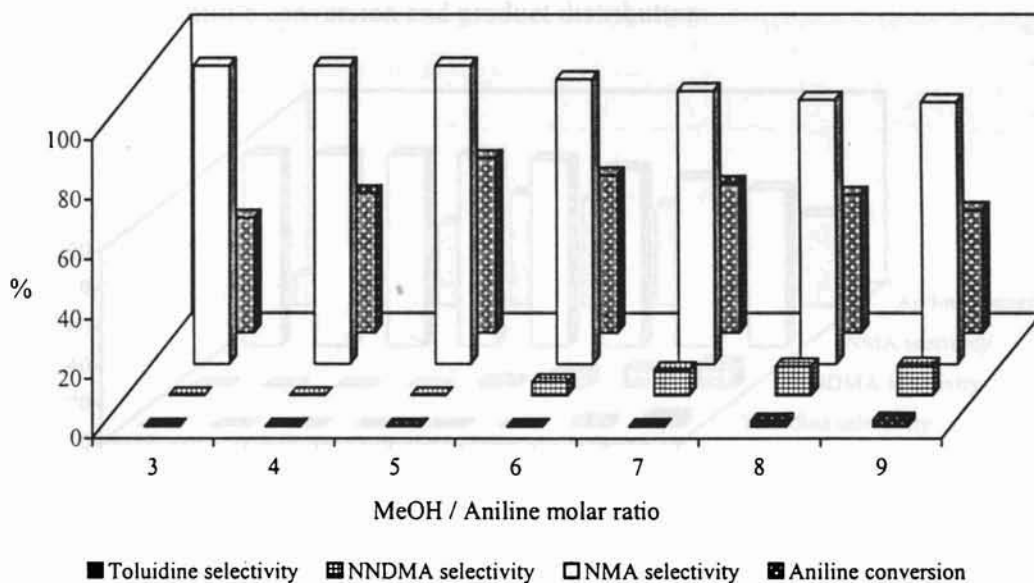


Fig. 4.2.2. Effect of MeOH/aniline molar ratio on conversion and selectivity of methylation of aniline over Cr_{0.8}Mn_{0.2}Fe₂O₄. Reaction temperature-350°C, TOS- 2 h, VHSV- 5 mL h⁻¹.

It is obvious from the figure that the major reaction product is N-methylaniline and its selectivity remained cent percent from a molar ratio of 3 up to a molar ratio of 5. Further increase in the molar ratio decreased the selectivity for NMA with corresponding increase in the selectivity for NNDMA. This suggests that higher molar ratios, favour

the consecutive methylation of NMA owing to the presence of large amount of methanol. Negligible amount of C-alkylated product, toluidines were observed even at higher molar ratios. When the molar ratio was 3, the aniline conversion was 38.44%, improved significantly up to a molar ratio of 5 (58.51%). However, excess of methanol beyond the molar ratio of 5 lowered the aniline conversion because the alcohol probably undergoes side reactions leading to the formation of coke. Therefore MeOH-aniline molar ratio of 5 was selected as the optimum feed mix ratio in the subsequent experiments.

4.2.1.2 Effect of reaction temperature

A series of aniline alkylation reactions were performed in the temperature range of 200 to 550°C over $\text{Cr}_{0.8}\text{Mn}_{0.2}\text{Fe}_2\text{O}_4$. Figure 4.2.3 shows the influence of reaction temperature on aniline conversion and product distribution.

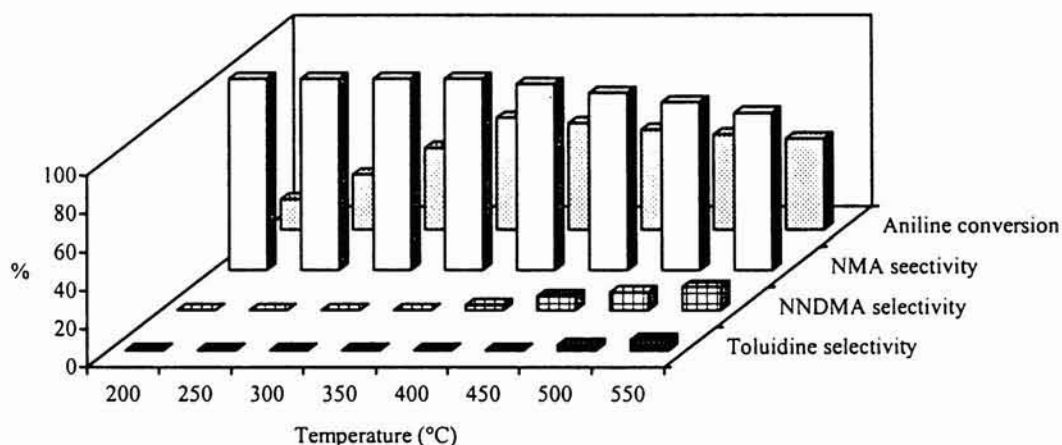


Fig.4.2.3. Effect of reaction temperature on aniline alkylation. Catalyst- $\text{Cr}_{0.8}\text{Mn}_{0.2}\text{Fe}_2\text{O}_4$, TOS- 2 h, VHSV- 5mL h^{-1} , MeOH/aniline molar ratio-5.

It can be seen that temperature has a marked influence on the aniline conversion and product selectivity. At all the temperatures, N-methylaniline was observed to be the major product. Its selectivity remained cent percent up to 350°C, but decreased on further rise in temperature. At higher temperatures NNDMA is formed by the successive alkylation of NMA. This reduced the NMA selectivity and increased the NNDMA

selectivity. Ring alkylation leading to toluidines was observed in the temperature region of 500 - 550°C. According to Prasad and Rao [44] the C-alkylated products are formed by the isomerization of N,N-dialkylated product at high reaction temperatures. The aniline conversion showed a significant increase with the rise of temperature from 200 to 350°C. However, further increase in temperature rather reduced the aniline conversion, which may be due to the coke deposition in this temperature range. Another possible reason for the reduced conversion is that methanol decomposition to C-oxides will be larger at higher temperatures. These results indicate that the optimum temperature range is 300-350°C for high aniline conversion and high selectivity for NMA.

4.2.1.3 Effect of flow rate

Figure 4.2.4 shows the influence of flow rate (VHSV) over $\text{Cr}_{0.8}\text{Mn}_{0.2}\text{Fe}_2\text{O}_4$ at 350°C and a MeOH/aniline molar ratio of 5.

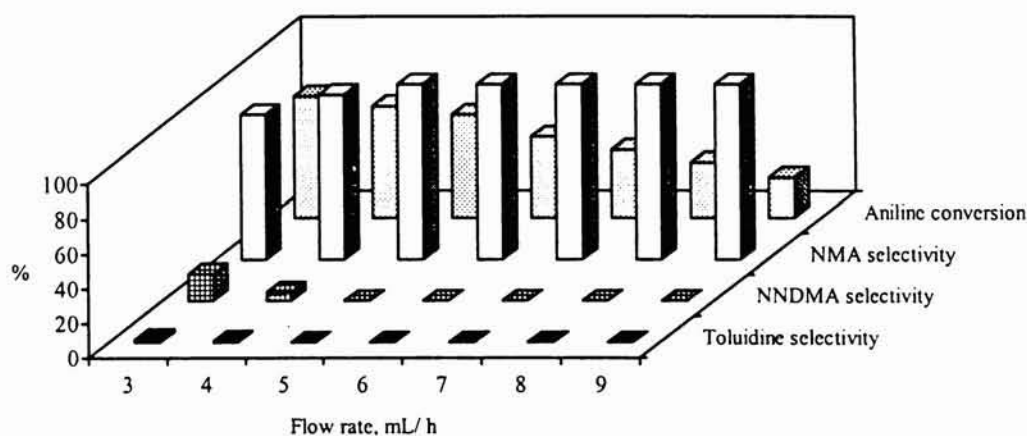


Fig. 4.2.4 Effect of flow rate on conversion and selectivity of methylation of aniline over $\text{Cr}_{0.8}\text{Mn}_{0.2}\text{Fe}_2\text{O}_4$. Reaction temperature- 350°C, MeOH/aniline molar ratio-5 and TOS- 2 h

Increase in feed rate increases the diffusion of the reactant molecules through the catalyst. So aniline gets much less time to go into the product side which will result in a decrease in aniline conversion and higher alkylated products of aniline. Yuvaraj *et al.* observed a similar trend over zeolites Y and β [41]. The ferrite samples follow the same drift as it can be seen from Fig.4.2.4. With the increase of VHSV, aniline conversion

decreased dramatically. The lower flow rate enhances the formation of dialkylated product, NNDMA and a negligible amount of C-alkylated product, toluidines were observed at the flow rate of 3 mL h⁻¹. As the flow rate was increased from 3 to 9 mL h⁻¹, the reaction shifted completely towards N-monoalkylation leading to the product, NMA.

4.2.2 Comparison of catalyst composition

For the catalyst comparison the aniline alkylation reactions were performed over the five series of the manganese ferros spinels.

(a) Cr_xMn_(1-x)Fe₂O₄ - type systems (x = 0, 0.2, 0.4, 0.6, 0.8 and 1.0)

The percentage conversion of aniline and the product distribution of aniline alkylation reaction carried out over the mixed Cr-Mn ferrite systems are presented in Table 4.2.2. It can be seen that the successive incorporation of chromium into the manganese ferros spinel increased both the aniline conversion and NMA yield.

Table 4.2.2 Alkylation of aniline with methanol over Cr_xMn_(1-x)Fe₂O₄ - type systems

Catalyst	Aniline conv.(%)	NMA Yield (wt %)	Selectivity (%)		
			NMA	NNDMA	Toluidine
MnFe ₂ O ₄	22.45	13.12	78.72	13.73	7.55
Cr _{0.2} Mn _{0.8} Fe ₂ O ₄	47.37	42.36	98.72	1.28	-
Cr _{0.4} Mn _{0.6} Fe ₂ O ₄	49.66	49.37	99.01	0.99	-
Cr _{0.6} Mn _{0.4} Fe ₂ O ₄	53.37	56.52	100	-	-
Cr _{0.8} Mn _{0.2} Fe ₂ O ₄	58.51	61.78	100	-	-
CrFe ₂ O ₄	51.27	54.73	100	-	-

Reaction temperature-350°C, MeOH/aniline-5, TOS- 2 h and flow rate –5mL /h.

The thermodesorption studies using 2,6-dimethylpyridine showed a decrease in the relative amount of Brönsted acidic sites by the replacement of Mn by Cr. The NH₃-TPD studies and the thermodesorption studies of pyridine adsorbed samples revealed the enhancement in the weak and medium acidic sites with increase in chromium content and this may be due to the presence of weak Lewis acid sites. But it is seen that the limiting concentrations of the electron acceptors adsorbed showed a proportionate

increase with increase in chromium content. The decrease in the dehydration activity from the cyclohexanol decomposition reaction confirmed the decrease in acidity with increase in 'x' values. Table 4.2.3 presents the acid-base properties of Cr-Mn series along with NMA yields.

Table 4.2.3. Dehydration activity, weak plus medium acidity, limiting amount and NMA yields of the system $\text{Cr}_x\text{Mn}_{1-x}\text{Fe}_2\text{O}_4$ ($x = 0, 0.2, 0.4, 0.6, 0.8$ and 1)

x	Dehydration	Brönsted acid sites (%)	Weak+medium Acidity (10^{-4} mmol m^{-2})	Limiting amount (10^{-4} mmol m^{-2})		NMA Yield (wt %)
	Activity (wt %)			TCNQ	Chloranil	
	Cyclohexene					
0	91.28	0.825	8.12	10.71	2.6	13.12
0.2	38.52	0.300	8.19	55.52	28.62	42.36
0.4	37.01	0.261	8.36	56.28	29.19	49.37
0.6	36.25	0.233	8.48	57.58	30.12	56.52
0.8	35.89	0.208	8.61	59.01	31.29	61.78
1	34.82	0.187	8.65	60.61	32.74	54.73

Though aniline alkylation is an acid catalyzed reaction, it is observed that acidity of the catalysts is not the sole factor determining the catalytic activity. The decisive role in determining the catalytic activity of the spinels is their cation distribution. The partially inverse MnFe_2O_4 spinel is shifted to the more inverse nature by the incorporation of chromium ions in the octahedral sites. This resulted in the isomorphic replacement of Fe^{3+} ions from the more exposed and active octahedral sites to the hindered tetrahedral sites. Cation valency distribution of mixed Cr-Mn series are presented in Table 4.2.4.

The cation valency distribution of the mixed Cr-Mn series reveals that $\text{Fe}_{\text{oct}}^{3+}/\text{Fe}_{\text{tet}}^{3+}$ ratio decreases with increase in 'x' value. The octahedral cations are more polar and more accessible to the reactant molecules than the tetrahedral cations [50, 51]. But, due to the easy electron hopping between the sites [52-54], tetrahedral ions can also influence the overall activity of the system, and this hopping mechanism is more pronounced in inverse spinels. The participation of Fe^{3+} ions in the octahedral sites as

Table 4.2.4. Cation valency distribution of $\text{Cr}_x\text{Mn}_{(1-x)}\text{Fe}_2\text{O}_4$ -type systems

Catalyst	Cation valency distribution
MnFe_2O_4	$(\text{Mn}_{0.5}^{2+}\text{Fe}_{0.5}^{3+})_{\text{tet}}[\text{Fe}_{0.5}^{2+}\text{Fe}^{3+}\text{Mn}_{0.5}^{3+}]_{\text{oct}}\text{O}_4^{2-}$
$\text{Cr}_{0.2}\text{Mn}_{0.8}\text{Fe}_2\text{O}_4$	$(\text{Mn}_{0.4}^{2+}\text{Fe}_{0.6}^{3+})_{\text{tet}}[\text{Fe}_{0.6}^{2+}\text{Fe}_{0.8}^{3+}\text{Mn}_{0.4}^{3+}\text{Cr}_{0.2}^{3+}]_{\text{oct}}\text{O}_4^{2-}$
$\text{Cr}_{0.4}\text{Mn}_{0.6}\text{Fe}_2\text{O}_4$	$(\text{Mn}_{0.3}^{2+}\text{Fe}_{0.7}^{3+})_{\text{tet}}[\text{Fe}_{0.7}^{2+}\text{Fe}_{0.6}^{3+}\text{Mn}_{0.3}^{3+}\text{Cr}_{0.4}^{3+}]_{\text{oct}}\text{O}_4^{2-}$
$\text{Cr}_{0.6}\text{Mn}_{0.4}\text{Fe}_2\text{O}_4$	$(\text{Mn}_{0.2}^{2+}\text{Fe}_{0.8}^{3+})_{\text{tet}}[\text{Fe}_{0.8}^{2+}\text{Fe}_{0.4}^{3+}\text{Mn}_{0.2}^{3+}\text{Cr}_{0.6}^{3+}]_{\text{oct}}\text{O}_4^{2-}$
$\text{Cr}_{0.8}\text{Mn}_{0.2}\text{Fe}_2\text{O}_4$	$(\text{Mn}_{0.1}^{2+}\text{Fe}_{0.9}^{3+})_{\text{tet}}[\text{Fe}_{0.9}^{2+}\text{Fe}_{0.2}^{3+}\text{Mn}_{0.1}^{3+}\text{Cr}_{0.8}^{3+}]_{\text{oct}}\text{O}_4^{2-}$
CrFe_2O_4	$(\text{Fe}^{3+})_{\text{tet}}[\text{Fe}^{2+}\text{Cr}^{3+}]_{\text{oct}}\text{O}_4^{2-}$

the alcohol adsorbing centers has already been reported [50]. Except for CrFe_2O_4 , all the other systems in this series possess some amount of Fe^{3+} ions in the octahedral sites and this may be the reason for reduced catalytic activity of CrFe_2O_4 compared to $\text{Cr}_{0.8}\text{Mn}_{0.2}\text{Fe}_2\text{O}_4$ and $\text{Cr}_{0.6}\text{Mn}_{0.4}\text{Fe}_2\text{O}_4$. Since aniline is a strong base, even the weak Lewis acid sites on the catalyst surface can make effective coordination with this molecule. It is also believed that only weak to moderate acidity favour the reaction [55] and the enhanced catalytic activity of mixed Cr-Mn systems is due to the improved weak Lewis acidity.

Effect of time-on- stream

The catalytic stability of different mixed Cr-Mn systems were checked by observing NMA yield over a period of seven hours. The reactions were carried out at 350°C , at a MeOH/aniline molar ratio of 5 and the product analysis was done at regular intervals of 60 minutes (Fig. 4.2.5). All the catalysts showed excellent stability and selectivity for NMA for a long reaction period.

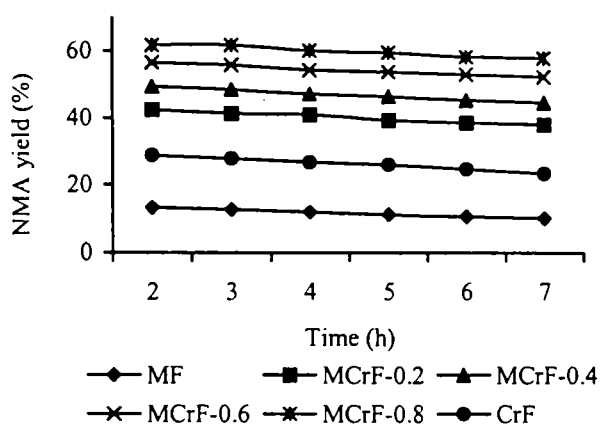


Fig.4.2.5. Effect of time-on-stream over the system, $\text{Cr}_x\text{Mn}_{1-x}\text{Fe}_2\text{O}_4$ ($x = 0, 0.2, 0.4, 0.6, 0.8$ and 1). Reaction temperature- 350°C , MeOH/aniline-5, and feed rate - 5mL h^{-1} .

(b) $\text{Co}_x\text{Mn}_{(1-x)}\text{Fe}_2\text{O}_4$ - type systems ($x = 0, 0.2, 0.4, 0.6, 0.8$ and 1.0)

A series of experiments were performed over mixed Co-Mn spinels at a reaction temperature of 350°C and MeOH/aniline molar ratio was maintained at 5 (Table 4.2.5). Though the selectivity for NMA is not as excellent as for Cr-Mn series, this series of ferrites exhibit rather pronounced selectivity. The yields of NNDMA and toluidines were decreased with increase in 'x' values.

Table 4.2.5. Alkylation of aniline with methanol over $\text{Co}_x\text{Mn}_{(1-x)}\text{Fe}_2\text{O}_4$ - type systems

Catalyst	Aniline conv.(%)	NMA Yield (wt %)	Selectivity (%)		
			NMA	NNDMA	Toluidine
MnFe_2O_4	22.45	13.12	78.72	13.73	7.55
$\text{Co}_{0.2}\text{Mn}_{0.8}\text{Fe}_2\text{O}_4$	27.73	18.36	85.12	9.28	5.60
$\text{Co}_{0.4}\text{Mn}_{0.6}\text{Fe}_2\text{O}_4$	30.57	20.37	89.01	6.84	4.15
$\text{Co}_{0.6}\text{Mn}_{0.4}\text{Fe}_2\text{O}_4$	32.16	23.52	91.52	4.98	3.50
$\text{Co}_{0.8}\text{Mn}_{0.2}\text{Fe}_2\text{O}_4$	35.79	26.78	94.64	3.13	2.23
CoFe_2O_4	37.29	28.73	97.71	1.37	0.92

Reaction temperature- 350°C , MeOH/ aniline molar ratio- 5, TOS- 2 h and flow rate -5mL h^{-1} .

Like the Cr-Mn mixed ferrites, in this case also the relative amount of Brönsted acid sites were diminished with increase in 'x' values, whereas the amount of weak plus medium acidic sites were slightly improved. Thus it can be inferred that the improved acidity may be due to the enhanced weak Lewis acidic sites by the successive incorporation of cobalt ions in the octahedral sites. The limiting concentrations of the electron acceptors showed a slight increase in values with increase in cobalt content, while the dehydration activity determined from the cyclohexanol decomposition reaction is reduced slightly. The limiting amounts of electron acceptors adsorbed, the relative amount of Brönsted acidic sites (from the thermodesorption studies of 2,6-dimethyl pyridine adsorbed samples), the acidity in the weak plus medium sites (from NH_3 -TPD measurements) and the dehydration activities along with NMA yields are presented in Table 4.2.6.

Table 4.2.6. Dehydration activity, weak plus medium acidity, limiting amount and NMA yield of the system $\text{Co}_x\text{Mn}_{1-x}\text{Fe}_2\text{O}_4$ ($x = 0, 0.2, 0.4, 0.6, 0.8$ and 1).

x	Dehydration	Brönsted acid sites (%)	Weak+medium Acidity (10^{-4} mmol m^{-2})	Limiting amount (10^{-4} mmol m^{-2})		NMA Yield (wt %)
	Activity (wt %)			TCNQ	Chloranil	
0	91.28	0.825	8.12	10.71	2.60	13.12
0.2	90.80	0.683	8.16	15.68	5.39	18.36
0.4	88.00	0.651	8.21	16.38	6.32	20.37
0.6	87.50	0.614	8.27	17.19	7.62	23.52
0.8	87.10	0.588	8.36	17.88	8.69	26.78
1	86.00	0.566	8.43	18.58	9.63	28.73

The cation valency distribution of mixed Co-Mn series are presented in Table 4.2.6. The partially inverse MnFe_2O_4 spinel is shifted to the more inverse nature by the incorporation of cobalt ions in the octahedral sites. It can be seen that the concentration of Fe^{3+} ions in the octahedral sites is the same for all compositions in this series. Therefore, the catalytic activity is mainly determined by the $\text{Co}^{2+}/\text{Mn}^{3+}$ ratio in the octahedral site. The enhanced weak Lewis acidity supplied by the incorporated cobalt ions in the octahedral sites of the pure manganese ferrite slightly improves the catalytic activity.

Table 4.2.6 Cation valency distribution of $\text{Co}_x\text{Mn}_{(1-x)}\text{Fe}_2\text{O}_4$ - type systems.

Catalyst	Cation valency distribution
MnFe_2O_4	$(\text{Mn}_{0.5}^{2+}\text{Fe}_{0.5}^{3+})_{\text{tet}}[\text{Fe}_{0.5}^{2+}\text{Fe}_1^{3+}\text{Mn}_{0.5}^{3+}]_{\text{oct}}\text{O}_4^{2-}$
$\text{Co}_{0.2}\text{Mn}_{0.8}\text{Fe}_2\text{O}_4$	$(\text{Mn}_{0.4}^{2+}\text{Fe}_{0.6}^{3+})_{\text{tet}}[\text{Fe}_{0.4}^{2+}\text{Fe}_1^{3+}\text{Mn}_{0.4}^{3+}\text{Co}_{0.2}^{2+}]_{\text{oct}}\text{O}_4^{2-}$
$\text{Co}_{0.4}\text{Mn}_{0.6}\text{Fe}_2\text{O}_4$	$(\text{Mn}_{0.3}^{2+}\text{Fe}_{0.7}^{3+})_{\text{tet}}[\text{Fe}_{0.3}^{2+}\text{Fe}_1^{3+}\text{Mn}_{0.3}^{3+}\text{Co}_{0.4}^{2+}]_{\text{oct}}\text{O}_4^{2-}$
$\text{Co}_{0.6}\text{Mn}_{0.4}\text{Fe}_2\text{O}_4$	$(\text{Mn}_{0.2}^{2+}\text{Fe}_{0.8}^{3+})_{\text{tet}}[\text{Fe}_{0.2}^{2+}\text{Fe}_1^{3+}\text{Mn}_{0.2}^{3+}\text{Co}_{0.6}^{2+}]_{\text{oct}}\text{O}_4^{2-}$
$\text{Co}_{0.8}\text{Mn}_{0.2}\text{Fe}_2\text{O}_4$	$(\text{Mn}_{0.1}^{2+}\text{Fe}_{0.9}^{3+})_{\text{tet}}[\text{Fe}_{0.1}^{2+}\text{Fe}_1^{3+}\text{Mn}_{0.1}^{3+}\text{Co}_{0.8}^{2+}]_{\text{oct}}\text{O}_4^{2-}$
CoFe_2O_4	$(\text{Fe}^{3+})_{\text{tet}}[\text{Fe}^{3+}\text{Co}^{3+}]_{\text{oct}}\text{O}_4^{2-}$

Effect of time-on-stream

In Fig. 4.2.6, the yield of NMA is plotted as a function of time-on-stream. The reactions were carried out at 350°C and at a MeOH/aniline molar ratio of 5 for 7 hours and the product analysis was done at a regular interval of 60 minutes. All the catalysts except CoFe_2O_4 showed excellent catalytic stability. The poor catalytic stability of CoFe_2O_4 is due to the formation of carbonaceous products over the catalyst surface.

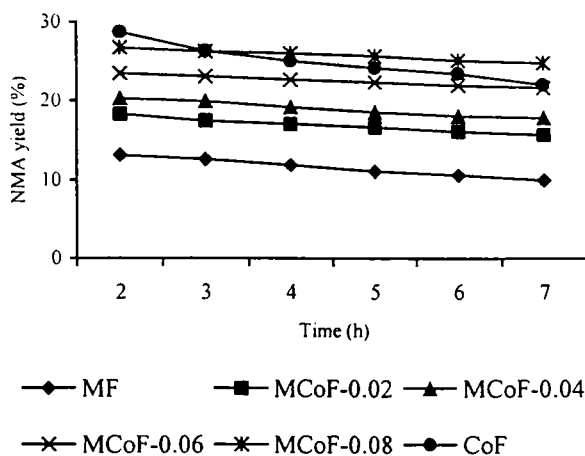


Fig.4.2.6. Effect of time-on-stream over the system, $\text{Co}_x\text{Mn}_{1-x}\text{Fe}_2\text{O}_4$. Reaction temperature- 350°C, MeOH/aniline molar ratio -5, and flow rate -5mL h^{-1}

(c) $\text{Ni}_x\text{Mn}_{(1-x)}\text{Fe}_2\text{O}_4$ - type systems (x = 0, 0.2, 0.4, 0.6, 0.8 and 1.0)

The product distribution and percentage of aniline conversion over different mixed Ni-Mn systems are presented in Table 4.2.7. The NMA selectivity increased with rise in ‘x’ values and all the compositions exhibited somewhat enhanced activity.

Table 4.2.7. Alkylation of aniline with methanol over $\text{Ni}_x\text{Mn}_{(1-x)}\text{Fe}_2\text{O}_4$ (x = 0, 0.2, 0.4, 0.6, 0.8 and 1.0)- type systems

Catalyst	Aniline conversion (%)	NMA Yield (wt %)	Product distribution (%)		
			NMA	NNDMA	Toluidine
MnFe_2O_4	22.45	13.12	78.72	13.73	7.55
$\text{Ni}_{0.2}\text{Mn}_{0.8}\text{Fe}_2\text{O}_4$	23.73	15.36	91.12	7.28	1.60
$\text{Ni}_{0.4}\text{Mn}_{0.6}\text{Fe}_2\text{O}_4$	25.57	17.37	93.01	5.81	1.18
$\text{Ni}_{0.6}\text{Mn}_{0.4}\text{Fe}_2\text{O}_4$	27.16	19.52	95.32	3.71	0.97
$\text{Ni}_{0.8}\text{Mn}_{0.2}\text{Fe}_2\text{O}_4$	28.79	21.78	97.41	2.59	---
NiFe_2O_4	30.29	23.73	98.83	1.17	---

Reaction temperature-350°C, MeOH/ aniline-5, TOS- 2 h and flow rate –5mL h⁻¹.

It is seen that the successive nickel doping increased the weak plus medium acidity as revealed from the NH₃-TPD studies and also, from the thermodesorption studies of pyridine adsorbed samples. The relative Brönsted acid sites remained more or less constant throughout the series and thus, the increase in weak plus medium acidity may be due to the slightly enhanced weak Lewis acidity. The dehydration activity of the catalysts diminished whereas the limiting concentration of the electron acceptors adsorbed showed a reasonable increase with increase in nickel content. The relevant acidity-basicity values and the catalytic activity of the mixed Ni-Mn ferrites are shown in Table 4.2.8.

Table 4.2.8. Dehydration activity, weak plus medium acidity, limiting amount and NMA yield of the system Ni_xMn_{1-x}Fe₂O₄ (x = 0, 0.2, 0.4, 0.6, 0.8 and 1).

x	Dehydration	Brönsted acid sites (%)	Weak+medium Acidity (10 ⁻⁴ mmol m ⁻²)	Limiting amount (10 ⁻⁴ mmol m ⁻²)		NMA Yield (wt %)
	Activity (wt %) Cyclohexene			TCNQ	Chloranil	
0	91.28	0.825	8.12	10.71	2.60	13.12
0.2	90.76	0.824	8.14	20.81	6.41	15.36
0.4	89.25	0.823	8.18	22.47	7.00	17.37
0.6	88.98	0.820	8.22	23.13	7.58	19.52
0.8	85.29	0.817	8.26	23.97	7.92	21.78
1	82.10	0.814	8.32	25.52	8.91	23.73

The spinel compositions and cation valency distribution of the mixed Ni-Mn spinel ferrites are depicted in Table 4.2.9. All the ferrites in this series are inverse in nature and the inverse nature increases with increase in 'x' values. Like the Co-Mn series, in this case also, the concentration of the Fe³⁺ ions in the octahedral sites is same for all the compositions. Hence the catalytic activity is mainly determined by the amount of incorporated nickel ions in the octahedral sites. Thus, the improved catalytic activity of the Ni-Mn series is due to the enhancement in weak Lewis acidity by the successive nickel doping.

Table 4.2.9 Cation valency distribution of $Ni_xMn_{(1-x)}Fe_2O_4$ ($x = 0, 0.2, 0.4, 0.6, 0.8$ and 1.0)- type systems.

Catalyst	Cation valency distribution
$MnFe_2O_4$	$(Mn_{0.5}^{2+}Fe_{0.5}^{3+})_{tet}[Fe_{0.5}^{2+}Fe_1^{3+}Mn_{0.5}^{3+}]_{oct}O_4^{2-}$
$Ni_{0.2}Mn_{0.8}Fe_2O_4$	$(Mn_{0.4}^{2+}Fe_{0.6}^{3+})_{tet}[Fe_{0.4}^{2+}Fe_1^{3+}Mn_{0.4}^{3+}Ni_{0.2}^{2+}]_{oct}O_4^{2-}$
$Ni_{0.4}Mn_{0.6}Fe_2O_4$	$(Mn_{0.3}^{2+}Fe_{0.7}^{3+})_{tet}[Fe_{0.3}^{2+}Fe_1^{3+}Mn_{0.3}^{3+}Ni_{0.4}^{2+}]_{oct}O_4^{2-}$
$Ni_{0.6}Mn_{0.4}Fe_2O_4$	$(Mn_{0.2}^{2+}Fe_{0.8}^{3+})_{tet}[Fe_{0.2}^{2+}Fe_1^{3+}Mn_{0.2}^{3+}Ni_{0.6}^{2+}]_{oct}O_4^{2-}$
$Ni_{0.8}Mn_{0.2}Fe_2O_4$	$(Mn_{0.1}^{2+}Fe_{0.9}^{3+})_{tet}[Fe_{0.1}^{2+}Fe_1^{3+}Mn_{0.1}^{3+}Ni_{0.8}^{2+}]_{oct}O_4^{2-}$
$NiFe_2O_4$	$(Fe^{3+})_{tet}[Fe^{3+}Ni^{2+}]_{oct}O_4^{2-}$

Effect of time-on-stream

All the compositions of this series were checked for catalytic stability at $350^\circ C$ and at a MeOH/aniline molar ratio of 5 for 7 h. The reaction mixture was collected at regular intervals of 1 h and analysed. The yield of NMA is plotted as a function of time-on-stream (Fig. 4.2.7.). All the mixed Ni-Mn compositions showed reasonable stability. $NiFe_2O_4$ and $MnFe_2O_4$ were found to be deactivated due to the formation of carbonaceous products over the catalyst surface.

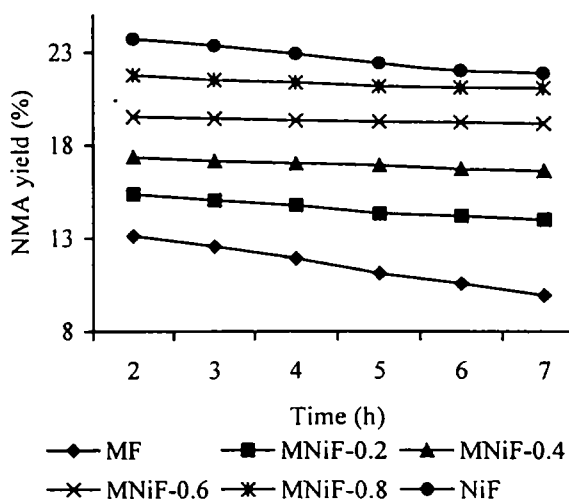


Fig.4.2.7. Effect of time-on-stream over the system $Ni_xMn_{1-x}Fe_2O_4$ ($x = 0, 0.2, 0.4, 0.6, 0.8$ and 1). Reaction temperature- $350^\circ C$, MeOH/ aniline molar ratio-5, and flow rate $-5mL h^{-1}$.

(d) $Cu_xMn_{(1-x)}Fe_2O_4$ ($x = 0, 0.2, 0.4, 0.6, 0.8$ and 1.0) - type systems

The percentage of aniline conversion and product distribution over various Cu-Mn series are depicted in the Table 4.2.10. The NMA selectivity is improved with successive copper addition and all the compositions performed with rather enhanced activity.

Table 4.2.10. Alkylation of aniline with methanol over $\text{Cu}_x\text{Mn}_{(1-x)}\text{Fe}_2\text{O}_4$ - type systems

Catalyst	Aniline conv.(%)	NMA Yield (wt %)	Product distribution (%)		
			NMA	NNDMA	Toluidine
MnFe_2O_4	22.45	13.12	78.72	13.73	7.55
$\text{Cu}_{0.2}\text{Mn}_{0.8}\text{Fe}_2\text{O}_4$	24.13	17.57	94.12	5.88	---
$\text{Cu}_{0.4}\text{Mn}_{0.6}\text{Fe}_2\text{O}_4$	26.12	21.48	96.11	3.89	---
$\text{Cu}_{0.6}\text{Mn}_{0.4}\text{Fe}_2\text{O}_4$	27.23	23.74	98.17	1.83	---
$\text{Cu}_{0.8}\text{Mn}_{0.2}\text{Fe}_2\text{O}_4$	28.19	24.94	99.41	2.59	---
CuFe_2O_4	29.49	27.76	98.83	1.17	---

Reaction temperature-350°C, MeOH/ aniline molar ratio-5, TOS- 2 h and flow rate – 5mL h⁻¹.

The acidity-basicity of the catalysts along with NMA yield are depicted in the Table 4.2.11. The weak Lewis acidic (weak plus medium acidity) sites were increased on successive copper doping into manganese ferros spinel as evident from the NH_3 -TPD studies and thermodesorption studies of pyridine and 2,6-dimethylpyridine adsorbed samples. The dehydration activity of the catalysts determined from the cyclohexanol decomposition reaction is diminished with rise in 'x' values, whereas the limiting amount of the electron acceptors adsorbed increased with increase in the copper content.

Table 4.2.11. Dehydration activity, weak plus medium acidity, limiting amount, aniline conversion and NMA yields of the system, $\text{Cu}_x\text{Mn}_{1-x}\text{Fe}_2\text{O}_4$.

x	Dehydration	Brönsted acid sites (%)	Weak+medium Acidity (10 ⁻⁴ mmol m ⁻²)	Limiting amount (10 ⁻⁴ mmol m ⁻²)		NMA Yield (wt %)
	Activity (wt %)			TCNQ	Chloranil	
	Cyclohexene					
0	91.28	0.825	8.12	10.71	2.60	13.12
0.2	47.23	0.810	8.15	22.91	8.37	17.57
0.4	46.36	0.791	8.19	24.65	9.52	21.48
0.6	42.18	0.777	8.24	26.95	10.65	23.74
0.8	38.98	0.752	8.28	28.32	11.82	24.94
1	34.91	0.731	8.32	30.01	12.80	27.76

The cation valency distribution of the mixed Cu-Mn series depicted in the Table 4.2.12 reveals that all the ferrites in this series are inverse and the concentration of Fe^{3+} ions in the octahedral sites for all compositions is the same. Thus, the catalytic activity of this series is mainly determined by the $\text{Cu}^{2+}/\text{Mn}^{3+}$ ratio in the octahedral sites and the slight enhancement in the catalytic activity is due to the increased weak Lewis acidity with copper doping.

Table 4.2.12. Cation valency distribution of $\text{Cu}_x\text{Mn}_{(1-x)}\text{Fe}_2\text{O}_4$ - type systems

Catalyst	Cation valency distribution
MnFe_2O_4	$(\text{Mn}_{0.5}^{2+}\text{Fe}_{0.5}^{3+})_{\text{tet}}[\text{Fe}_{0.5}^{2+}\text{Fe}_{1}^{3+}\text{Mn}_{0.5}^{3+}]_{\text{oct}}\text{O}_4^{2-}$
$\text{Cu}_{0.2}\text{Mn}_{0.8}\text{Fe}_2\text{O}_4$	$(\text{Mn}_{0.4}^{2+}\text{Fe}_{0.6}^{3+})_{\text{tet}}[\text{Fe}_{0.4}^{2+}\text{Fe}_{1}^{3+}\text{Mn}_{0.4}^{3+}\text{Cu}_{0.2}^{2+}]_{\text{oct}}\text{O}_4^{2-}$
$\text{Cu}_{0.4}\text{Mn}_{0.6}\text{Fe}_2\text{O}_4$	$(\text{Mn}_{0.3}^{2+}\text{Fe}_{0.7}^{3+})_{\text{tet}}[\text{Fe}_{0.3}^{2+}\text{Fe}_{1}^{3+}\text{Mn}_{0.3}^{3+}\text{Cu}_{0.4}^{2+}]_{\text{oct}}\text{O}_4^{2-}$
$\text{Cu}_{0.6}\text{Mn}_{0.4}\text{Fe}_2\text{O}_4$	$(\text{Mn}_{0.2}^{2+}\text{Fe}_{0.8}^{3+})_{\text{tet}}[\text{Fe}_{0.2}^{2+}\text{Fe}_{1}^{3+}\text{Mn}_{0.2}^{3+}\text{Cu}_{0.6}^{2+}]_{\text{oct}}\text{O}_4^{2-}$
$\text{Cu}_{0.8}\text{Mn}_{0.2}\text{Fe}_2\text{O}_4$	$(\text{Mn}_{0.1}^{2+}\text{Fe}_{0.9}^{3+})_{\text{tet}}[\text{Fe}_{0.1}^{2+}\text{Fe}_{1}^{3+}\text{Mn}_{0.1}^{3+}\text{Cu}_{0.8}^{2+}]_{\text{oct}}\text{O}_4^{2-}$
CuFe_2O_4	$(\text{Fe}^{3+})_{\text{tet}}[\text{Fe}^{3+}\text{Cu}^{2+}]_{\text{oct}}\text{O}_4^{2-}$

Effect of time-on-stream

A set of reactions was performed to ensure the catalytic stability of the Cu-Mn ferrite series at 350°C for 7 hours. The MeOH/aniline molar ratio was maintained at 5. The reaction mixture was collected and analyzed at regular intervals. Fig.4.2.8 shows the variation of NMA yield (%) with time. All the compositions of the series showed moderate stability for a long period of reaction.

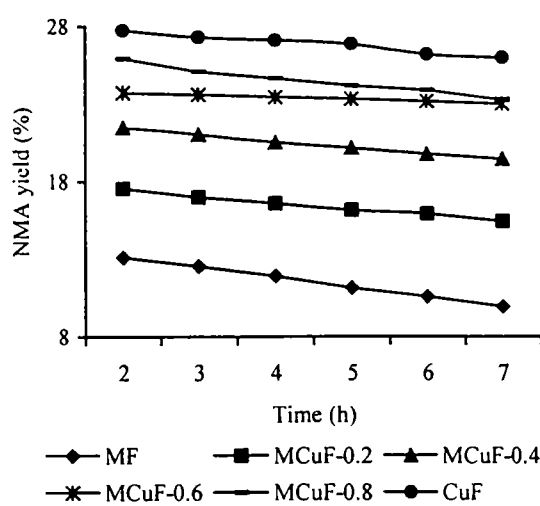


Fig.4.2.8. Effect of time-on-stream over the system $\text{Cu}_x\text{Mn}_{1-x}\text{Fe}_2\text{O}_4$ Reaction temperature- 350°C , MeOH/ aniline-5, and flow rate -5mL h^{-1} .

(d) $Zn_xMn_{(1-x)}Fe_2O_4$ ($x = 0, 0.2, 0.4, 0.6, 0.8$ and 1.0) - type systems .

Table 4.2.13 presents the percentage of aniline conversion and product distribution of aniline alkylation reactions with methanol for mixed Zn-Mn ferrite series. All the compositions showed privileged activity with shoddier NMA selectivity.

Table 4.2.13 Alkylation of aniline with methanol over $Zn_xMn_{(1-x)}Fe_2O_4$ - type systems

Catalyst	Aniline conv.(%)	NMA Yield (wt %)	Product distribution (%)		
			NMA	NNDMA	Toluidine
$MnFe_2O_4$	22.45	13.12	78.72	13.73	7.55
$Zn_{0.2}Mn_{0.8}Fe_2O_4$	13.31	12.75	72.37	20.52	7.11
$Zn_{0.4}Mn_{0.6}Fe_2O_4$	12.21	11.48	69.47	23.53	7.00
$Zn_{0.6}Mn_{0.4}Fe_2O_4$	10.32	10.74	67.54	25.61	6.85
$Zn_{0.8}Mn_{0.2}Fe_2O_4$	8.91	9.94	65.12	28.81	6.07
$ZnFe_2O_4$	6.94	8.76	64.82	29.17	6.01

Reaction temperature-350°C, MeOH/aniline-5, TOS- 2 h and flow rate $-5mL h^{-1}$.

The analysis of the data in Table 4.2.14 shows that the weak plus medium acidity and Brönsted acid sites are decreased with rise in 'x' values. The limiting amount of the electron acceptors adsorbed decreased while the dehydration activity slightly enhanced by the successive replacement of Mn by Zn. Therefore, it can be confirmed that acidity is not the sole factor determining the catalytic activity of the ferrites.

Table 4.2.14. Dehydration activity, weak plus medium acidity, limiting amount, aniline conversion and NMA yields of the system, $Zn_xMn_{1-x}Fe_2O_4$.

x	Dehydration	Brönsted acid sites (%)	Weak+medium Acidity ($10^4 mmol m^{-2}$)	Limiting amount ($10^4 mmol m^{-2}$)		NMA Yield (wt %)
	Activity (wt %)			TCNQ	Chloranil	
	Cyclohexene					
0	91.28	0.825	8.12	10.71	2.60	13.12
0.2	87.23	0.784	3.48	10.21	2.58	12.75
0.4	85.36	0.750	3.09	10.02	2.51	11.48
0.6	83.18	0.728	2.75	9.91	2.49	10.74
0.8	81.98	0.691	2.34	9.62	2.46	9.94
1	79.91	0.606	2.07	9.37	2.43	8.76

The cation distribution of the mixed Zn-Mn ferrite systems is depicted in Table 4.2.15 reveals that the progressive incorporation of Zn^{2+} ions into the tetrahedral sites shifted the partially inverse $MnFe_2O_4$ to the normal ferrites. Thus, the $Fe_{oct}^{3+}/Fe_{tet}^{3+}$ ratio increases with rise in 'x' values thereby promoting the catalytic activity for the series.

Table 4.2.15 Cation valency distribution of $Zn_xMn_{(1-x)}Fe_2O_4$ - type systems

Catalyst	Cation valency distribution
$MnFe_2O_4$	$(Mn_{0.5}^{2+}Fe_{0.5}^{3+})_{tet}[Fe_{0.5}^{2+}Fe_{1.5}^{3+}Mn_{0.5}^{3+}]_{oct}O_4^{2-}$
$Zn_{0.2}Mn_{0.8}Fe_2O_4$	$(Zn_{0.2}^{2+}Mn_{0.4}^{2+}Fe_{0.4}^{3+})_{tet}[Fe_{0.4}^{2+}Fe_{1.2}^{3+}Mn_{0.4}^{3+}]_{oct}O_4^{2-}$
$Zn_{0.4}Mn_{0.6}Fe_2O_4$	$(Zn_{0.4}^{2+}Mn_{0.3}^{2+}Fe_{0.3}^{3+})_{tet}[Fe_{0.3}^{2+}Fe_{1.4}^{3+}Mn_{0.3}^{3+}]_{oct}O_4^{2-}$
$Zn_{0.6}Mn_{0.4}Fe_2O_4$	$(Zn_{0.6}^{2+}Mn_{0.2}^{2+}Fe_{0.2}^{3+})_{tet}[Fe_{0.2}^{2+}Fe_{1.6}^{3+}Mn_{0.2}^{3+}]_{oct}O_4^{2-}$
$Zn_{0.8}Mn_{0.2}Fe_2O_4$	$(Zn_{0.8}^{2+}Mn_{0.1}^{2+}Fe_{0.1}^{3+})_{tet}[Fe_{0.1}^{2+}Fe_{1.8}^{3+}Mn_{0.1}^{3+}]_{oct}O_4^{2-}$
$ZnFe_2O_4$	$(Zn^{2+})_{tet}[Fe_2^{3+}]_{oct}O_4^{2-}$

Effect of time-on-stream

The catalytic stability of the catalysts was checked by noting the NMA yield (%) for 7 hours. All the mixed Zn-Mn ferrites showed prolonged stability. The deactivation of $MnFe_2O_4$ is due to the deposition of carbonaceous products over the catalyst surface. The reduction of Fe^{3+} ions in the reaction medium and the normal spinel structure of $ZnFe_2O_4$ restricts the redistribution of electrons to regain the original oxidation state is the cause for its poor stability.

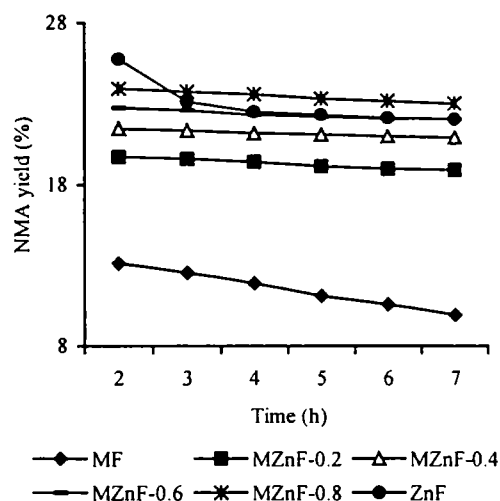


Fig.4.2.9Effect of time-on-stream over the system $Zn_xMn_{1-x}Fe_2O_4$. Reaction temperature-350°C, MeOH/aniline-5 and flow rate -5mL h⁻¹.

4.2.3 Mechanism of aniline alkylation

From the results obtained for the reaction over the ferrite catalysts, it is clear that N-alkylation of aniline is a facile reaction. The reaction is supposed to be consecutive or sequential and follows the order: Aniline → NMA → NNDMA → Others. It is also

believed that only weak to moderate acidity favours the reaction and the presence of certain minimum number of acidic and basic sites are enough to trigger the reaction. Any excess number of acid sites even if present will not be involved in the reaction and will be surplus. Strong acidity on the other hand, if present will only deactivate the catalyst by coking due to cracking of the alcohol and there by making it unavailable for alkylation. The presence of more Lewis acid sites is preferred for the reaction. Aniline being a stronger base than methanol gets adsorbed preferentially over the Lewis sites. The participation of Fe^{3+} ions in the octahedral sites as the alcohol adsorbing centers has already been reported [50]. Fig. 4.2.10 depicts a plausible mechanism of aniline alkylation over ferrite catalysts.

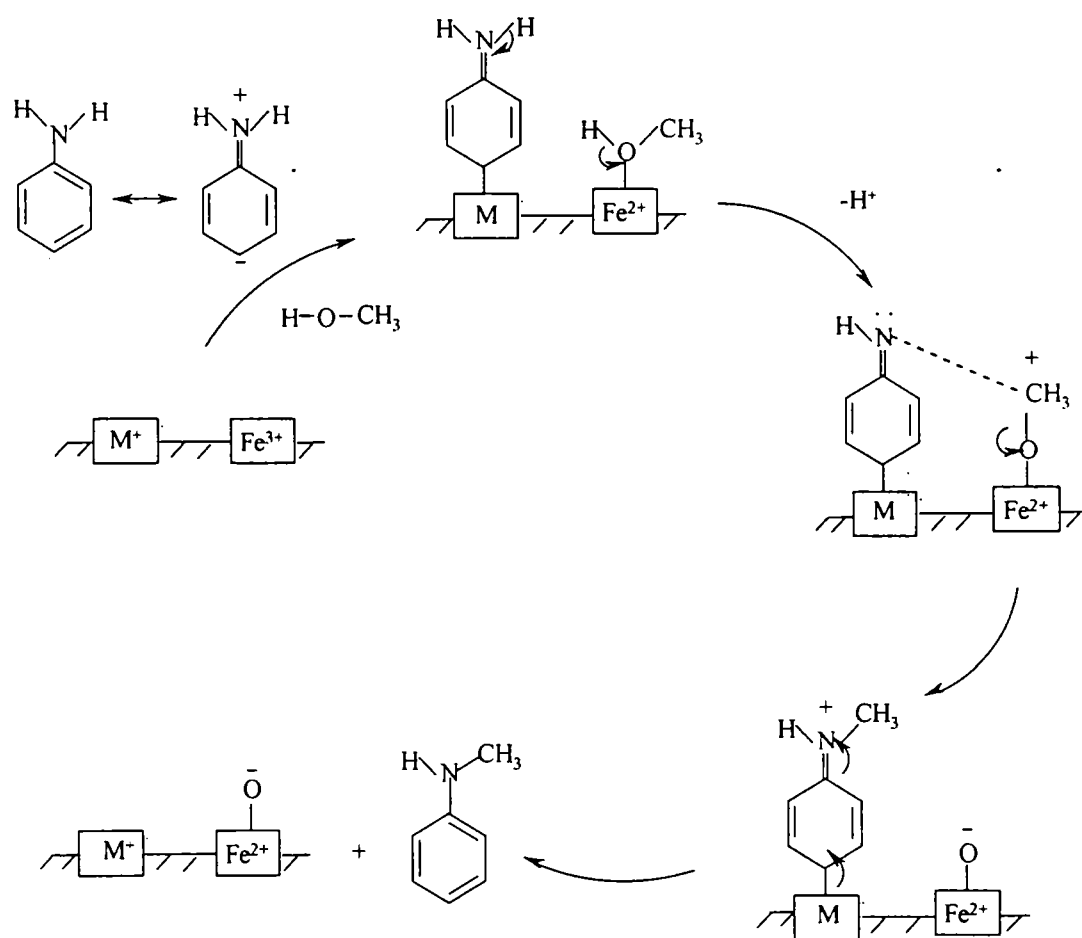


Fig. 4.2.10. A plausible mechanism for aniline alkylation over ferrite catalysts.

4.3 Section III – Phenol Alkylation

Alkylation of phenol with methanol is an industrially important reaction as the reaction products, *o*-cresol is an important organic intermediate for herbicides and insecticides, 2,6-xyleneol is used in the manufacture of polyphenylene oxide (PPO) and special grade paints and anisole is an additive in gasoline to boost octane [1, 2]. Other alkylated phenols such as *p*-cresol, *m*-cresol and other xyleneol isomers are also industrially important as antioxidants, herbicides, and insecticides and are used for stabilizing natural and synthetic rubber. So, the choice of a suitable catalyst and the proper operating conditions is of primary importance in determining the industrial convenience of the process. A schematic representation of the various reaction pathways of phenol alkylation using methanol as the alkylating agent is presented in Fig. 4.3.1.

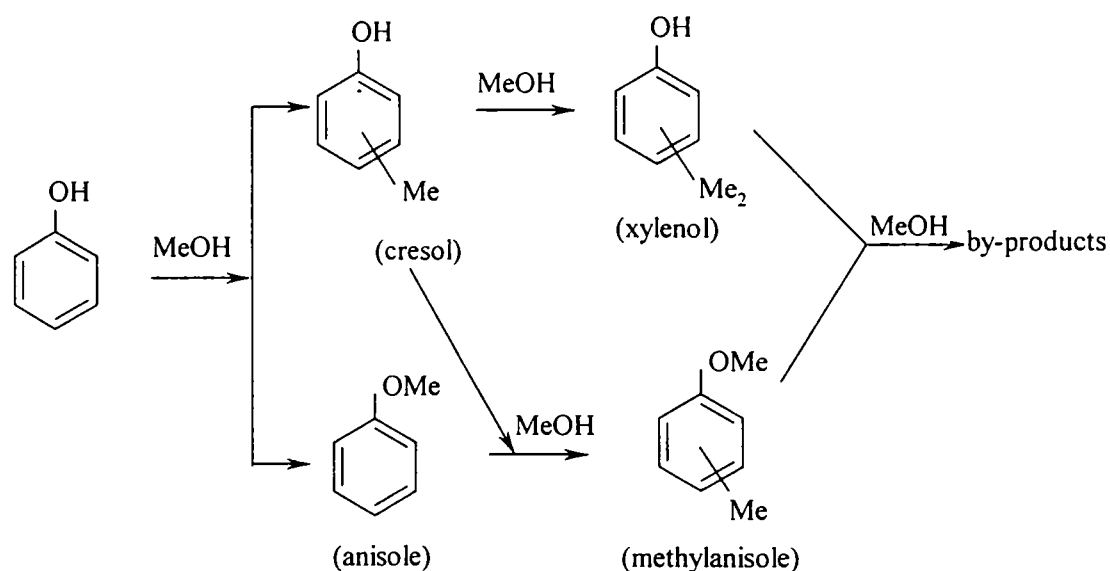


Fig. 4.3.1 Reaction scheme of phenol alkylation using methanol as the alkylating agent.

Earlier, Friedel-Crafts catalysts have been used for the alkylation of phenol, but the selective methylation of phenol on the aromatic carbon atoms has not been successful [3]. The environmentally friendly solid acid catalysts are very good alternatives to proton acids or Friedel-Crafts-type catalysts. The catalysts employed for this reaction include γ -alumina [4-9], silica-alumina [10], supported phosphoric acid [11, 12], magnesium oxide [13], titania [14], mixed oxides [14- 18], acid solids such as BaSO_4 , SrSO_4 and $\text{La}_2(\text{HPO}_4)_3$ [6], Nafion -H [19] and zeolites [22-28].

The alkylation of phenol with methanol is basically an acid-base reaction. So, the difference in activity and product selectivity could be explained on the basis of difference in acid-base properties of the catalysts. However, there is a continuous debate on the correlation between acid-base properties and product selectivity. There is always a competition between O- and C-alkylation [20, 22, 29] and the strength of the acidic sites play a crucial role in the product selectivity. Acidic catalysts generally produce a mixture of cresols and xylenols and also get deactivated with time due to coking.

It has been reported by Benzouhanava *et al.* [30] that strongly acidic catalysts favour O-alkylation to give anisole as a predominant product while weak acidic sites or strong basic sites favour C-alkylation. Tliemat-Manzalji *et al.* [31] and Marczewski *et al.* [32] have claimed that weak acidic sites favour C-alkylation. Again, Samalada *et al.* have reported that existence of medium strength acid sites is selective towards O-alkylation. According to Rao *et al.* [33-35] increase in acidity enhances the phenol conversion and selectivity for 2,6-xyleneol at the expense of *o*-cresol. Balsama *et al.* [22] have studied the alkylation of phenol with methanol in the presence of X and Y zeolites exchanged with various cations and of pentasil-type molecular sieves and claimed that strongly acidic catalysts promote ring alkylation.

Tanabe and Nishizaki [3] have reported that basic catalysts such as MgO selectively alkylate phenol at the *ortho*-position. Rao *et al.* have reported the involvement of acidic sites to give predominantly *ortho*-alkylation [33]. Velu and Swami [36] have done the alkylation of phenol with methanol over magnesium-aluminium calcined hydrotalcites (MgAl-CHT). According to them, the reaction proceeded predominantly through anisole as the intermediate and they suggested the participation of combined acidic and basic sites in calcined hydrotalcites for alkylation. The same authors [37] further studied the phenol alkylation over CuAl-CHT and the selective C-alkylation to give *o*-cresol and 2,6-xyleneol could be attributed to the higher acidity of these catalysts.

Santhacesaria *et al.* [38] evaluated the catalytic activity of different catalysts with different acid strengths for phenol alkylation and concluded that the selectivity of the products greatly depend on the geometrical factors of the adsorbed reagents.

Furthermore, they observed that the Brønsted acid sites are responsible for coke formation.

This section gives detailed discussion on vapour-phase phenol alkylation reaction with methanol as the alkylating agent over the five series of manganese ferros spinels. We observed that in majority of the cases manganese ferros spinels could produce *o*-cresol with high selectivity and in a few cases 2,6-xyleneol was also formed. *O*-alkylation leading to anisole was observed in negligible amount. A thorough depiction of process optimization such as effect of reaction temperature, flow rate, methanol to phenol molar ratio and water in the feed are also included in this section.

4.3.1 Process optimization

The vapour-phase alkylation of phenol with methanol was carried out at atmospheric pressure using a vertical flow-type reactor of 2 cm ID and 30 cm length, kept in a cylindrical double walled furnace mounted vertically. 0.5 g of the catalyst activated at 500°C for 2 h was placed in the middle of the reactor and packed with silica beads. The temperature of the reactor was maintained by a Cr-Al thermocouple placed inside the reactor. A pre-mixed phenol- methanol solution was introduced at the top of the reactor by means of a syringe pump. The products were analysed by gas chromatography (Chemito GC 8610, flame ionization detector, SE 30 column, 2 m length). A blank run was carried out at 350°C with no catalyst in the reactor indicating negligible thermal reaction.

4.3.1.1 Effect of methanol to phenol molar ratio

In order to choose an optimum feed mix ratio, the alkylation reactions on $Zn_{0.8}Mn_{0.2}Fe_2O_4$ was carried out at 350°C using several methanol/phenol molar ratios. The *C*-alkylated products such as *o*-cresol and 2,6-xyleneol were the major reaction products observed. Phenol conversion and product selectivities are plotted against methanol/phenol molar ratio (Fig. 4.3.2).

It can be seen from the figure that the phenol conversion gradually increases with rise in methanol/phenol molar ratio. The *O*-alkylated product, anisole remained more or less constant through out the molar ratios studied. Since the phenol conversion and

selectivities towards *o*-cresol and 2,6-xylene were maximal at a methanol/phenol molar ratio of 7, this feed mix ratio was selected for further studies.

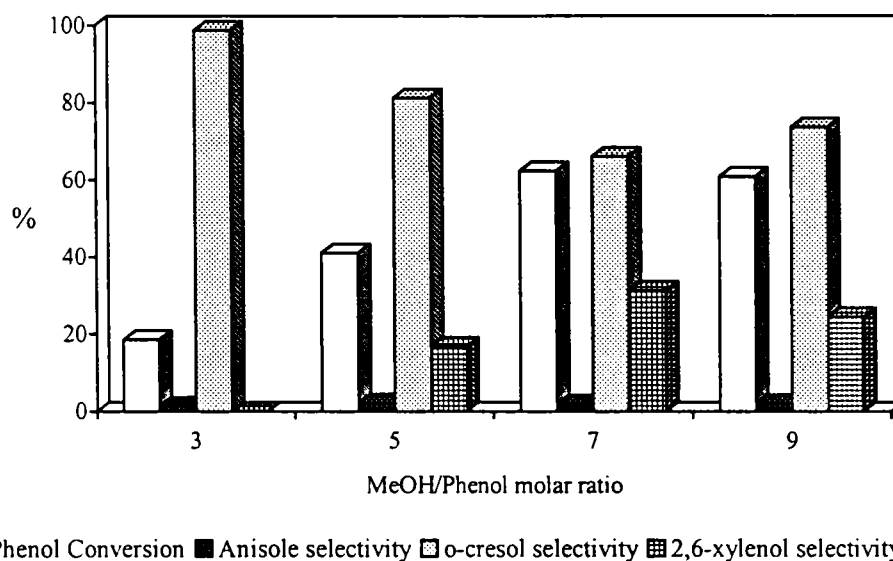


Fig. 4.3.2. Effect of MeOH to phenol molar ratio on conversion and selectivity of methylation of phenol over $Zn_{0.8}Mn_{0.2}Fe_2O_4$. Reaction temperature- 350°C, TOS- 2 h and VHSV- 4 mL h⁻¹.

4.3.1.2 Effect of reaction temperature

The alkylation reactions were carried out in the temperature range 300-450°C over $Zn_{0.8}Mn_{0.2}Fe_2O_4$ at a MeOH/phenol molar ratio of 7. The phenol conversion and product selectivities are depicted in the Table 4.3.1.

Phenol conversion showed an increase with rise in temperature up to 350°C. The O-alkylation leading to anisole formation was detected to be less than 3% throughout the temperature region studied. The manganese ferros spinels were found to be more prone to C-alkylation at any temperature region. At lower temperatures *o*-cresol was detected as the major reaction product. With the rise in temperature, consecutive methylation of *o*-cresol to 2,6-xylene was increased and the maximum yield of 2,6-xylene was observed at 350°C. Further rise in temperature did not show an enhancement in the alkylation rate, but phenol underwent decomposition reaction

forming benzene and toluene. Again, at higher temperatures methanol undergoes decomposition in greater extent decreasing the reaction rate.

Table 4.3.1 Product distribution (wt%) for the phenol alkylation reaction- Effect of reaction temperature.

Products distribution	Reaction Temperature (°C)						
	300	325	350	375	400	450	500
C-oxides	---	---	0.33	0.72	1.93	2.13	2.72
Benzene	---	---	---	---	0.98	1.62	3.01
Toluene	---	---	---	0.98	2.72	3.01	4.17
Anisole	2.97	2.56	1.72	1.61	1.11	0.91	0.52
Unreacted	68.63	57.68	37.68	39.48	46.61	50.64	57.63
Phenol							
<i>o</i> -cresol	26.67	33.08	40.81	42.85	36.88	32.01	28.59
2,6-xylenol	1.83	6.68	19.46	14.46	11.77	9.69	3.36
Phenol	31.37	42.32	62.32	60.52	55.39	49.36	42.37
conversion							
Selectivity (%)							
<i>o</i> -cresol	85.01	78.16	65.48	70.64	66.58	64.82	67.48
2,6-xylenol	5.83	15.78	31.22	23.89	21.25	19.63	7.93

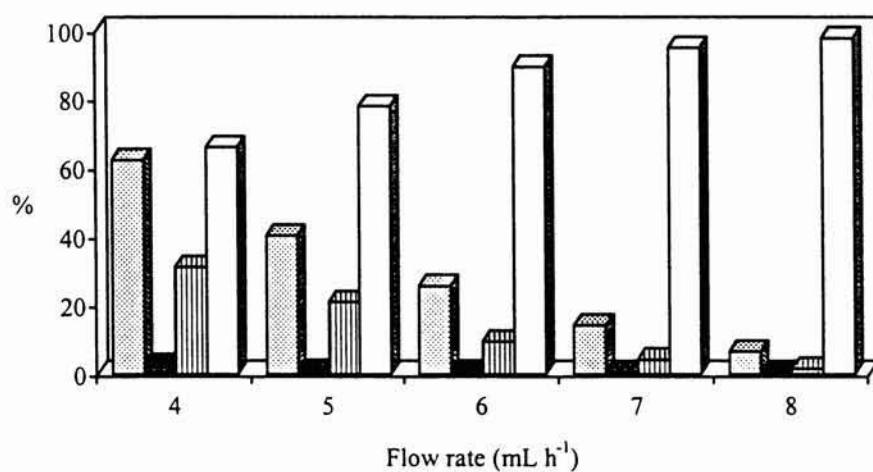
Reaction temperature-350°C, MeOH/phenol-7, TOS- 2 h and flow rate – 4mL/h.

4.3.1.3 Effect of flow rate

The effect of contact time (VHSV) on phenol conversion and product selectivity at 350°C performed over $Zn_{0.8}Mn_{0.2}Fe_2O_4$ at a MeOH/phenol molar ratio of 7 is shown in Fig. 4.3.3.

As the flow rate increases from 4 to 8 mL h⁻¹ the phenol conversion drastically declines from 62% to 6.5%. At higher flow rates, the residence time of the reactant molecules over the catalyst surface is less compared to the lower flow rates resulting in the lower conversions. At lower contact time, *o*-cresol was observed as a major product

with negligible amount of 2,6-xylenol. Higher contact time resulted in an increased in the formation of 2,6-xylenol, and this was allied with a resultant decrease in the *o*-cresol yield. This is an indication of the consecutive methylation of *o*-cresol over the catalyst surface at high contact time.



□ Phenol conversion ■ Anisole selectivity ▨ 2,6-xylenol selectivity □ *o*-cresol selectivity

Fig. 4.3.3. Effect of flow rate on conversion and selectivity of methylation of phenol over $Zn_{0.8}Mn_{0.2}Fe_2O_4$. Reaction temperature- 350°C, TOS- 2 h, MeOH to phenol molar ratio- 7.

4.3.1.4 Effect of water in the feed

In order to study the effect of water in the feed, alkylation reaction with four different molar ratios of methanol-to-water-to-phenol were done and the results obtained were compared (Table 4.3.2). It can be seen from the above discussions that C-alkylation of phenol with methanol occurred efficiently at a methanol to phenol molar ratio of 7 and at a temperature of 350°C over $Zn_{0.8}Mn_{0.2}Fe_2O_4$. In a vapour-phase set-up with excess of methanol there is every chance of loss of methanol due to decomposition or side reactions. With the intention of reducing these side reactions and to suppress the coke formation over the catalyst surface, we have added some water in the feed mix and studied its effect on the reaction. Interestingly, it was observed that water in the feed significantly suppressed the using up of methanol without much affecting the product yields.

Table 4.3.2. Product distribution (wt%) and selectivity for the phenol alkylation reaction- Effect of water in the feed.

Product distribution	Feed composition (MeOH: H ₂ O : Phenol)			
	7:0:1	6:1:1	5:2:1	4:3:1
C-oxides	0.33	---	---	---
Benzene	---	0.42	0.51	0.50
Toluene	---	0.79	0.88	0.92
Anisole	1.72	0.31	0.20	0.18
Unreacted Phenol	37.68	40.43	44.80	60.88
<i>o</i> -cresol	40.81	41.67	40.60	36.38
2,6-xylenol	19.46	16.38	13.55	11.14
Phenol conversion	62.32	59.57	55.20	49.12
Methanol conversion	51.71	42.71	33.89	21.07
Selectivity (%)				
<i>o</i> -cresol	65.84	69.95	73.55	75.08
2,6-xylenol	31.22	27.49	24.55	22.68

Reaction temperature-350°C, MeOH/ phenol-7, TOS- 2 h and flow rate –4 mL h⁻¹.

4.3.2 Comparison of catalyst composition

The alkylation of phenol with methanol was done over five series of manganese ferros spinels at 350°C and at a methanol/phenol molar ratio of 7 and flow rate was kept at 4 mLh⁻¹. The catalytic activity was correlated to the acid-base properties of the samples. C-alkylation was dominant over O-alkylation with the ferrites.

(a) Cr_xMn_(1-x)Fe₂O₄ (x = 0, 0.2, 0.4, 0.6, 0.8 and 1.0) - type systems

A series of experiments were performed to evaluate the catalytic activity of Cr-Mn ferrites. The phenol conversion and selectivities are depicted in Table 4.3.3.

Even though the selectivity for *o*-cresol is enhanced tremendously, the phenol conversion reduced radically by the incorporation of Cr-ions. The secondary alkylated product, 2,6-xylenol produced by the consecutive methylation of *o*-cresol is not observed in this series.

Table 4.3.3. Alkylation of phenol with methanol over $\text{Cr}_x\text{Mn}_{(1-x)}\text{Fe}_2\text{O}_4$ - type systems.

Catalyst	Phenol Conv. (wt%)	<i>o</i> -cresol yield (wt%)	2,6-xylenol yield (wt%)	Product selectivity (%)		
				Anisole	<i>o</i> -cresol	2,6-xylenol
MnFe_2O_4	40.75	39.63	---	1.37	98.63	---
$\text{Cr}_{0.2}\text{Mn}_{0.8}\text{Fe}_2\text{O}_4$	18.68	17.90	---	0.98	99.02	---
$\text{Cr}_{0.4}\text{Mn}_{0.6}\text{Fe}_2\text{O}_4$	16.42	16.42	---	---	100	---
$\text{Cr}_{0.6}\text{Mn}_{0.4}\text{Fe}_2\text{O}_4$	15.18	15.18	---	---	100	---
$\text{Cr}_{0.8}\text{Mn}_{0.2}\text{Fe}_2\text{O}_4$	14.02	14.02	---	---	100	---
CrFe_2O_4	13.61	13.61	---	---	100	---

Reaction temperature-350°C, MeOH/ phenol-7, TOS- 2 h and flow rate 4 mL h^{-1} .

The total acidity, especially acidity in the high acid strength region was decreased by the successive incorporation of Cr ions in the octahedral positions of the pure manganese ferrosphenel as evident from the NH_3 -TPD studies and thermodesorption studies of the pyridine adsorbed samples. This is supported by the dehydration activity from the cyclohexanol decomposition reaction. The limiting concentration of the electron acceptors adsorbed showed a fair increase with increase in chromium content. The acid-base properties of the Cr-Mn series along with phenol conversion (wt%) are presented in Table 4.3.4.

Table 4.3.4. Dehydration activity, total acidity, limiting amount and phenol conversion of the system $\text{Cr}_x\text{Mn}_{1-x}\text{Fe}_2\text{O}_4$ ($x = 0, 0.2, 0.4, 0.6, 0.8$ and 1).

x	Dehydration Activity (wt %)	Total Acidity (10^{-4} mmol m^{-2})	Limiting amount (10^{-4} mmol m^{-2})		Phenol Conversion (wt%)
	Cyclohexene		TCNQ	chloranil	
0	91.28	16.50	10.71	40.75	39.63
0.2	38.52	10.56	55.52	18.68	17.90
0.4	37.01	10.48	56.28	16.42	16.42
0.6	36.25	10.43	57.58	15.18	15.18
0.8	35.89	10.41	59.01	14.02	14.02
1	34.82	10.36	60.61	13.61	13.61

Since phenol is a polar molecule, even the very weak basic sites can easily remove a H^+ from phenolic O-H bond forming phenolate ion. The phenolate ion then coordinate with the acidic site of the catalyst. Therefore, in phenol alkylation it is the acidity rather than the basicity that controls the catalytic activity. The decrease in the acidity of the series by chromium substitution is the prime cause for their reduced phenol conversion.

Effect of time-on-stream

A set of experiments were performed over mixed Cr-Mn series at 350°C and at a methanol-to-phenol molar ratio of 7 over a period of 6 h to evaluate the stability of the system. The product analysis was done at regular intervals of 60 minutes. The deactivation studies of the mixed Cr-Mn series are depicted in the following figure (Fig. 4.3.4). Among the systems, MnFe_2O_4 showed excellent stability where as other systems showed slight deactivation with time.

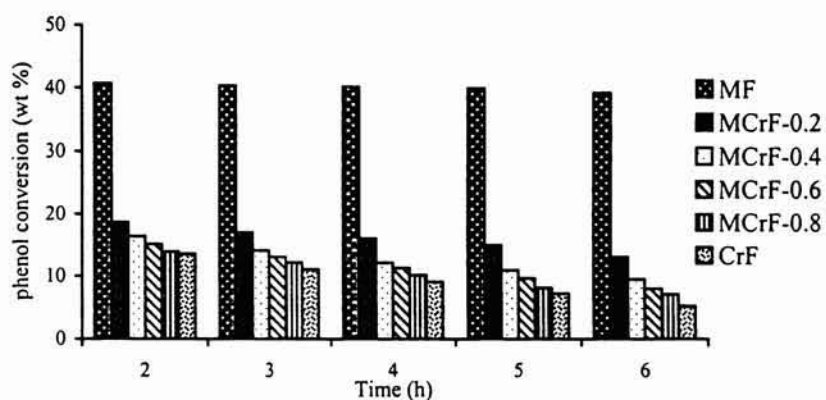


Fig. 4.3.4. Effect of time-on-stream over the system, $\text{Cr}_x\text{Mn}_{1-x}\text{Fe}_2\text{O}_4$ ($x = 0, 0.2, 0.4, 0.6, 0.8$ and 1) Reaction temperature- 350°C , MeOH/ aniline- 5, TOS- 2 h and flow rate 4mL h^{-1} .

(b) $\text{Co}_x\text{Mn}_{(1-x)}\text{Fe}_2\text{O}_4$ ($x = 0, 0.2, 0.4, 0.6, 0.8$ and 1.0) - type systems

The phenol conversion and product selectivity of phenol alkylation reaction done over mixed Co-Mn series is depicted in Table 4.3.5. It is clear from the table that the replacement of Mn by Co in the pure manganese ferrosphenel decreased the phenol conversion and *o*-cresol selectivity slightly. Though negligible amount of

O-alkylated product, anisole is observed all along the system, the secondary alkylated product 2,6-xylenol is not detected.

Table 4.3.5. Alkylation of phenol with methanol over $\text{Co}_x\text{Mn}_{(1-x)}\text{Fe}_2\text{O}_4$ - type systems

Catalyst	Phenol Conv. (wt%)	<i>o</i> -cresol yield (wt%)	2,6-xylenol yield (wt%)	Product selectivity (%)		
				Anisole	<i>o</i> -cresol	2,6-xylenol
MnFe_2O_4	40.75	39.63	---	1.37	98.63	---
$\text{Co}_{0.2}\text{Mn}_{0.8}\text{Fe}_2\text{O}_4$	37.81	36.80	---	1.22	98.78	---
$\text{Co}_{0.4}\text{Mn}_{0.6}\text{Fe}_2\text{O}_4$	35.29	35.57	---	0.91	99.09	---
$\text{Co}_{0.6}\text{Mn}_{0.4}\text{Fe}_2\text{O}_4$	34.13	34.44	---	0.88	99.12	---
$\text{Co}_{0.8}\text{Mn}_{0.2}\text{Fe}_2\text{O}_4$	32.92	33.18	---	0.79	99.21	---
CoFe_2O_4	30.67	30.13	---	0.77		---

Reaction temperature-350°C, MeOH/ phenol-7, TOS- 2 h and flow rate 4 mL h^{-1} .

The variation in total acidity is smooth and decreases from MnFe_2O_4 to CoFe_2O_4 as the cobalt content increases in the system. This observation was confirmed by the dehydration of cyclohexanol carried out on these catalysts which is taken as a measure of the acidity index. The limiting amount of the electron acceptors adsorbed showed a slight increase with Co-substitution. Table 4.3.6 depicts the acid-base properties along with phenol conversion (wt%).

Table 4.3.6. Dehydration activity, total acidity, limiting amount, *o*-cresol and 2,6-xylenol yields of the system $\text{Co}_x\text{Mn}_{1-x}\text{Fe}_2\text{O}_4$ ($x = 0, 0.2, 0.4, 0.6, 0.8$ and 1).

x	Dehydration	Total Acidity (10^{-3} mmol m^{-2})	Limiting amount (10^{-4} mmol m^{-2})		Phenol Conversion (wt%)
	Activity (wt %)		TCNQ	chloranil	
	Cyclohexene				
0	91.28	16.50	10.71	40.75	39.63
0.2	90.80	16.36	15.68	37.81	36.80
0.4	88.00	16.27	16.38	35.29	35.57
0.6	87.50	15.79	17.19	34.13	34.44
0.8	87.10	15.70	17.88	32.92	33.18
1	86.00	15.63	18.58	30.67	30.13

Though phenol alkylation is essentially an acid-base reaction, the acidity of the catalysts has a decisive role in determining the rate of the reaction. Since the cobalt substitution decreased the total acidity slightly, the same trend is reflected in the phenol alkylation activity.

Effect of time-on-stream

The phenol alkylation reactions were done over $\text{Co}_x\text{Mn}_{1-x}\text{Fe}_2\text{O}_4$ - type system at 350°C and at a flow rate of 4 mLh^{-1} for 6 h to check the stability of the system. The product analysis was done at regular interval of 60 minutes (Fig.4.3.5). All the systems showed excellent stability for a long period of reaction time.

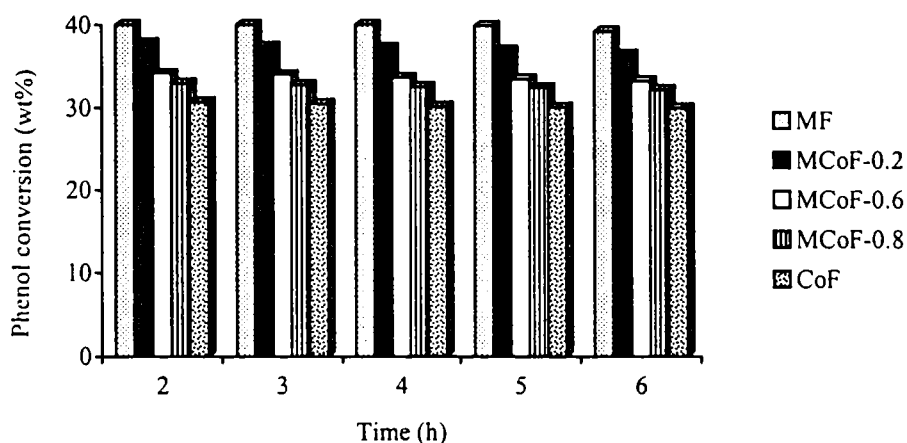


Fig. 4.3.5. Effect of time-on-stream over the system, $\text{Co}_x\text{Mn}_{1-x}\text{Fe}_2\text{O}_4$ ($x = 0, 0.2, 0.4, 0.6, 0.8$ and 1). Reaction temperature- 350°C , MeOH/ aniline- 5, TOS- 2 h and flow rate 4 mL h^{-1} .

(c) $\text{Ni}_x\text{Mn}_{(1-x)}\text{Fe}_2\text{O}_4$ ($x = 0, 0.2, 0.4, 0.6, 0.8$ and 1.0) - type systems

Table 4.3.7 represents the phenol conversion and product selectivities of phenol alkylation performed over mixed Ni-Mn ferrites.

Ni-Mn mixed series showed poor activity for phenol methylation with progressive incorporation of Ni. The selectivity for *o*-cresol remained more or less cent percent through out the series. The secondary methylation leading to 2,6- xylene is not detected throughout the series.

The acid-base properties of the series determined by various methods along with phenol conversion (wt %) are shown in Table 4.3.8. The total acidity of this series decreased with successive Ni-doping as determined by NH₃-TPD method. The decrease in the dehydration activity from the cyclohexanol decomposition reaction confirmed the decrease in acidity with increase in 'x' values. But, it is seen that the limiting concentrations of the electron acceptors adsorbed on the catalyst showed a proportionate increase with increase in nickel content.

Table 4.3.7. Alkylation of phenol with methanol over Ni_xMn_(1-x)Fe₂O₄ - type systems

Catalyst	Phenol Conv. (wt%)	<i>o</i> -cresol yield (wt%)	2,6-xylenol yield (wt%)	Product selectivity (%)		
				Anisole	<i>o</i> -cresol	2,6-xylenol
MnFe ₂ O ₄	40.75	39.63	---	1.37	98.63	---
Ni _{0.2} Mn _{0.8} Fe ₂ O ₄	25.22	24.91	---	0.58	99.42	---
Ni _{0.4} Mn _{0.6} Fe ₂ O ₄	23.92	23.84	---	0.41	99.59	---
Ni _{0.6} Mn _{0.4} Fe ₂ O ₄	22.16	21.91	---	0.42	99.58	---
Ni _{0.8} Mn _{0.2} Fe ₂ O ₄	21.87	21.36	---	0.31	99.69	---
NiFe ₂ O ₄	20.34	20.03	---	0.27	99.73	---

Reaction temperature-350°C, MeOH/ phenol-7, TOS- 2 h and flow rate -4mL h⁻¹.

Table 4.3.8. Dehydration activity, total acidity, limiting amount and *o*-cresol yield of the system Ni_xMn_{1-x}Fe₂O₄ (x = 0, 0.2, 0.4, 0.6, 0.8 and 1).

x	Dehydration	Total Acidity	Limiting amount		Phenol Conversion (wt%)
	Activity (wt %)	(10 ⁻⁴ mmol m ⁻²)	(10 ⁻⁴ mmol m ⁻²)		
	Cyclohexene		TCNQ	chloranil	
0	91.28	16.50	10.71	40.75	39.63
0.2	73.76	15.14	20.81	25.22	39.63
0.4	70.25	15.06	22.47	23.92	24.91
0.6	68.98	15.00	23.13	22.16	23.84
0.8	65.29	14.96	23.97	21.87	21.91
1	62.10	14.90	25.52	20.34	21.36

Ni-addition progressively removes the acidic sites originally present in pure manganese ferros spinel system and correspondingly possessed lesser activity for phenol alkylation.

Effect of time-on-stream

The Ni-Mn series were checked for catalytic stability by noting the phenol conversion for 6h. The reaction temperature was kept at 350°C and methanol-to-phenol molar ratio was 7. The product analysis was done at a regular interval of 60 minutes and the results are presented in the figure 4.3.6. $MnFe_2O_4$ performed excellent stability. $Ni_{0.2}Mn_{0.8}Fe_2O_4$, $Ni_{0.4}Mn_{0.6}Fe_2O_4$ and $Ni_{0.6}Mn_{0.4}Fe_2O_4$ showed slight deactivation where as $Ni_{0.8}Mn_{0.2}Fe_2O_4$ and $NiFe_2O_4$ showed rapid deactivation.

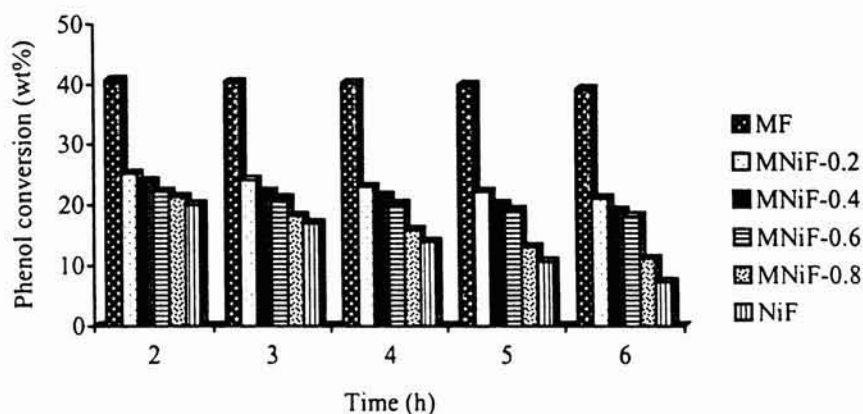


Fig. 4.3.6. Effect of time-on-stream over the system, $Ni_xMn_{1-x}Fe_2O_4$ ($x = 0, 0.2, 0.4, 0.6, 0.8$ and 1). Reaction temperature- 350°C, MeOH/ aniline- 5, TOS- 2h and flow rate $4 mL h^{-1}$.

(d) $Cu_xMn_{(1-x)}Fe_2O_4$ ($x = 0, 0.2, 0.4, 0.6, 0.8$ and 1.0) - type systems

The phenol alkylation with methanol was performed over mixed Cu-Mn series at 350°C. The results obtained are depicted in Table 4.3.9. The phenol conversion first showed a decrease on incorporating Cu^{2+} ions into the octahedral position and then increased with increase in copper content. The selectivity for *o*-cresol remained more or less constant all along the series. Negligible amount of O-alkylated product, anisole is detected through out the series. 2,6-xyleneol, which is produced by the secondary methylation of *o*-cresol is not observed throughout the series.

Table 4.3.9. Alkylation of phenol with methanol over $\text{Cu}_x\text{Mn}_{(1-x)}\text{Fe}_2\text{O}_4$ - type systems

Catalyst	Phenol Conv. (wt%)	<i>o</i> -cresol yield (wt%)	2,6-xylene yield (wt%)	Product selectivity (%)		
				Anisole	<i>o</i> -cresol	2,6-xylene
MnFe_2O_4	40.75	39.63	---	2.75	97.25	---
$\text{Cu}_{0.2}\text{Mn}_{0.8}\text{Fe}_2\text{O}_4$	24.62	24.19	---	1.75	98.25	---
$\text{Cu}_{0.4}\text{Mn}_{0.6}\text{Fe}_2\text{O}_4$	28.71	28.16	---	1.91	98.08	---
$\text{Cu}_{0.6}\text{Mn}_{0.4}\text{Fe}_2\text{O}_4$	30.61	29.95	---	2.15	97.84	---
$\text{Cu}_{0.8}\text{Mn}_{0.2}\text{Fe}_2\text{O}_4$	32.93	32.17	---	2.30	97.70	---
CuFe_2O_4	33.59	32.90	---	2.05	97.95	---

Reaction temperature-350°C, MeOH/ phenol-7, TOS- 2 h and flow rate 4 mL h^{-1} .

Table 4.3.10 presents the acid-base properties of the $\text{Cu}_x\text{Mn}_{1-x}\text{Fe}_2\text{O}_4$ - system. The total acidity of the system first decreased and then increased with successive Cu-addition. The dehydration activity did not follow the same trend; it goes on increasing with increase in Cu-content. The limiting concentration of the electron acceptors adsorbed remained rather constant throughout the series.

Table 4.3.10. Dehydration activity, total acidity, limiting amount and phenol conversion yield of the system $\text{Cu}_x\text{Mn}_{1-x}\text{Fe}_2\text{O}_4$ ($x = 0, 0.2, 0.4, 0.6, 0.8$ and 1).

x	Dehydration	Total Acidity	Limiting amount		Phenol Conversion (wt%)
	Activity (wt %)	(10^{-4} mmol m^{-2})	(10 ⁻⁴ mmol m^{-2})		
	Cyclohexene		TCNQ	chloranil	
0	91.28	16.50	10.71	40.75	40.75
0.2	92.23	13.99	10.21	24.62	24.62
0.4	93.36	14.13	10.02	28.71	28.71
0.6	94.18	14.71	9.91	30.61	30.61
0.8	95.98	15.61	9.62	32.93	32.93
1	96.91	16.42	9.37	33.59	33.59

Effect of time-on-stream

A series of phenol alkylation experiments were performed at 350°C over $\text{Cu}_x\text{Mn}_{1-x}\text{Fe}_2\text{O}_4$ system for 6 h and the product analysis was done at regular intervals of 60 minutes to check the catalytic stability. The results are presented in Fig. 4.3.7. Except for the pure manganese ferrosphenel, MnFe_2O_4 all the other samples in this series exhibit poor stability.

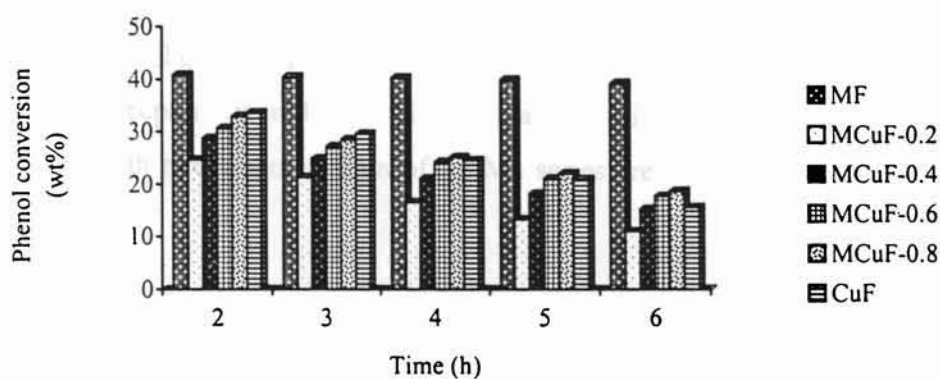


Fig. 4.3.7. Effect of time-on-stream over the system, $\text{Cu}_x\text{Mn}_{1-x}\text{Fe}_2\text{O}_4$. Reaction temperature- 350°C, MeOH/ aniline- 5, TOS- 2 h and feed flow 4mL h^{-1} .

(e) $\text{Zn}_x\text{Mn}_{(1-x)}\text{Fe}_2\text{O}_4$ ($x = 0, 0.2, 0.4, 0.6, 0.8$ and 1.0) - type systems

The phenol conversion and product selectivities obtained from phenol alkylation experiments done over Zn-Mn series is shown in Table 4.3.11.

Table 4.3.11. Alkylation of phenol with methanol over $\text{Zn}_x\text{Mn}_{(1-x)}\text{Fe}_2\text{O}_4$ - type systems

Catalyst	Phenol Conv. (wt%)	<i>o</i> -cresol yield (wt%)	2,6-xyleneol yield (wt%)	Product selectivity (%)		
				Anisole	<i>o</i> -cresol	2,6-xyleneol
MnFe_2O_4	40.75	39.63	---	2.75	97.25	---
$\text{Zn}_{0.2}\text{Mn}_{0.8}\text{Fe}_2\text{O}_4$	50.03	47.56	1.38	2.17	95.06	2.75
$\text{Zn}_{0.4}\text{Mn}_{0.6}\text{Fe}_2\text{O}_4$	53.97	46.66	6.23	2.00	86.46	11.54
$\text{Zn}_{0.6}\text{Mn}_{0.4}\text{Fe}_2\text{O}_4$	58.52	43.98	13.28	2.15	75.15	22.69
$\text{Zn}_{0.8}\text{Mn}_{0.2}\text{Fe}_2\text{O}_4$	62.32	40.81	20.46	1.68	65.48	32.83
ZnFe_2O_4	61.91	41.37	19.17	2.21	66.82	30.97

Reaction temperature-350°C, MeOH/ phenol-7, TOS- 2 h and flow rate 4mL h^{-1} .

The Zn-Mn series performed enhanced activity for phenol alkylation. The concentration of anisole obtained through out the series remained less than 3%. Moreover, the formation of the secondary alkylated product, 2,6-xyleneol is enhanced with successive Zn-addition.

The substitution of zinc into the manganese ferrite increased the total acidity as evident from the NH₃-TPD profiles. This results are propped up by the dehydration activity from the cyclohexanol decomposition studies whereas the limiting concentration of the electron acceptors is reduced with increase in zinc content. The acid-base properties along with phenol conversion of Zn-Mn series are depicted in the following table (Table. 4.3.12).

Table 4.3.10. Dehydration activity, total acidity, limiting amount and phenol conversion of the system Zn_xMn_{1-x}Fe₂O₄ (x = 0, 0.2, 0.4, 0.6, 0.8 and 1).

x	Dehydration	Total Acidity (10 ⁻⁴ mmol m ⁻²)	Limiting amount (10 ⁻⁴ mmol m ⁻²)		Phenol Conversion (wt%)
	Activity (wt %) Cyclohexene		TCNQ	Chloranil	
0	91.28	16.50	10.71	2.60	40.75
0.2	92.23	13.99	10.21	2.58	50.03
0.4	93.36	14.13	10.02	2.51	53.97
0.6	94.18	14.71	9.91	2.49	58.52
0.8	95.98	15.61	9.62	2.46	62.32
1	96.91	16.42	9.37	2.43	61.91

The enhanced catalytic activity of the Zn-Mn series can be attributed to the improved total acidity possessed by the system.

Effect of time-on-stream

To establish the catalytic stability of the Zn-Mn series a set of phenol alkylation experiments were performed and noted the phenol conversion at regular intervals of 60 minutes. The reaction temperature was kept at 350°C and the methanol-to-phenol molar

ratio was maintained at 7. The results obtained are presented in the figure 4.3.8. All the systems in this series, except ZnFe_2O_4 exhibited excellent stability.

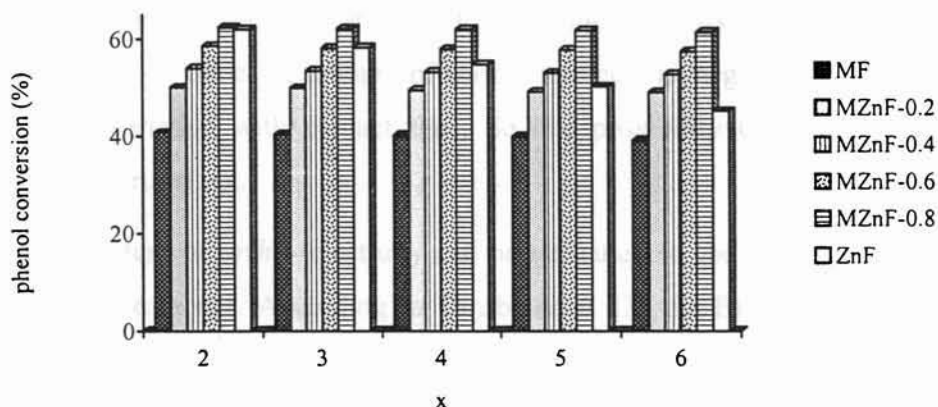


Fig. 4.3.8. Effect of time-on-stream over the system, $\text{Zn}_x\text{Mn}_{1-x}\text{Fe}_2\text{O}_4$ ($x = 0, 0.2, 0.4, 0.6, 0.8$ and 1). Reaction temperature- 350°C , MeOH/ aniline- 5, TOS- 2 h and flow rate – 4mL h^{-1} .

4.3.3 Mechanism of phenol alkylation

Alkylation of phenol with methanol is essentially an acid-base reaction. Therefore, the catalytic activity and product selectivity depend strongly on the acid-base properties of the catalysts and up to a certain extent on the reaction conditions. According to Velu and Swami [35], in the case of strong acid catalysts phenol methylation initially accelerates the formation of O-alkylated product, anisole. Anisole, then undergoes intramolecular rearrangement of methyl group to form *o*-cresol. At higher temperatures, *o*-cresol further undergoes isomerization to form *meta*- and *para*-isomers. Xylenol isomers are also produced by the consecutive methylation of cresol isomers. But, in the case of less acidic and bifunctional systems, direct C-alkylation occurs without the intervention of anisole as an intermediate [37]. Phenol dissociates to form a protonic site and a phenolate ion, which gets adsorbed on the basic and acidic sites of these catalysts, respectively. The proton site promotes methanol to produce a carbonium ion, which attacks the ortho position of the adjacently adsorbed phenolate species. Thus, in such cases methylation of phenol is more selective to ortho positions yielding *o*-cresol and 2,6-xylenol.

From the above discussions, it can be seen that manganese ferros spinels produce *ortho*-alkylated products (formation of *o*-cresol and 2,6-xyleneol, but not *meta*- or *para*-cresols and xyleneol isomers.) and the total *ortho*-selectivity always exceeded 97%. Additionally, in all the cases amount of anisole formed was negligible and did not show any marked variation with contact time. So, the possibility of anisole acting as an intermediate is ruled out.

The extent of *ortho*-selectivity can be attributed to the nature of adsorption of phenol on the catalysts. According to Tanabe *et al.* [3] the Brønsted acid sites in the catalysts interact with the aromatic ring and consequently, the phenol molecule will lie parallel to the catalyst surface. This parallel orientation of the phenol molecule is shown in the following figure (Fig. 4.3.9). Thus, all positions of the aromatic ring of the phenol molecule will become evenly accessible for the attacking group. This leads to the formation of all possible alkyl phenols resulting to poor selectivity for *ortho*-alkylation.

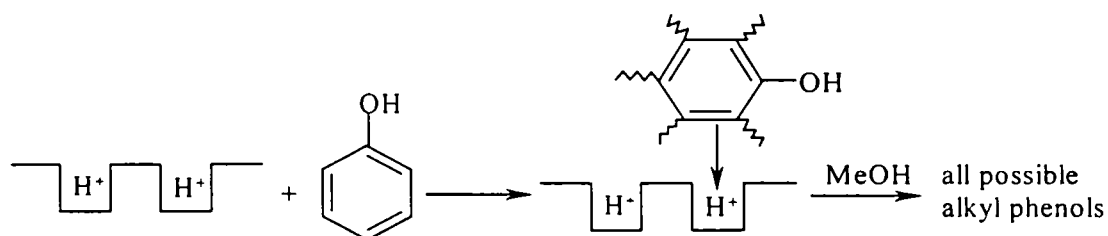


Fig.4.3.9. Parallel orientation of the aromatic ring on the catalyst surface

But, if the orientation of the aromatic ring is vertical to the catalyst surface, as suggested by Klemm *et al.* [38] and Santacesaria *et al.* [37] interaction of the aromatic ring with the strong acid sites on the catalyst surface is prevented, resulting in high *ortho*-selectivity. This is possible in bifunctional catalysts where a Lewis acid site exists beside a Lewis basic site. Phenol molecule will interact with the catalyst by giving a phenolate ion adsorbed on the acid site and a hydrogen ion bound to the basic one. Hydrogen ions thus formed should have sufficient mobility to activate the methyl groups of methanol and alkylation at the ring, in the *ortho* position occurs effectively. A

plausible scheme for the alkylation of phenol with methanol is shown in the following figure (Fig. 4.3.10).

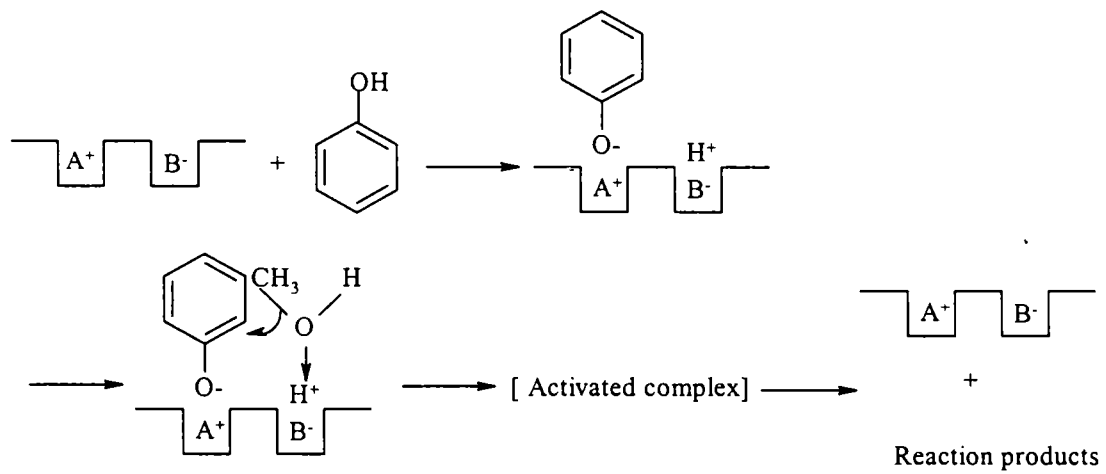


Fig. 4.3.10. Reaction mechanism of phenol alkylation using methanol

References

Section-I

- [1] C. Friedel and J. M. Crafts; *Compt. Rend.*, 84 (1877) 1392, 1450.
- [2] H. W. Kouwenhoven and H van Bekkum; (Eds., G. Ertl, H. Knozinger and J. Weitkamp) "Handbook of Heterogenous Catalysis", 5, (1997) 2358.
- [3] J. March; "Advanced Organic Chemistry", 4th Edn., Wiley, New York, 1992.
- [4] G.A. Olah; "Friedel-Crafts and Related Reactions", Vols.1-4, Wiley-Interscience, New York, London, 1963-1964.
- [5] G. A. Olah; "Friedel-Crafts Chemistry", Wiley-Interscience, New York, London, Sydney, Toronto, 1973.
- [6] G. A. Olah, G. K. S. Prakash and J. Sommer; "Superacids", Wiley-Interscience, New York, London, Brisbane, Toronto, 1985.
- [7] M. Spagnol, L. Gilbert and D. Alby; (Eds., J. R. Desmurs and S. Rattoy), "The Roots of Organic Development", Elsevier, Amsterdam, 1996, p.29.
- [8] P. R. Kurek; U.S. Patent, 5 126 489, 1992.
- [9] M. Misono; *Adv. Catal.*, 41 (1996) 113.
- [10] G. A. Olah, R. Malhotra, S.C. Narang and J.A. Olah; *Synthesis*, (1978) 672.
- [11] M. Harmer; Patent PCT, Int. Appl. WO 95 19 222 1995.
- [12] M. A. Harmer, A. J. Vega, Q.Sun, W. E. Farneth, A. Heldukum and W. F. Hoelerich; *Green Chem.*, 2 (2000) 7.
- [13] S. Gotto, M. Gotto and Y. Kimura; *React. Kinet. Catal. Lett.*, 41 (1991) 27.
- [14] A. Pandey and A. P. Singh; *Catal. Lett.*, 44 (1997) 129.
- [15] I. Neves, F. Jayat, P. Magnoux, G. Perot, F. R. Rlbelro, M. Gubelmann and M. Guisnet; *J. Mol. Catal.*, 93 (1994) 164.
- [16] I. Neves, F. Jayat, P. Magnoux, G. Perot, F.R. Rlbelro, M. Gubelmann and M. Guisnet; *J. Chem. Soc., Chem. Commun.*, (1994) 717.
- [17] R. Sreekumar and R. Padmakumar; *Synth. Commun.*, 27(5) (1997) 777.
- [18] R. Fang, G. Harvey, H. W. Kouwenhoeven and R. Prins; *Appl. Catal.*, 130 (1995) 67.
- [19] G. Harvey, A. Vogt, H. W. Kouwenhoeven and R. Prins; Proc. 9th Int. Zeol. Conf., 2 (1993) 363.
- [20] B. Chiche, A. Finiels, C. Gauthier, P. Genbeste, J. Graille and D. Pioch; *J. Org. Chem.*, 51 (1986) 2128.
- [21] A. Corma, M. J. Climent, H. Garcia and J. Primo; *J. Appl. Catal.*, 49 (1989)109.
- [22] K. Smith, Z. Zhenhua and K.G. Hodgson; *J. Mol. Catal.*, 134 (1998) 121.
- [23] U. Freese, F. Hienrich and F. Roessner; *Catal. Today*, 49 (1999) 237.

- [24] A. P. Singh, D. Bhattacharya and S. Sarama; *J. Mol. Catal.*, 102 (1995) 139.
- [25] K. Arata and M. Hino; *Appl. Catal.*, 59 (1990) 197.
- [26] P. Botella, A. Corma, J. M. Lopez-Nieto, S. Valencia and R. Jacquot; *J. Catal.*, 195 (2000) 161.
- [27] J. Bindhu, S. Sugunan and A. P. Singh; *J. Mol. Catal.*, 139 (1999) 43.
- [28] V. Paul, A. Sudalai, T. Daniel and K.V. Srinivasan; *Tetra. Lett.*, 35(16) (1994) 2602.
- [29] M. Hino and K. Arata; *J. Chem. Soc., Chem. Commun.*, (1985) 112.
- [30] K. Arata and M. Hino (Eds., M. J. Philips and M. Ternan); Proc. 9th Int. Congr. on Catalysis, Chem. Soc., Canada, 1988, 1727.
- [31] K. Arata, H. Nakamura and M. Shouji; *Appl. Catal.*, 197 (2000) 213.
- [32] D. Baudry, A. Dormond and F. Momagnac; *New J. Chem.*, 18 (1994) 871.
- [33] D. Baudry-Barbier, A. Dormond and F. Duriac-Momagnac; *C.R. Acad. Sci. Ser. Iic.*, (1998) 41.
- [34] D. Baudry-Barbier, A. Dormond and F. Duriac-Momagnac; *J. Mol. Catal.*, 149 (1999) 215.
- [35] C. de Castro, J. Primo and A. Corma; *J. Mol. Catal.*, 134 (1998) 215.
- [36] A. Cornelis, A. Gerstmans, P. Laszlo, A. Mathy and I. Zieba; *Catal. Lett.*, 6 (1990) 103.
- [37] A. Cornelis, C. Dony, P. Laazlo, K.M. Nsunda; *Tetra. Lett.*, 32 (1991) 1423, 2901, 2903.
- [38] A. Cornelis, P. Laazlo and S. Wang; *Tetra. Lett.*, 34 (1993) 3849.
- [39] C.G. Ramankutty and S. Sugunan; *Appl. Catal.*, 5608 (2001) 1.
- [40] D. E. Pearson and C. A. Buehler; *Synthesis*, (1972) 533.
- [41] F. Effenberger and G. Epple; *Angew. Chem. Int. Ed. Engl.*, 11 (1972) 300.
- [42] M. Hino and K. Arata; *Chem. Lett.*, (1978) 325.
- [43] T. Yamaguchi, A. Mitoh and K. Tanabe; *Chem. Lett.*, (1982) 1229.
- [44] T. Mukaiyama, H. Nagaoka, M. Ohshima and M. Murakami; *Chem. Lett.*, (1986) 165.
- [45] F. Effenberger and D. Steegmuller; *Chem. Ber.*, 121(1988) 117.
- [46] F. Effenberger, D. Steegmuller, V. Null and T. Ziegler; *Chem. Ber.*, 121(1988) 125.
- [47] G. A. Olah, O. Garooq, S. Morteza, F. Farnia and J. A. Olah; *J. Am. Chem. Soc.*, 110 (1988) 2560.
- [48] T. Mukaiyama, T. Ohno, T. Nishimura, S. Suda and S. Kobayashi; *Chem. Lett.*, (1991) 1059.
- [49] T. Harada, T. Ohno, S. Kobayashi and T. Mukaiyama; *Synthesis*, (1991) 1216.
- [50] K. Mikami, O. Kotera, Y. Motoyama, H. Sakaguchi, M. Marutha; *Syn. Lett.*, (1996) 171.
- [51] J. Izumi and T. Mukaiyama; *Chem. Lett.*, (1996) 739.
- [52] K. Suzuki, H. Kitagawa and T. Mukaiyama; *Bull. Chem. Soc. Jpn.*, 66 (1993) 3729.
- [53] S. Kobayashi and S. Iwamoto; *Tetra. Lett.*, 39 (1998) 4697.
- [54] S. Repichet, C. L. Roux, J. Dubac and J. Desmurs; *J. Org. Chem.*, (1998) 2743.
- [55] D. Rohan, C. Canaff, E. Romentin and M. Guismet; *J. Catal.*, 177 (1998) 298.
- [56] S. P. Ghorpade, V. S. Darshane and S. G. Dixit; *Appl. Catal.*, 166 (1998) 135.

- [57] O. Saur, M. Bensitel, A. B. M. Saad, J. C. Lavalley, C. P. Tripp and B. A. Morrow; *J. Catal.*, 99 (1986) 104.
- [58] H. van Bekkum, A. J. Hoefenagel, M. A. Vankoten, E. A. Gunnewegh, A. H. G. Vog and H. W. Kouwenhoven; *Stud. Surf. Sci. Catal.*, 83 (1994) 379
- [59] R. Fang, H. W. Kouwenhoven and R. Prins; *Stud. Surf. Sci. Catal.*, 83 (1994) 1441.
- [60] I. Neves, F. Jayat, P. Magnoux, G. Perot, F. R. Riebero, M. Gubelman and M. Guisnet; *J. Chem. Soc. Chem. Commun.*, (1994) 717.
- [61] Y. V. Subba Rao, S. J. Kulkarni, M. Subrahmanyam and A. V. Rama Rao; *J. Chem. Soc. Chem. Commun.*, (1993) 1456
- [62] A. P. Singh and D. Bhattacharya; *Catal. Lett.*, 32 (1995) 327.
- [63] D. Bhattacharya, S. Sharma and A. P. Singh; *Appl. Catal.*, 150 (1997) 53.
- [64] A. K. Pandey and A. P. Singh; *Catal. Lett.*, 44 (1997) 129.
- [65] K. Arata, K. Yabe and I. Toyoshima; *J. Catal.*, 44 (1976) 385.
- [66] D. B. Barbier, A. Dormond and F. D. Montagne; *J. Mol. Catal.*, 149 (1999) 215.
- [67] V. R. Choudhari, S. K. Jana and B. P. Kiran; *J. Catal.*, 192 (2000) 257.
- [68] G. Harvey, A. Vogt, H. W. Kouwenhoven and R. Prins; *Catalysis*, 1994, 363.

Section-II

- [1] The Merck Index , 11th edn., (Eds., S. Budavari. Merck and Co. Inc., Rahway, N J), 1989.
- [2] M. Sittig; "Handbook of Toxic and Hazardous Chemicals and Carcinogens", 2nd Edn., Noyes Publications, Park Ridge, N J, 1985.
- [3] Y. Ki Park, K. Yon Park and S. Ihl Woo; *Catal. Lett.*, 26 (1994) 169.
- [4] A. K. Bhattacharya and D. K. Nandi; *Ind. Eng. Chem. Prod. Res. Dev.*, 14 (1975) 162.
- [5] A. B. Brown and E. E. Reid; *J. Am. Chem. Soc.*, 46 (1924) 1836.
- [6] C. E. Andrews; U. S Patent, 2 073 671.
- [7] A. G. Hill, J.H. Shipp and A. J. Hill; *Ind. Eng. Chem.*, 43 (1951) 1579.
- [8] Y. Ono; *Catal. Tech.*, 1997.
- [9] A. N. Ko, C. L. Yang, W. Zhu and H. Lin; *Appl. Catal.*, 134 (1996) 53.
- [10] S. Narayanan and B. P. Prasad; *J. Chem. Soc. Chem. Commun.*, (1992) 1204.
- [11] S. Narayanan, B. P. Prasad and V. Vishwanathan; *React. Kinet. Catal. Lett*, 48 (1992) 561.
- [12] S. Narayanan, B. P. Prasad and V. Vishwanathan; *React. Kinet. Catal. Lett*, 48 (1992) 497.
- [13] S. Narayanan and B. P. Prasad; *J. Mol. Catal.*, 96 (1995) 57.
- [14] J. M. Parera, A. Gonzalez and M. A. Barral; *Ind. Eng. Chem. Prod. Res. Dev.*, 7 (1968) 259.
- [15] N. Takamiya, Y. Koinuma, K. Ando and S. Murai; *Nippon Kagakukaishi*, (1979) 1452.
- [16] M. Rusek; Proc. 9th. Int. Conf. Catal. Cagary., Vol. 3, Canada, p. 1138.
- [17] R. G. Rice and E. J. Kohn; *J. Am. Soc.*, 77 (1955) 4052.

- [18] S. Narayanan, A. Sulthana, K. Krishna, P. Meriaudeau and C. Naccache; *Catal. Lett.*, 34 (1995) 129.
- [19] S. Narayanan, A. Sulthana and K. Krishna; *React. Kinet. Catal. Lett.*, 52 (1994) 205.
- [20] S. Narayanan, A. Sulthana, P. Meriaudeau, C. Naccache, A. Auroux and C. Viomery; *Appl. Catal.*, 143 (1996) 337.
- [21] S. Narayanan and A. Sulthana; *Stud. Surf. Sci. Catal.*, 113 (1998) 667.
- [22] S. Narayanan, A. Sulthana, Quoc Thinh Le and A. Auroux; *Appl. Catal.*, 168 (1998) 373.
- [23] P. R. H. P Rao, P. Massiani and D. Bartomeuf; *Stud. Surf. Sci. Catal.*, 84 (1994) 1449.
- [24] O. V. Kikhtyanin, K.G. Ione, L.V. Malysheva and A.V. Toktarev; (Eds., T. Inni, S. Namba and T. Tsumi), Proc. Int. Symp. On Chemistry of Microporous Crystals, Tokyo, Elsevier, Amsterdam, 1991, p.319.
- [25] S. Narayanan and A. Sulthana; *Appl. Catal.*, 167 (1998) 103.
- [26] B. L. Su and D. Bartomeuf; *Appl. Catal.*, 124 (1995) 73, 81.
- [27] P. S. Singh, R. Bandyopadhyay and B. S Rao; *Appl. Catal.*, 136 (1996) 177.
- [28] S. P. Elangovan, C. Kannan, B. Arabindoo and V. Murugesan; *Appl. Catal.*, 174 (1998) 213.
- [29] S. Narayanan, K. Deshpande and B.P. Prasad; *J. Mol. Catal.*, 88 (1994) 271.
- [30] S. Narayanan and K. Deshpande; *J. Mol. Catal.*, 104 (1995) 109.
- [31] S. Narayanan and K. Deshpande; *Appl. Catal.*, 135 (1996) 125.
- [32] S. Narayanan and K. Deshpande; *Microporous Mater.*, 11 (1997) 77.
- [33] S. Narayanan and K. Deshpande; *Stud. Surf. Sci. Catal.*, 113 (1998) 773.
- [34] S. Narayanan and K. Deshpande; *Bull. Catal. Soc. Ind.*, 9 (1990) 53.
- [35] J. G. Earl and A.G. Hills, *J. Chem. Soc.*, (1947) 973.
- [36] C. Naccache and Y. Ben Tarit; *J. Catal.*, 22 (1971) 171.
- [37] P. Y. Chen, M. C. Chen, H.Y. Chu, N. S. Chang and T. K. Chuang; Proc. 7th Int. Zeolite Conf., (Eds., A. Iijima, J. Ward and Y. Murakami), Kodansha/ Elsevier, Tokyo, (1986) 739.
- [38] F. Trotta, P. Tundo and G. Moraglio; *J. Org. Chem.*, 52 (1987) 1300.
- [39] Z. H. Fu and Y. Ono; *Catal. Lett.*, 22 (1993) 277.
- [40] S. Narayanan, V. Durga Kumari and A. Sudhakar Rao; *Appl. Catal.*, 111 (1994) 133.
- [41] S. Yuvaraj and M. Palanichami; "Catalysis: Modern Trends" (Eds., N. M. Gupta and D. K. Chakrabarty) Narosa Publishing House, New Delhi, India, 1995.
- [42] K. G. Ione and O. V. Kikhtyanin; "Zeolites: Facts, Figures, Future" (Eds., P. A. Jacob and R. van Santen), *Stud. Surf. Sci. Catal.*, Vol. 49, Elsevier, Amsterdam, (1989), 1073.
- [43] P. Y. Chen, S. J. Chu, N. S. Chang and T. K. Chuang; "Zeolites: Facts, Figures, Future" (Eds., P. A. Jacob and R. Santen) *Stud. Surf. Sci. Catal.*, Vol. 49, Elsevier, Amsterdam, (1989) 1105.
- [44] S. Prasad and B. S. Rao; *J. Mol. Catal.*, 62 (1990) 12.

- [45] M. A. Aramendia, V. Borau, C. Jimenez, J. M. Marinas and F. J. Romero; *Appl. Catal.*, 183 (1999) 73.
- [46] M. A. Aramendia, V. Borau, C. Jimenez, J. M. Marinas and F. J. Romero; *Colloids and Surfaces*; 170 (2000) 51.
- [47] S. I. Woo, J. K. Lee, S. B. Hong, Y. K. Park and Y. S. Uh; *Stud. Surf. Sci. Catal.*, 49 (1989) 1905.
- [48] Y. K. Park, K.Y. Park and S. I. Woo; *Catal. Lett.*, 26 (1994) 169.
- [49] I. I. Ivanova, E.B. Pomakhina, Y.G. Kolyagin, A.I. Rebrov and M. Hunger; 12th Int. Congress on Catalysis, Granada, Spain, July 9-14, (2000) R117.
- [50] C. S. Narasimhan and C.S. Swami; *Appl. Catal.*, 2 (1982) 315
- [51] J. P. Jacobs, A. Maltha, J. G. H. Reintjes, J. Drimal, V. Ponec and H. H. Brongersma; *J. Catal.*, 147 (1994) 294.
- [52] E. J. W. Verwey and J. H. de Boer; *Rec. Trav. Chim. Phys. Bas.*, 55 (1936) 531.
- [53] A. A. Samokhvalov and A. G. Rustamov; *Sov. Phys. Solid State*, 6 (1964) 749.
- [54] A. A. Samokhvalov and A. G. Rustamov; *Sov. Phys. Solid State*, 7 (1965) 961.
- [55] S. Narayanan and K. Deshpande; *Appl. Catal.*, 199 (2000) 1.

Section III

- [1] S. Miyata; *Clays Clay Miner.*, 23 (1975) 369.
- [2] T. Kwon and T. J. Pinnavaia; *J. Mol. Catal.*, 74 (1992) 23.
- [3] K. Tanabe and T. Nishizaki; in G. C. Bond (Eds. P.B Wells and F.C Tompkins), Proc. 6th. Int. Conf. On Catalysis, Vol II, *The Chemical Soc.*, London, 1977, p.863.
- [4] N. M. Cullinane and S. J. Chard; *J. Chem. Soc.*, (1945) 821.
- [5] P. Beltrame, P. L. Beltrame, P. Carnity, A. Castelli and L. Forni; *Appl. Catal.*, 29 (1987) 327.
- [6] R. Pierantozzi and A. F. Nordqist; *Appl. Catal.*, 263 (1986) 21.
- [7] M. Chirca, M. Caldarn, N. Jonescu, E. Meroin and J. Herscovici; *Rev. Chem.*, 21 (1981) 1167.
- [8] N. M. Cullinane and W. C. Davis; Brit. Patent, 600 837 (1948).
- [9] H. L. Schlichting, G. Island, A. D. Barbapoulos and W. H. Prah; U. S. Patent, 3 426 358 (1969).
- [10] M. B. Neuworth; U.S. Patent, 2 777 881 (1957)
- [11] N. D. Limankina, E. A. Vdovtsova and A. S. Sultanov; *Uzb. Khim. Zh.*, 6 (1977) 34.
- [12] N. D. Limankina, E. A. Vdovtsova and A. S. Sultanov; *Chem. Abst.*, 89 (1976) 17640.
- [13] F. Nozaki, I. Kimura; *Bull. Chem. Soc. Japan*, 50 (1977) 614.
- [14] J. A. Sharp and R. E. Dean; Brit. Patent, 1 125 087 (1968).
- [15] S. Enamoto and M. Inone; *Am. Meeting. Catal. Soc. Japan Sendai*, (1968).
- [16] Y. Fuduka, T. Nishizaki and K. Tanabe; *Nippon Kagaku Zasshi*, (1972) 1754.

- [17] T. Kotanigawa, M. Yamamoto, K. Shimotawa and Y. Yoshida, *Bull. Chem. Soc. Japan*, 44 (1971) 1961.
- [18] M. Froitzheim, K. F. Lang, T. Rupertshain, L. Rappen and J. Turowski; U. S Patent, 3 347 936 (1967).
- [19] J. Kaspi and G. A. Olah; *J. Org. Chem.*, 43 (1978) 3142.
- [20] S. Namba, T. Yashima, Y. Itaba and N. Hara; "Studies in Surface Science and Catalysis", (Eds., B. Imelik, C. Naccache, Y. Ben Taarit, J. C. Vedrine, G. Coudurier and H. Praliaud), Vol. 5, Catalysis by Zeolites, Elsevier, Amsterdam (1980) p.105.
- [21] P. Beltrame, P. L. Beltrame, P. Carnity, A. Castelli and L. Forni; *Gazz. Chim. Ital.*, 116 (1986) 473.
- [22] S. Balsama, P. Beltrame, P. L. Beltrame, P. Carnity, L. Forni and G. Zuretti; *Appl. Catal.*, 13 (1984) 161.
- [23] P. D. Chantal, S. Kaliaguine and J. L. Grandmaison; *Appl. Catal.*, 18 (1985) 133.
- [24] M. Renaud, P. D. Chantal and S. Kaliaguine; *Can. J. Chem. Eng.*, 64 (1986) 787.
- [25] R. F. Parton, J. M. Jacobs, H. V. Ooteghem and P. A. Jacobs; (Eds., H. G. Karge and J. Weitkamp), Studies in Surface Science and Catalysis, Vol. 46, Zeolites as Catalysts, Sorbents and Detergent Builders, Elsevier, Amsterdam (1989).
- [26] N. S. Chang, C. C. Chen, S. J. Chu, P. Y. Chen and T. K. Chuang ; (Eds., H.G. Karge and J. Weitkamp), Studies in Surface Science and Catalysis, Vol. 46, Zeolites as Catalysts, Sorbents and Detergent Builders, Elsevier, Amsterdam (1989).
- [27] G. Papparatto and E. Moretti; Ital. Patent, 19727 (1983).
- [28] G. Papparatto and E. Moretti; Ital. Patent 20729 (1983).
- [29] S. Karupannasamy, K. Narayanan and C. N. Pillai; *J. Catal.*, 66 (1980) 281.
- [30] C. Benzouhanava and M. A. Al-Zihari; *Appl. Catal.*, 8 (1992) 45.
- [31] R. T. Tlietmat-Manzalji, D. B. Bianchi and G. M. Pajonk; *Appl. Catal.*, 101 (1993) 339.
- [32] M. Marcezewski, J. P. Bodibo, G. Perofand and M. Guisnet, *J. Mol. Catal.*, 50 (1989) 211.
- [33] V. V. Rao, K. V. R. Chary, V. Durgakumari and S. Narayanan; *Appl. Catal.*, 49 (1989) 165.
- [34] V. V. Rao, K. V. R. Chary, V. Durgakumari and S. Narayanan; *Appl. Catal.*, 61 (1990) 89.
- [35] S. Narayanan, V. V. Rao and V. Durgakumari; *J. Mol. Catal.*, 52 (1989) 29.
- [36] S. Velu and C. S. Swami; *Appl. Catal.*, 119 (1994) 241.
- [37] S. Velu and C. S. Swami; *Appl. Catal.*, 145 (1996) 141.
- [38] S. Santhacesaria, D. Grasso, D. Gelosa and S. Carra; *Appl. Catal.*, 64 (1990) 83.
- [39] L.H. Klemm, C. E. Klopfenstein and J. Shabtai; *J. Org. Chem.*, 35 (1970) 1069.

Oxidation Reactions

Catalytic oxidation is widely employed in the manufacture of bulk chemicals from aromatics and more recently, as an environmentally attractive method for the production of fine chemicals [1-3]. The present chapter is divided into two sections. The first section depicts the liquid-phase hydroxylation of phenol using hydrogen peroxide as the oxidant over different manganese ferrosinels and the effects of various reaction parameters on the product distribution. The vapour-phase oxidative dehydrogenation of ethylbenzene and effect of various reaction parameters for styrene production are presented in the second section.

5.1 Section I – Phenol Hydroxylation

Phenol hydroxylation is one of the industrially important reactions as the products namely catechol and hydroquinone are extensively used as photographic developers, ingredients for food and pharmaceutical applications and antioxidants [4]. This reaction has an added importance for the reduction of refractory organic pollutants such as phenol in the aqueous effluents from industries such as pharmaceutical, chemical, petrochemical etc. The heterogeneous catalytic oxidation mineralized these refractory organic compounds to CO_2 and H_2O . This technique allows a significant reduction of the temperature and necessary pressure employed by the non-catalytic oxidation techniques and thereby improving the economy of the process [5-7]. The oxidation and hydroxylation of aromatic compounds using molecular oxygen are not in common practice either in the laboratory or in the industry. Hydrogen peroxide is found to be a superior alternative as it is a good weight efficient oxidizing agent, which yields water and oxygen only on decomposition [8, 9]. In recent years, due to the tightening of the environmental regulations, diphenols from phenol hydroxylation and reduction of phenolic pollutants in waste waters using heterogeneous catalysts with hydrogen peroxide as the oxidant has become one of the promising approaches because it demands for the simple techniques and produce little environmental pollution.

A schematic representation of the various reaction pathways of phenol hydroxylation using hydrogen peroxide as the oxidant is presented below (Fig. 5.1.1).

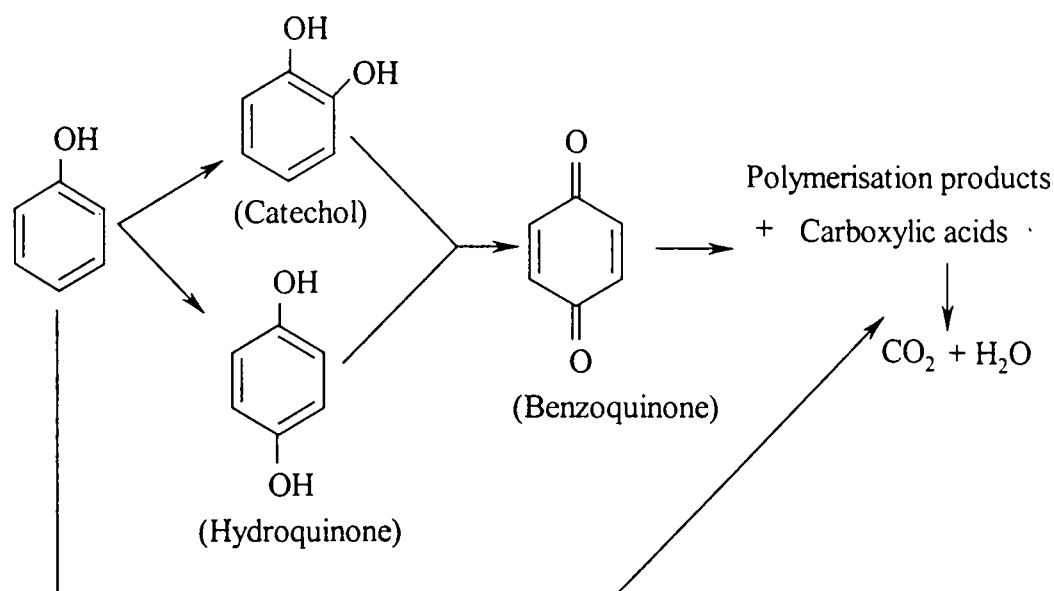


Fig. 5.1.1 Reaction scheme for phenol hydroxylation using hydrogen peroxide as the oxidant.

Since 1970, hydroxylation of phenol catalyzed by mineral acids [10-12], simple metal ions and their complexes in homogeneous liquid-phase [13-15] with hydrogen peroxide as oxidant, has been extensively studied. Although some of these showed potential catalytic activities, the disadvantages of homogeneous reactions are very distinct to prevent their wide use in phenol catalytic oxidation.

A wide range of heterogeneous catalysts have been introduced, due to their eco-friendly nature and their potential to replace the conventional homogenous systems. Pure metal oxides or supported oxides have been found to catalyze the hydroxylation of phenol viz., Fe₂O₃ [16], Co₃O₄ [17], Fe₂O₃/Al₂O₃ [18], CaO/SiO₂ [19], MoO₃ [20] V₂O₅ and colloidal TiO₂ [21], but neither the catalytic activity nor the product selectivity of these catalysts is satisfactory.

Molecular sieves such as TS-1 [22], TS-2 [23], Ti-ZSM-48 [24], Ti-β[25], TAPO-11 [26], Ti-MCM-41 [27], VS-2 [28], zirconotitanosilicates [29] were intensively studied and were found to exhibit unique catalytic activity including high activity,

minimal non-productive hydrogen peroxide decomposition and high catalyst stability [30]. These positive aspects have led to an extraordinary series of work on the use of transition metal substituted silicate zeolites as catalysts for phenol hydroxylation. Despite the obvious attractiveness of these titanium silicate zeolite as catalysts, the somewhat complicated synthesis, small pore size and low reaction rate [31] will perhaps limit their application as a popular tool for oxidation in organic chemistry. The compound, $H_xV_2Zr_2O_9 \cdot H_2O$ is found to be a novel complex oxide with two transition metals, showing many advantages compared with TS-1, such as cheaper preparation and high stability [32]. These compounds with smaller crystallite size exhibited much higher catalytic activity for phenol hydroxylation by hydrogen peroxide.

Complex oxides containing transition metals such as $La_{1.9}Sr_{0.1}CuO_{4 \pm \lambda}$ [33] and V-Zr-O [34, 35] were used for hydroxylation of phenol, however both the diphenol yield and reaction rate were low. Iron oxide nanoparticles [36] prepared by the *in situ* forced hydrolysis of Fe^{3+} ions chemisorbed at the pore walls, showed hydroxylation activity, but the active component of such catalysts was lost easily, and the phenol conversion of such catalysts was not high enough.

Heteropoly acids such as molybdovanadophosphoric acid [37] and molybdotungstophosphoric acid [38] were tried for the hydroxylation of phenol by hydrogen peroxide, but the decomposition of H_2O_2 was obvious and acetonitrile was the only solvent medium applicable.

The present part of the thesis deals with the detailed investigation of $Cr_xMn_{(1-x)}Fe_2O_4$, $Co_xMn_{(1-x)}Fe_2O_4$, $Ni_xMn_{(1-x)}Fe_2O_4$, $Cu_xMn_{(1-x)}Fe_2O_4$ and $Zn_xMn_{(1-x)}Fe_2O_4$ -type manganese ferrosphinel systems for phenol hydroxylation using hydrogen peroxide as the oxidant. The objectives are to investigate the reaction pathways and associated mechanisms and to correlate the activity with the amount of holes or cation vacancies present in the systems and composition of the catalysts. In addition, the influence of the reaction parameters such as amount of catalyst, phenol to hydrogen peroxide molar ratio, reaction temperature, pH and solvents are studied. We observed that manganese ferrites, particularly, $Cu_xMn_{(1-x)}Fe_2O_4$ were the most active series of systems for the reaction.

5.1.1 Process optimization

The liquid-phase hydroxylation of phenol using 30% H₂O₂ as the oxidant was carried out in a 50 mL round bottom flask equipped with an air condenser. The reaction mixture was stirred using a magnetic stirrer. About 0.1 g of the catalyst was taken and prior to each reaction they were activated at 500°C for 2 h. Phenol and the solvent were taken in the round bottom flask at the desired temperature. The required amount of the hydrogen peroxide was added drop wise to the reaction medium and the reaction was allowed to proceed for 30 minutes. The products were analyzed using Chemito GC chromatograph fitted with FID. The influence of various reaction parameters on phenol conversion and product selectivity is presented in the ongoing sections.

5.1.1.1 Effect of catalyst loading

The catalyst amount required for the maximum phenol conversion (%) was optimized by taking CuFe₂O₄ as the catalyst and water as the solvent. The amount of the catalyst was varied from 0.05 g to 0.30 g and all the reactions were carried out at room temperature for 30 minutes. The effect of amount of catalyst on phenol conversion and product selectivity are shown in Fig. 5.1.2.

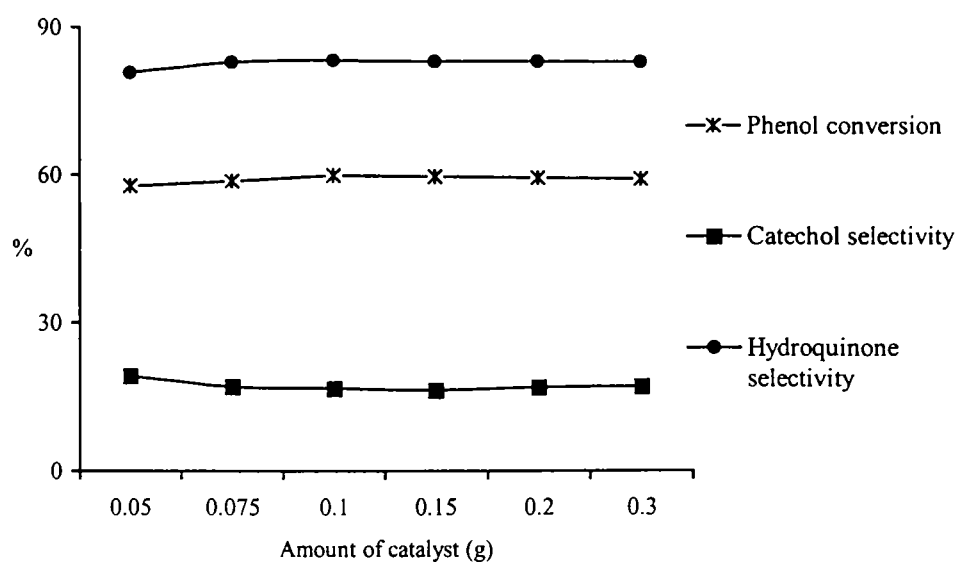


Fig. 5.1.2 Effect of catalyst loading. Catalyst- CuFe₂O₄, Reaction temperature- room temperature, H₂O₂/Phenol volume ratio-10, Reaction time-30 minutes and Solvent-water.

From the figure, it can be seen that the catalyst concentration has no influence on phenol conversion. The product selectivity remained more or less constant at any catalyst loading. According to Santos *et al.* [39], catalyst concentration has scarcely any influence on phenol conversion and at low catalyst concentrations an important contribution of the homogeneous reaction is inferred. They suggested a homogeneous mechanism for the oxidation of phenol, while the oxidation of intermediates is mainly due to the heterogeneous reaction. This is supported by the observations by Yu *et al.* over V-Zr-O complex [32] that excess of catalyst has no advantage in the phenol conversion and a large excess of catalyst reduced the yield significantly. 0.1 g of the catalyst was used for the subsequent studies of the reaction.

5.1.1.2 Effect of reaction temperature

A set of reactions was performed over CuFe_2O_4 at different temperatures for 30 minutes. The hydrogen peroxide to phenol volume ratio was kept at 5. Figure 5.1.3 shows the variation of phenol conversion and the product distribution with reaction temperature.

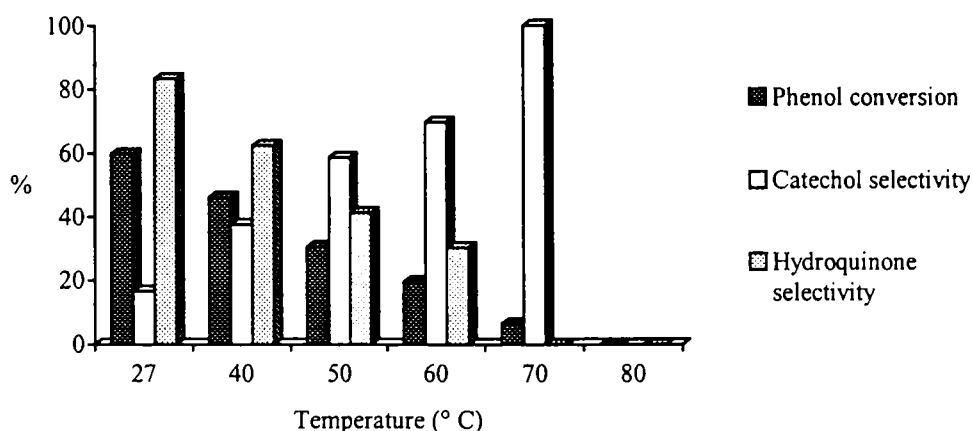


Fig. 5.1.3 Effect of reaction temperature, Catalyst- CuFe_2O_4 , amount of catalyst-0.1 g, H_2O_2 /Phenol volume ratio-5, Reaction time- 30 minutes, solvent-water.

The phenol hydroxylation reaction was observed to be exothermic and the conversion of phenol decreased with reaction temperature. That is, the lower temperature is found beneficial for higher conversion of phenol. The phenol conversion is maximum

at room temperature (59.81%) and no phenol conversion is observed beyond 70°C. The product selectivity showed a marked difference with varying temperature. The rise in temperature favoured the increase in catechol selectivity. The fact that the percentage conversion of phenol decreased with increasing temperature suggests that the activation energy for hydrogen peroxide decomposition is lower than that for the hydroxylation of phenol [32].

5.1.1.3 Effect of reaction time

The appropriate reaction time is the main assurance for a perfect reaction. For optimizing the reaction time for the phenol hydroxylation, the reaction was carried out over CuFe_2O_4 at room temperature for 60 minutes and the hydrogen peroxide to phenol volume ratio was 5. The filtrate was collected from the reaction mixture at a regular interval of 10 minutes for the GC analysis. Figure 5.1.4 illustrates the conversion of phenol and product selectivity with time.

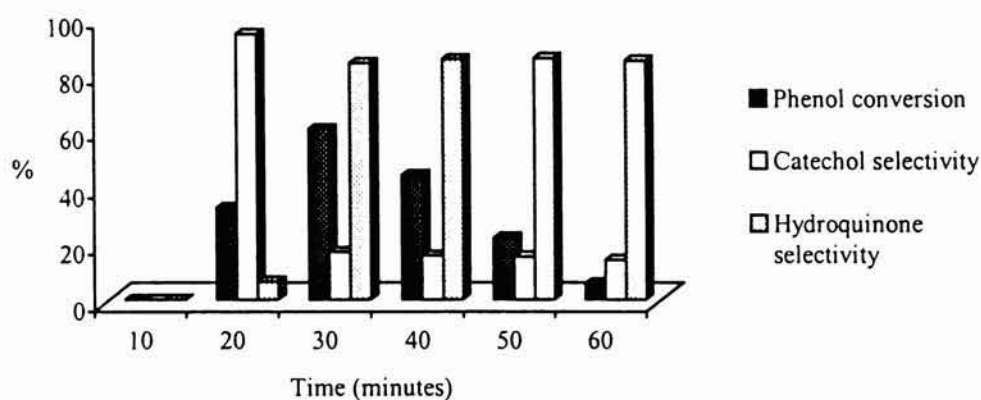


Fig. 5.1.4. Effect of reaction time, Catalyst- CuFe_2O_4 , Reaction temperature- room temperature, amount of catalyst-0.1 g, H_2O_2 /Phenol volume ratio-5, solvent-water.

In the first 10 minutes we could not observe any phenol conversion; but a sudden rise in conversion of phenol was obtained at 20 minutes, which reached the maximum at 30 minutes and then, turned to decline. Thus, extended reaction time appeared to be unfavourable for the phenol hydroxylation. In the whole process of the reaction the yield of catechol declined sharply (from 93.67% to 13.88%) and at the same time, the selectivity for hydroquinone increased remarkably. With increase in reaction time,

significant amount of the tarry products was detected in the reaction mixture, indicative of the polymerization of the reaction products, catechol and hydroquinone.

5.1.1.4 Effect of hydrogen peroxide to phenol volume ratio

Table 5.1.1 summarized the catalytic hydroxylation results under various volume ratios of H₂O₂ /phenol. All the reactions were done over CuFe₂O₄ at room temperature for 30 minutes.

Table 5.1.1 Effect of Hydrogen peroxide to phenol volume ratio on phenol hydroxylation

H ₂ O ₂ (mL)/phenol(mL) volume ratio	Phenol conversion(%)	Product selectivity (%)	
		Catechol	Hydroquinone
1	10.32	67.65	32.25
2	21.62	52.68	47.32
3	32.05	48.67	51.33
4	45.09	35.32	64.38
5	59.81	16.76	83.24
6	42.67	47.39	52.61
7	23.72	46.36	53.64
8	10.67	46.01	53.99
9		No desired products	

Catalyst- CuFe₂O₄, Reaction temperature- room temperature, amount of catalyst-0.1 g, Reaction time- 30 minutes, solvent-water.

The H₂O₂ to phenol volume ratio was varied from 1 to 9. It is observed that phenol conversion increased with increase in hydrogen peroxide to phenol volume ratio, reached a maximum conversion and then declined. A large excess of 30% hydrogen peroxide reduced the product yields very significantly. The probable reason for the lower yield is that a large excess of hydrogen peroxide enhances its decomposition rather than the hydroxylation of phenol. Catechol and hydroquinone were the products observed at all volume ratios. The formation of secondary oxidation product, benzoquinone was not observed at higher amount of hydrogen peroxide, but at this condition, increased formation of tarry products and evolution of CO₂ were detected. The tarry products are

due to the deep oxidation of the reaction products with large excess of hydrogen peroxide. The proportion of the products seemed to be sensitive to the variation in H₂O₂ to phenol volume ratio. At lower H₂O₂/ phenol volume ratios catechol was detected with greater selectivity.

5.1.1.5 Effect of pH of the reaction medium

The pH values used for this study- 3, 7 and 10, were attained by adding dilute H₂SO₄, H₂O and Na₂CO₃, respectively. The reactions were performed at room temperature for 30 minutes and the results obtained are presented in Fig. 5.1.5.

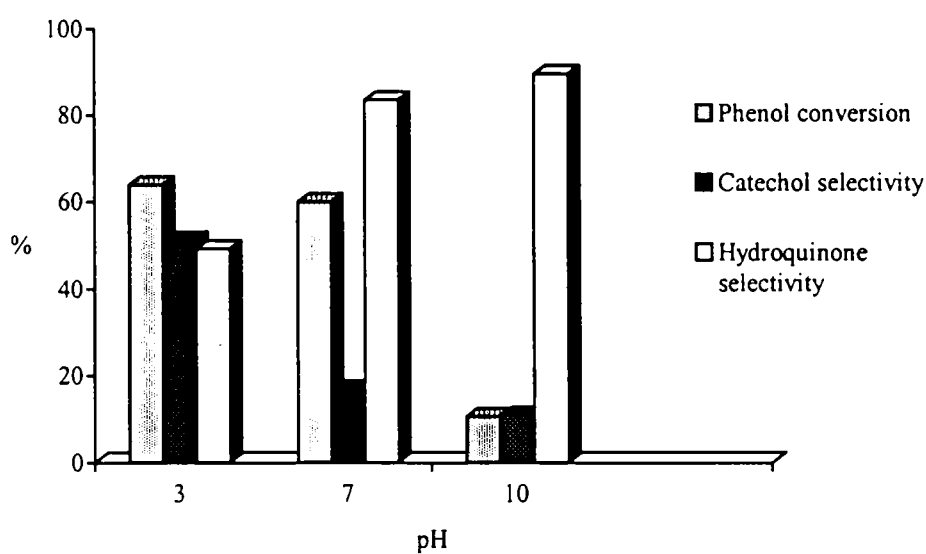


Fig. 5.1.5. Effect of pH of the reaction medium, Catalyst- CuFe₂O₄, Reaction temperature- room temperature, amount of catalyst-0.1 g, H₂O₂/Phenol volume ratio-5, solvent-water and reaction time- 30 minutes.

The phenol conversion was found to be greater for acidic rather than for basic media. But the desired product selectivity was very low in acidic medium. Though the basic media showed greater selectivity for hydroquinone, phenol conversion reduced tremendously. At neutral reaction medium (pH-7), both the conversion of phenol and selectivity for the hydroquinone were appreciable. Thus, neither the acidic nor the basic environment is good for phenol hydroxylation. A neutral reaction medium is a better choice for phenol hydroxylation.

5.1.1.6 Effect of solvent

Table 5.1.2 presents the catalytic data for phenol hydroxylation over CuFe_2O_4 catalyst with different solvents such as water, acetonitrile, methanol, 1,4-dioxane and acetone. All the experiments were performed at room temperature for 30 minutes.

Table 5.1.2. Effect of solvent.

Solvent	Phenol Conversion (%)	Product distribution (%)	
		Catechol	Hydroquinone
Water	59.81	16.76	83.24
Acetonitrile	44.84	59.76	40.54
1,2-dioxane	18.78	67.52	32.48
Methanol	5.76	---	100
Acetone	No desired products		

Catalyst- CuFe_2O_4 , Reaction temperature- room temperature, amount of catalyst-0.1 g, Reaction time- 30 minutes, H_2O_2 /Phenol volume ratio-5.

When acetone was chosen as the solvent, the catalytic reaction did not take place while with methanol as a solvent, the catalytic reaction gave low conversion with cent percent selectivity to hydroquinone. The phenol conversion with 1,2-dioxane was three times greater than that with methanol as the solvent. It can be seen that acetonitrile is a good solvent favourable for improving phenol conversion. The best conversion was observed with water as the solvent. The reduction of catalytic activity with other solvents is probably due to the adsorption of these solvents on the active sites of the catalyst. Since a high conversion of phenol was observed with water as the solvent, this technique can be used for the reduction of phenolic pollutants in aqueous effluents from industries.

5.1.2 Comparison of catalyst composition

Under the optimized reaction conditions the phenol hydroxylation was done over the five series of manganese ferros spinels. The catalytic activity is correlated with the number of holes or cation vacancies and their mobility determined from the Hall effect measurements.

(a) Cr_xMn_(1-x)Fe₂O₄- type systems (x = 0, 0.2, 0.4, 0.6, 0.8 and 1.0)

The data for the phenol hydroxylation carried out over Cr-Mn series is presented in Table 5.1.3.

Table 5.1.3 Hydroxylation of phenol over Cr_xMn_(1-x)Fe₂O₄ (x = 0, 0.2, 0.4, 0.6, 0.8 and 1.0)- type systems

Catalyst	Phenol Conversion (%)	Product selectivity (%)	
		Catechol	Hydroquinone
MnFe ₂ O ₄	6.03	51.57	48.43
Cr _{0.2} Mn _{0.8} Fe ₂ O ₄	17.57	55.39	44.61
Cr _{0.4} Mn _{0.6} Fe ₂ O ₄	18.62	52.46	47.54
Cr _{0.6} Mn _{0.4} Fe ₂ O ₄	22.73	50.06	49.94
Cr _{0.8} Mn _{0.2} Fe ₂ O ₄	24.69	49.18	50.82
CrFe ₂ O ₄	25.01	49.54	50.45

Reaction temperature- room temperature, amount of catalyst-0.1 g, Reaction time- 30 minutes, H₂O₂/Phenol volume ratio-5.

The incorporation of the Cr³⁺ ions in the octahedral sites of the manganese ferrosinels enhanced the catalytic activity. But a considerable amount of unidentified polymerization products were formed in the reaction mixture catalyzed by chromium incorporated systems. This series of catalysts mainly produced catechol and hydroquinone as the reaction products and no benzoquinones were detected. In the case of MnFe₂O₄, considerable evolution of CO₂ was noted. This can be either due to the transformation of reaction products to CO₂ or by the direct complete oxidation of phenol.

The type, amount and mobility of the carriers present in the systems along with the phenol conversion of Cr-Mn series are presented in the following table (Table 5.1.4). It can be seen that the type of carriers were changed from electrons to holes by the incorporation of chromium ions into the manganese ferrosinels. The amount and mobility of the charge carriers were also improved with chromium content. The change in the catalytic activity with increase in the chromium content can be accounted for in terms of the enhanced cation vacancies (holes), resulting in the increased formation of diphenol product.

Table 5.1.4. Type, amount and mobility of the charge carriers and phenol conversion of the system, $\text{Cr}_x\text{Mn}_{1-x}\text{Fe}_2\text{O}_4$ ($x = 0, 0.2, 0.4, 0.6, 0.8$ and 1)

Catalyst	Type of carriers	Amount of holes/ electrons (cm^{-3})	Mobility of the carriers ($\text{cm}^2/\text{V s}$)	Phenol Conversion (%)
MnFe_2O_4	Electrons	2.60×10^{13}	- 84.20	6.03
$\text{Cr}_{0.2}\text{Mn}_{0.8}\text{Fe}_2\text{O}_4$	Holes	2.07×10^9	+ 0.58	13.57
$\text{Cr}_{0.4}\text{Mn}_{0.6}\text{Fe}_2\text{O}_4$	Holes	2.79×10^9	+ 0.67	17.62
$\text{Cr}_{0.6}\text{Mn}_{0.4}\text{Fe}_2\text{O}_4$	Holes	3.76×10^9	+ 0.76	20.73
$\text{Cr}_{0.8}\text{Mn}_{0.2}\text{Fe}_2\text{O}_4$	Holes	4.37×10^9	+ 0.84	22.69
CrFe_2O_4	Holes	4.52×10^9	+ 0.93	23.01

(b) $\text{Co}_x\text{Mn}_{(1-x)}\text{Fe}_2\text{O}_4$ - type systems ($x = 0, 0.2, 0.4, 0.6, 0.8$ and 1.0)

Table 5.1.5 reports the catalytic activity of Co-Mn series in phenol hydroxylation at room temperature with water as solvent.

Table 5.1.5. Hydroxylation of phenol over $\text{Co}_x\text{Mn}_{(1-x)}\text{Fe}_2\text{O}_4$ ($x = 0, 0.2, 0.4, 0.6, 0.8$ and 1.0)- type systems

Catalyst	Phenol Conversion (%)	Product selectivity (%)	
		Catechol	Hydroquinone
MnFe_2O_4	6.03	51.57	48.43
$\text{Co}_{0.2}\text{Mn}_{0.8}\text{Fe}_2\text{O}_4$	23.68	52.05	47.95
$\text{Co}_{0.4}\text{Mn}_{0.6}\text{Fe}_2\text{O}_4$	37.69	56.22	43.76
$\text{Co}_{0.6}\text{Mn}_{0.4}\text{Fe}_2\text{O}_4$	42.69	59.72	40.28
$\text{Co}_{0.8}\text{Mn}_{0.2}\text{Fe}_2\text{O}_4$	46.17	63.76	36.24
CoFe_2O_4	47.93	64.18	35.82

Reaction temperature- room temperature, amount of catalyst-0.1 g, Reaction time- 30 minutes, H_2O_2 /Phenol volume ratio-5.

The progressive incorporation of Co into the manganese ferros spinels increased the catalytic activity in phenol hydroxylation. Product analysis showed that Co-Mn

series catalyzes the formation of diphenols such as catechol and hydroquinone with high selectivity. Deep oxidation products such as quinones, carboxylic acids, tarry products and evolution of CO₂ were not observed.

Table 5.1.6 presents the type, amount and mobility of the carriers present in the systems along with the phenol conversion of Co-Mn series.

Table 5.1.6. Type, amount and mobility of the carriers and phenol conversion of the system Co_xMn_{1-x}Fe₂O₄ (x = 0, 0.2, 0.4, 0.6, 0.8 and 1)

Catalyst	Type of carriers	Amount of holes/ electrons (cm ⁻³)	Mobility of the carriers (cm ² /V s)	Phenol Conversion (%)
MnFe ₂ O ₄	Electrons	2.60 x 10 ¹³	- 84.20	6.03
Co _{0.2} Mn _{0.8} Fe ₂ O ₄	Holes	1.03 x 10 ¹²	+ 2.58	23.68
Co _{0.4} Mn _{0.6} Fe ₂ O ₄	Holes	6.83 x 10 ¹²	+ 3.07	37.69
Co _{0.6} Mn _{0.4} Fe ₂ O ₄	Holes	12.37 x 10 ¹²	+ 3.36	42.69
Co _{0.8} Mn _{0.2} Fe ₂ O ₄	Holes	18.32 x 10 ¹²	+ 3.64	46.17
CoFe ₂ O ₄	Holes	28.57 x 10 ¹²	+ 3.97	47.93

The type of charge carriers changes from electrons to holes by the progressive addition of Co into the octahedral sites of the manganese ferros spinels. Also, the mobility and the amount of the carriers improved radically by the addition of Co. The aforementioned factors play decisive role in enhancing the catalytic activity of the Co-Mn series for phenol hydroxylation.

(c) Ni_xMn_(1-x)Fe₂O₄- type systems (x = 0, 0.2, 0.4, 0.6, 0.8 and 1.0)

The percentage conversion of phenol and product selectivity for phenol hydroxylation done over Ni-Mn series are presented in Table 5.1.7.

The data in the table clearly reveal that the incorporation of Ni²⁺ ions into the octahedral positions of the manganese ferros spinel improve the catalytic activity fairly to yield diphenols with high selectivity. Only a negligible amount of the tarry products were detected. No quinones and carboxylic acids were found, but a considerable evolution of CO₂ was noted.

Table 5.1.7. Hydroxylation of phenol over $Ni_xMn_{(1-x)}Fe_2O_4$ ($x = 0, 0.2, 0.4, 0.6, 0.8$ and 1.0)- type systems

Catalyst	Phenol Conversion (%)	Product selectivity (%)	
		Catechol	Hydroquinone
MnFe ₂ O ₄	6.03	51.57	48.43
Ni _{0.2} Mn _{0.8} Fe ₂ O ₄	6.76	57.16	42.84
Ni _{0.4} Mn _{0.6} Fe ₂ O ₄	16.32	60.37	39.63
Ni _{0.6} Mn _{0.4} Fe ₂ O ₄	22.72	62.71	37.29
Ni _{0.8} Mn _{0.2} Fe ₂ O ₄	25.18	63.76	36.09
NiFe ₂ O ₄	25.72	64.81	35.19

Reaction temperature- room temperature, amount of catalyst-0.1 g, Reaction time- 30 minutes, H₂O₂/Phenol volume ratio-5.

The characteristics of the charge carriers along with phenol conversion of Ni-Mn series are depicted in Table 5.1.8.

Table 5.1.8. Type, amount and mobility of the carriers and phenol conversion of the system $Ni_xMn_{1-x}Fe_2O_4$ ($x = 0, 0.2, 0.4, 0.6, 0.8$ and 1)

Catalyst	Type of carriers	Amount of holes/ electrons (cm ⁻³)	Mobility of the carriers (cm ² /V s)	Phenol Conversion (%)
MnFe ₂ O ₄	Electrons	2.60 x 10 ¹³	- 84.20	6.03
Ni _{0.2} Mn _{0.8} Fe ₂ O ₄	Holes	0.03 x 10 ¹⁰	+ 1.85	6.76
Ni _{0.4} Mn _{0.6} Fe ₂ O ₄	Holes	4.23 x 10 ¹⁰	+ 2.31	16.32
Ni _{0.6} Mn _{0.4} Fe ₂ O ₄	Holes	8.37 x 10 ¹⁰	+ 2.66	22.72
Ni _{0.8} Mn _{0.2} Fe ₂ O ₄	Holes	11.63 x 10 ¹⁰	+ 2.81	25.18
NiFe ₂ O ₄	Holes	14.07 x 10 ¹⁰	+ 3.12	25.72

Similar to the previous systems, the charge carriers are shifted from electrons to holes by the successive incorporation of Ni²⁺ into the octahedral sites of pure manganese ferrite. The number of holes and their mobility in the catalyst systems were appreciable and these are the decisive factors enhancing the catalytic activity of this series.

(d) $\text{Cu}_x\text{Mn}_{(1-x)}\text{Fe}_2\text{O}_4$ - type systems ($x = 0, 0.2, 0.4, 0.6, 0.8$ and 1.0)

The percentage of phenol conversion and product selectivity for phenol conversion carried out over Cu-Mn series is shown in Tale 5.1.9.

Table 5.1.9. Hydroxylation of phenol over $\text{Cu}_x\text{Mn}_{(1-x)}\text{Fe}_2\text{O}_4$ ($x = 0, 0.2, 0.4, 0.6, 0.8$ and 1.0)- type systems

Catalyst	Phenol Conversion (%)	Product selectivity (%)	
		Catechol	Hydroquinone
MnFe_2O_4	6.03	51.57	48.43
$\text{Cu}_{0.2}\text{Mn}_{0.8}\text{Fe}_2\text{O}_4$	25.66	47.35	52.35
$\text{Cu}_{0.4}\text{Mn}_{0.6}\text{Fe}_2\text{O}_4$	36.37	44.30	55.70
$\text{Cu}_{0.6}\text{Mn}_{0.4}\text{Fe}_2\text{O}_4$	47.57	33.63	66.37
$\text{Cu}_{0.8}\text{Mn}_{0.2}\text{Fe}_2\text{O}_4$	54.79	22.54	77.46
CuFe_2O_4	59.81	16.76	83.24

Reaction temperature- room temperature, amount of catalyst-0.1 g, Reaction time- 30 minutes, H_2O_2 /Phenol volume ratio-5.

It can be seen from the above table that the step-wise increment in Cu-content proportionally increased the phenol conversion and the maximum conversion was obtained for CuFe_2O_4 . Unlike other systems, the increase in Cu content enhanced the selectivity for hydroquinone. No quinones, carboxylic acids and tarry products were detected and only a negligible evolution of CO_2 was noted.

Most of the catalysts tested for the catalytic oxidation in aqueous phase have been based on copper oxide with different supports [40-43]. It has been found that the catalysts which contain copper as the active element exhibit higher ability for accelerating the catalytic oxidation of phenol [44, 45].

Table 5.1.10 presents the type, amount and mobility of the charge carriers present in the Cu-Mn series along with phenol conversion.

Table 5.1.10. Type, amount and mobility of the carriers and phenol conversion of the system $\text{Cu}_x\text{Mn}_{1-x}\text{Fe}_2\text{O}_4$ ($x = 0, 0.2, 0.4, 0.6, 0.8$ and 1).

Catalyst	Type of carriers	Amount of holes/ electrons (cm^{-3})	Mobility of the carriers ($\text{cm}^2/\text{V s}$)	Phenol Conversion (%)
MnFe_2O_4	Electrons	2.60×10^{13}	- 84.20	6.03
$\text{Cu}_{0.2}\text{Mn}_{0.8}\text{Fe}_2\text{O}_4$	Holes	0.07×10^{13}	+ 1.38	25.66
$\text{Cu}_{0.4}\text{Mn}_{0.6}\text{Fe}_2\text{O}_4$	Holes	1.18×10^{13}	+ 1.79	36.37
$\text{Cu}_{0.6}\text{Mn}_{0.4}\text{Fe}_2\text{O}_4$	Holes	3.78×10^{13}	+ 1.86	47.57
$\text{Cu}_{0.8}\text{Mn}_{0.2}\text{Fe}_2\text{O}_4$	Holes	9.72×10^{13}	+ 1.94	54.79
CuFe_2O_4	Holes	13.76×10^{13}	+ 2.12	59.81

The Cu-incorporated systems have holes as the charge carriers and their number and mobility in the systems are appreciable. These characteristics of the Cu added systems account for their high catalytic activity towards phenol hydroxylation.

(e) $\text{Zn}_x\text{Mn}_{(1-x)}\text{Fe}_2\text{O}_4$ - type systems ($x = 0, 0.2, 0.4, 0.6, 0.8$ and 1.0)

The data obtained for the hydroxylation of phenol over Zn-Mn series are presented in the Table 5.1.11.

Table 5.1.11. Hydroxylation of phenol over $\text{Zn}_x\text{Mn}_{(1-x)}\text{Fe}_2\text{O}_4$ ($x = 0, 0.2, 0.4, 0.6, 0.8$ and 1.0)- type systems

Catalyst	Phenol Conversion (%)	Product selectivity (%)	
		Catechol	Hydroquinone
MnFe_2O_4	6.03	51.57	48.43
$\text{Zn}_{0.2}\text{Mn}_{0.8}\text{Fe}_2\text{O}_4$	20.76	52.73	47.26
$\text{Zn}_{0.4}\text{Mn}_{0.6}\text{Fe}_2\text{O}_4$	36.72	55.90	44.08
$\text{Zn}_{0.6}\text{Mn}_{0.4}\text{Fe}_2\text{O}_4$	39.56	58.28	41.70
$\text{Zn}_{0.8}\text{Mn}_{0.2}\text{Fe}_2\text{O}_4$	42.07	59.70	40.28
ZnFe_2O_4	43.93	64.33	35.67

Reaction temperature- room temperature, amount of catalyst-0.1 g, Reaction time- 30 minutes, H_2O_2 /Phenol volume ratio-5.

Phenol hydroxylation over Zn-added manganese ferros spinels produced diphenols such as catechol and hydroquinone with high selectivity. Benzoquinones and carboxylic acids were not observed. But, a negligible amount of unidentified tarry products along with evolution of CO₂ were noted.

Table 5.1.12 illustrates the characteristics of charge carriers possessed by the Zn-Mn series.

Table 5.1.12. Type, amount and mobility of the carriers and phenol conversion of the system Zn_xMn_{1-x}Fe₂O₄ (x = 0, 0.2, 0.4, 0.6, 0.8 and 1).

Catalyst	Type of carriers	Amount of holes/ electrons (cm ⁻³)	Mobility of the carriers (cm ² /V s)	Phenol Conversion (%)
MnFe ₂ O ₄	Electrons	2.60 x 10 ¹³	- 84.20	6.03
Zn _{0.2} Mn _{0.8} Fe ₂ O ₄	Holes	0.12 x 10 ¹¹	+ 2.18	20.76
Zn _{0.4} Mn _{0.6} Fe ₂ O ₄	Holes	1.01 x 10 ¹¹	+ 2.99	36.72
Zn _{0.6} Mn _{0.4} Fe ₂ O ₄	Holes	4.66 x 10 ¹¹	+ 3.16	39.56
Zn _{0.8} Mn _{0.2} Fe ₂ O ₄	Holes	10.52 x 10 ¹¹	+ 3.34	42.07
ZnFe ₂ O ₄	Holes	15.18 x 10 ¹¹	+ 3.62	43.93

The enhanced amount of holes and their appreciable mobility in the catalyst systems are the decisive factors which determine the improved the catalytic activity in phenol hydroxylation of Zn-Mn series.

5.1.3 Mechanism of phenol hydroxylation

Several mechanisms have been proposed for hydroxylation of phenol over solid catalysts. Wilkenhoner *et al.* [48] have carried out phenol hydroxylation over titanosilicates and proposed that hydrogen peroxide is the best oxidant for the reaction and the terminal OH of the titanium hydroperoxo group is the electrophile that attacks the aromatic ring. According to them, solvents have a profound influence in determining the reaction product. The major product formed on the surface is solvent dependent; catechol is preferred in acetone and hydroquinone in protic solvents. Especially in water

as a solvent, a significant part of phenol conversion is due to external surface activity, while in the pores of the titanosilicates, hydroquinone is clearly the preferred product.

Sadana *et al.* [41] proposed a heterogeneous-homogeneous free-radical reaction mechanism for oxidation of phenol over copper oxides which was supported by Lui *et al.* for the hydroxylation of phenol over the complex oxide $\text{La}_{1.9}\text{Sr}_{0.1}\text{CuO}_{4\pm\lambda}$ [33]. Initially Mayer *et al.* suggested this heterogeneous-homogenous free-radical reaction mechanism in liquid-phase oxidations over solid catalysts [46]. In this type of reactions, free radicals are formed on the surface of the solid catalysts and undergo propagation and termination in solution. Xiong *et al.* [47] suggested two ways for the generation of free radicals on the catalyst surface; (1) the catalyst accelerates the decomposition of hydrogen peroxide into radicals or (2) the catalyst activates the phenol molecules directly and facilitates the formation of phenoxy radicals. In the first case, the formation of OH radicals from hydrogen peroxide over the catalyst surface is the initiation step of the reaction, and the propagation of the reaction chain occurs in the solution. But in the second case, the phenoxy radicals are formed from the phenol molecule over the catalyst surface via hydrogen abstraction in the initiation step of the reaction.

From the aforementioned sections, it can be inferred that a free radical mechanism is operating in phenol hydroxylation over the different manganese ferrite catalysts. It is also observed from the results on the comparison of spinel catalysts that the catalytic activity in phenol hydroxylation improved proportionally with increase in the amount of the holes or cation vacancies (\square) in the system. These cation vacancies can abstract proton from the phenol molecule forming phenoxy radicals on the catalyst surface. This is the initiation step of the reaction which is taking place over the catalyst surface. The phenoxy radicals formed undergo propagation step of the reaction chain in the solution. It is assumed that the formation of hydroquinones proceeds in the same way as that of catechol. A plausible mechanism for phenol hydroxylation with hydrogen peroxide as the oxidant over manganese ferros spinels is depicted in the Fig. 5.1.6.

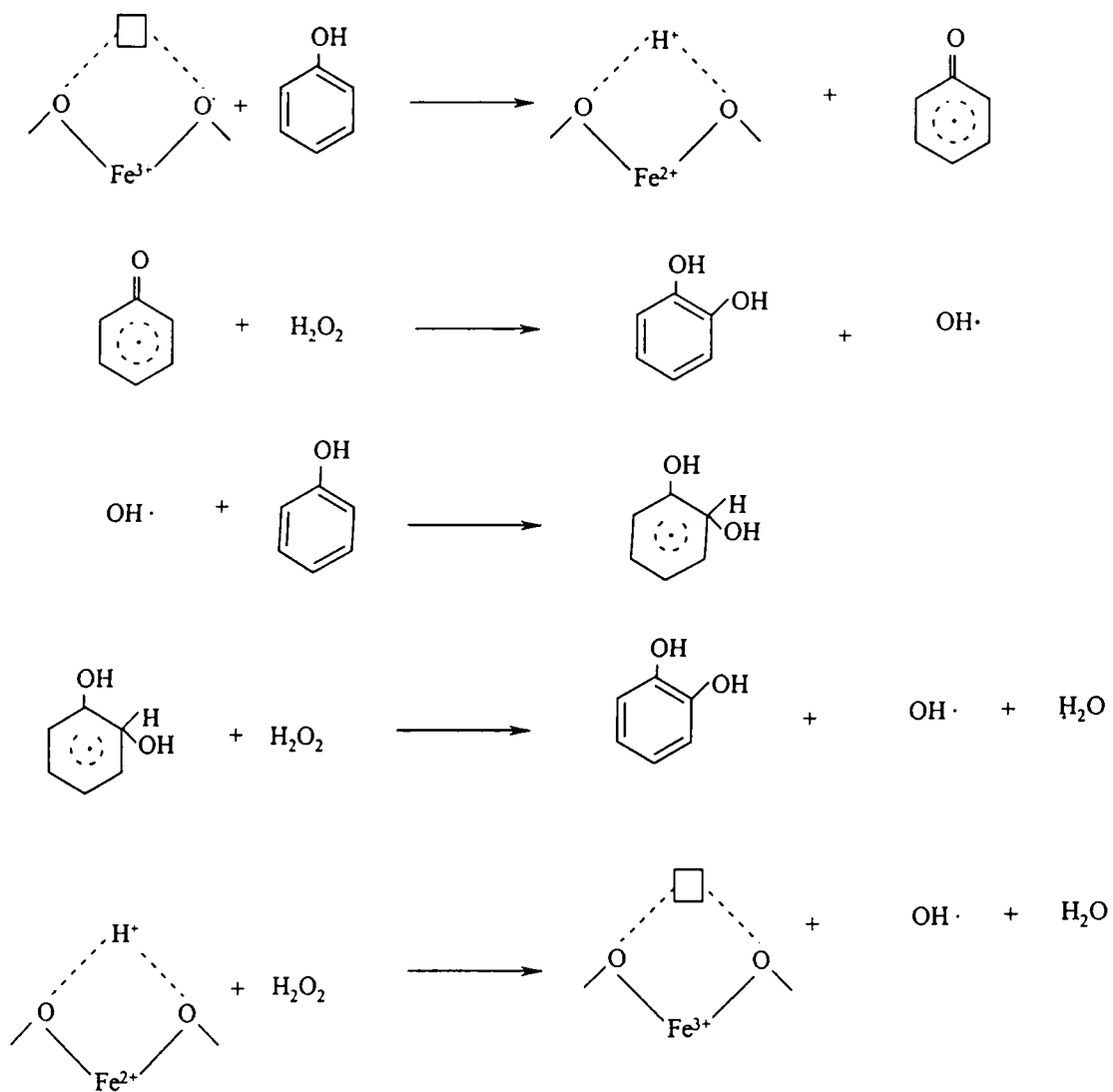


Fig. 5.1.6. A plausible mechanism for phenol hydroxylation with hydrogen peroxide as the oxidant over manganese ferrosphenels.

The intermediates formed in the propagation step of the reaction chain undergoes side reactions (presented in Fig.5.1.7).

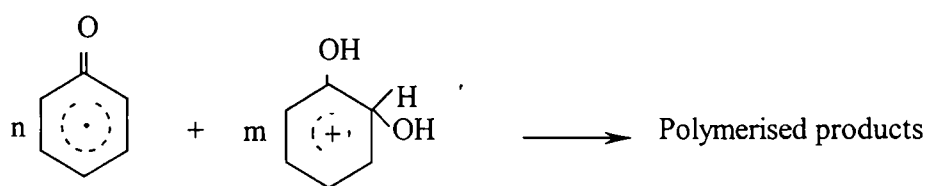


Fig. 5.1.7. A plausible side reaction during phenol hydroxylation.

The cation vacancies present in the catalyst systems are electron rich and make the surrounding oxygen ions more basic [47]. These basic oxygens can abstract protons from the adsorbed diphenol radical ions to balance the excess charge. This enhances the formation of the diphenol product and lowers the concentration of diphenol radical ion in liquid-phase. Thus, the side reaction shown in Fig. 5.1.7 leading to polymerized products is reduced and the diphenol selectivity is enhanced.

5.2 Section II - Oxidative Dehydrogenation of Ethylbenzene

Styrene is one of the fundamental materials used to obtain synthetic rubbers and numerous thermoplastics. The monomer is produced by the catalytic dehydrogenation of ethylbenzene [1, 2]. The industrial process for dehydrogenation of ethylbenzene to styrene employs a promoted iron oxide catalyst [2, 3]. This direct dehydrogenation is an endothermic reaction and is limited by equilibrium, high reactor temperatures are required and also the typical conversions are low. For these reasons, there has been a great deal of interest in oxidative dehydrogenation methods [4-11]. The formation of water as a byproduct of the oxidation process makes the process exothermic and theoretically enables the complete conversion at much lower temperatures.

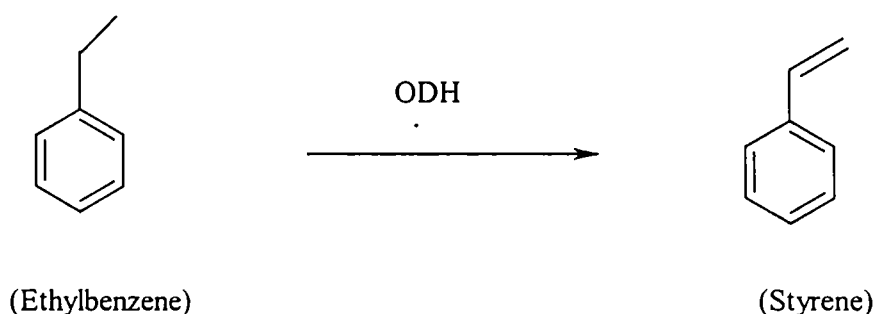


Fig. 5.2.1. Oxidative dehydrogenation of ethylbenzene to styrene.

For this reaction, the economically preferred oxidant is air if high selectivity can be maintained. Various promoters like primarily halides and sulphur compounds were tried [12, 13]. Though these provided high conversions and selectivities, the severe problems are arised in terms of corrosion, recovery, recycle of the catalysts and removal of the impurities from the reaction product. So, these have not been extended into commercial processes.

In oxydehydrogenation, the formation of carbon oxides is often a side reaction. The process economy rapidly deteriorates when ethylbenzene is extensively oxidized to carbon oxides. The formation of carbon oxides requires large quantities of oxygen, which limits the conversion to styrene. Moreover, formation of carbon oxides is extremely exothermic. Therefore the catalyst should be very selective in the minimum

production of carbon oxides and reasonably active in order to limit the reactor size. Too much activity can cause problems with heat transfer and runaway reaction. Thus most of the work on ethylbenzene has been devoted to the selection of suitable catalysts and appropriate reaction conditions for improved styrene yields and selectivities [14].

Catalysts based on phosphates of nickel-zirconium, aluminium, cerium and calcium have been reported as active catalysts in oxydehydrogenation reactions [15, 16]. Emig and Hofmann investigated the catalytic properties of zirconium phosphate, concluding that it acts as a carrier for the formation of an active coke, which is the true catalyst for the selective formation of styrene [8]. Vrieland [9] reported a variety of metal phosphate catalysts which are very active and selective in the oxidative dehydrogenation of ethylbenzene and suggested that the actual catalytic surface is a carbonaceous layer formed on the surface of the pyrophosphates. The mixed metal phosphates such as Zr-Sn and Sn-Ge systems display improved catalytic performances with respect to the corresponding single metal phosphates [17-19].

Alumina, a typical catalyst for acid-base reactions, has been reported [20-23] to be an active catalyst for oxidative dehydrogenation of ethylbenzene. This activity for the formation of styrene from ethylbenzene and oxygen was interpreted on the basis of a two center mechanism involving adjacent electron-acceptor and electron-donor sites [24, 25]. Fiedrow *et al.* [26, 27] observed that the high activity of alumina is achieved when treated with mineral acids. γ -alumina when modified by introducing iron oxide and chromia showed high positive effect on its activity in the hydrogenation of ethylbenzene [28].

In order to promote rare earth oxides as catalysts for the oxidative dehydrogenation of ethylbenzene, Kim *et al.* studied the reaction over molybdena-alumina promoted with lanthana, ceria, praseodymia and neodymia [29]. Of the four lanthanides tested, praseodymia showed the highest promoting effect with respect to both conversion and selectivity. Rare earth-promoted sulphated tin oxide displays a better oxidation activity in the oxidative dehydrogenation of ethylbenzene to styrene compared to non-sulphated analogues and sulphated tin oxide [30].

This section presents the exhaustive investigation on vapour-phase oxidative dehydrogenation of ethylbenzene over different series of manganese ferros spinels. It was observed that the catalytic performance of the manganese ferros spinel systems for the oxidative dehydrogenation of ethylbenzene was fairly good. Both ethylbenzene conversion and styrene selectivity were maximum for $\text{Co}_{0.8}\text{Mn}_{0.4}\text{Fe}_2\text{O}_4$. In all cases, some amount of benzene, toluene and carbon oxides were detected as by-products. The detailed representation of process optimization by studying the effect of reaction temperature, flow rate and air flow rate are also included in this section.

5.2.1 Process optimization

The reactions were performed in a vapour-phase down-flow silica reactor kept in a cylindrical double walled furnace mounted vertically. 0.5 g of the catalysts activated at 500°C for 2 h was placed in the middle of the reactor. A soap bubble meter was used to regulate the flow of air. A 20 ml of air/minute along with ethylbenzene was passed through the reactor in the temperature range $400\text{--}550^\circ\text{C}$. The products were analysed by gas chromatography (Chemito GC 8610, flame ionization detector, FFAP column, 2 m length). A blank run was carried out at 500°C with no catalyst in the reactor indicating negligible thermal reaction.

5.2.1.1 Effect of air flow rate

The dehydrogenation of ethylbenzene to styrene over oxide catalysts may take place either in the presence or absence of oxygen. In the absence of oxygen, lattice oxygen directly participates in the reaction resulting in the bulk reduction of the catalyst [31, 32]. A series of experiments were conducted in the absence of oxygen over $\text{Co}_{0.8}\text{Mn}_{0.2}\text{Fe}_2\text{O}_4$ catalyst. These experiments were carried out at 500°C and the flow rate was maintained at 6 ml/h for 7h. The reaction products were collected and analysed at regular intervals of 1h and the data of the reactions are depicted in Fig. 5.2.2. It was observed that the conversion of ethylbenzene was lowered drastically with time. But, the selectivity for styrene remained more or less constant throughout the reaction period. The formation of C-oxides was observed only at the initial runs of the reaction. The reduction in conversion of ethylbenzene is due to the lack of oxygen needed for abstraction of hydrogen by reoxidizing the catalyst. Besides, deposition of carbonaceous

materials is also another factor, which leads to poisoning of the active sites of the catalyst.

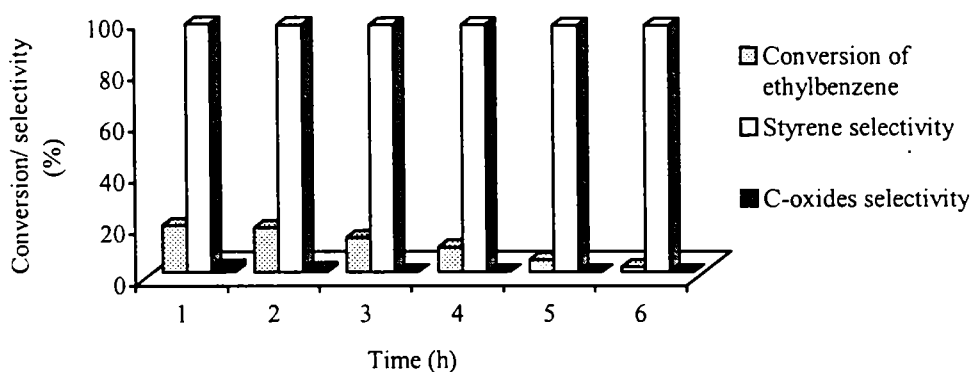


Fig. 5.2.2. Dehydrogenation of ethylbenzene in the absence of oxygen. Catalyst- $\text{Co}_{0.8}\text{Mn}_{0.2}\text{Fe}_2\text{O}_4$, Reaction temperature- 500°C and Flow rate – 6ml/h .

Another set of reactions was conducted over the same catalyst and under the similar reaction conditions except with varying amounts of oxygen (air flow rate) for 2h. The data are given in the following table (Table 5.2.1).

Table 5.2.1. Effect of air flow rate on ethylbenzene conversion and product selectivity .

Air flow rate (ml/min)	Ethylbenzene conversion (%)	Selectivity (%)			
		Benzene	Toluene	c-oxides	Styrene
0	17.32	1.32	0.76	1.07	96.85
5	28.72	1.41	0.62	3.76	94.21
10	46.75	1.43	0.56	4.07	93.94
20	64.72	1.47	0.47	4.58	93.48

Catalyst- $\text{Co}_{0.8}\text{Mn}_{0.2}\text{Fe}_2\text{O}_4$, Reaction Temperature – 500°C , Flow rate - 6ml/h and TOS- 2h.

It can be seen from Table 5.1.1 that the concentration of oxygen radically enhanced the conversion of ethylbenzene. The improved conversion of ethylbenzene in the presence of the oxygen is due to the fact that the additional air supply reoxidizes the catalyst and thereby providing the oxygen needed for hydrogen abstraction. But the

selectivity for styrene remained constant at different air flow rates. However, it was slightly less than that observed for the reaction in the absence of oxygen. The increased availability of oxygen seemed to enhance the formation of C-oxides, thereby reducing the styrene selectivity by a very insignificant value.

With 20 ml/minute air flow rate and at the reaction temperature of 500°C, the reaction was tried over the catalyst, $\text{Co}_{0.8}\text{Mn}_{0.2}\text{Fe}_2\text{O}_4$ for 6 h. At regular intervals of 1 h the reaction products were collected and analysed. The data are depicted in Fig. 5.2.3.

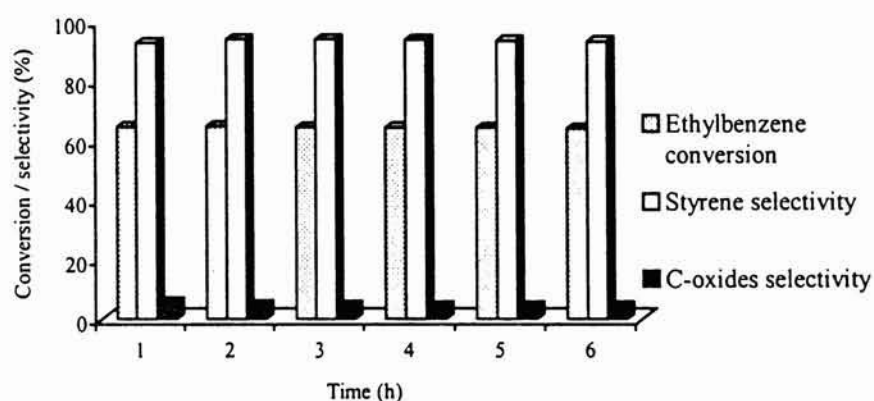


Fig. 5.2.3. Oxidative dehydrogenation of ethylbenzene in the absence of oxygen. Catalyst- $\text{Co}_{0.8}\text{Mn}_{0.2}\text{Fe}_2\text{O}_4$, Reaction temperature- 500°C, air flow rate-20 ml/minute and flow rate – 6ml/ h.

Interestingly, it can be seen from the above figure (Fig. 5.2.3) that the conversion of ethylbenzene and styrene selectivity remained constant throughout the reaction period. Therefore, 20 ml/minute is selected as the optimum air flow rate for the subsequent reactions.

5.2.1.2 Effect of reaction temperature

In order to understand the effect of reaction temperature on oxidative dehydrogenation of ethylbenzene a set of reactions were performed over $\text{Co}_{0.8}\text{Mn}_{0.2}\text{Fe}_2\text{O}_4$ at different temperatures. The airflow rate and flow rate were maintained at 20 ml/ min. and 6 ml/ h respectively. The data obtained were presented in the Table 5.2.2. The data reveal that the ethylbenzene conversion increased with rise in temperature. But, the selectivity for styrene was slightly decreased on increasing the

Table 5.2.2. The product distribution (wt%) and selectivity for ethyl benzene conversion- Effect of temperature.

Product distribution	Temperature (°C)				
	400	450	475	500	525
Benzene	0.08	0.28	0.51	0.95	2.53
Toluene	0.015	0.070	0.14	0.30	0.98
Unreacted EB	91.68	74.27	58.68	35.58	30.8
C-oxides	0.085	0.66	1.55	2.95	5.19
Styrene	8.14	24.72	39.12	60.22	60.50
EB conversion	8.32	25.73	41.32	64.42	69.20
Selectivity (%)					
Benzene	0.96	1.08	1.23	1.47	3.65
Toluene	0.18	0.27	0.34	0.47	1.41
C-oxides	1.02	2.56	3.75	4.58	7.52
Styrene	97.84	95.70	94.33	93.48	87.42

Catalyst- $\text{Co}_{0.8}\text{Mn}_{0.2}\text{Fe}_2\text{O}_4$, Air flow rate-20 ml/minute and Flow rate – 6ml/ h.

temperature. Beyond 500°C the formation of side products like benzene, toluene and C-oxides were greatly enhanced. So, a reaction temperature of 500°C was selected for the further studies.

5.2.1.3 Effect of flow rate

For studying the effect of flow rate on ethylbenzene conversion and product selectivity, five flow rates (4, 5, 6, 7 and 8 ml/h) were selected. The reactions were done over $\text{Co}_{0.8}\text{Mn}_{0.2}\text{Fe}_2\text{O}_4$ at 500°C, maintaining the air flow rate of 20 ml/ minute. The results obtained are depicted in Fig. 5.2.4.

Lower flow rates increase the residence time of the reactant molecules on the catalyst surface resulting in the higher conversion. This is clear from figure 5.2.4. However, higher residence time resulted in the drastic loss in selectivity for styrene as the by-products like benzene, toluene and C-oxides were produced in greater yield.

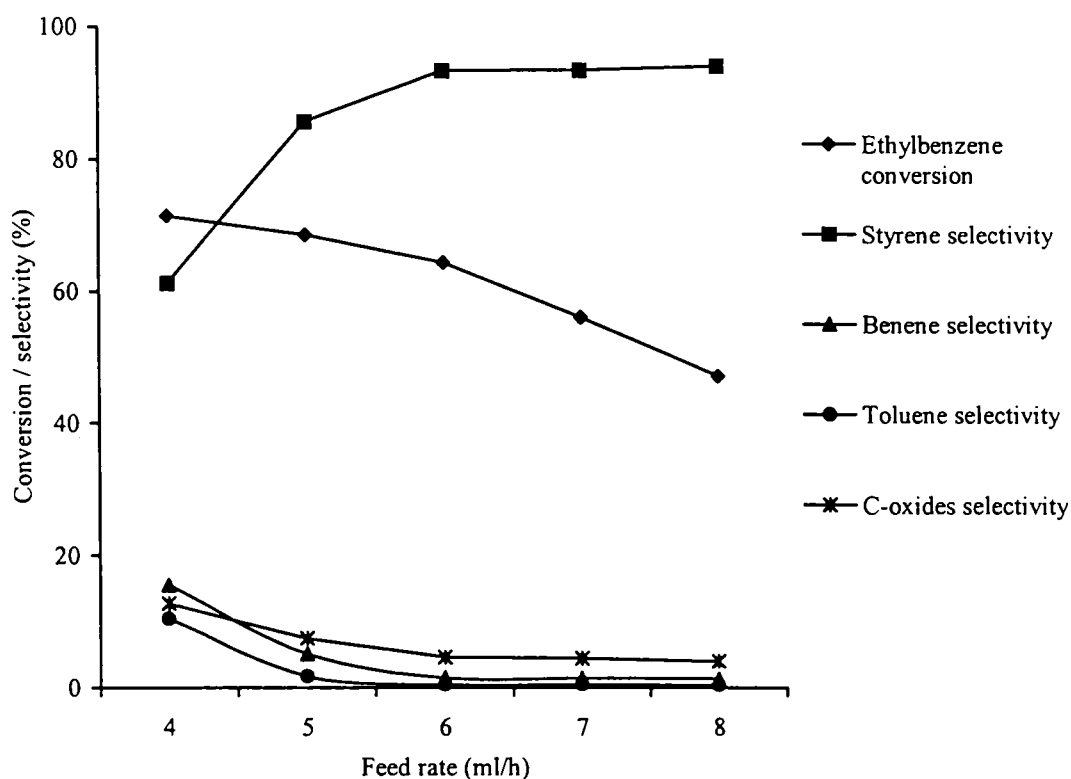


Fig. 5.2.3. Effect of flow rate on ethylbenzene conversion and product selectivity. Catalyst- $\text{Co}_{0.8}\text{Mn}_{0.2}\text{Fe}_2\text{O}_4$, Reaction temperature- 500°C , air flow rate-20 ml/minute.

5.2.2 Comparison of catalyst comparison

To understand the effect of catalyst composition for the oxidative dehydrogenation of ethylbenzene, a sequence of reactions was performed over the different series of manganese ferros spinels under the optimized reaction conditions. Here, we attempt to correlate the catalytic activity with the acid-base properties of the systems. All the prepared catalysts gave styrene as the major product with varying amounts of benzene, toluene and C-oxides as the by-products. It is also interesting to note that for toluene oxidation over the ferrite catalysts, the only products formed were carbon oxides and water. Again, no oxygenated products such as benzaldehyde or benzoic acid were detected. This demonstrates the difference between the oxidative properties of the ternary ferrites and bismuth molybdate. In the case of bismuth molybdate, benzaldehyde is produced as one of the non-selective products in the oxidative dehydrogenation of ethylbenzene [33].

(a) Cr_xMn_(1-x)Fe₂O₄- type systems (x = 0, 0.2, 0.4, 0.6, 0.8 and 1.0)

The percentage conversion of ethylbenzene and product distribution for oxidative dehydrogenation of ethylbenzene done over Cr-Mn series is depicted in the table below (Table 5.2.5).

Table 5.2.5 Product distribution (wt%) and selectivity for ODH of ethylbenzene.

Product distribution	Cr _x Mn _(1-x) Fe ₂ O ₄ - type systems					
	x = 0	x = 0.2	x = 0.4	x = 0.6	x = 0.8	x = 1.0
Benzene	1.23	1.12	1.26	1.32	1.42	1.44
Toluene	1.02	1.62	1.93	2.03	2.10	2.15
Unreacted EB	43.27	78.43	81.42	84.21	86.25	88.88
C-oxides	2.96	0.97	1.1	1.02	0.92	0.85
Styrene	51.52	17.86	14.23	11.42	9.31	6.68
EB conversion	56.73	21.57	18.52	15.79	13.75	11.12
Selectivity (%)						
Benzene	2.19	5.19	6.80	8.35	10.32	12.94
Toluene	1.79	7.51	10.42	12.85	15.27	19.33
C-oxides	5.21	4.49	5.93	6.48	6.69	7.64
Styrene	90.81	82.80	76.83	72.32	67.70	62.14

Reaction temperature- 500 °C , flow rate- 6mL h⁻¹ and air flow rate-20 ml/minute

It can be seen that successive addition of Cr- ions into the octahedral sites of pure manganese ferrosipinel decreased both ethylbenzene conversion and styrene selectivity. The formation of non-selective products such as benzene, toluene and C-oxide were enhanced by the Cr- doping.

The chromium incorporation into the manganese ferrosipinel decreased the medium plus strong acidity as evident from the NH₃-TPD methods and thermodesorption studies of pyridine adsorbed sample. The dehydration activity of the systems revealed from the cyclohexanol decomposition reaction also decreased with increase in chromium content while, the limiting concentration of the electron acceptors adsorbed were increased. Table 5.2.6 presents acid-base properties along with ethylbenzene conversion and styrene selectivity.

Table 5.2.6 Dehydration activity, medium plus strong acidity, limiting amount, ethylbenzene (EB) conversion and styrene yield (%) of the system $\text{Cr}_x\text{Mn}_{1-x}\text{Fe}_2\text{O}_4$ ($x = 0, 0.2, 0.4, 0.6, 0.8$ and 1)

x	Dehydration	medium+strong	Limiting amount		EB	Styrene
	Activity (wt%)	Acidity	(10 ⁻⁴ mmol m ⁻²)		conversion	Selectivity
	Cyclohexene	(10 ⁻⁴ mmol m ⁻²)	TCNQ	Chloranil	(%)	(%)
0	91.28	12.65	10.71	2.6	56.73	90.81
0.2	38.52	6.68	55.52	28.62	21.57	82.80
0.4	37.01	6.51	56.28	29.19	18.52	76.83
0.6	36.25	6.39	57.58	30.12	15.79	72.32
0.8	35.89	6.29	59.01	31.29	13.75	67.70
1	34.82	6.18	60.61	32.74	11.12	62.14

The poor catalytic activity of Cr-Mn series is due to decrease in acidity in the medium- high strength regions.

Effect of time-on-stream

In order to check the catalytic stability of the Cr-Mn series, a set of reactions were carried out at 500°C for 6 h. The flow rate and air flow rate were maintained at 6 mL h⁻¹ and 20 ml/min. respectively. All the compositions of the series possess reasonable stability. The metal ions reduced during the reaction were reoxidized by the external supply of oxygen providing a long-term catalytic stability to the systems.

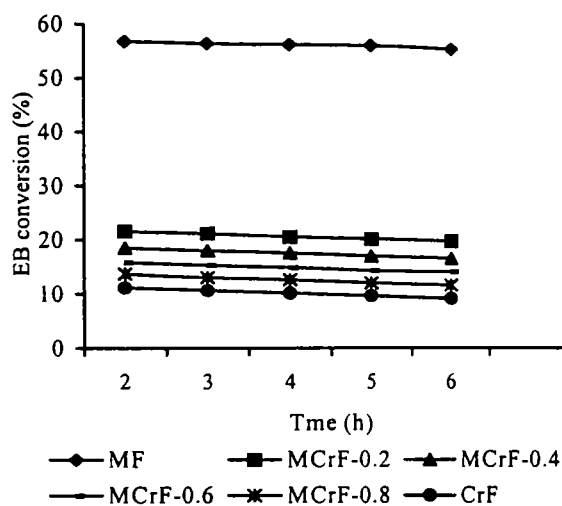


Fig .5.2.4. Effect of time-on-stream over the system, $\text{Cr}_x\text{Mn}_{1-x}\text{Fe}_2\text{O}_4$. Reaction temperature-500°C, flow rate -6mL h⁻¹, air flow rate- 20 ml/min.

(b) $\text{Co}_x\text{Mn}_{(1-x)}\text{Fe}_2\text{O}_4$ - type systems ($x = 0, 0.2, 0.4, 0.6, 0.8$ and 1.0)

The results obtained for oxidative dehydrogenation done over Ni-Mn series are presented in Table 5.2.7.

Table 5.2.7. Product distribution (wt%) and selectivity for ODH of ethylbenzene.

Product distribution	$\text{Co}_x\text{Mn}_{(1-x)}\text{Fe}_2\text{O}_4$ - type systems					
	x = 0	x = 0.2	x = 0.4	x = 0.6	x = 0.8	x = 1.0
Benzene	1.23	1.37	1.36	1.20	0.95	1.31
Toluene	1.02	0.70	0.56	0.48	0.30	0.33
Unreacted EB	43.27	41.73	40.05	37.91	35.58	36.83
C-oxides	2.96	2.97	2.91	2.89	2.95	2.90
Styrene	51.52	53.23	55.12	57.52	60.22	58.63
EB conversion	56.73	58.27	59.95	62.09	64.42	63.17
Selectivity (%)						
Benzene	2.19	2.35	2.26	1.93	1.47	2.07
Toluene	1.79	1.20	0.93	0.77	0.47	0.52
C-oxides	5.21	5.09	4.85	4.65	4.58	4.59
Styrene	90.81	91.35	91.94	92.64	93.48	92.81

Reaction temperature- 500°C , flow rate- 6mL h^{-1} and air flow rate- 20 ml/minute .

The substitution of Mn by Co in the octahedral sites of manganese ferrosipinel enhanced the catalytic activity. Both ethylbenzene conversion and styrene selectivity were improved. Thus, Co-Mn series were found to be good catalysts for oxidative dehydrogenation of ethylbenzene.

The cobalt ion substitution in manganese ferropspinels enhanced the medium plus strong acidity as revealed from the NH_3 -TPD method and thermodesorption studies of pyridine adsorbed sample. The dehydration activity, which is mainly due to weak plus medium acidity, is lowered to some extent. The limiting amount of the electron acceptors adsorbed improved only slightly. The acid-base properties of the Co-Mn series are depicted in Table 5.2.8.

Table 5.2.8. Dehydration activity, medium plus strong acidity, limiting amount, ethylbenzene (EB) conversion and styrene yield (%) of the system $\text{Co}_x\text{Mn}_{1-x}\text{Fe}_2\text{O}_4$ ($x = 0, 0.2, 0.4, 0.6, 0.8$ and 1)

x	Dehydration	medium+strong	Limiting amount		EB	Styrene
	Activity (wt %)	Acidity	$(10^{-4} \text{ mmol m}^{-2})$		conversion	Selectivity
	Cyclohexene	$(10^{-4} \text{ mmol m}^{-2})$	TCNQ	Chloranil	(%)	(%)
0	91.28	12.65	10.71	2.6	56.73	90.81
0.2	90.80	12.72	15.68	5.39	58.27	91.35
0.4	88.00	12.80	16.38	6.32	59.95	91.94
0.6	87.50	12.84	17.19	7.62	62.09	92.64
0.8	87.10	12.93	17.88	8.69	64.42	93.48
1	86.00	12.88	18.58	9.63	63.17	92.81

Surface acidity of medium and stronger acid sites play an important role in the improved catalytic activity of Co-Mn series of ferrites.

Effect of time-on-stream

For the deactivation studies a series of experiments were performed over Co-Mn series of ferrites for 6 h. A plot is drawn with conversion of ethylbenzene as a function of reaction time. These studies revealed that the systems showed moderate catalytic stability. The ethylbenzene conversion of the series remained more or less constant, and hence the reoxidation of the catalyst system by the external supply of oxygen is elucidated.

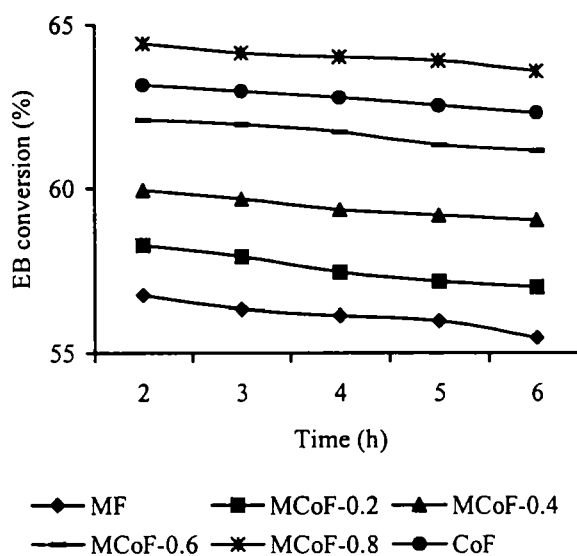


Fig. 5.2.5 Effect of time-on-stream over the system $\text{Co}_x\text{Mn}_{1-x}\text{Fe}_2\text{O}_4$ ($x = 0, 0.2, 0.4, 0.6, 0.8$ and 1). Reaction temperature- 500°C , flow rate - 6 mL h^{-1} air flow rate- 20 mL/min .

(c) $\text{Ni}_x\text{Mn}_{(1-x)}\text{Fe}_2\text{O}_4$ type systems ($x = 0, 0.2, 0.4, 0.6, 0.8$ and 1.0)

The data for the oxidative dehydrogenation of ethylbenzene over Ni-Mn series of ferrites are depicted in the Table 5.2.9.

Table 5.2.9 Product distribution (wt%) and selectivity for ODH of ethylbenzene.

Product distribution	$\text{Ni}_x\text{Mn}_{(1-x)}\text{Fe}_2\text{O}_4$ - type systems					
	x = 0	x = 0.2	x = 0.4	x = 0.6	x = 0.8	x = 1.0
Benzene	1.23	1.91	2.16	2.47	3.30	3.78
Toluene	1.02	2.52	2.72	3.12	3.57	4.18
Unreacted EB	43.27	52.41	54.82	55.43	56.82	59.28
C-oxides	2.96	3.07	3.05	3.09	3.12	3.21
Styrene	51.52	40.09	37.25	35.89	33.19	29.55
EB conversion	56.73	47.59	45.18	44.57	43.18	40.72
Selectivity (%)						
Benzene	2.19	4.01	4.78	5.54	7.64	9.28
Toluene	1.79	5.29	6.02	7.00	8.26	10.27
C-oxides	5.21	6.45	6.75	6.93	7.22	7.89
Styrene	90.81	84.24	82.44	80.53	76.86	72.56

Reaction temperature- 500°C , flow rate- 6mL h^{-1} and air flow rate- 20 ml/minute .

Nickel doping decreased ethylbenzene conversion to some extent and styrene selectivity was also reduced radically. Thus, Ni substitution in the octahedral sites of manganese ferrosinell is found to have a negative effect on the oxidative dehydrogenation of ethylbenzene.

Ni-doping in manganese ferrosinells reduced the medium plus strong acidity. This result obtained from the NH_3 -TPD measurements were supported by the thermodesorption studies of the pyridine adsorbed samples. The dehydration activity of this series decreases with increase in Ni content, whereas the limiting concentration of electron acceptors increased. The acid-base properties along with ethylbenzene conversion and styrene selectivity are depicted in the Table 5.2.10.

Table 5.2.10. Dehydration activity, medium plus strong acidity, limiting amount, ethylbenzene (EB) conversion and styrene yield (%) of the system $Ni_xMn_{1-x}Fe_2O_4$ ($x = 0, 0.2, 0.4, 0.6, 0.8$ and 1)

x	Dehydration	medium+strong	Limiting amount		EB	Styrene
	Activity (wt %)	Acidity	$(10^{-4} \text{ mmol m}^{-2})$		conversion	Selectivity
	Cyclohexene	$(10^{-4} \text{ mmol m}^{-2})$	TCNQ	Chloranil	(%)	(%)
0	91.28	12.65	10.71	2.6	56.73	90.81
0.2	73.76	11.32	20.81	6.41	47.59	84.24
0.4	70.25	11.23	22.47	7.00	45.18	82.44
0.6	68.98	11.14	23.13	7.58	44.57	80.53
0.8	65.29	11.08	23.97	7.92	43.18	76.86
1	62.10	10.99	25.52	8.91	40.72	72.56

The data in Table 5.2.10 clearly show that the acidity in the medium-strong region play the decisive role for the catalytic activity of Ni-Mn series in the oxidative dehydrogenation reaction.

Effect of time-on-stream

In order to check the stability of Ni-Mn series of ferrites for the oxidative dehydrogenation, a set of experiments were conducted at 500°C for 6 h. The flow rate and the air flow rate were kept at 6 mL h^{-1} and 20 ml/min , respectively. All the compositions of this series showed reasonable stability and the ethylbenzene conversion remained more or less constant for a long time. The external supply of oxygen replenishes the catalyst and provides the stability throughout the reaction.

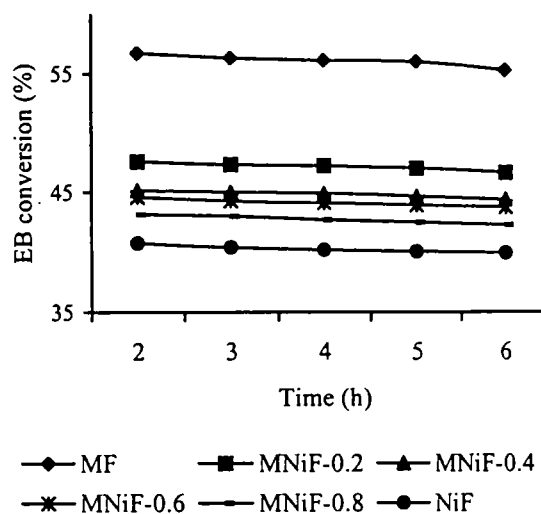


Fig. 5.2.6. Effect of time-on-stream over the system $Ni_xMn_{1-x}Fe_2O_4$ ($x = 0, 0.2, 0.4, 0.6, 0.8$ and 1). Reaction temperature- 500°C , feed flow rate - 6 mL h^{-1} , air flow rate- 20 ml/min .

(d) $\text{Cu}_x\text{Mn}_{(1-x)}\text{Fe}_2\text{O}_4$ - type systems ($x = 0, 0.2, 0.4, 0.6, 0.8$ and 1.0)

Table 5.2.11 shows the percentage conversion of ethylbenzene and product selectivity for oxidative dehydrogenation of ethylbenzene carried out over Cu-Mn series of ferrites.

Table 5.2.11 Product distribution (wt%) and selectivity for ODH of ethylbenzene.

Product distribution	$\text{Cu}_x\text{Mn}_{(1-x)}\text{Fe}_2\text{O}_4$ - type systems					
	x = 0	x = 0.2	x = 0.4	x = 0.6	x = 0.8	x = 1.0
Benzene	1.23	1.36	1.58	1.84	2.18	2.49
Toluene	1.02	3.78	3.42	2.57	0.54	0.49
Unreacted EB	43.27	63.68	61.54	57.33	50.28	46.88
C-oxides	2.96	2.67	2.92	3.38	4.02	2.65
Styrene	51.52	28.51	30.54	34.88	42.98	47.83
EB conversion	56.73	36.32	38.46	42.67	49.72	53.46
Selectivity (%)						
Benzene	2.19	3.75	4.10	4.31	4.38	4.66
Toluene	1.79	10.23	8.89	6.02	1.08	0.91
C-oxides	5.21	7.33	7.60	7.92	8.08	4.96
Styrene	90.81	78.69	79.40	81.74	86.44	89.46

Reaction temperature- 500°C , flow rate- 6 mL h^{-1} and air flow rate- 20 ml/minute .

The addition of copper to the octahedral sites of manganese ferrosponels initially decreased the EB conversion and styrene selectivity. But, successive copper doping gradually increased both the EB conversion and styrene selectivity. The formation of nonselective products was also enhanced in Cu-Mn series.

The medium plus strong acidity of the Cu-Mn series first decreased and then increased with copper content as evident from the NH_3 -TPD studies and thermodesorption studies of pyridine adsorbed samples. The dehydration activity, which is mainly due to the weak plus medium acidity decreased with copper addition, while the limiting value of the electron acceptors, enhanced. These characteristics of Cu-Mn series are presented in the Table 5.2.12.

Table 5.2.12 Dehydration activity, medium plus strong acidity, limiting amount, ethylbenzene (EB) conversion and styrene yield (%) of the system $\text{Cu}_x\text{Mn}_{1-x}\text{Fe}_2\text{O}_4$ ($x = 0, 0.2, 0.4, 0.6, 0.8$ and 1).

x	Dehydration	medium+strong	Limiting amount		EB	Styrene
	Activity (wt %)	Acidity	$(10^{-4} \text{ mmol m}^{-2})$		conversion	Selectivity
	Cyclohexene	$(10^{-4} \text{ mmol m}^{-2})$	TCNQ	Chloranil	(%)	(%)
0	91.28	12.65	10.71	2.6	56.73	90.81
0.2	55.23	10.15	22.91	8.37	36.32	78.69
0.4	52.36	10.27	24.65	9.52	38.46	79.40
0.6	51.18	10.83	26.95	10.65	42.67	81.74
0.8	49.98	11.71	28.32	11.82	49.72	86.44
1	47.91	12.51	30.01	12.80	53.46	89.46

The trend in medium plus strong acidity is same as the trend showed in EB conversion and hence it is concluded that the acidity in this range are responsible for the catalytic activity of Cu-Mn series.

Effect of time-on-stream

All compositions of the Cu-Mn series of ferrites were checked for their catalytic stability by carrying out the reaction at 500°C and maintaining the flow rate and air flow rate at 6 mL h^{-1} and 20 ml/min. , respectively. In the presence of gaseous oxygen, all the systems in this series showed moderate stability for long period of reaction run. The styrene selectivity for all the systems in this series remained constant throughout the reaction period.

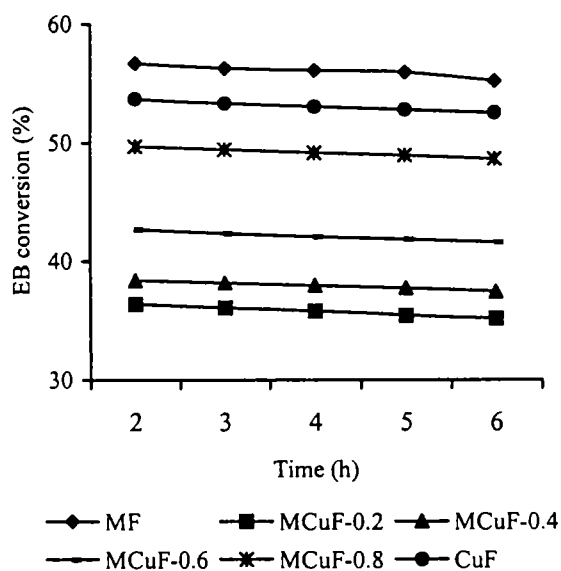


Fig. 5.2.7. Effect of time-on-stream over the system $\text{Cu}_x\text{Mn}_{1-x}\text{Fe}_2\text{O}_4$. Reaction temperature- 500°C , flow rate - 6 mL h^{-1} , air flow rate- 20 ml/min.

(e) $Zn_xMn_{(1-x)}Fe_2O_4$ - type systems (x = 0, 0.2, 0.4, 0.6, 0.8 and 1.0)

The details of the oxidative dehydrogenation of EB over Zn-Mn series are depicted in Table 5.2.13.

Table 5.2.13 Product distribution (wt%) and selectivity for ODH of ethylbenzene.

Product distribution	$Zn_xMn_{(1-x)}Fe_2O_4$ - type systems					
	x = 0	x = 0.2	x = 0.4	x = 0.6	x = 0.8	x = 1.0
Benzene	1.23	3.20	3.01	2.84	2.53	2.19
Toluene	1.02	2.47	2.83	3.69	4.26	4.36
Unreacted EB	43.27	60.11	62.79	63.98	65.78	68.13
C-oxides	2.96	2.09	2.19	2.37	2.42	2.69
Styrene	51.52	32.13	29.18	27.12	25.01	22.63
EB conversion	56.73	39.89	37.21	36.02	34.22	31.87
Selectivity (%)						
Benzene	2.19	8.02	8.08	7.88	7.39	6.87
Toluene	1.79	6.19	7.60	10.24	12.44	13.68
C-oxides	5.21	5.23	5.88	6.57	6.71	8.44
Styrene	90.81	80.54	78.42	75.29	73.09	71.00

Reaction temperature- 500°C, flow rate- 6 mL h⁻¹ and air flow rate-20 ml/minute.

The addition of zinc into the manganese ferros spinels increases the zinc content in the tetrahedral sites and decreases the catalytic activity of the Zn-Mn series of ferrites. Both the EB conversion and styrene selectivity were decreased to certain extent.

The incorporation of Zn into the manganese ferros spinel decreased the medium-high strength acidity as revealed from the NH₃-TPD studies and thermodesorption studies of pyridine adsorbed samples. The dehydration activity, which is due to the weak plus medium acidity was increased with Zn content, whereas the limiting amounts of the electron acceptors adsorbed decreased. All these characteristics of Zn-Mn series are presented in the following Table 5.2.14.

Table 5.2.14. Dehydration activity, medium plus strong acidity, limiting amount, ethylbenzene (EB) conversion and styrene yield (%) for the system $Zn_xMn_{1-x}Fe_2O_4$ ($x = 0, 0.2, 0.4, 0.6, 0.8$ and 1).

x	Dehydration	medium+strong	Limiting amount		EB	Styrene
	Activity (wt %)	Acidity	$(10^{-4} \text{ mmol m}^{-2})$		conversion	Selectivity
	Cyclohexene	$(10^{-4} \text{ mmol m}^{-2})$	TCNQ	Chloranil	(%)	(%)
0	91.28	12.65	10.71	2.6	56.73	90.81
0.2	92.23	10.42	10.21	2.58	39.89	80.54
0.4	93.36	10.38	10.02	2.51	37.21	78.42
0.6	94.18	10.37	9.91	2.49	36.02	75.29
0.8	95.98	10.32	9.62	2.46	34.22	73.09
1	96.91	10.30	9.37	2.43	31.87	71.00

The decreased catalytic activity of the Zn-Mn series as evident from the Table 5.2.14 is due to the reduction in medium-high strength acidity. Both the ethylbenzene conversion and styrene selectivity were decreased on zinc incorporation.

Effect of time-on-stream

The catalytic stability of the Zn-Mn series was examined. For this a set of experiments were done over the Zn-Mn series at 500°C for 6 hours; the air flow rate and flow rate being 20 ml/min and 6 mL h^{-1} respectively. The products were collected at regular intervals of 1 h and analyzed. The conversion of ethylbenzene is plotted as a function of time and is shown in Fig. 5.2.8. It can be seen that all compositions of this series exhibited reasonable stability during the reaction period in presence of oxygen.

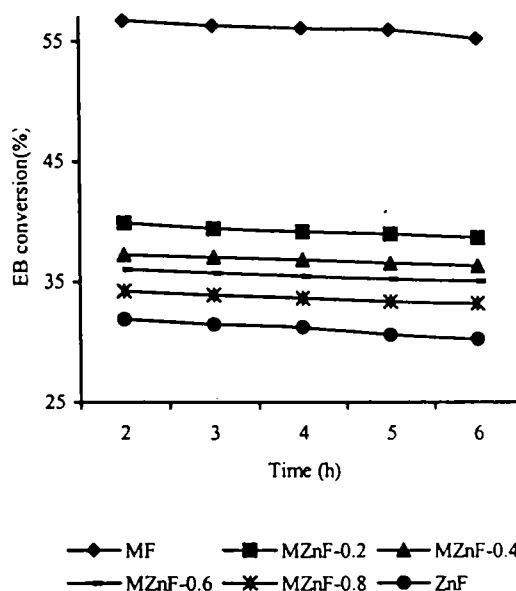


Fig. 5.2.8 Effect of time-on-stream over the system $Zn_xMn_{1-x}Fe_2O_4$ ($x = 0, 0.2, 0.4, 0.6, 0.8$ and 1). Reaction temperature- 500°C , flow rate - 6 mL h^{-1} , air flow rate- 20 ml/min .

5.2.3 Mechanism of ODH of ethylbenzene

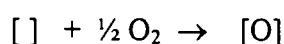
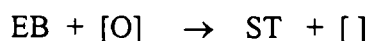
From the ethylbenzene conversion and styrene selectivity values given in the aforementioned parts it can be seen that,

- The catalytic activity and percentage conversion were significantly reduced when the reaction was carried out in the absence of air showing the decisive role of gaseous oxygen in the reaction.
- Whenever a conjugated product can be produced by oxidative dehydrogenation, it is the predominant product. In the oxidative dehydrogenation of ethylbenzene using different series of manganese ferrosinels as catalysts, we observed styrene as the major product.
- The non-selective products observed were benzene, toluene, C-oxides and water. No further oxidation products such as benzaldehyde or benzoic acid were detected.
- Acid-base sites with suitable ranges are found to be the active sites for the ethylbenzene oxydehydrogenation. Acidity in the medium-high strength plays a relevant role in the reaction.

Several mechanisms have been proposed for the oxidative dehydrogenation of ethylbenzene. The most probable one is that, which consists of abstraction of hydrogen from ethylbenzene by the lattice oxygen on the surface to form styrene through π allyl intermediate and reoxidation of the catalyst [4, 34, 35]. This mechanism is known as Mars-van Krevelen mechanism [36, 37]. A condition for the operation of the Mars-van Krevelen mechanism is that the catalyst contains metal ions with variable valencies, notably transition metal ions able to cope with the varying degree of surface oxidation [38]. On manganese ferrosinels systems, oxidative dehydrogenation is supposed to occur through this mechanism. The reoxidation of the reduced ferrites involve chemisorption of an oxygen molecule from gas phase. In the case of manganese ferrites, the redox cycle involves Fe^{3+} and Fe^{2+} , and in the absence of gas-phase oxygen, the oxidative dehydrogenation of ethylbenzene will not proceed once the surface reduction of the catalyst has been achieved. It has been shown [39] that for ferrites, the Fe^{3+} is not

reduced beyond the Fe^{2+} even under high temperature reduction under hydrogen. So when this catalyst is reduced, the reduction of Fe^{3+} to Fe^{2+} occurs only to the extent that a monolayer of lattice oxygen is reduced.

In non-oxidative dehydrogenation, the absence of gaseous oxygen may lower the activity. The following sequence is suggested by Tagawa *et al.* on Si-Al system [5].



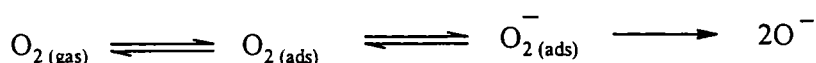
where, EB is ethylbenzene, ST is styrene, [O] is the lattice oxygen and [] is the anion vacancy.

Bautista *et al.* [40] explained the dehydrogenation of ethylbenzene as a concerted process over the Lewis acid sites. According to this mechanism direct transfer of two oxygen atoms to a triplet oxygen molecule is considered. Activation to the triplet state is achieved by the action of Lewis acid sites. According to the authors, the gas-phase dehydrogenation mechanism in non-oxidative as well as in oxidative conditions can be explained within the framework of a concerted process.

The acid-base properties of the catalysts have shown to modify the catalytic activity and selectivity of oxidative dehydrogenation of ethylbenzene [6, 8, 41-45]. From the oxidative dehydrogenation of ethylbenzene over $\text{SnO}_2\text{-P}_2\text{O}_5$ catalysts, Murakami *et al.* [41] suggested that the basic component contributes to the increase in activity by the adsorption of oxygen and its supply to the surface reaction while, the acidic component contributes to the adsorption of ethylbenzene in the active form for the reaction. The mutual interaction of the acidic and basic components increases the activity and the selectivity for the reaction. The moderate and weak acid sites of alumina are responsible for the formation of styrene as propounded by Fiedorow *et al.* [44]. However, Tagawa *et al.* [5] investigated $\text{SnO}_2\text{-P}_2\text{O}_5$ and other solid acid catalysts, and arrived at the conclusion that acid-base sites with suitable strengths are the active sites for ethylbenzene oxydehydrogenation. According to Bagnasco *et al.* [46] surface acid sites of medium-high strength play a significant role in the oxidative dehydrogenation of ethylbenzene. From the investigations over rare earth-promoted sulphated tin oxide, Sugunan *et al.* [30] suggest that the strong acid sites generated by the sulphate treatment

is accountable in the activation of ethylbenzene and enhanced catalytic activity. The strong basic sites enhanced the formation of the nonselective product, toluene.

In oxidative dehydrogenation of ethylbenzene the adsorption and activation of gas-phase oxygen are important. It is proposed that basic sites of suitable strength can adsorb and activate the gas-phase oxygen [5, 47, 48]. The molecular oxygen is dissociated to O^- species over the basic sites of the catalyst according to the following scheme.



Kaliaguine *et al.* [49] and Aika *et al.* [50, 51] have determined that the reaction of O^- with hydrocarbons is initiated by the abstraction of hydrogen by O^- to form OH^- species. The same mechanism has been proposed to explain the activity of ferrites for the dehydrogenation reaction [39, 52-54]. A similar role of O^- species can be expected in the ODH of ethylbenzene over manganese ferrites, i.e., the O^- species abstracts the α -hydrogen of the adsorbed intermediate of ethylbenzene to form surface OH group. If an acidic site of suitable range lies adjacent of the basic site, ethylbenzene is coordinated to this acid site and the ring electron is transferred to the acid site [5]. This donation of ring electron to the acid site makes the acidic nature of α -hydrogen pronounced.

A plausible mechanism for oxidative dehydrogenation of ethylbenzene over manganese ferros spinels is shown in Fig. 5.2.9. At first, the ethylbenzene is coordinated to the acid site and the basic group adjacent to the acid site abstracts the α -hydrogen from the coordinated ethylbenzene to give a stable adsorbed species. The OH group thus formed over the catalyst surface then abstracts the β -hydrogen and the subsequent desorption of water activates the molecular oxygen. The reversibly adsorbed oxygen is converted to O^- species over the catalyst surface, which regenerates the active site.

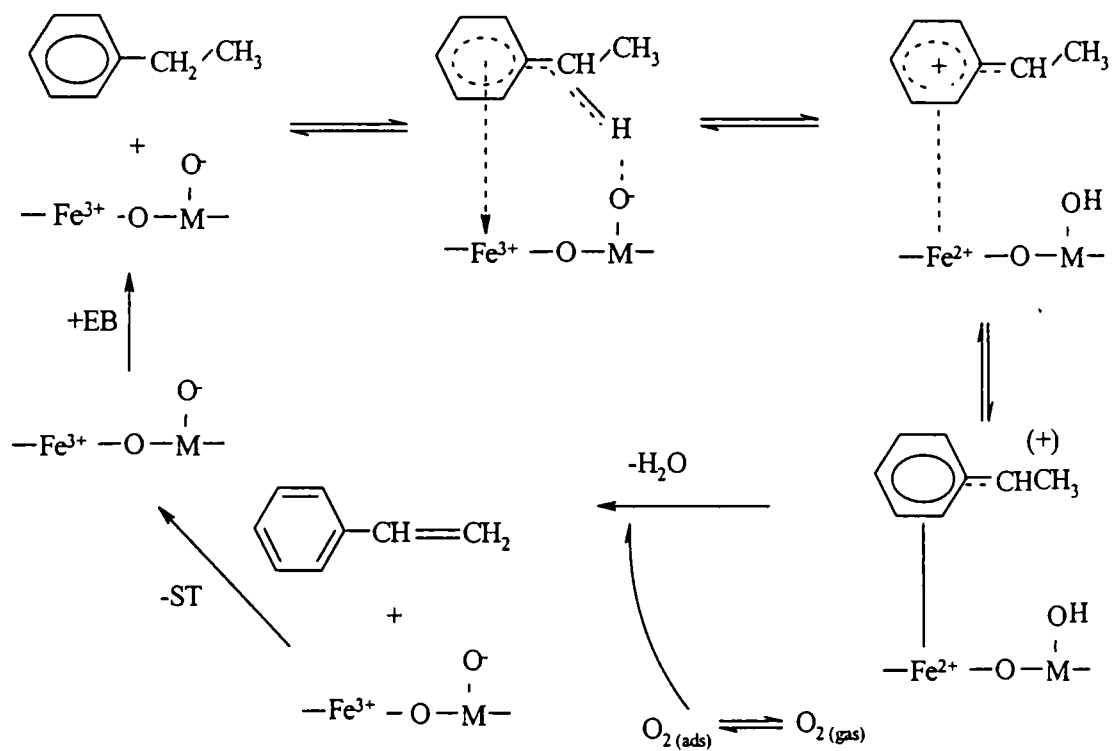


Fig. 5.2.9 A plausible mechanism for the oxidative dehydrogenation of ethylbenzene.

References

Section- I

- [1] R. A. Sheldon and J. K. Koshi; "Metal Catalysed Oxidations of Organic Compounds", Academic Press, New York, 1981.
- [2] R. A. Sheldon; *Chem. Tech.*, (1991) 566.
- [3] R. A. Sheldon; *J. Mol. Catal.*, 107 (1996) 75.
- [4] Shen Lin, Yin Zhen, Shi-Ming Wang and Yu-Mei Dai; *J. Mol. Catal.*, 156 (2000) 113.
- [5] A. Pintar and J. Levecc; *Catal. Today*, 24 (1995) 51.
- [6] Z. Ding, S. N. Aki and M. A. Abraham; *Environ. Sci. Technol.*, 29 (1995) 2748.
- [7] S. H. Lin and S. J. Ho; *Appl. Catal.*, 9 (1996) 133.
- [8] D. Rohan and B. K. Hodnett; *Appl. Catal.*, 151 (1997) 409.
- [9] R. Raja and P. Ratnaswamy; *Appl. Catal.*, 143 (1996) 145.
- [10] C. Skepalik; Ger.Offen, 2138735, 1973.
- [11] M. Uohama; Japan Patent, 0334 948 , 91 34948, 1991.
- [12] S. W. Brown; Br. Pat. Appl., 913323, 1991.
- [13] L. Y. Litvintsv; *Kinet. Catal.*, 34 (1993) 71.
- [14] D. R. C Hytbrechts; *Catal. Lett.*, 8 (1991) 273.
- [15] A. A. Danopoulos, S. M. Paraskevas and E. Kohle; *Erdgas. Petrochem.*, 47 (1994) 240.
- [16] S. M. Imamura; *Gjjustu*, 22 (1981) 201.
- [17] M. Ai; *J. Catal.*, 54 (1978) 223.
- [18] N. Ai-Heyck; *Water Res.*, 19 (1985) 657.
- [19] A. Njnibeako; *Prepr. Can. Symp. Catal.*, 5 (1997) 170.
- [20] T. A. Tatarinova; *Katal. Kal.*, 23 (1985) 54.
- [21] S. Goldstein, G. Czapski and J. Robani; *J. Phys. Chem.*, 98 (1994) 6586.
- [22] A. Thankaraj, R. Kumar and P. Ratnaswamy; *Appl. Catal.*, 57 (1990) L1.
- [23] J. S. Reddy and S. Sivasankar; *Catal. Lett.*, 11 (1992) 241.
- [24] D. P. Serrano, H. X. Liand and M. E. Davis; *J. Chem. Soc Chem. Commun.*, 1992, 745.
- [25] M. A. Camblor, A. Corma, A. Martinez and J. Perez-Pariente; *J. Chem. Soc. Chem. Commun.*, 1992, 589.
- [26] N. Vlagappan and V. Rishani; *J. Chem. Soc. Chem. Commun.*, (1995) 374.
- [27] K. R. Jiri, Z. Amost and H. Jiri; *Collect. Czech. Chem. Commun.*, 60 (1995) 451.
- [28] P. R. Hari Prasad Rao and A. V Ratnaswami; *Appl. Catal.*, 93 (1993) 123.
- [29] O. Kondo, T. Sugsi and S. Yoshida; Jpn Kakai Tokyo Koho, Japan Patent, 1 640 978 (94 40978) (1994).
- [30] G. Bellasti and V. Fatore; *Stud. Surf. Sci. Catal.*, 69 (1991) 79.

- [31] H. Norman; *J. Coord. Chem.*, 19 (1988) 25.
- [32] R. Yu, F. Xiao, D. Wang, G. Pang, S. Feng, S. Qiu and R. Xu; *Catal. Lett.*, 49 (1997) 49.
- [33] C. B. Lui, Z. Zhang, X.G. Yang and Y. Wu; *J. Chem. Soc. Commun.*, (1996) 1019.
- [34] R. B. Yang, F. S. Xiao, D. Wu, Y. Lui, S. L. Qui and R. R. Xu; *Catal. Lett.*, 49 (1997) 49.
- [35] R. B. Yang, F. S. Xiao, D. Wu, Y. Wu, Y. Lui and R. R. Xu; *Catal. Today*, 51 (1997) 39.
- [36] D. Y. Wang, Z. Q. Liu and F. Q. Liu; *Appl. Catal.*, 174 (1998) 25.
- [37] J. F. Yu, Y. Yang and T. H. Wu; *Chem. J. Chin. Univ.*, 17 (1996) 126.
- [38] Y. Yang, J. F. Yu, T. H. Wu and J. Z. Sun, *Chin. J. Catal.*, 18 (1997) 126.
- [39] A. Santos, E. Barroso and G. Felix; *Catal. Today*, 48 (1999) 109.
- [40] Y. I. Matatov-Meytal and M. Sheintuch; *Ind. Eng. Chem. Res.*, 37 (1998) 309.
- [41] A. Sadana and J. R. Katzer; *J. Catal.*, 35 (1974) 140.
- [42] J. Levee; *Appl. Catal.*, 63 (1996) L1.
- [43] A. Pintar and J. Levee; *Chem. Eng. Sci.*, 47 (1992) 2395.
- [44] Q. Wu, X. Hu, P. L. Yue, X. S. Zhao and Q. G. Lu; *Appl. Catal. B*, 32 (3) (2001) 151.
- [45] J. Barrault, C. Bouchoule, K. Echachoui, N. Frini-Srosra, M. Trahelsi and F. Bergaya; *Appl. Catal.*, 15 (1998) 269.
- [46] C. Meyer, G. Clement and J. C. Balaceanu, Proc. 3rd Int. Congr. On Catalysis, vol.1 (1965) p.184.
- [47] C. Xiong, Q. Chen, W. Lu, H. Gao, W. Lu and Z. Gao; *Catal. Lett.*, 69 (2000) 231.
- [48] U. Wilkenhoner, G. Langendries, F. van Laar, G. V. Baron, D. W. Gammon, P. A. Jacobs and E. van Steen; (in press).

Section-II

- [1] J. Jarecki and M. Konopka; *Prezm. Chem.*, 57 (1978) 226.
- [2] W. W. Kaeding; *Catal. Rev.*, 8 (1973) 307.
- [3] E. H. Lee, *Catal. Rev.*, 8 (1973) 285.
- [4] Y. Murakami, K. Iwayama, H. Uchida, T. Hattori and T. Tagawa; *J. Catal.*, 71 (1981) 257.
- [5] T. Tagawa, T. Hattori and Y. Murakami; *J. Catal.*, 75 (1982) 66.
- [6] T. Tagawa, K. Iwayama, Y. Ishida, T. Hattori and Y. Murakami; *J. Catal.*, 79 (1983) 47.
- [7] J. R. Ghublikian; U.S. Patent, 3 502 737.
- [8] G. Emig and H. Hofmann; *J. Catal.*, 84 (1983) 15
- [9] G. E. Vrieland; *J. Catal.*, 111 (1988) 1.
- [10] G. E. Vrieland; *ibid.*, (1988) 14.
- [11] L. E. Cadus, L. A. Arrua, O. F. Gorriz and J. B. Rivarola; *Ind. Eng. Chem. Res.*, 27 (1988) 2241.
- [12] R. M. Manell and L. Bajars; U.S. Patent, 3 247 273 (1966).

- [13] C. R. Adams and T. J. Jennings; *J. Catal.*, 17 (1970) 157.
- [14] A. Cortes and J. L. Seoane; *J. Catal.*, 34 (1974) 7.
- [15] C. F. Crum and S. J. Paton; U.S. Patent, 4 291 184 (1981).
- [16] C. F. Crum and S. J. Paton; U.S. Patent, 4 291 183 (1981).
- [17] P. Galli, A. La Ginestra, P. Patrono, M. A. Massucci, C. Ferragina, P. Ciambelli and G. Bagnasco; Italian Pat. N. 21587 A / 86 (1986).
- [18] M. Turco, G. Bagnasco, P. Ciambelli, A. La Ginestra and G. Russo; *Studies Surf. Sci. Catal.*, 55 (1990) 327.
- [19] G. Bagnasco, P. Ciambelli, A. Frezza, P. Galli and A. La Ginestra; *Appl. Catal.*, 68 (1991) 55.
- [20] T. G. Alkhozov, A. E. Lisovski, M. Safarov and A. M. Dadasheva; *Kinet. Katal.*, 13 (1972) 509.
- [21] P. Ciambelli, S. Crescitelli, V. De Simone and G. Russo; *Chim. Ind. Milan*, 55 (1973) 634.
- [22] K. Tazaki, R. Kitahama, F. Nomura and T. Yokoji; Japan Pat., 74 39 246.
- [23] K. Tazaki, R. Kitahama, F. Nomura and T. Yokoji; *Chem. Abstr.*, 83 (1975) 44002 v.
- [24] T. G. Alkhozov, A. E. Lisovski, M. Safarov, V. B. Lapin and N. A. Kurbanow; *Kinet. Katal.*, 14 (1973) 1182.
- [25] A. E. Lisovski, T. G. Alkhozov and M. Safarov; *Kinet. Katal.*, 13 (1972) 1504.
- [26] R. Fiedorow, W. Kania, K. Nowinska, M. Sopa and M. Wojciechowska; *Bull. Acad. Pol. Sci., Ser. Sci. Chim.*, 27 (1978) 641.
- [27] R. Fiedorow, M. Sopa and W. Przystajko; *Pol. Pat.*, 219 898, 1981.
- [28] W. Kania and K. Jurczyk; *Appl. Catal.*, 61 (1990) 35.
- [29] J. J Kim and S. W. Weller; *Appl. Catal.*, 33 (1987) 15.
- [30] T. M Jyothi, K. Sreekumar, M. B Talwar, A. A. Belhekar, B. S Rao and S. Sugunan; *Bull. Chem. Soc. Jpn.*, 73 (2000) 1.
- [31] A. P. H. Batist, A. Kapteijns, B. C. Lippens and G. C. A. Schutit; *J. Catal.*, 7 (1967) 33.
- [32] M. A. Woskow, P. M. Colling and O. C. Karkaliits; U.S. Patent, 3 440 299, 1969.
- [33] C. R. Adams; *Ind. Eng. Chem.*, 61 (1969) 30.
- [34] J. Hanuza and B. Jezowska-Trzebiatowska; *J. Mol. Catal.*, 4 (1978) 271.
- [35] I. Aso, M. Nakao, M. Egashira, N. Yamazoe and T. Seiyama; *Shokubai*, 18 (1976) 106.
- [36] P. Mars and D. W. van der Krevelen; *Chem. Eng. Sci.*, 8 (1954) 41.
- [37] A. Maltha, T. L. F. Favre, H. F. Kist, A. P. Zuur and V. Ponec; *J. Catal.*, 149 (1994) 364.
- [38] S. Meijers, T. P. Pruys van der Hoeven, V. Ponec, J. P. Jacobs and H. H. Brongersma; *J. Catal.*, 161 (1996) 459.
- [39] R. J. Rennard and W. L. Kehl; *J. Catal.*, 21 (1971) 282.
- [40] F. M. Bautista, J. M. Campelo, A. Garcia and V. M. Marinas; *J. Catal.*, 116 (1989) 338.
- [41] Y. Murakami, K. Iwayama, H. Uchida, T. Hattori and T. Tagawa; *J. Catal.*, 2 (1982) 67.

- [42] A. Schraut, G. Emig and H. G. Sockel; *Appl. Catal.*, 29 (1987) 311.
- [43] T. Hattori, H. Hanai and Y. Murakami; *J. Catal.*, 84 (1979) 294.
- [44] R. Fiedorow, W. Przystajko, M. Sopa and I. G. Della Lana; *J. Catal.*, 68 (1981) 33.
- [45] K. Brozyana and Dziewcki; *Appl. Catal.*, 35 (1987) 211.
- [46] G. Bagnasco, P. Ciambelli, M. Turco, A. La Ginestra and P. Patrono; *Appl. Catal.*, 68 (1991) 69.
- [47] J. H. Lunsford; *Catal. Rev.*, 8 (1973) 135.
- [48] A. Bielanski and J. Haber; *J. Catal.*, 19 (1979) 1.
- [49] S. L. Kaliaguine, B. N. Shelimov and V. B. Kazanski; *J. Catal.*, 55 (1978) 384.
- [50] K. Aika and J. H. Lunsford; *J. Phys. Chem.*, 81 (1977) 1393.
- [51] K. Aika and J. H. Lunsford; *J. Phys. Chem.*, 82 (1978) 1794.
- [52] W. R. Cares and J. W. Hightower; *J. Catal.*, 23 (1971) 193.
- [53] M. A. Gibson and J. W. Hightower; *J. Catal.*, 41 (1976) 420.
- [54] K. M. Sancier, P. R. Wentreck and H. Wise; *J. Catal.*, 39 (1975) 141.

Summary And Conclusions

6.1 Summary of the work

Spinels of simple (AFe_2O_4) type and mixed ($A_{(1-x)}B_xFe_2O_4$) type ferrites are known. These special group of inorganic compounds attracted the attention of physicists, technologists and chemists due to their peculiar cation distribution, thermal and mechanical stability and interesting electrical and magnetic properties. Also, they are found to be effective catalysts for various reactions due to the following reasons. (a) The ease with which iron can change its oxidation state between 2 and 3, (b) the reduction of Fe^{3+} to Fe^{2+} takes place without altering the lattice configurations so that upon reoxidation the original state can be regained and (c) individual metal oxides lose their catalytic activity rapidly owing to ageing and formation of the coke over the catalyst surface whereas the spinel lattice imparts extra stability to the catalysts under various reaction conditions so that these systems have sustained activity for longer periods. For studying the catalytic properties, the low temperature co-precipitation method is preferred over the usual ceramic method as the former method yields homogeneous, and fine ferrite particles. The present study, accordingly, employed low temperature co-precipitation method for the preparation of $Mn_{(1-x)}B_xFe_2O_4$ specimens, where B is a metal cation such as Cr, Co, Ni, Cu and Zn. The prepared ferrite samples were characterized by adopting various physico-chemical techniques. The catalytic activities of the systems were investigated for liquid-phase benzoylation of aromatic compounds and phenol hydroxylation and for vapour-phase reactions such as aniline alkylation, phenol methylation and ODH of ethylbenzene. The description of the work is presented in six chapters.

Chapter 1 presents an introduction to heterogeneous catalysis and a literature survey on catalysis by transition metal oxides and spinel ferrites. A detailed description on various methods of preparation of ferrites, spinel structure, electrical and acid-base properties of ferrites and catalytic effectiveness for various reactions are also given in this chapter.

Chapter 2 deals with various experimental procedures and principles of characterization methods employed for the present work.

Chapter 3 reports the results and discussion of the catalyst characterization procedure. The spinel phase formation at the calcination temperature of 500°C has been ascertained by the XRD data. The unit cell parameters of the pure manganese ferrite were found to be increasing by the incorporation of various metal cations. The crystallite size characterized from the XRD broadening is in the range 21-58 nm. The SEM analysis for MnFe₂O₄ at three different calcination temperatures is in concordance with the XRD data. The stoichiometries of the compositions checked by the ICP analysis were found to be in good agreement with the theoretical values. The spinel phase formation is further confirmed by the appearance of two strong infrared bands ν_1 and ν_2 around 700 cm⁻¹ and 500 cm⁻¹, respectively. The spinel ferrites prepared by low temperature co-precipitation method possess sufficiently large surface area. The transport studies revealed that the different series of manganese ferrites are semiconductors and possess holes as the major charge carriers except for MnFe₂O₄ where electrons are the major charge carriers. Activation energy or energy gap determination by the DC conductivity studies showed that incorporation of Cr, Ni and Zn cations increased the energy gap whereas the incorporation of the other metal cations decreased the same. The Mössbauer spectra revealed the presence of Fe²⁺ and Fe³⁺ ions in MnFe₂O₄. Also, the inherent magnetic behaviour of the sample is proved by the Mössbauer hyperfine splitting. NH₃-TPD studies revealed that the weak plus medium acidity is increased by the incorporation of Cr, Ni, Co and Cu ions whereas the strong acidity is increased by the progressive substitution of Zn ion. The thermodesorption studies of pyridine adsorbed samples well supported the NH₃-TPD results. The thermodesorption studies of 2,6-dimethylpyridine adsorbed samples showed that incorporation of metal cations decreased the Brønsted acidity of pure manganese ferrites. The electron donating property studies revealed that the limiting amount of the electron acceptors adsorbed on the catalyst surface is enhanced with metal ion incorporation in manganese ferrite and is more pronounced in Cr-substituted manganese ferrites. Cyclohexanol decomposition reactions were performed to evaluate the acidity of the

systems. Since dehydration is an acid catalyzed reaction, the dehydration activities of the systems leading to cyclohexene has been taken as measure of their acid strength.

Chapter 4 is divided into three sections. The first section gives the detailed discussion of the liquid-phase benzoylation of the aromatic compounds using benzoyl chloride as the benzoylating reagent over different manganese ferrite catalysts and also the effect of various reaction parameters on product distribution of toluene benzoylation. The decisive properties in the catalytic activity for activated and deactivated benzenes are observed to be different. It is evident that in the case of activated benzenes like toluene, xylenes and anisole, the aromatic ring is highly activated and therefore less acidity of the samples is sufficient to bring about such reactions and activation energy of the catalysts is seemed to be more involved than the acidity. But in the case of benzene and halobenzenes, the aromatic ring is not activated or deactivated respectively, the adsorption of the aromatic substrate over the catalyst surface is difficult and hence the acidity of the catalysts plays the decisive role. It was observed that various reaction parameters such as amount of catalyst, reaction temperature, catalyst composition, presence of moisture in the reaction mixture as well as in the catalyst and aromatic substrate /BOC molar ratio have crucial roles in determining the catalytic performance. The second section deals with a thorough investigation of alkylation of aniline using methanol over the prepared systems. The detailed discussion regarding the influence of factors such as reaction temperature, molar ratio, time-on-stream and contact time are also presented in this section. The weak plus medium acidity of the catalyst was involved in determining the catalytic activity towards aniline alkylation and Cr-substituted manganese ferrites are found as good options for this reaction. The alkylation of phenol using methanol over all the catalyst systems and effects of various reaction parameters are depicted in the third section. It is seen that manganese ferros spinels produce *ortho*-alkylated products (formation of *o*-cresol and 2,6-xyleneol, but not *meta*- or *para*-cresols and xyleneol isomers) and the total *ortho*-selectivity always exceeded 97%, whereas the individual selectivities depend greatly on reaction parameters. The manganese ferrites in which Zn progressively substitutes Mn are particularly selective and active for *ortho* methylation of phenol. $Zn_{0.8}Mn_{0.2}Fe_2O_4$ is found to be the most active and selective catalyst for this reaction.

Chapter 5 is divided into two sections. The first section depicts the liquid-phase phenol hydroxylation using hydrogen peroxide as the oxidant over different manganese ferros spinels and the effects of various reaction parameters on the product distribution. The enhanced amount of holes or cation vacancies and their appreciable mobility in the systems are the decisive factors determining the improved catalytic activity in phenol hydroxylation of different series of manganese ferrites. A heterogeneous-homogeneous free-radical reaction mechanism is proposed for phenol hydroxylation over different manganese ferrites. The second section focuses on the vapour-phase oxidative dehydrogenation of ethylbenzene and effect of various reaction parameters for styrene conversion. The acidity in the medium-strong region was found to determine the catalytic activity of different manganese ferrite series in the oxidative dehydrogenation reaction.

6.2 Conclusions

- ❖ Manganese ferros spinels prepared by the low temperature co-precipitation technique provides homogeneous, fine and reproducible ferrite powders with high surface areas.
- ❖ All the peaks in the XRD pattern matched well with the characteristic reflections of the ferrites. Close resemblance of the 'd' values with the standard values indicated the formation of spinel phase at the calcination temperature of 500°C. The spinel phase formation is again confirmed by the appearance of two strong infrared bands below 1000 cm⁻¹.
- ❖ The successive incorporation of metal cations such as Cr, Co, Ni, Cu and Zn decreased the total acidity of MnFe₂O₄ as evident from the NH₃-TPD studies. The weak plus medium acidity is improved by the progressive addition of Cr, Co, Ni and Cu whereas the strong acidity is enhanced with Zn ion substitution.
- ❖ The thermodesorption data of pyridine adsorbed samples is in concordance with the NH₃-TPD results.
- ❖ The general observation that dehydration is favoured by acid sites and dehydrogenation is favoured by both acidic and basic sites is confirmed by the

cyclohexanol decomposition reaction carried over different series of manganese ferrites.

- ❖ Liquid-phase benzoylation of various aromatic compounds proceeded efficiently over different series of manganese ferrites. It is observed that for activated benzenes, activation energy of the systems play the decisive role in determining the conversion of BOC. But in the case of benzene and activated benzenes, increase in strong acidity of the systems has the key role in the conversion of BOC.
- ❖ Among the various systems studied, $\text{Cr}_{0.8}\text{Mn}_{0.2}\text{Fe}_2\text{O}_4$ exhibits excellent selectivity and high yield for N-methylaniline even at comparatively low temperatures and methanol to aniline molar ratios. Only a minimum acidity is required for the reaction and surplus acidity does not favour the reaction.
- ❖ The manganese ferrites in which Zn progressively substitutes Mn are particularly selective and active for *ortho*-methylation of phenol leading to *o*-cresol and 2,6-xyleneol. $\text{Zn}_{0.8}\text{Mn}_{0.2}\text{Fe}_2\text{O}_4$ is found to be the most active and selective catalyst for this reaction. Under the optimized reaction conditions the *ortho*-selectivity (*o*-cresol and 2,6-xyleneol) exceeded 97% whereas the individual selectivities depended on the reaction parameters.
- ❖ Optimization process for hydroxylation of phenol revealed that the reaction parameters such as amount of catalyst, reaction temperature, H_2O_2 /phenol volume ratio, solvent and pH have critical influence on the reaction. CuFe_2O_4 is found to be most efficient for the hydroxylation of phenol since both giving maximum conversion of phenol and selectivity for diphenol.
- ❖ Catalytic studies of oxidative dehydrogenation of ethylbenzene pointed out that sufficient number of both acidic and basic sites is needed for the conversion of ethylbenzene and selective formation of styrene. $\text{Co}_{0.8}\text{Mn}_{0.2}\text{Fe}_2\text{O}_4$ is found to be most efficient for this reaction. Increase in temperature and decrease of flow rate enhance the conversion of ethylbenzene. However, increase of temperature above 500°C reduces styrene selectivity.



6.3 Further scope of the work

The different series of manganese ferrites are proved to be excellent catalysts for various industrially important reactions such as Friedel-Crafts benzoylation of aromatic compounds, methylation of aniline and phenol, hydroxylation of phenol and oxidative dehydrogenation of ethylbenzene. These catalysts were found to be active not only for benzoylation of activated benzenes but also for deactivated benzenes. Thus, the work can be extended to the development of environmentally friendly ferrite catalysts for the acylation/ benzoylation of various aromatic compounds using different acylating agents. Interestingly, it is observed that Cr-Mn series of ferrites are very good catalysts for the active and selective formation of N-methylamine. Thus, this series of ferrites can be further modified for the alkylation of substituted aniline using various alkylating agents. Again, the different series of manganese ferrites yield *ortho*-alkylated products and total *ortho*-selectivity always exceeded 97% for phenol methylation. The activity and selectivity can be further improved by incorporating suitable metal cations into the pure manganese ferrite and can be used for the alkylation of substituted phenols. Various manganese ferrites, especially copper substituted ones, are found to be potential catalysts for the production of diphenols under mild reaction conditions and prolonged reaction resulted in the complete conversion of phenol to C-oxides and tar. Due to the tightening of the environmental regulations, production of diphenols from phenol hydroxylation and reduction of phenolic pollutants in waste waters using these catalysts can be a promising approach because it demands only simple techniques and produce little environmental pollution.